Identification and Characterization of Novel Determinants of Epithelial Apical-Basal Polarity and Lumen Formation

A thesis by

Li-Ting Wang, M.Sc.

Division of Experimental Medicine,
McGill University, Montreal
March 2021

A thesis submitted to McGill University in partial fulfillment of the requirements for the degree of Doctor of Philosophy

Abstract

Epithelial cells line most organ and tissue surfaces and provide an essential barrier that separates physiological compartments. A nearly universal feature of epithelial cells is their polarization into distinct apical and basolateral membrane domains that allows groups of cells to organize into complex structures such as tubes and acini with a characteristic central lumen. This process requires that cells coordinately orient their polarity axis so that the basolateral domain is on the outside and apical domain inside epithelial structures. However, the cues that initiate internalization of apical proteins from the periphery to establish an internal apical site are incompletely understood.

To identify potential novel regulators of apical-basal polarity and lumen formation, I used a biotin identification (BioID) approach coupled with mass spectrometry in epithelial cells cultured in a three-dimensional matrix. I report in this thesis several novel proteins involved in lumen formation, including CD13, PARD3B, RALB, and HRNR, each of which is necessary for epithelial organization and lumen formation. I also identified PTPN14 as a novel polarity-associated protein, which regulates epithelial organization during oncogene-induced malignant transformation.

I report that CD13 (Aminopeptidase N/APN/ANPEP) associates with the apical Crumbs/Par6. Loss of CD13 induces an inverted polarity phenotype in which apical components fail to accumulate at the appropriate location during cell division. I propose that CD13 acts as a surface membrane receptor for Rab11-mediated endocytosis of apical cargo that is necessary to reorient apical proteins from the periphery to internal sites necessary for lumen formation.

Furthermore, I identified PTPN14 as a proximal protein for aPKC and PAR6 that localizes to the apical membrane. Depletion of PTPN14 had a modest effect on the degree of aPKC-enrichment at the apical membrane and did not affect lumen formation. However, PTPN14 protein expression was down-regulated in $KRAS^{G12V}$-expressing epithelial cells and re-introduction of PTPN14 suppressed $KRAS^{G12V}$-induced overgrowth and restored apical-basal polarity and a central lumen. This suggests that PTPN14 is an important tumour suppressor that maintains cell polarization to restrict cancer development.

Together, these results identify several novel players that regulate epithelial organization, which have potentially important roles in the progression of cancer.

Résumé

Les cellules épithéliales tapissent la plupart des organes ainsi que la surface des tissus et assurent une fonction de barrière indispensable, afin de séparer les compartiments physiologiques. Une caractéristique presque universelle des cellules épithéliales est leur polarisation en domaines membranaires apicaux et basolatéraux distincts, qui permettent aux groupes de cellules de s'organiser en structures complexes, telles que des tubes et des acini avec une lumière centrale caractéristique. Ce processus requiert que les cellules orientent leur axe de polarité de façon coordonnée, afin que le domaine basolatéral se situe à l'extérieur et le domaine apical à l'intérieur des structures épithéliales. Cependant, les signaux qui initient l'internalisation des protéines apicales à partir de la périphérie, afin d'établir un site apical interne, ne sont pas encore complètement compris.

Afin d'identifier de potentiels nouveaux régulateurs de la polarité apico-basale et de la formation de la lumière, j'ai utilisé une approche d'identification de la biotine (BioID) couplée à la spectrométrie de masse, sur des cellules épithéliales cultivées dans une matrice en trois dimensions. Je rapporte dans cette thèse de nombreuses nouvelles protéines impliquées dans la formation de la lumière, incluant CD13, PARD3B, RALB et HRNR, chacune étant nécessaire à l'organisation épithéliale et à la formation de la lumière. J'ai également identifié PTPN14 comme une nouvelle protéine associée à la polarité, qui régule l'organisation épithéliale au cours de la transformation maligne, induite par un oncogène.

J'ai montré que CD13 (Aminopeptidase N/APN/ANPEP) s'associe au niveau apical avec Crumbs/Par6. La perte de CD13 induit un phénotype de polarité inversée dans lequel les composants apicaux ne s'accumulent pas au bon endroit, au cours de la division cellulaire. Je

suggère que CD13 agit comme un récepteur membranaire de surface pour Rab11 qui joue un rôle de médiateur dans l'endocytose des protéines cargo apicales, étape nécessaire à la réorientation des protéines apicales depuis la périphérie jusqu'aux sites internes, essentielle à la formation de la lumière.

De plus, j'ai identifié PTPN14 comme une protéine proximale pour aPKC et PAR6, qui se localise au niveau de la membrane apicale. La déplétion de PTPN14 avait un effet modeste sur le degré d'enrichissement de aPKC au niveau de la membrane apicale et n'affectait pas la formation de la lumière. Cependant, l'expression de la protéine PTPN14 était diminuée dans les cellules épithéliales exprimant $KRAS^{G12V}$ et la réintroduction de PTPN14 supprimait l'augmentation de la croissance induite par $KRAS^{G12V}$ et restaurait la polarité apico-basale ainsi que la lumière centrale. Cela suggère que PTPN14 est un suppresseur de tumeur important qui maintient la polarisation cellulaire afin de restreindre le développement de cancers.

Ensemble, ces résultats identifient plusieurs nouveaux acteurs qui régulent l'organisation épithéliale et qui ont des rôles potentiellement importants dans la progression du cancer.

Acknowledgements

I would like to greatly appreciate the Canadian Institutes of Health Research for funding my work. I would also like to acknowledge receipt of the Rolande & Marcel Gosselin Studentship, The McGill Integrated Cancer Research Training Program and The Charlotte and Leo Karassik Foundation PhD Fellowship Awards.

I would like to express my sincere gratitude and appreciation to my supervisor Dr. Luke McCaffrey for accepting me into his lab and providing me an opportunity to conduct my studies. I am honoured to be part of his lab and have guidance from him, he has always given his profound knowledge, patience, time, continuous support, and encouragement. My research and study would not have been possible without his help.

I would like to thank my advisor, Dr. Maxime Bouchard, and committee members: Dr. Yojiro Yamanaka, Dr. William Muller, and Dr. Peter Siegel for their advice and invaluable feedback that has helped me to enrich my work throughout my study.

I would also like to acknowledge all members of the McCaffrey lab both past and present. They have always been providing practical scientific discussions and thoughtful assistance whenever I needed it. I am lucky to work with so many intelligent people. On top of that, they made the lab a pleasant working environment with their kind nature. Thank you to the members of the fourth floor of GCRC especially the McBouYa group.

To Virginie, thank you for helping me to translate the abstract of my thesis from English to French. I really appreciate the time you put into this.

To all the people in the Department of Experimental Medicine and GCRC centre, for providing a great research environment to conduct my studies and people for their friendly care

and timely help. I would also like to thank the staffs of Advanced BioImaging Facility, the Flow Cytometry and Cell Sorting Facility of McGill, and The Proteomics Core Facility of Université de Montréal for their technical expertise.

I would also like to thank you to have all my friends in McGill for their continuous support and genuine friendship throughout my doctoral studies.

To all my family, teachers and friends in Taiwan and Canada, I would like to thank you for your understanding, friendship, and support during these years.

Most of all, I would like to extend my utmost gratitude to my beloved parents, my four lovely sisters, my two brothers in law for their constant support and encouragement with their best wishes. Especially Lydia and Jasper for guidance, support, and encouragement over all these years. I dedicate this thesis to my parents, sisters, and brothers.

I would like to end my acknowledgements with a deeply grateful to Heavenly Mother that continue to flow into my life.

Table of Contents

List of Figures

Contribution to Original Knowledge

During my studies, I have made three main contributions to original knowledge that I highlight in this thesis:

1. I established three dimensional organotypic cultures for proximity proteomics screen as an architecturally relevant system for identifying novel regulators of cell polarization and lumen formation.
2. I discovered that CD13 is necessary to reorient apical proteins from the periphery to internal sites, which is necessary for lumen formation.
3. I discovered that PTPN14 associates with aPKC/PAR6B complex and is important for suppressing $KRAS^{G12V}$-induced transformation.

Contribution of Authors

1. All the work presented in this thesis is my original research, designed, performed, and analyzed by myself, supervised by Dr. Luke McCaffrey.
2. Sara Banerjee performed the SAINT analysis in Figure 2.3 and Figure 4.2.
3. Abira Rajah, and Dr. Claire M Brown provided technical assistance with TIRF data in Figure 3.5 F,G,H.
4. Dr. Virginie Lelarge performed the staining in Supplemental Figure S4.5 C.
5. Dr. Luke McCaffrey performed the staining in Figure 5.1 A.

Refereed Journal Publications

1. **Li-Ting Wang** and Luke McCaffrey. A Proximity Proteomics Screen in Three-Dimensional Organotypic Cultures Identifies Novel Regulators of Lumen Formation. *Manuscript in preparation*
2. **Li-Ting Wang**, Abira Rajah, Claire M Brown, Luke McCaffrey. (2021) CD13 orients the apical-basal polarity axis necessary for lumen formation. *manuscript under revision for Nature Communications*
3. **Li-Ting Wang** and Luke McCaffrey. Protein tyrosine phosphatase N14 associates with the Par complex and regulates KRAS-dependent transformation. *Manuscript in preparation*
4. Cornélia Biehler, **Li-Ting Wang**, Myriam Sévigny, Alexandra Jetté, Clémence L. Gamblin, Rachel Catterall, Elise Houssin, Luke McCaffrey, Patrick Laprise. (2020) Girdin is a component of the lateral polarity protein network restricting cell dissemination. *PLOS Genetics* 16(3) e1008674

5. Maia Al Masri, Karina Paliotti, Raymond Tran, Ruba Halaoui, Virginie Lelarge, Sudipa Chatterjee, **Li-Ting Wang**, Christopher Moraes, Luke McCaffrey. (2021) Architectural Control of Metabolic Plasticity in Epithelial Cancer Cells*. Communications Biology*

Refereed Conference Abstracts

1. **Li-Ting Wang** and Luke M. McCaffrey. "Characterization of aPKC-Related Signalling Pathways in Normal and Oncogene-Transformed Cells". American Society for Cell Biology|European Molecular Biology Organization Meeting (ASCB|EMBO) (2017, Philadelphia, PA, USA)
2. **Li-Ting Wang** and Luke M. McCaffrey. "Characterization of the novel role of CD13 in apical-basal polarity". EMBO Workshop (2019, Sant Feliu de Guixols, Spain)

Abbreviations

2D	Two-dimensional
3D	Three-dimensional
AMIS	Apical membrane initiation site
aPKC	Atypical protein kinase C
APN/ANPEP	Aminopeptidase N
ARE	Apical recycling endosomes
ASE	Apical sorting endosome
ATCC	American type culture collection
Baz	Bazooka
BCAR1	Breast cancer anti-estrogen resistance protein 1
BioID	Biotin identification
BME	Basement membrane extract
BSE	Basal sorting endosome
CCD	Charged coupled device
CEA	Carcinoembryonic antigen
CGN	Cingulin
CLPI	Cysteine-leucine-proline-isoleucine
CRB	Crumbs
CRC	Colorectal cancer
CRE	Common recycling endosome

CRIB	Cdc42/Rac interaction binding
CRISPR	Clustered regularly interspaced short palindromic repeats
DIC	Differential interference contrast
DLG	Discs large
DMEM	Dulbecco's modified Eagle's medium
DNA	Deoxyribonucleic acid
DOX	Doxycycline
DTT	Dithiothreitol
ECM	Extracellular matrix
EDTA	Ethylenediaminetetraacetic acid
EFGP	Enhanced green fluorescent protein
EGF	Epidermal growth factor
EGTA	Ethylene glycol tetraacetic acid
EMT	Epithelial to mesenchymal transition
ERK	Extracellular regulated kinase
ERLI	Glutamic acid-arginine-leucine-isoleucine
FACS	Fluorescent activated cell sorting
F-actin	Filamentous actin
FDR	False discovery rate
FERM	Four-point-one, ezrin, radixin, moesin
GAPDH	Glyceraldehyde-3-phosphate dehydrogenase
GAPs	GTPase activating proteins

GDP	Guanosine diphosphate
GEF	Guanine-nucleotide exchange factor
GFP	Green fluorescent protein
GTP	Guanosine triphosphate
HRAS	Harvey rat sarcoma viral oncogene
HRNR	Hornerin
HRP	Horseradish peroxidase
Insc	Inscuteable
IP	Immunoprecipitation
IRES	Internal ribosomal entry site
JAK	The Janus kinase
JAM	Junctional adhesion molecules
KIBRA	Kidney and Brain Protein
KRAS	Kirsten rat sarcoma viral oncogene
LAP	LRR (for leucine-rich repeats) and PDZ (for PSD-95/Discs-large/ZO-1)
LATS1	Large tumor suppressor kinase 1
LED	Light emitting diode
LGL	Lethal giant larvae
LKB	Liver kinase B
LRRs	Leucine-rich repeats
MAGUK	Membrane-associated guanylate kinase
MAPK	Mitogen-activated protein kinase

MCS	Multiple cloning site
MDCK	Madin-Darby canine kidney
MEK	Mitogen-activated protein kinase
MHC	Histocompatibility complex
MOI	Multiplicity of infection
NA	Numerical aperture
NRAS	Neuroblastoma RAS viral oncogene
Nrx-IV	Neurexin IV
NSCLC	Non-small cell lung cancer
PALS1	Protein associated with Lin-7 one
PAP	Pre-luminal apical patch
PAR	Partitioning defective
PATJ	Pals1-associated tight junction
PBS	Phosphate-buffered saline
PCR	Polymerase chain reaction
PDAC	Pancreatic ductal adenocarcinoma
PDZ	PSD-95, discs large, ZO-1
PEG	Polyethylene glycol
PEI	Polyethylenimine
PI3K	Phospho-inositol-3-kinase
Pins	Partner of Inscuteable
PJS	Peutz-Jeghers syndrome

PKD	Protein kinase D
PMSF	Phenylmethylsulfonyl fluoride
PRKCD	Protein kinase C delta
PRKCI	Protein kinase C iota
PRKCZ	Protein kinase C zeta
PRNRP	Papillary renal neoplasm with reverse polarity
PSD-95	Post-synaptic density protein 95
PTEN	Protein tyrosine phosphatase and tensin homologue
PTP	Protein tyrosine phosphatase
PTPN14	Tyrosine-protein phosphatase non-receptor 14
RAB11FIP5	RAB11 family interacting protein 5
RAF	Rapidly accelerated fibrosarcoma
RALB	Ras like proto-oncogene B
RE	Recycling endosome
RIN1	Ras and Rab interactor 1
RING-finger	Really Interesting New Gene-finger protein
RIPA	Radioimmunoprecipitation assay
RNA	Ribonucleic acid
ROCK	Rho-associated protein kinase
ROS	Reactive oxygen species
SAINT	Significance Analysis of interactome
SCRIB	Scribble

SDS	Sodium dodecyl sulfate
SDS-PAGE	SDS-Polyacrylamide gel
STX	Syntaxin
TAL6	Tumor-associated antigen L6
TGF	Transforming growth factor
TGN	Trans-Golgi network
tICM	Temporal image correlation microscopy
TIRF	Total internal reflectance fluorescence
UBA	Ubiquitin-associated
VEGFR3	Vascular endothelial growth factor receptor 3
VSVG	Vesicular stomatitis virus G
YAP	Yes-associated protein
ZO	Zonula occludens

Chapter 1: Introduction

Epithelial cells are major constituents of many tissues and can organize into complex structures such as stratified sheets, alveoli, and tubes. A major function of epithelial cells is to act as permeability barriers to separate internal from external environments and between tissue compartments. Epithelial cells require exquisite control over cell-cell adhesions and cell-matrix adhesions to ensure accurate cellular organization necessary to establish and maintain epithelial structure and form a lumen (Bernascone et al., 2017; Carthew, 2005). A fundamental property of simple epithelial cells is that they have an apical cortex facing a lumen and a basolateral cortex facing extracellular matrix (ECM). This polarized organization is critical to maintain epithelial homeostasis. Defects in epithelial tubular organization leads to developmental abnormalities including human renal and intestinal disorders, such as polycystic kidney disease, renal tubular acidosis, microvilli inclusion disease, and diabetes insipidus (Deen et al., 1995; Jarolim et al., 1998; Mulders et al., 1997; Schneeberger et al., 2018; Wilson, 2011). Moreover, more than 80% of human cancers arise from epithelial cells, and disruption of epithelial homeostasis is considered a prerequisite for tumour formation and progression (McCaffrey and Macara, 2011; Sternlicht, 2006).

1.1 Polarity and epithelial organization

Cell polarity is involved in epithelial morphogenesis and presents as planar cell polarity, apical-basal polarity, front-rear polarity, and mitotic spindle polarity (Muthuswamy and Xue, 2012). The cooperation of proteins that control polarity play fundamental roles in regulating many aspects of epithelial biology by controlling the localization of key mediators involved in regulating stem cell renewal, proliferation, apoptosis, survival, differentiation, cell motility, cell

adhesion, spindle orientation, genomic integrity, and tissue organization, processes with strong links to development and cancer progression (Aranda et al., 2006; Bilder, 2004; Desai et al., 2009; Dias Gomes et al., 2019; Durgan et al., 2011; Etienne-Manneville, 2008; Lee et al., 2006; Lin et al., 2000; Rodriguez-Boulan and Macara, 2014; Saadaoui et al., 2014; Yamashita et al., 2010). The homeostasis of cell polarity occurs through a network of polarity complexes consisting of proteins and phospholipids that integrate and interpret cues from extracellular environment to regulate intracellular signalling programs. Many studies have shown that disrupting polarity can alter cell and tissue homeostasis, which contributes to carcinoma development (Halaoui et al., 2017; Huang and Muthuswamy, 2010; Huebner et al., 2014). Therefore, polarity is a central process relevant to normal development and disease progression.

1.1.1 Polarity complexes

Three major complexes regulate apical-basal polarization within epithelial cells: the PAR, SCRIB, and CRB complexes, which localize at apical-lateral border (tight junction), basolateral domain, and apical domain, respectively (Rodriguez-Boulan and Macara, 2014).

1.1.1.1 PAR complex

The Par proteins (for Partitioning defective, Par1-6) were first identified in *Caenorhabditis elegans* embryos in which Par mutants disrupted an asymmetric first cell division. Par1 and Par4 are serine/threonine kinases, Par2 is a zinc-finger protein, Par3 is the scaffold core for the complex, Par5 is a 14-3-3 protein and Par6 is an adaptor that regulates another polarity kinase, aPKC. All of these except Par2 are conserved in other species (Kemphues et al., 1988; Tabuse et al., 1998; Watts et al., 1996). The Par complex consists of aPKC, Par3, Par6, and the small GTPase Cdc42 (cell division control protein 42) and localizes to tight junctions. (Assemat et al., 2008;

Joberty et al., 2000; Lin et al., 2000) (Figure 1.1). Par1 and Par4 are localized to the basolateral membrane whereas Par5/14-3-3 proteins are not polarized but control the localization of other Par proteins through phosphorylation-dependent binding. The Par complex interacts with diverse effector proteins that establish and maintain their asymmetric distribution within cells to regulate lumen formation, cell division orientation, cell migration, and plays a crucial role in oncogenic signalling (Aranda et al., 2008; Archibald et al., 2015a; Archibald et al., 2015b; McCaffrey et al., 2012).

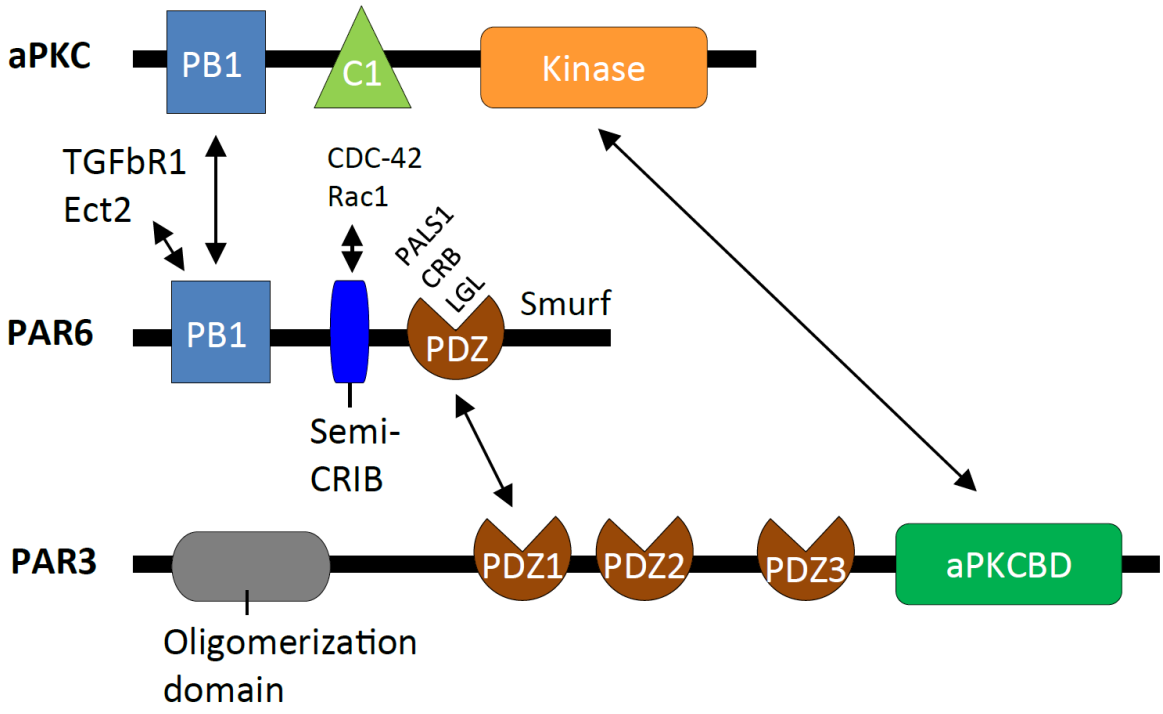

Figure 1.1 A schematic diagram showing the interaction domains of PAR complex proteins

Atypical PKC isoforms (PKCι/PRKCI and PKCζ/PRKCZ) are 75 kDa serine/threonine protein kinases that belong to the PKC family (Steinberg, 2008). All PKCs have a conserved catalytic domain at the C-terminus, and the difference between atypical and other PKC isoforms is that aPKCs have a regulatory PB1 (Phox Bem1) domain at N-terminal which directly interacts with Par6 and is regulated by Cdc42, whereas conventional and novel PKC isoforms depend on Ca^{2+} or diacyl glycerol for their activation (Moscat et al., 2006; Noda et al., 2001; Rosse et al., 2010).

aPKCs are constitutively bound to Par6 and in addition to associating with Par3 in the Par complex (Gunaratne et al., 2013) and can also associate with the Crumbs complex in mature epithelial cells. Moreover, aPKC protects Par6 from proteasomal degradation in kinase-independent manner, conversely, Par6 regulates the localization of aPKC and its kinase activity (Durgan et al., 2011). A primary polarity role for apical aPKCs is to phosphorylate lethal giant larvae (LGL; including LLGL1 and LLGL2), PAR1 and other basal lateral proteins to exclude them from apical cortex (Rodriguez-Boulan and Macara, 2014; Smith et al., 2007; Suzuki et al., 2004). aPKC-Par6 bind to Par3 through the catalytic domain of aPKC and the PDZ (post-synaptic density protein 95 (PSD-95), discs large, Zonula occludens (ZO-1)) domain of Par6 (Bilder et al., 2003; Hirose et al., 2002). Moreover, aPKCs have been implicated in the regulation of cell signaling that contributes to signaling that promotes cancer (Fields and Regala, 2007; Rosse et al., 2010).

Par3 is a multidomain scaffolding protein that exist from two genes in humans and other mammals, *PARD3* and *PARD3B*. *PARD3* encodes three splice forms with molecular weights of 180 kDa, 150 kDa, 100 kDa, which all contain three PDZ domains. Par3 resides at tight junctions in epithelial cells (Izumi et al., 1998), and knockdown of Par3 in MDCK (Madin-Darby canine kidney) cells delayed tight junciton assembly (Chen and Macara, 2005). Par3 (PARD3) also has a

conserved N-terminal region that can form self-associations (Liu et al., 2020) and binds to the junctional adhesion molecule-A (JAM-A) and phosphoinositide lipids (Krahn et al., 2010; Mizuno et al., 2003). Since JAM-A forms cell-cell contacts prior to Par3 localization to the plasma membrane, it is considered that JAM-A recruits Par3 (PARD3) to tight junctional complexes (Ebnet et al., 2001; Itoh et al., 2001). Once Par3 is anchored to nascent tight junctions, it can recruit Par6 and aPKC (Joberty et al., 2000) (Chen and Macara, 2005; Suzuki et al., 2001). Loss of Par3, or expression of a mutant that cannot bind to aPKC, results in the mislocalization of aPKC and the inappropriate activation of signalling pathways that promote tumour invasion and metastasis (McCaffrey et al., 2012).

Par3B is a 140 kDa product of *PARD3B*, and is a homologue of cell polarity protein Par3 with a similar domain structure, however, it was shown not to interact with aPKC, and little is known about the binding with Par6 (Gao et al., 2002; Kohjima et al., 2002). Par3B is highly expressed in the kidney, lung, and skeletal muscle and has been shown that Par3B is localized at tight junction with tight junction protein ZO-1 (Kohjima et al., 2002). Ectopically expressed the N-terminal region of Par3B can disrupt the formation of tight junctions in MDCK cells (Gao et al., 2002). A recent study indicated that Par3B binds to tumour suppressor protein LKB1 and suppresses its kinase activity, and that ablation of Par3B causes rapid and profound stem cell loss, indicating that it is vital for mammary gland stem cell maintenance (Huo and Macara, 2014).

Par6 is a 37 kDa adaptor protein that is expressed as multiple isoforms from different genes (*PARD6A*, *PARD6B*, and *PARD6G*). It contains conserved PB1, Cdc42/Rac interaction binding (CRIB), and PDZ domain that mediates binding to aPKC, Cdc42 or Rac GTPase in the GTP-bound state (Johansson et al., 2000; Noda et al., 2001), and Par3, respectively. The PDZ domain

also mediates the association between Par6 and other proteins, including Llgl, Pals1, and Crb3 (Assemat et al., 2008; Gao and Macara, 2004; Lemmers et al., 2004; Lin et al., 2000). Llgl is thought to regulate aPKC/Par6 trafficking to the plasma membrane, where it becomes activated by Cdc42, leading to phosphorylation of Llgl and association with Par3. Phosphorylation of Par3 by aPKC subsequently releases the complex and enables Par6/aPKC to associate with the Crumbs complex at the apical membrane (Hayase et al., 2013; Hurd et al., 2003).

The different isoforms of Par6 localize in cells differently, which indicates that they may have distinct functions. For example, Pals1 binds strongly to Par6B but weakly to Par6A (Assemat et al., 2008; Gao and Macara, 2004). Par6 proteins have many functions including cell migration, organization of tight junctions, and cell growth (Suzuki and Ohno, 2006). For example, previous studies demonstrated that overexpressed Par6B and Crb3 can disrupt tight junctions (Hurd et al., 2003; Joberty et al., 2000; Lemmers et al., 2004). In addition, Par6B plays a major role with aPKC, in regulating mitotic spindle orientation during epithelial morphogenesis (Durgan et al., 2011).

1.1.1.2 Scrib complex

The Scribble (Scrib) complex includes a group of proteins (Scrib, Lgl and Dlg) that localize to the basolateral membrane, first discovered and characterized in *Drosophila,* and are highly conserved in mammals (Bilder and Perrimon, 2000; Mechler et al., 1985; Stephens et al., 2018). Proteins from the Scrib complex are crucial regulators of tissue development and homeostasis, such as establishing basolateral identity in polarity, directing cell migration, maintaining cell-cell contacts through adherens junctions integrity, responses to growth factors during morphogenesis, vesicle trafficking, tissue growth, differentiation, and regulating mitotic spindle asymmetry in epithelial cells (Albertson and Doe, 2003; Humbert et al., 2006; Khursheed and

Bashyam, 2014; Qin et al., 2005; Rodriguez-Boulan and Macara, 2014; Stephens et al., 2018; Yamanaka et al., 2003). Unlike the Par complex, the Scrib complex has a minor effect on tight junctions, indicating that different polarity complexes influence apical and lateral junctions (Rodriguez-Boulan and Macara, 2014).

Scrib is a 175 kDa cytoplasmic multidomain scaffold protein that has many functions in diverse organisms. Scrib belongs to the LAP (LRR and PDZ) protein family and has 16 leucine-rich repeats (LRRs) at its N-terminal, two LAP-specific domains (LAPSADa and LAPSADb), a linker region, and four PDZ domains (Assemat et al., 2008). These domains are essential for protein-protein interaction to allow proper localization of Scrib to the basolateral membrane of epithelial cells and maintains the integrity of basolateral domain (Bilder and Perrimon, 2000; Kallay et al., 2006; Legouis et al., 2003; Mathew et al., 2002; Metais et al., 2005; Navarro et al., 2005; Qin et al., 2005; Sun et al., 2009; Zeitler et al., 2004). Scrib has multiple phosphorylation sites that are involved in regulating signaling pathways including mitogen-activated protein kinase (MAPK), Phospho-Inositol-3-Kinase (PI3K), Hippo, Wnt, and protein tyrosine phosphatase and tensin homologue (PTEN) to mediate their localization and organize signaling modules (Adey et al., 2000; Stephens et al., 2018).

DLG has five isoforms from separate genes in humans and the protein contains three PDZ domains, a Src homology 3 (SH3) domain, a hook domain (also known as 4.1 binding domain) and a guanylate kinase-like (GUK) domain at C-terminal, which are conserved in other membrane-associated guanylate kinase (MAGUK) scaffold protein family, and a L27 domain. These diverse protein-protein interaction domains allow Dlg to regulate apical-basal polarity, adherens junction integrity, cell division orientation, apoptosis, and multiple signaling pathways including MAPK,

PI3K and PTEN, Hippo, and Wnt to mediate localization of various proteins (Adey et al., 2000; Etienne-Manneville et al., 2005; Gaudet et al., 2011; Iizuka-Kogo et al., 2007; Laprise et al., 2004; Lee et al., 2002; Porter et al., 2019; Stephens et al., 2018; Ventura et al., 2020).

Llgl has two isoforms in humans and other mammals, *LLGL1* (115 kDa) and *LLGL2* (113 kDa) and regulates cell polarity establishment, basolateral exocytotic machinery, actin-myosin contractility, cell migration, cell-cell adhesion, mitotic spindle orientation and multiple signaling pathways including MAPK, PI3K, Hippo, and Wnt to mediate cell localization (Bell et al., 2015; Dahan et al., 2014; Dahan et al., 2012; Jossin et al., 2017; Musch et al., 2002; Stephens et al., 2018; Zhang et al., 2005). Both isoforms contain N-terminal WD40 repeats (six in LLGL1 and five in LLGL2), and a C-terminal region containing a polybasic region containing aPKC and Aurora kinase phosphorylation sites (Cao et al., 2015; Kallay et al., 2006; Stephens et al., 2018). Phosphorylation of LLGL by aPKC is required for excluding LLGL from the apical membrane and facilitating its recruitment to the basolateral membrane during epithelial polarity establishment (Kallay et al., 2006; Linch et al., 2013; Musch et al., 2002; Yamanaka et al., 2003). On the other hand, LLGL also inhibits aPKC activity by binding to Par6 in the aPKC/Par6 complex and competing with the binding of Par3 (Stephens et al., 2018).

1.1.1.3 CRB complex

The Crumbs complex (Crumbs/Crb, Pals1 and Patj) localizes to the apical membrane (Rodriguez-Boulan and Macara, 2014) and recruits aPKC and PAR6 to the apical cortex during polarization (Margolis, 2018). There are three Crb isoforms, Crb1, Crb2, and Crb3. Crb1 (154 kDa) and Crb2 (134 kDa) are type I transmembrane proteins with large extracellular domains that contain a N-terminal signal peptide, EGF motifs (19 and 14 in Crb1 and Crb2, respectively), three

Laminin A/G motifs (Assemat et al., 2008). In contrast, Crb3 (13 kDa) has a short extracellular domain with O- and N-glycosylation sites (Medina et al., 2002).

CRB3 is the major CRB isoform in mammalian epithelia (Fogg et al., 2005; Lemmers et al., 2004; Makarova et al., 2003) and exists as two alternate splicing forms: Crb3a and Crb3b (Lemmers et al., 2004). The cytoplasmic domain of Crb3a contains a FERM (four-point-one, ezrin, radixin, moesin) protein-binding domain and a C-terminal PDZ-binding domain consisting of glutamic acid-arginine-leucine-isoleucine (ERLI) residues. Crb3b is similar but has C-terminal sequence CLPI (cysteine-leucine-proline-isoleucine) that does not bind to PDZ domains (Margolis, 2018). Crb3b associates with the PDZ-domains of Par6 and Pals1, which is essential for regulating apical polarity. Moreover, Crb3 links to the actin cytoskeleton through its FERM domain and is required for tight junction development, apical membrane expansion, cilia biogenesis, and lumen formation in cultured epithelial cells (Bryant et al., 2010; Meder et al., 2005; Schluter et al., 2009b). However, studies were not able to show obvious defects of polarity and cell-cell junctions in CRB3 knockout mice, suggesting that there may be redundancy in CRB3-mediated polarity mechanisms (Charrier et al., 2015; Margolis, 2018; Whiteman et al., 2014). Additionally, Crb3 links cell polarity with tissue mechanics and proliferation through regulation of the Hippo/Yes-associated protein (Yap) pathway (Ling et al., 2010; Szymaniak et al., 2015). The Crb complex is negatively regulated by the Coracle group, which consists of Moesin, Yurt, Coracle, Neurexin IV (Nrx-IV) and Na^+, K^+-ATPase, and is required for establishing basolateral membrane identity (Laprise et al., 2009).

Pals1, also known as membrane-associated palmitoylated protein 5 (MPP5), is a 77 kDa scaffold protein and associated with tight junction formation and cell polarity by linking Crb3 and

Patj (Fogg et al., 2005; Roh et al., 2002b). Pals1 belongs to the MAGUK family (Kamberov et al., 2000), it has multiple protein-protein interaction domains including two L27 domains, a PDZ domain, an SH3 domain, a hook domain and a GUK domain (Rodriguez-Boulan and Macara, 2014). The first L27 domain interacts with Patj and the second associates with Lin7 which functions in tight junction formation (Straight et al., 2006). A previous study indicated that loss of Pals1 resulted in loss of expression of Patj, a delay in the polarization of MDCK monolayers, and failure to form luminal cyst in MDCK 3D organoids (Straight et al., 2004). Moreover, loss of Pals1 leads to the accumulation of E-cadherin puncta in the cell periphery, and disruption of E-cadherin trafficking, suggesting that Pals1 is also required for adherens junctional functions (Wang et al., 2007).

Patj is a 196 kDa scaffold protein that is expressed mainly in epithelial tissues and localizes to tight junctions. Patj contains an N-terminal L27 domain binds to Pals1, and multiple PDZ domains that mediate diverse interactions with tight junction proteins, including ZO-3 and Claudin1 (Lemmers et al., 2002; Roh et al., 2002a; Roh et al., 2002b). Similar to other members of the Crb copmplex, Patj is also involved in tight junctions assembly (Lemmers et al., 2002; Michel et al., 2005; Shin et al., 2005) and the depletion of Patj leads to the mislocalization of Crb3 and Pals1, as well as tight junction markers (occludin and ZO-3), suggesting that Patj stabilizes the Crb complex between the apical domain and tight junctions (Michel et al., 2005). Moreover, Patj also plays a crucial role in directional migration of MDCK cell by regulating the localization of aPKC and Par3 to the leading edge (Shin et al., 2007).

1.1.1.4 Other polarity regulators

Apical-basal polarity is also regulated by additional proteins not part of the three canonical polarity complexes, including the protein serine/threonine kinases Par1, Par4/Lkb1, and phospho-protein interactor Par5/14-3-3ζ. These proteins play an important role in epithelial polarity organization. Par1 has a kinase and an ubiquitin-associated (UBA) domains, which is phosphorated and regulated by aPKC and LKB1. Par1 is recruited to the basolateral cortex and phsophorylates Par3 to disrupt the Par complex and therefore exclude it from basolateral cortex (Lizcano et al., 2004; Suzuki et al., 2004). Par1 also regulates cell division orientation through regulating RhoA activity, which affects recruitment of the core spindle orientation machinery (G α i, LGN, and NuMA) (Lazaro-Dieguez et al., 2013). Par5 is distributed in cytoplasm and it can bind to phosphorylated Par3, Par1, or Llgl to relocate these proteins to the cytoplasm, thereby ensuring the fidelity of apical and basolateral segregation (Benton and St Johnston, 2003).

Cdc42, Rac1, and RhoA belong to RHO GTPase family and crosstalk with each other to regulate multiple cellular processes, including polarization (Iden and Collard, 2008). For example, Cdc42 is a master regulator of cell polarity that interacts with Par6 and changes its conformation, which in turn activates aPKC kinase activity to phosphorylate substrates in the apical domain (Yamanaka et al., 2001). Cdc42 can also influence the spatio-temporal activation of Rac1, which suppresses RhoA activity at adherens juctions (ten Klooster et al., 2006; Wildenberg et al., 2006). In turn, RhoA inhibits Rac1 activity by disrupting the Par complex, which is a scaffold for GTPase regulators (Nakayama et al., 2008).

Phosphoinositides are required for many biological functions, including regulation of membrane traffic, the cytoskeleton, nuclear events and the permeability and transport functions

of membrane (Di Paolo and De Camilli, 2006). There are seven phosphoinositide isoforms and are regulated by phosphoinositide kinases and phosphatases in different organelles such as plasma membrane, endoplasmic reticulum, Golgi complex, early endosome, and late endosome (Di Paolo and De Camilli, 2006). Phosphoinositides are implicated in defining cell polarity identity though crosstalk with small GTPases (Krahn and Wodarz, 2012). In yeast, phosphatidylserine regulates Cdc42 targeting and activation during cell division (Fairn et al., 2011). Phosphatidylinositol-3,4,5-trisphosphate (PtdIns(3,4,5)P_3) is stably localized at the basolateral plasma membrane (Gassama-Diagne et al., 2006) and PtdIns-4,5-bisphosphate (PtdIns(4,5)P_2) is localized at apical plasma membrane (Martin-Belmonte et al., 2007). This balance is regulated by the phosphatase PTEN, which is localized at the apical domain through an interacting with Par3 and is antagonized by PI3K (Maehama and Dixon, 1998; von Stein et al., 2005).

1.1.2 The regulation of protein-protein interactions in polarity

The spatiotemporal coordination of polarity protein interactions is crucial to establish and maintain epithelial organization. The asymmetric segregation of the plasma membrane into unique domains is positively or negatively regulated through a network of protein-protein interactions, controlled largely by phosphorylation (Rodriguez-Boulan and Macara, 2014). Par3 associates with nascent tight junctions through JAM-A which then recruits aPKC through either a direct interaction or through an indirect association with Par6 to form interdependent Par complex at the apical-lateral membrane. After being recruited to the apical Par complex, aPKC kinase activity is positively regulated by Cdc42, which is localized to the apical membrane by PTEN through annexin 2 (Joberty et al., 2000; Martin-Belmonte et al., 2007). Activated aPKC then phosphorylates and dissociates from Par3, and then binds to the Crb complex via PAR6 (Morais-

de-Sa et al., 2010). Apical aPKC/Par6 is necessary to stabilize the Crb complex and promote the formation of mature epithelial structures from the premature junctional structures (Morais-de-Sa et al., 2010).

Not only does aPKC kinase activity act as a determinant for apical complexes, but it is also crucial for restricting the localization of basolateral proteins. For example, aPKC phosphorylates Llgl, Par1, and Yurt, causing them to dissociate from the apical plasma membrane (Suzuki et al., 2004). Conversely, Par1 phosphorylates Par3 to exclude it from the basolateral membrane, which consequently precludes aPKC/Par6 from the basolateral membrane. Yurt also negatively regulates Crb to promote basolateral membrane stability (Laprise et al., 2009).

1.1.3 Polarity and cancer

Over 80% of cancers arise from epithelial cells, which are called carcinoma. Polarity plays a significant role in regulating multiple aspects of epithelial growth control and tissue morphogenesis and disruption of epithelial homeostasis is considered a prerequisite for tumour formation (Aranda et al., 2006; McCaffrey and Macara, 2011; Rodriguez-Boulan and Macara, 2014). A polarized epithelial architecture organizes cells so that they can interpret both intrinsic and extrinsic signals from the microenvironment to regulate cell behaviors such as proliferation, apoptosis, and migration, which when they become dysregulated promote cancer initiation, growth, and metastasis (Bergstralh and St Johnston, 2012; Ellenbroek et al., 2012; Halaoui and McCaffrey, 2015b; Huang and Muthuswamy, 2010; Huebner et al., 2014). Previous studies from our lab demonstrated that apical-basal polarity is progressively lost during breast carcinoma development, but surprisingly, polarity genes are not necessarily down-regulated at the mRNA level (Catterall et al., 2020; Halaoui et al., 2017). Instead, loss of polarity occurs through

asymmetric cell divisions that produce a polarized and non-polarized cell, the latter which proliferate faster and likely outcompete the polarized population (Halaoui et al., 2017). Remarkably, the process is reversible, and inactivation of the driver oncogene results in re-acquisition of the polarity program and lumen formation through apoptosis-mediated cavitation (Halaoui et al., 2017).

aPKC isoforms (iota and zeta) are reported to have oncogenic or tumour-suppressive functions depending on the isoform and cancer type. aPKCι (PRKCI) is amplified and overexpressed in multiple cancers, including hepatocellular carcinoma, pancreatic adenocarcinoma, and breast cancer (Halaoui and McCaffrey, 2015b). In lung cancer, PKCι associates with a guanine nucleotide exchange factor Ect2 that activates a pathway involving RAC1/Mek1/2-Erk1/2 to promote malignant transformation and proliferation (Murray et al., 2011; Regala et al., 2005). PKCι cooperates with other oncogenes and was shown to be required for oncogenic RAS transformation of the colon epithelium *in vivo* (Murray et al., 2004). On the other hand, PKCζ was shown to act as a tumor suppressor in invasive prostate carcinoma *in vivo*, by regulating c-myc function (Kim et al., 2013).

Par6 is overexpressed and amplified in breast cancer (Nolan et al., 2008), and displays diverse localization patterns (polarized/apical, uniform membrane, cytoplasmic, and nuclear) in preinvasive and advanced breast cancers (Catterall et al., 2020; Halaoui et al., 2017). Mislocalized Par6 results in loss of tissue organization downstream of oncogenic signalling (Aranda et al., 2008) and correlates with increasing grade and the presence of nodal metastasis (Catterall et al., 2020). Par6 contributes to cancer progression in part by associating with the transforming growth factor (TGF)β receptor type-1 to promote EMT (Ozdamar et al., 2005). Moreover, human epidermal

growth factor receptor 2 (HER2/ErbB2) is amplified or overexpressed in about 25% of breast cancers and uncouples Par6/aPKC from Par3 to disrupt apical-basal polarity in human mammary epithelial cells to promote malignant transformation (Aranda et al., 2006). Furthermore, Par6 has also been shown to cooperate with Par3 to regulate actomyosin contractility and collective cell migration by interacting with discoidin domain receptor 1 (DDR1) (Hidalgo-Carcedo et al., 2011).

Par3 functions as a tumor promoter or a suppressor, depending on context. For example, our lab demonstrated that loss of Par3 promotes breast tumorigenesis and metastasis through active aPKC-dependant regulation of matrix remodelling (McCaffrey et al., 2012). Moreover, in ErbB2-induced tumour epithelial cells, loss of Par3 also contributes to metastasis through decreasing cell-cell cohesion (Murray et al., 2004). However, in keratinocytes, knockout Par3 impairs Ras-activated Erk1/2 and Akt signaling, which leads to reduce proliferation and increase apoptosis, which protects cells from cancer development (Iden et al., 2012).

A common theme is that polarity proteins have diverse roles in cancer to support or suppress cancer development and progression. For example, the role of Crb3 as a tumor suppressor is supported by a study reporting that repression of Crb3 was associated with tumor migration and metastasis in immortal baby mouse kidney epithelial cells (Karp et al., 2008). The Scrib complex also exerts a tumor suppressive role in mammalian epithelial cancers including lung, prostate, breast, and colon, and regulates various signaling pathways which are related to cell proliferation, survival and migration (Stephens et al., 2018). For example, deregulation of Scrib results in mammary tumorigenesis (Zhan et al., 2008) and premalignancy and tumour progression in the mammary gland by modulating the MAPK/Fra1 pathway (Godde et al., 2014). However, Scrib also has protumorigenic activity since reduction of Scrib slows breast cancer cell

MDA-MB-231 migration and prevents mammary tumorigenesis *in vivo* (Anastas et al., 2012). Loss of Llgl1/2 induces a mesenchymal phenotype, tissue overgrowth, and loss apical-basal polarity in mammary epithelial cells (Russ et al., 2012). A study has shown that Dlg is targeted by high risk oncogenic human papillomavirus E6 proteins for proteasome mediated degradation (Gardiol et al., 1999). Lkb1 has been widely investigated for its tumor suppressor function, which contributes to deregulate cell polarity, metabolism, extracellular matrix deposition, and signaling (Halaoui and McCaffrey, 2015b). Moreover, germline mutations in Lkb1 are linked with Peutz-Jeghers syndrome (PJS), which is a disorder that predisposes to gastrointestinal polyposis and cancer. Additionally, loss of Lkb1 in mice induces intestinal polyposis, however, this does not cause transformation, suggesting that Lkb1 is involved in establishing a pre-cancerous niche (Bardeesy et al., 2002). Furthermore, loss of Lkb1 reduces the latency of ErbB2-mediated mammary gland tumorigenesis compared with ErbB2 expression alone, indicating the suppressive role of Lkb1 in cancer (Andrade-Vieira et al., 2013).

Epithelial-mesenchymal transition (EMT) plays an important role in epithelial-derived cancers, it is characterized by loss of polarity and junctions. EMT can be induced by TGFβ signaling and transcription factors including Zeb1, Twist and Snail (Thiery et al., 2009). Zeb1 and Snail have been shown to directly repress Crb3, Llgl2, and E-cad mRNA expression (Davalos et al., 2012). In turn, polarity proteins also can regulate EMT. For example, Llgl has been demonstrated to suppress Snail carcinogenesis and induce epithelial markers (Kashyap et al., 2013). On the other hand, a tyrosine phosphatase, Shp2, interacts with Par3 through its SH2 domain and ectopic expression of Shp2 has been shown to diminish the phosphorylation of Par3 which prevents formation of the Par complex and enhances EMT (Zhang et al., 2016). In summary, most, if not

all, core polarity regulators have important roles in diverse cancer types. However, there remain significant gaps in knowledge regarding how polarity proteins integrate diverse pathways in normal and disease states. Furthermore, it is not yet fully clear how loss of polarity and organization at the cell and tissue level enable cancer progression.

1.1.4 Cell polarization/lumen morphogenesis

1.1.4.1 Morphological steps of lumenogenesis

The formation of a lumen is essential to create epithelial tubes and acini during tissue morphogenesis. Moreover, the lumen is often filled or disrupted during cancer progression. Lumenogenesis can occur by three major mechanisms: 1) budding - polarized epithelial sheets bud or fold to entrap a central lumen from the apical space (Jewett and Prekeris, 2018); 2) cavitation - solid epithelial structures create a hollow space by eliminating cells at the core through apoptosis; 3) apicalization - de novo lumen formation in which a cell-cell contact is converted to a free membrane surface that expands to form a lumen. There are many different cell and animal models for which *de novo* lumen formation occurs via apicalization, including the vertebrate vasculature, zebrafish notochord, and MDCK tubules grown in 3D cultures (Iruela-Arispe and Beitel, 2013; Jewett and Prekeris, 2018; Lubarsky and Krasnow, 2003). During *de novo* lumen formation by apicalization, the midbody, which is a microtubule-rich structure that forms during cell division, is considered the first symmetry-breaking cue that determines the time and site of the prospective lumen. Recruitment of apical proteins and formation of a lumen progresses through a well-defined set of steps, for which the molecular mechanisms are incompletely understood. Apical proteins are initially recruited to the cell-cell junction by trafficking along midbody microtubules to establish an apical membrane initiation site (AMIS)

(Blasky et al., 2015; Li et al., 2014; Peterman and Prekeris, 2019; Schluter et al., 2009b; Wang et al., 2014). Further recruitment of apical proteins excludes basolateral determinants which allows the AMIS to mature into a pre-apical patch (PAP) which is bordered by tight junctions and requires recruitment of Cingulin (CGN) and ZO1 through trafficking and membrane rearrangements (Bryant et al., 2010; Ferrari et al., 2008). It is hypothesized that apical glycoproteins such as podocalyxin (gp135) push opposing apical membranes apart to initiate lumen formation, which proceeds via rho-associated protein kinase (ROCK)-mediated contractility of cells at the apical cortex assists lumen formation (Ferrari et al., 2008; Meder et al., 2005). With tight junctions in place to create a permeability barrier, aquaporins (water channels) generate hydrostatic pressure to further drive lumen opening (Ferrari et al., 2008). Therefore, a combination of polarized vesicle exocytosis, hydrostatic pressure, electrostatic repulsion, and cytoskeletal mechanics establish a nascent lumen. This complex series of events requires the precise coordination through multiple protein networks including Rho GTPases (Cdc42, Rac1, RhoA) and their regulators, polarity complexes (Par, Crb), phosphatidylinositol phosphatases, microtubule binding proteins, and Rab-GTPases. How trafficking of apical proteins is regulated during this process remains incompletely understood (Jewett and Prekeris, 2018).

The extracellular matrix (e.g. collagens and laminins) acting through integrin receptors and the cytoskeleton can control the orientation of apical-basal polarity, and therefore also contributes to lumen formation (Bedzhov and Zernicka-Goetz, 2014; Lee and Streuli, 2014; Monteleon et al., 2012; O'Brien et al., 2001; Taniguchi et al., 2015; Vogel et al., 2015).

1.1.4.2 Rab GTPases

Rab proteins are a family of small Ras-like GTPases that act as master regulators to establish the secretory and endocytic pathways. They cycle between active (GTP-bound) and inactive (GDP-bound) states that are established by GEFs and GAPs, respectively. In the active GTP-bound configuration, Rabs recruit a variety of effector proteins, including cytoskeletal motors, vesicle tethering proteins, and the SNARE (soluble N-ethyl-maleimide-sensitive factor protein attachment protein receptor) complex, which together target vesicles to mediate diverse functions at multiple trafficking steps, including vesicle budding, uncoating, motility, tethering, and fusion (Hutagalung and Novick, 2011). Approximately 1/4 of the 70 different Rab proteins have been implicated in regulating polarity trafficking machinery (Rab4, Rab5, Rab6, Rab7, Rab8, Rab10, Rab11, Rab13, Rab14, Rab17, Rab22, Rab25, Rab27, and Rab35) (Blum et al., 2020; Hutagalung and Novick, 2011; Klinkert and Echard, 2016; Klinkert et al., 2016; Lu and Wilson, 2016; Rodriguez-Boulan and Macara, 2014; Zerial and McBride, 2001). Rab GTPase-driven membrane trafficking is a highly coordinated event through the spatiotemporal regulation of various proteins that are context specific (Novick, 2016; Rink et al., 2005). For example, Rab GTPases mediate apical trafficking of Podocalyxin, however, different sets of Rab GTPases coordinate its delivery during cell polarization in 2D and 3D epithelial cultures (Mrozowska and Fukuda, 2016).

Among Rab proteins, the functional role of the Rab11 subfamily and their effector proteins have been widely investigated in epithelial trafficking (Casanova et al., 1999). The Rab11 family consists of Rab11a, Rab11b, and Rab25, which play a crucial role in transcytosis and lumenogenesis in diverse systems (Bhartur et al., 2000; Bryant et al., 2010; Casanova et al., 1999;

Desclozeaux et al., 2008; Li et al., 2007; Rathbun et al., 2020; Roman-Fernandez and Bryant, 2016; Shaye et al., 2008). More specifically, the Rab11 subfamily is apically localized and are known to mediate recycling and transport of apical polarity proteins during lumen establishment (Elias et al., 2015; Fremont and Echard, 2018; Golachowska et al., 2010; Goldenring et al., 1996; Prekeris et al., 2000; Shivas et al., 2010; Winter et al., 2012).

During lumen formation, Rab11 recruits its effector Rabin8 (a Rab8 GEF), which activates Rab8A on recycling endosome (RE) and thereby the vesicles tether and fuse at the nascent apical membrane through recruiting the exocyst component Sec15. This process is important for recruiting Myosin-5b to recycling endosomes, and subsequently with STX-3 and Munc18-2 to regulate Rab11-Rab8 cascade during polarity establishment (Li et al., 2007; Roland et al., 2011; Vogel et al., 2015). Furthermore, phosphatidylinositol (*4*,*5*)-bisphosphate-binding protein, Annexin2 (Anx2) and Cdc42 mediate the interaction with aPKC through associating with Rab8a/Rab11a vesicles, suggesting that the membrane traffic and polarity machineries cooperate to generate the apical identity during lumenogenesis (Bryant et al., 2010). Another Rab11 effector is FIP5, which sequentially interacts with SNX18, KIF3A, and CGN to mediate apical vesicle delivery (Roland et al., 2011) and targets to the AMIS during initial steps of lumen formation (Li et al., 2014; Mangan et al., 2016; Willenborg et al., 2011). FIP5-SNX18 interaction can only occur during telophase and cytokinesis and is inhibited by GSK3-dependent phosphorylation of FIP5 during metaphase and anaphase, showing FIP5 is a key temporal regulator during lumen formation (Li et al., 2014). CGN is recruited to the AMIS through interaction with ZO-1 and interacts and regulates Rab11FIP5 vesicle (Mangan et al., 2016). Another FIP family member, FIP2, is also required for lumen formation via interacting with the

clathrin-adaptor protein Eps15 which are necessary in establishing junctions (Lapierre et al., 2012; Lapierre et al., 2017). Gp135 is part of the CD34 family of transmembrane sialomucin proteins and is an apical membrane marker in lumenogenesis (Meder et al., 2005). A previous study indicated that Rab11a-containing endosomes assists apical glycoprotein Gp135 recycling and delivery to the apical surface (Bryant et al., 2010). Furthermore, synaptotagmin-like protein Slp2-a targets Rab27-containing vesicles for apical delivery to the AMIS and initiates single lumen formation through binding membrane enriched PtdIns(4,5)P_2. Moreover, Slp4-a as an effector of Rab27, Rab8, and Rab3 and together with STX3 to regulate vesicle tethering and fusion in epithelial cells (Galvez-Santisteban et al., 2012).

In parallel to the Rab11-regulated trafficking pathway, Rab35 is another regulator for docking apical vesicles by interacting with cytoplasmic domain of gp135 directly and tethering apical vesicles contain aPKC, Cdc42, and Crumbs3 to the AMIS during lumenogenesis. Studies have demonstrated that Rab35 inactivation results in inverted apical-basal polarity in 3D cysts, suggesting the crucial role of Rab35 in polarity establishment (Klinkert et al., 2016; Mrozowska and Fukuda, 2016). Furthermore, a recent study has shown that IRSp53 is required for directing the trafficking of gp135 to AMIS and stabilizing the Rab35 to control lumen formation (Bisi et al., 2020).

Small GTPase ARF6 modulates apical trafficking (Altschuler et al., 1999) and tubulogenesis (Tushir et al., 2010). EFA6 regulates lumen coalescence and enlargement by interacting with α-actinin 1 and is a GEF for ARF6 (Eva et al., 2017). A recent study shows that Rab14 regulates vesicles trafficking to the apical membrane by affecting ARF6 and Cdc42 activation, and midbody positioning during cell division (Lu and Wilson, 2016). Moreover, another study demonstrated

that Rab14 colocalized with Rab22 in endosomes, and acts as upstream of Rab22 which transport EFA6 to the AMIS to modulate ARF6 in the establishment of polarity (Blum et al., 2020).

1.1.5 Polarity and trafficking

The trafficking machinery involved in polarization is composed of secretory organelles (the endoplasmic reticulum (ER) and Golgi complex) and endosomal compartments that form a dynamic network that is crucial for tissue function and organization. The secretory organelles and endosomal compartments including apical sorting endosome (ASE), apical recycling endosome (ARE), common recycling endosome (CRE), multi-vesicular body, *Trans*-Golgi network (TGN), Golgi complex, and basal sorting endosome (BSE). Various sorting events, including indirect post-endocytic recycling and transcytotic routes and direct biosynthetic trafficking routes, contribute to the asymmetric distribution of membrane-associated proteins in polarized epithelial cells (Jewett and Prekeris, 2018). Each vesicular trafficking event is mediated through distinct mechanisms. For example, dynamin-2 is involved in apical routes by mediating the fission of apical transport vesicles at the level of AREs (Thuenauer et al., 2014), however, protein kinase D (PKD) regulates vesicles trafficking from TGN in the basolateral routes (Yeaman et al., 2004).

Another essential component of the intracellular trafficking machinery are microtubule and actin motors (myosin, dynein, and kinesin), that serve as tracks for recycling and biosynthetic vesicle delivery (Aguilar-Aragon et al., 2020; Rodriguez-Boulan et al., 2005). For instance, the actin-binding motor Myosin5b (Myo5B) associates with different Rab GTPase to modulate different membrane trafficking pathways (Roland et al., 2011). The exocyst complex is another regulator for trafficking, acts as tethering complex that is required for vesicles docking and fusion to plasma membranes at junctional complexes, as well as apical and basolateral membrane

domains (Grindstaff et al., 1998; Oztan et al., 2007). Vesicle fusion with apical or basolateral membranes is mediated by vesicular SNAREs (v-SNAREs or VAMPs) and target SNAREs (t-SNAREs or syntaxins) proteins (Rodriguez-Boulan et al., 2005).

Cell polarity proteins have been shown to be involved in regulating trafficking pathways. For example, Par5/14-3-3 is required for in Rab11-positive ARE positioning and apical-basal polarity in *C. elegans* intestines (Balklava et al., 2007). In MDCK cells the Par complex modulates membrane trafficking by affecting cortical polarization and apical exocytosis during lumen formation and Llgl is involved in basolateral exocytic machinery via integrating with STX4 (Bryant et al., 2010; Musch et al., 2002).

Therefore, a complex network of trafficking proteins coordinates with polarity regulators to establish and maintain lumen in epithelial tissues. Understanding the mechanisms of lumen formation is of importance for understanding tissue development, and in cancer, in which the lumen is filled as an early event.

1.2 Model systems to study epithelial morphogenesis

Epithelial cells are an essential cell type in multicellular organisms. Many of the fundamental properties that underlie their organization and function are conserved across species, and the core set of molecular tools are also highly conserved. However, the assembly of epithelial molecular networks can be modified to achieve specific functions in different contexts. Invertebrate and mammalian models are widely used and have been instrumental in understanding cell polarity.

1.2.1 Invertebrate model organisms

Polarity has been widely studied in yeast, worms, and flies, which have been essential for identifying many major polarity proteins and fundamental concepts of cell polarity regulation, which are often evolutionarily conserved across the animal kingdom.

The yeast *Saccharomyces cerevisiae* performs a process known as budding, it is an experimental model system for understanding cell asymmetry and growth polarity. Yeast cells break symmetry and establish polarity through positively modulating the actin cytoskeleton, membrane trafficking machinery, and the small GTPase Cdc42 signaling network, and orienting the site of asymmetry amplification when there are spatial cues such as bud scars and pheromone gradients (Slaughter et al., 2009). Cdc42 was shown to localize to plasma membrane and define the site for budding when yeast cells begin to divide. Moreover, Cdc42 is able to polarize and perform budding without cues and acts upstream of cytoskeletal polarization (Irazoqui et al., 2003). These discoveries in yeast also are essential for cell polarity in other organisms.

C. elegans is another invertebrate model which has been widely studied in polarity. The *C. elegans* embryo has the anterior-posterior cortex that becomes polarized by GPR1 and GPR2 and LIN-5 after fertilization and triggers an asymmetric first cell division (St Johnston and Ahringer, 2010). Zygote (fertilized oocyte) is oriented by the position of the sperm centrosome and Par genes which were discovered and defined as crucial genes for localization in early *C. elegans* embryos (Kemphues et al., 1988). Par1 and Par3 are evolutionarily conserved and are part of Par-aPKC molecular machinery which is implicated in cell polarity in many model systems. Several studies suggest that Par complex and kinase protein Par1 or RING (really interesting new gene)-

finger protein Par2 are mutually exclusive and are localized at different domains (Suzuki and Ohno, 2006). Moreover, Par1 and Par2 are associated with Llgl and localized to the posterior of the zygote (Hoege et al., 2010), whereas Par3, Par6, aPKC and Cdc42 are localized to the anterior of the zygote (Ajduk and Zernicka-Goetz, 2016).

The fruit fly *Drosophila* was the first model investigated that establishes epithelial apical-basal polarity in the early embryo. Therefore, epithelial polarization, spindle orientation and asymmetric cell division has been extensively studied in *Drosophila* (Ajduk and Zernicka-Goetz, 2016; Franz and Riechmann, 2010). Cdc42 and Par proteins are conserved and control polarity in fly epithelia, and many apical-basal polarity regulators were also discovered in this model system (Tepass, 2012). For example, Lgl, Scrib, Dlg have been shown to regulate the belt of adherens junctions, polarity, and growth control in *Drosophila* epithelia (Bilder et al., 2000). Cdc42, aPKC and Par6 form a complex with either Bazooka (Baz)/Par3 or Crumbs and its PDZ domain-containing binding partner Stardust (Crb-Sdt complex) at apical cortex which are important for polarity establishment and maintaining epithelial polarity (Franz and Riechmann, 2010). A study demonstrated that Baz/Par3 acts as a regulator in modulating localization of adherens junctions when epithelial folding (Wang et al., 2012). Moreover, aPKC/Par-6/Baz have been shown to interact with Inscuteable (Insc) which is required for recruiting Partner of Inscuteable (Pins) to the apical cortex and orients asymmetric cell divisions (Schober et al., 1999). On the other hand, Par1 phosphorylates the CR1 and CR3 domain of Baz which contains both lipid-binding and aPKC-binding regions to prevent Baz recruiting to the plasma membrane via interacting with 14-3-3 (Benton and St Johnston, 2003). Another polarity regulator Patj was found to be in a complex with Crb-Sdt and support apical-basal polarity (Zhou and Hong, 2012). A previous study

demonstrated that apical FERM-domain proteins Expanded and Merlin bind to Crb and deliver Crb to the apical domain (Ling et al., 2010). Moreover, Expanded and Merlin are in a complex and function together with Kibra which can be phosphorylated by aPKC and are localized at the apical domain of epithelial cells (Buther et al., 2004; Yu et al., 2010). Whereas basolateral FERM-domain proteins Yurt and Coracle together with the membrane proteins Nrx-IV and Na^+, K^+-ATPase and can restrict Crb localization from the basolateral membrane (Laprise et al., 2009). Overall, invertebrate model studies provide many important conserved polarity characteristic and functions which are also found in many higher organisms.

1.2.2 Mammalian polarity models

Mammalian polarity models have been used for various research since they are most closely related to human. *In vitro* studies in human cells or *in vivo* studies in mouse have been widely applied for understanding cell biology, cell development, drug discovery, tissue morphology, mechanisms of diseases. Mammalian *in vitro* study tools include two-dimensional (2D) and three-dimensional (3D) cell cultures, which provide a platform for examining epithelial biology. 2D cultures have been used widely in cell biology since 1900s, however, traditional 2D cultures do not share many features of the *in vivo* environment. Over the past few decades, and accelerated in the past few years, studies have shifted toward 3D cultures instead of 2D cultures by optimizing and manipulating the cell environment to better mimic organ physiology.

1.2.2.1 Two-Dimensional (2D) cultures

In 2D cell cultures, cells attach and are grown on flat dishes as a monolayer. Various 2D cell culture conditions such as culture media apply on different cell types in culture, specialized cell culture media is required for specialized cell types. 2D cells receive equal amounts of growth

factors and nutrition from culture media and are susceptible to external factors such as drugs or inhibitors. Since there are no regional confinement, 2D cells typically have lower sub-culturing times than 3D cultures with an increased proliferation rate compared to 3D and *in vivo* contexts (Edmondson et al., 2014). Moreover, plastic or glass dishes are very stiff, which provide unnatural mechanical environments for cells. Since cells grow as sheets, 2D cultures are not suitable for studies of epithelial morphogenesis and lumen formation.

1.2.2.2 Three-dimensional (3D) cultures

In vitro 3D cell cultures more closely resemble the *in vivo* environment in terms of mechanical properties and epithelial organization. 3D cultures allow more complex cell-cell contact and cell-microenvironment contact with co-culture techniques and the intercellular signalling programme is similar to *in vivo* (Chaicharoenaudomrung et al., 2019; Edmondson et al., 2014; Lancaster and Knoblich, 2014; Langhans, 2018). The environment of mammalian cell cultures are ECM-like matrices containing collagen, entactin, fibronectin, laminin, and polyethylene glycol (PEG)-based hydrogels, which can help the communication between cells and microenvironment and have been considered to be crucial for determining the basal cortex and generating cell polarity in the epithelial cells (Baker and Chen, 2012; Yonemura, 2014). For example, basal membrane determinants, such as integrins, act as a receptor to the surface of the cells and tether to the ECM to integrate and interpret signals from surroundings (Lee and Streuli, 2014). Interestingly, cells show different sensitivity to ECM and present different phenotypes in polarity establishment when cells are coated with the same ECM components but using a hanging drop method, suggesting that the approach to perform 3D cultures affects the morphology or response of cells (Yonemura, 2014). Moreover, 3D culture cells can also be grown as spheroids

(Breslin and O'Driscoll, 2013) or organoids which have the ability to renew and self-organize into complex structures with some functionality of an intact organ (Lancaster and Knoblich, 2014). Studies have shown that 3D culture have multiple characteristics and processes which is different from 2D culture: 3D culture has great viability, 3D culture are more resistant to drugs treatment, 3D culture has low stiffness, the gene or protein expression are more similar to *in vivo*, and 3D culture exhibit different stages of cell cycle (Edmondson et al., 2014; Kapalczynska et al., 2018). Currently, there are many options to implement 3D culture, including scaffolds, scaffold-free platforms for spheroid growth, gels, bioreactors, and microchips. There are two major types of 3D culture for studing polarity: cells grown on matrix or cells embedded within matrix.

3D MDCK and Caco-2 have been used for studying cell polarity since they can establish apical-basal polarity and form prominent hollow lumen in 3D spheroids with high efficiency. Moreover, a previous study has shown that the environment of 3D culture facilitates cell differentiation and cells are able to form the complex structures via developmental processes (Cukierman et al., 2002). 3D cultures recapitulate several molecular mechanisms, which are conserved in vivo (Beauchamp et al., 2015; Kadoshima et al., 2013; Nam et al., 2010; Park et al., 2006). Therefore, 3D culture is a practical and applicable tool for filling the gap between *in vitro* and *in vivo* research, which might decrease the use of animal models.

However, different 3D culture experiments are designed by considering factors such as cell types, research needs, application, and the budgets. There are limitations for 3D culture system: it cannot yet fully recapitulate the full complexity of in vivo environments; the capacity to scale up or down a single 3D culture format is hard to manipulate; it is hard to handle the post culturing processing; it is challenging to perform large-scale studies or high throughput screening

(Edmondson et al., 2014; Montanez-Sauri et al., 2015). To date, 3D cultures can be easily analyzed by imaging microscopy such as light fluorescence, and confocal microscopy. In summary, 3D culture systems show great potential and advantages for research compared to 2D cell culture and provide a better understanding of cell biology and diseases which will facilitate the development of novel therapies for epithelial diseases like cancer.

1.3 General hypothesis and Objectives

The organization of epithelial apical-basal polarity and lumen formation are complex processes that are essential for normal physiology in many tissues and are disrupted in cancer. However, the regulation of these events are incompletely understood. Thus, the hypothesis of this thesis is that novel effectors of the cell polarity programme direct lumen formation in epithelial cells. In Chapter 2, I present work on development of a 3D suspension culture method for efficient lumen formation that is amenable to generate sufficient quantities of cells for proteomic studies. Using this, I used BioID to identify novel proteins in proxmity to PAR6B and investigated their role in apical-basal polarity and lumen formation. In Chapter 3, I present a study on CD13 that revealed an unexpected role for this protein in the orientation of apical-basal cell polarity and establishing the prospective site for lumen formation by regulating apical-determinant trafficking. In Chapter 4, I present a study on a role for the tumour suppressor PTPN14 in regulating cell polarity in the context of KRAS cell transformation. In Chapter 5, I present a general discussion on mechanisms of cell polarity and lumen formation, and proposed future directions of the work presented in this thesis.

Chapter 2: A Proximity Proteomics Screen in Three-Dimensional Organotypic Cultures Identifies Novel Regulators of Lumen Formation

Authors: Li-Ting Wang[1,2] and Luke McCaffrey[1,2,3,4]

[1]Rosalind and Morris Goodman Cancer Research Centre, McGill University, Montreal, QC, Canada H3A 1A3
[2]Division of Experimental Medicine, McGill University, Montreal, QC, Canada H4A 3J1
[3]Gerald Bronfman Department of Oncology, McGill University, QC, Canada H4A 3T2
[4]Correspondence: luke.mccaffrey@mcgill.ca

Keywords: cell polarity, PAR6B, atypical protein kinase C, BioID, 3D, Par complex, Protein-Protein Interaction, PARD3B, RALB, HRNR, Caco-2

Abstract

Apical-basal cell polarity plays a fundamental role in regulating many aspects of epithelial cell biology including stem cell renewal, proliferation, survival, differentiation, cell motility, cell adhesion, and tissue organization, processes with strong contributions to normal development and cancer progression. Polarity proteins are known to contribute to lumen formation by coordinating apical membrane specification between cells. Here we used proximity-dependent biotin identification (BioID) to identify novel proximity proteins of the apical protein PAR6B in 2D and 3D cultures. Whereas the core Par-polarity complex was conserved in 2D and 3D culture, we identified novel PAR6B proximity proteins enriched in 2D or 3D environments, including PARD3B, HRNR, and RALB. We show that PARD3B is more highly expressed in 3D cultures and is required for lumen formation, whereas its expression is lower in 2D cultures with no apparent phenotype when depleted using shRNA. We also identified Hornerin/HRNR and RALB as PAR6B-proximity proteins that are novel regulators of epithelial organization and lumen formation. These results provide an applicable approach to explore functional protein networks linking cell polarity and lumen formation.

2.1 Introduction

Cell polarity is a fundamental property of epithelial cells that is crucial for their organization and homeostasis. The establishment of apical-basal polarity allows epithelial cells to adopt different structures in which the apical membranes are juxtaposed in neighbouring cells. For example, epithelial cells cultured on flat 2D surfaces form polarized monolayers with the apical membrane exposed to culture medium, whereas they organize into monolayer acini with a central lumen when cultured in 3D extracellular matrix (Baker and Chen, 2012). 3D cultures have multiple characteristics and processes that differ from 2D cultures including greater viability, more resistance to drug treatments, and lower stiffness in 3D environments (Baker and Chen, 2012). The differences in cell organization in 2D and 3D cultures are accompanied by changes in gene expression, with some genes involved in lumen formation upregulated in 3D environments (Edmondson et al., 2014; Kapalczynska et al., 2018; Roman-Fernandez et al., 2018). 3D culture systems therefore show many advantages and offer great potential for understanding development of tissue organization in normal and disease states.

The apically positioned Par complex consists of PARD3, PAR6B, and aPKC, which regulates many aspects of epithelial organization including apical-basal polarity, tight junction formation, cell division orientation, and cell migration (Assemat et al., 2008; Joberty et al., 2000; Lin et al., 2000; Rodriguez-Boulan and Macara, 2014) (Figure 2.3 B). PAR6B has many physiological functions and is required for efficient lumen formation in epithelial cells in 3D culture (Durgan et al., 2011). Moreover, PAR6B is overexpressed and amplified in breast cancers, and some oncogenes disrupt epithelial organization by uncoupling PAR6B from the Par complex (Aranda et al., 2006; Nolan et al., 2008; Ozdamar et al., 2005). PAR6B and aPKC also associate with a second

apical complex, the Crumbs complex, through direct interactions with PALS1 and CRB3 (Assemat et al., 2008; Gao and Macara, 2004; Lemmers et al., 2004; Lin et al., 2000). PAR6B is a multidomain adaptor that controls aPKC localization and activity, and conversely, aPKC protects PAR6B from proteasomal degradation in kinase-independent manner (Durgan et al., 2011). PAR6B also couples with the two apical complexes through protein-protein interaction domains including a PB1, Cdc42/Rac interaction binding (CRIB) and a PDZ domain. The PB1 domain of PAR6B couples with the PB1 domain of aPKC, the CRIB domain of PAR6 binds to Cdc42 or Rac GTPase (Johansson et al., 2000; Noda et al., 2001), whereas the PDZ domain binds diverse partners including LLGL, PALS1, CRB3 and PARD3 (Figure 2.3 B). Therefore, PAR6B is a dynamic polarity regulator that associates with multiple apical complexes and is necessary to maintain epithelial organization.

PARD3B is a homologue of cell polarity protein PARD3 and has a similar domains structure, however, studies have indicated that unlike PARD3, PARD3B does not interact with aPKC and the association with PAR6B is controversial (Gao et al., 2002; Kohjima et al., 2002). The function of PARD3B in epithelial cell polarity is unclear. PARD3B is highly expressed in the kidney, lung, and skeletal muscle and has been shown that PARD3B is localized at tight junctions with tight junction protein ZO-1 (Kohjima et al., 2002). Ectopically expressed the N-terminal region of PARD3B can disrupt the formation of tight junctions in MDCK cells (Gao et al., 2002). Recent studies indicate that PARD3B binds to tumour suppressor protein Lkb1 and suppresses its kinase activity, whereas ablation of PARD3B causes rapid and profound stem cell loss that is vital for mammary gland stem cell maintenance (Huo and Macara, 2014).

Proximity-dependent biotin identification (BioID) was developed to characterize protein-protein interaction networks and has been applied successfully in different model systems to screen a wide range of proteins and investigate protein networks and functions (Choi-Rhee et al., 2004; Cronan, 2005; Kim and Roux, 2016; Li et al., 2017; Varnaite and MacNeill, 2016). BioID is based on proximity-dependent cellular biotinylation by fusing a biotin ligase to either the N- or C-terminus of a protein-of-interest over a period of time (typically 24-48 hrs) in living cells. The biotinylated proteins are isolated using streptavidin affinity purification and can be analyzed by mass spectrometry (Roux et al., 2012). Whereas wild-type BirA specifically biotinylates acetyl-CoA carboxylase through releasing a primed bioAMP molecule, which covalently attaches to a specific lysine of its substrate peptide (Kwon and Beckett, 2000; Kwon et al., 2000), modification of the biotin ligase BirA from *Escherichia coli* (R118G, BirA*) allows promiscuous biotinylation of proximal proteins (~10nm radius), irrespective of whether they are directly or indirectly interacting in the same neighborhood, by generating high reactive and short-lived bioAMP (Roux et al., 2012). Since the proximal proteins are attached by stable covalent modification, harsh lysis condition can be applied to solubilize most proteins (Lambert et al., 2015). Moreover, promiscuous biotin ligase (BioID2) from *A. aeolicus* is a smaller, more biotin-sensitive biotin ligase, thus improving on the original BioID (Kim et al., 2016). This technique will allow for understanding of signaling networks in previously inaccessible biological settings.

Here, we apply an integrative approach using BioID2 in 2D and 3D epithelial cultures to identify potential novel PAR6B-proximity proteins as potential regulators of apical-basal polarity and lumen formation. Our results show that PAR6B has a common set of proteins in 2D and 3D environments, as well as unique proteins in each condition. We report that PAR6B is in proximity

to PARD3B in epithelial cells cultured in 3D and both are required for lumen formation. Moreover, we identify HRNR and RAS like proto-oncogene B (RALB) as PAR6B proximal proteins that are essential for lumen formation and epithelial organization. Collectively, these results demonstrate that 3D epithelial cultures are amenable to proteomics studies and that proximity-based methods can identify novel regulators of lumen formation.

2.2 Results

2.2.1 Suspension culture of Caco-2 supports lumen formation

To identify potential novel regulators of lumen formation we chose to first identify proteins in proximity to PAR6B, an apical protein involved in lumen formation in 3D Caco-2 cysts, using proximity biotinylation (BioID). Caco-2 cells were implemented in this study because they efficiently form lumen in 3D culture (Figure 2.1 A) (Jaffe et al., 2008). Culture of cells in 3D environments for lumen formation typically involved embedding cells in solid basement membrane extract (BME), or culturing cells on top of a solid layer of BME with 2-4% soluble BME in the culture medium (Figure 2.1 B). While these formats efficiently generate 3D structures with a lumen, there are limitations for their use in proteomic analysis. First, embedding cells within or on top of solid BME is costly to obtain sufficient cells for proteomic screening. Second, cells need to be extracted from the solid BME gels and processed prior to proteomic analysis, which can lead to sample loss. Therefore, we sought to develop a suspension culture format to culture 3D Caco-2 cysts that would alleviate these challenges.

For suspension cultures, we generated non-adhesion dishes by coating standard tissue culture dishes with polyHEMA, an inert biopolymer that prevents cell adhesion to the plastic

surface (Figure 2.1 B). To determine if cells could grow into 3D structures with a central lumen in suspension culture, we seeded single cell suspensions in the presence 0-2% BME and cultured them for 10 days. Whereas cells in the absence or low concentration (0.5%) of soluble BME failed to form 3D structures with a central lumen, cells in 1-2% BME efficiently formed lumen (Figure 2.1 C, D). Cells grown in 1 and 1.5% BME tended to clump together, whereas clumping was minimal in 2% BME. Therefore, 2% BME represents the optical concentration for lumen formation in suspension Caco-2 cells. Immunostaining for apical (aPKC, PAR6, F-actin) markers and ECM proteins like laminin confirmed that cell polarity and epithelial architecture was indistinguishable between Caco-2 cells cultured in semi-embedded or non-adherent conditions (Figure 2.1 E, F). An advantage of non-adherent cultures is the potential to scale cell production. To this end, we examined lumen formation efficiency at a range of cell concentrations (3.75-15x10^4 cells/ml). Up to 6.25x10^4 cells/ml, >90% of cells generated 3D structures with a single lumen, similar to semi-embedded cysts, whereas above this the efficiency deteriorated with increased proportion of fused cysts or cysts with no lumen (Figure 2.1 G).

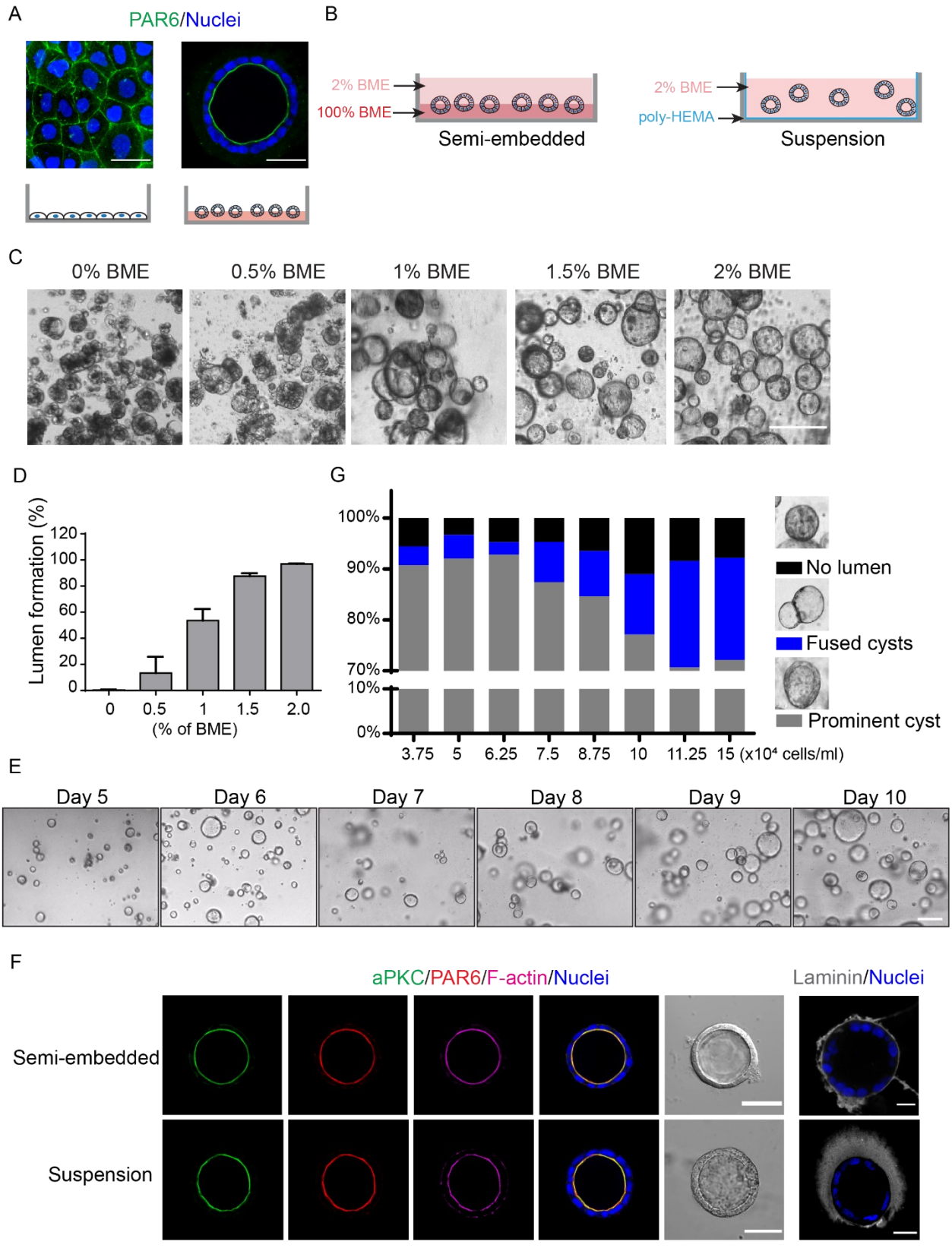
A
PAR6/Nuclei
B
2% BME
100% BME
Semi-embedded
2% BME
poly-HEMA
Suspension
C
0% BME
0.5% BME
1% BME
1.5% BME
2% BME
D
Lumen formation (%)
120
100
80
60
40
20
0
0
0.5
1
1.5
2.0
(% of BME)
G
100%
90%
80%
70%
10%
0%
3.75
5
6.25
7.5
8.75
10
11.25
15 (x10⁴ cells/ml)
No lumen
Fused cysts
Prominent cyst
E
Day 5
Day 6
Day 7
Day 8
Day 9
Day 10
F
aPKC/PAR6/F-actin/Nuclei
Laminin/Nuclei
Semi-embedded
Suspension

Figure 2.1: The condition for 3D organotypic cell culture model of Caco-2 cells. (A) Confocal images for PAR6B (green) in 2D and 3D Caco-2 cells. (B) Schematic showing 3D organotypic cell culture model for semi-embedded and suspension Caco-2 cells. (C) Brightfield images showing the phenotype of 3D organotypic suspension Caco-2 cells in different percentage (0-2%) of BME with complete DMEM culture media. (D) Quantification of the percentage of lumen formation in different percentage (0-2%) of BME. (E) Brightfield images of 3D organotypic suspension Caco-2 cells were captured from day5 to day10. (F) Confocal images were captured for 3D organotypic cells for semi-embedded and suspension Caco-2 cells immunostained for aPKC (green), PAR6B (red), F-actin (magenta), and Laminin (grey) showing both 3D culture cells have the same phenotype with apical-basal polarity and form a single prominent lumen. (G) Quantification of the percentage of different Caco-2 cells phenotype (no lumen, fused cysts, single prominent cyst) at different cell numbers (3.75-15x10^4 cells/ml) in 3D organotypic suspension cell culture. Cells were seeded in 8-well Ibidi plates. Scale Bars: A, 50µm; C, 100µm; E, 200µm; F, 50µm (left panel); 20µm (right panel).

2.2.2 Identification of known and novel PAR6B proximity proteins

To initially validate expression of BirA*PAR6B, HEK293 cells were transiently transfected with pWPI-BirA*-PAR6B or a control plasmid expressing mCherry (pWPI-BirA*-mCherry), which produced fusion proteins at the expected sizes (BirA*-PARD6B, 85kDa; BirA*-mCherry, 50kDa) (Figure 2.2 B). These plasmids express a myc-tag before BirA* and the fusion protein, as well as an IRES-GFP cassette to identify transduced cells (Figure 2.2 A). Expression was further confirmed by blotting for a myc-tag and the expression of the fusion protein were detected by anti-myc, and anti-PAR6B (Figure 2.2 B) and the biotinylation of the proximity interactors of the BirA*-PAR6B or BirA*-mCherry were detected by HRP (horseradish peroxidase) streptavidin (Supplemental Figure S2.1).

We next used lentivirus to generate stable expression of BirA*-PAR6B and BirA*-mCherry in Caco-2 cells. To obtain exogenous expression levels of BirA*-fused PAR6B similar to endogenous levels of PAR6B, we used a low dose of lentivirus virus (multiplicity of infection (MOI = 0.2) and used fluorescent activated cell sorting (FACS) to split cells into three groups based on GFP expression (lowest 25%, middle 50%, highest 75%). The expression BirA*-PAR6B was evaluate by western blot, and it was determined that it was expressed similar to endogenous PAR6B in the cells with lowest GFP-expression (Figure 2.2 C). These cells were used for subsequent experiments. BirA*-PAR6B localized to the apical membrane, similar to endogenous PAR6B and did not disrupt lumen formation (Figure 2.2 D, E).

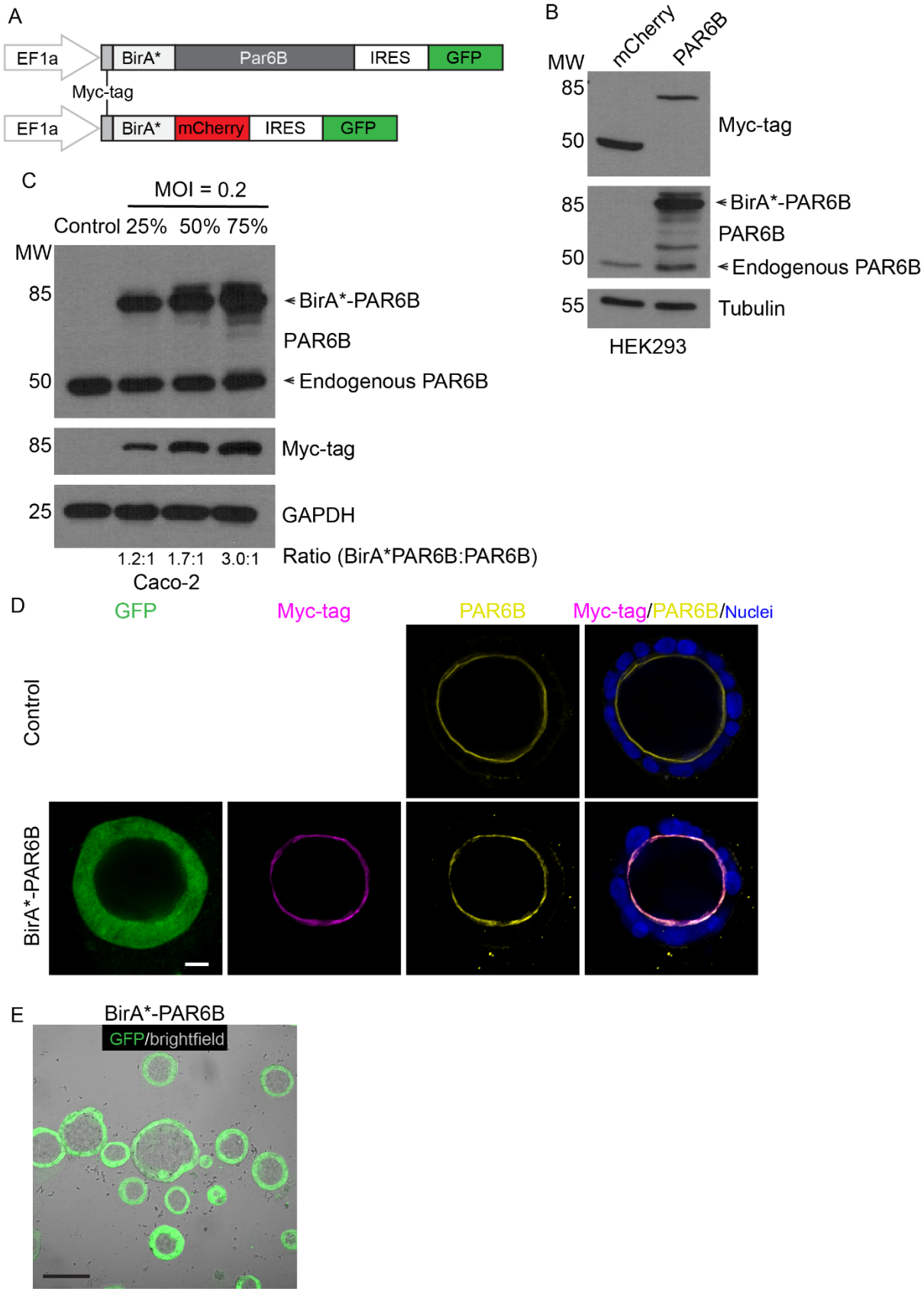
A
EF1a
BirA*
Par6B
IRES
GFP
Myc-tag
EF1a
BirA*
mCherry
IRES
GFP
B
MW
mCherry
PAR6B
85
50
Myc-tag
85
50
BirA*-PAR6B
PAR6B
Endogenous PAR6B
55
Tubulin
HEK293
C
MOI = 0.2
Control 25% 50% 75%
MW
85
50
BirA*-PAR6B
PAR6B
Endogenous PAR6B
85
Myc-tag
25
GAPDH
1.2:1 1.7:1 3.0:1
Ratio (BirA*PAR6B:PAR6B)
Caco-2
D
GFP
Myc-tag
PAR6B
Myc-tag/PAR6B/Nuclei
Control
BirA*-PAR6B
E
BirA*-PAR6B
GFP/brightfield

Figure 2.2: The validation for BioID method. (A) Diagram showing lentiviral constructs for the expression of BirA*PAR6B and BirA*-mCherry. Expression is driven by an EF1α promoter and an internal ribosomal entry site (IRES) directs expression of GFP. (B) Myc-tagged BirA*-mCherry (control) and BirA*-PAR6B expression were confirmed in HEK293 cells by western blot analysis. (C) To provide consistent expression levels, Caco-2 cells were infected with lentiviral constructs shown in (A) at a low multiplicity of infection (MOI = 0.2) to ensure single site integration. Three levels of expression were isolated by FACS of the coupled GFP marker: lowest 25%, the middle 50%, and the highest 75%. The expression of BirA*-PAR6B was determined by western blot with PAR6B antibodies. The ratio of BirA*-PAR6B: endogenous PAR6B is denoted at the bottom of the blot. (D) Confocal images were captured for control (uninfected) and BirA*-PAR6B-expressing 3D Caco-2 cells immunostained for myc-tag (magenta) and PAR6B (yellow) to demonstrate that BirA*-PAR6B localizes to the apical membrane, similar to endogenous PAR6B. GFP was visualized by direct fluorescence. (E) Widefield images (brightfield and GFP fluorescence) were captured and overlaid, demonstrating that BirA*-PAR6B-expressing 3D Caco-2 cells form a single prominent lumen. Scale Bars: D, 10µm; E, 100µm.

2.2.3 Identification of PAR6B proximity proteins in polarized Caco-2 cells

To identify apical proteins proximal to PAR6B, we grew cells for 8 days in suspension culture, a time when the lumen is fully established. At this time, we added biotin for 48 hrs, then lysed cells and pulled-down biotinylated proteins using streptavidin beads. In parallel, we performed experiments on Caco-2 cells cultured in tissue culture dishes in standard two-dimensional (2D) format, to determine if unique proteins could be identified in Caco-2 cells that form a lumen (3D) and those that polarize in the absence of lumen formation (2D). From triplicate experiments, 8645 peptides from 526 proteins were identified in 3D samples, whereas 13329 peptides from 600 proteins were identified in 2D samples. We filtered the list of PAR6B-proximity proteins using the following criteria: 1) peptides were detected in at least two of the three replicates; 2) the average peptide count was at least twice the count in the control; 3) the peptide count was <10 for each control replicates. This filtering process resulted in 47 proteins in 3D samples and 34 proteins in 2D. This filter is justified, since it includes known PAR6B-associated proteins, whereas more stringent cut-offs excluded some known interactions. Proteins that are associated with PAR6B are listed in Figure 2.3 A. High confidence hits (Saint Score > 0.75) included polarity proteins known to directly associated with PARD6B (LLGL1, LLGL2, PARD3, PRKCI (aPKCι), PRKCZ (aPKCζ), and CDC42) as well PARD3B, an ortholog of PARD3 (Kohjima et al., 2002). As expected, the Par proteins and LLGL were also identified as high-confidence hits from cells grown in 2D (Supplementary Fig. S2.2 A). We also identified PTPN14 and HRNR as high-confidence hits with unknown roles in cell polarity or lumen formation. Additional proteins known to associate with the Par complex (WWC1/Kibra, TP53BP2/ASPP2, SQSTM1/p62) were also identified as lower confidence interactions (Saint Score < 0.75) (Supplementary Fig. S2.2 A) (Joberty et al., 2000;

Yamanaka et al., 2003). Strikingly, we did not observe any proteins from the Crumbs complex in proximity to PAR6B in either 2D or 3D experiments, despite reported data supporting PAR6B as a component of both the Par and Crumbs complexes. To further explore relationships between PAR6B proximity proteins, we used STRING protein-protein interaction networks as well as Gene Ontology for candidates from 3D and 2D samples (Figure 2.3 C, D and Supplementary Fig. S2.2 B, C). This identified three clusters related to 1) Apical basal polarity and trafficking, 2) protein translation and folding, 3) metabolic processes. Of the PAR6B-proximal proteins identified in 3D and 2D screens, 40 were common, 19 specific to 3D samples and 10 specific to 2D samples (Figure 2.4 A). Furthermore, for two proteins (PARD3B and RALB), peptide spectra were identified in both 2D and 3D samples but were enriched > 5-fold in the 3D samples, indicating some differences in proximity networks between 2D and 3D samples (Figure 2.4 B). To determine if differences in observed peptide spectral counts between 2D and 3D could result from differences in gene expression, we compared 2D and 3D using RNA-seq. However, mRNA expression was not substantially different for these genes (Figure 2.4 C).

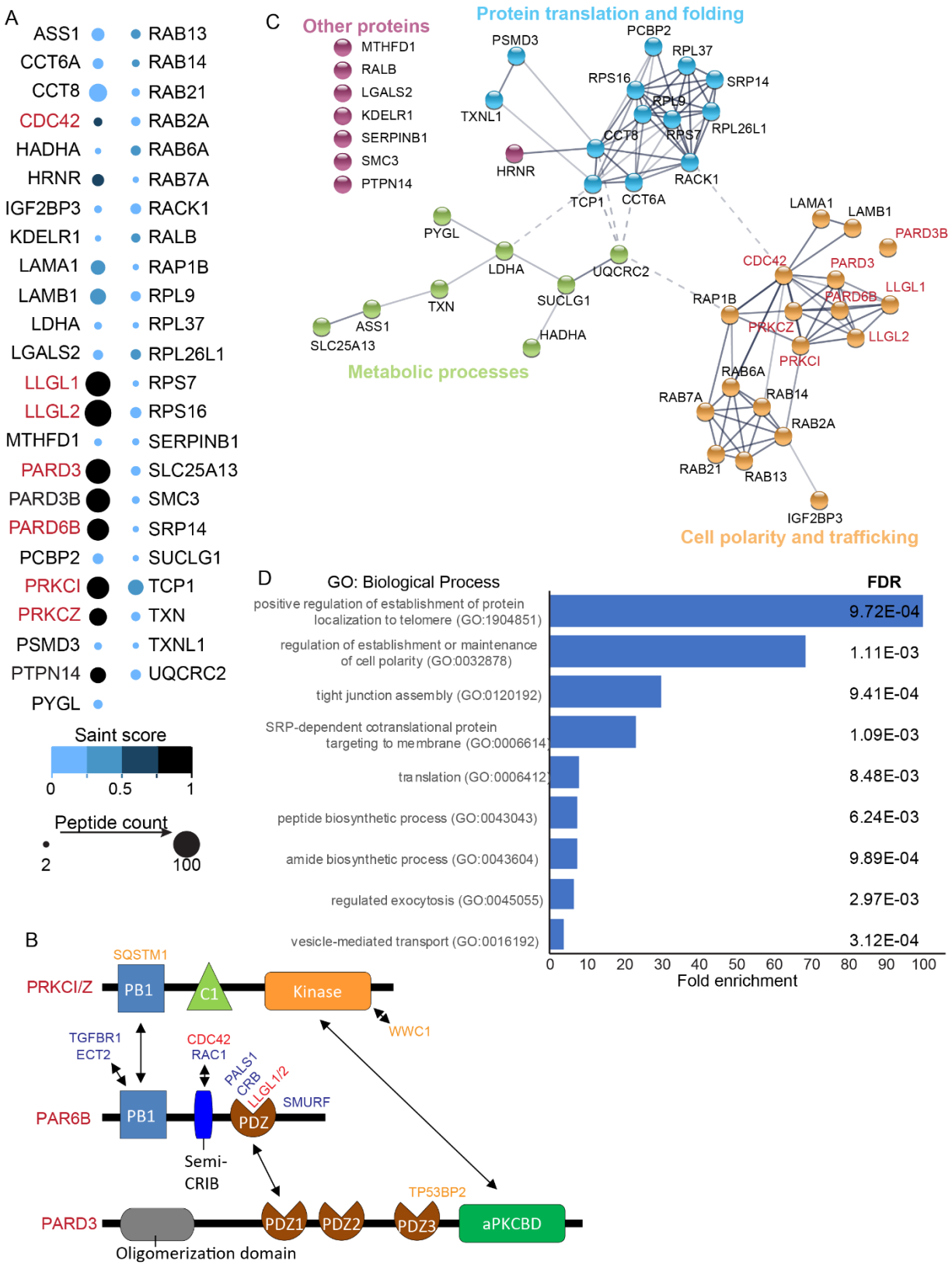
A
ASS1
CCT6A
CCT8
CDC42
HADHA
HRNR
IGF2BP3
KDELR1
LAMA1
LAMB1
LDHA
LGALS2
LLGL1
LLGL2
MTHFD1
PARD3
PARD3B
PARD6B
PCBP2
PRKCI
PRKCZ
PSMD3
PTPN14
PYGL
RAB13
RAB14
RAB21
RAB2A
RAB6A
RAB7A
RACK1
RALB
RAP1B
RPL9
RPL37
RPL26L1
RPS7
RPS16
SERPINB1
SLC25A13
SMC3
SRP14
SUCLG1
TCP1
TXN
TXNL1
UQCRC2
Saint score
0
0.5
1
Peptide count
2
100
C
Other proteins
MTHFD1
RALB
LGALS2
KDELR1
SERPINB1
SMC3
PTPN14
Protein translation and folding
PSMD3
PCBP2
RPL37
RPS16
SRP14
RPL9
TXNL1
RPS7
RPL26L1
CCT8
HRNR
RACK1
TCP1
CCT6A
PYGL
LDHA
UQCRC2
TXN
SUCLG1
ASS1
SLC25A13
HADHA
Metabolic processes
LAMA1
LAMB1
PARD3B
CDC42
PARD3
LLGL1
PARD6B
RAP1B
PRKCZ
LLGL2
PRKCI
RAB6A
RAB7A
RAB14
RAB2A
RAB21
RAB13
IGF2BP3
Cell polarity and trafficking
D
GO: Biological Process
FDR
positive regulation of establishment of protein localization to telomere (GO:1904851)
9.72E-04
regulation of establishment or maintenance of cell polarity (GO:0032878)
1.11E-03
tight junction assembly (GO:0120192)
9.41E-04
SRP-dependent cotranslational protein targeting to membrane (GO:0006614)
1.09E-03
translation (GO:0006412)
8.48E-03
peptide biosynthetic process (GO:0043043)
6.24E-03
amide biosynthetic process (GO:0043604)
9.89E-04
regulated exocytosis (GO:0045055)
2.97E-03
vesicle-mediated transport (GO:0016192)
3.12E-04
0 10 20 30 40 50 60 70 80 90 100
Fold enrichment
B
SQSTM1
PRKCI/Z
PB1
C1
Kinase
WWC1
TGFBR1
ECT2
CDC42
RAC1
PALS1
CRB
LLGL1/2
SMURF
PAR6B
PB1
PDZ
Semi-
CRIB
TP53BP2
PARD3
PDZ1
PDZ2
PDZ3
aPKCBD
Oligomerization domain

Figure 2.3: Identification of BirA*-PAR6B vicinal proteins in 3D cell culture samples by proteomics analysis. (A) The Saint score and peptide counts for PAR6B targets identified in 3D BirA*-PAR6B-expressing Caco-2 cells are shown with different color and size, which were analysed by SAINT analysis. BioID was successful at identifying known interaction partners for PAR6B such as CDC42, LLGL1/2, PARD3, and aPKC, novel vicinal proteins were also identified. (B) Graph showing the known interaction domains and interactors for Par complex (aPKC, PAR6B, PARD3). Proteins in red are known interactors for PAR6B and were identified in BirA*-PAR6B mass spectrometry data. Proteins in blue are known interactors for PAR6B and were not identified in BirA*-PAR6B mass spectrometry data. Proteins in orange indirectly associate with PAR6B and were identified in BirA*-PAR6B mass spectrometry data. (C) The interaction between proteins which were identified in 3D BirA*-PAR6B-expressing Caco-2 cells by BioID based on the STRING database. Line darkness indicates the strength of the predicted relationship between the proteins. (D) The graph showing fold enrichment of different biological processes of BirA*-PAR6B vicinal proteins in 3D samples based on Gene Ontology. FDR: False Discovery Rates.

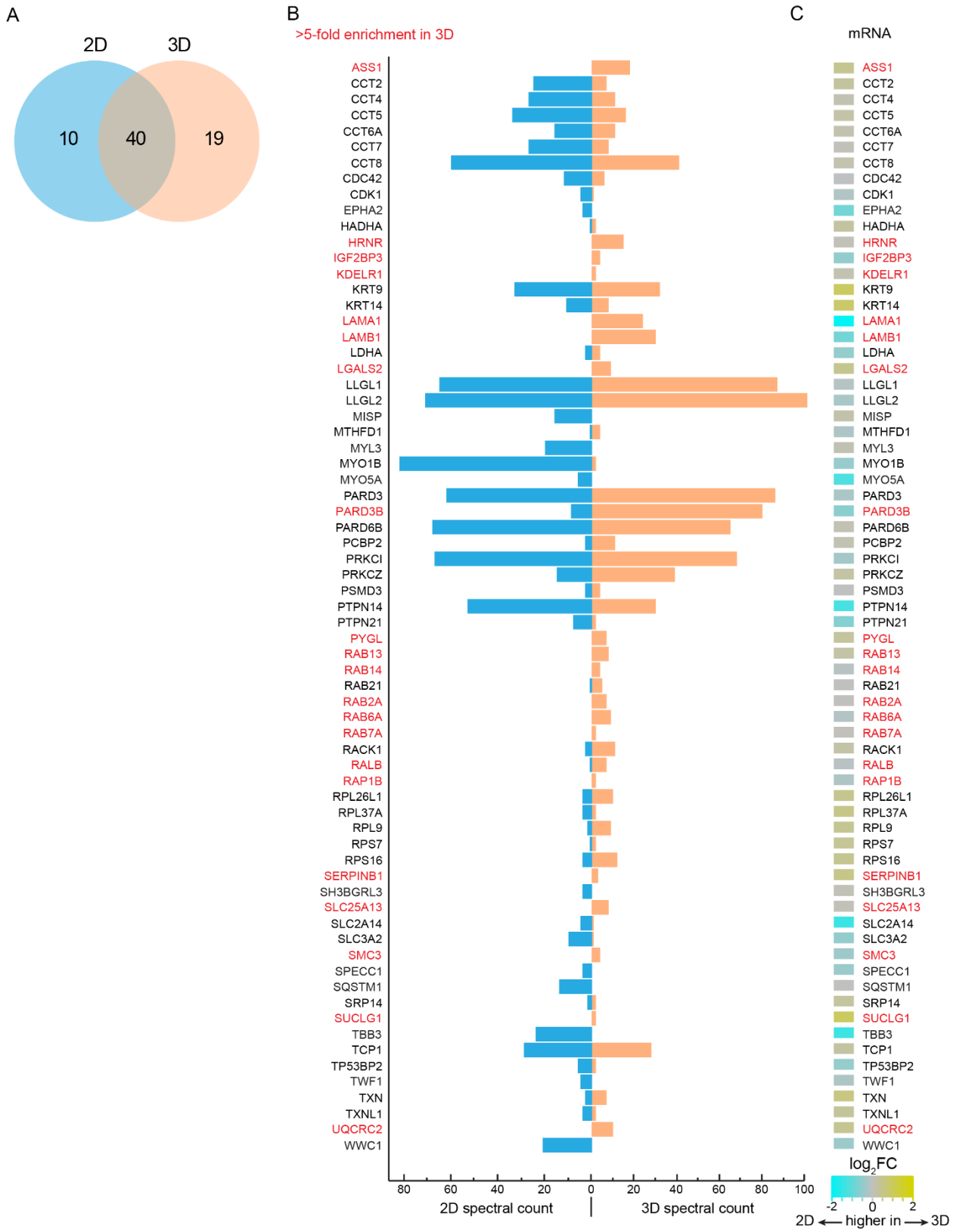
A
2D
3D
10
40
19
B
>5-fold enrichment in 3D
ASS1
CCT2
CCT4
CCT5
CCT6A
CCT7
CCT8
CDC42
CDK1
EPHA2
HADHA
HRNR
IGF2BP3
KDELR1
KRT9
KRT14
LAMA1
LAMB1
LDHA
LGALS2
LLGL1
LLGL2
MISP
MTHFD1
MYL3
MYO1B
MYO5A
PARD3
PARD3B
PARD6B
PCBP2
PRKCI
PRKCZ
PSMD3
PTPN14
PTPN21
PYGL
RAB13
RAB14
RAB21
RAB2A
RAB6A
RAB7A
RACK1
RALB
RAP1B
RPL26L1
RPL37A
RPL9
RPS7
RPS16
SERPINB1
SH3BGRL3
SLC25A13
SLC2A14
SLC3A2
SMC3
SPECC1
SQSTM1
SRP14
SUCLG1
TBB3
TCP1
TP53BP2
TWF1
TXN
TXNL1
UQCRC2
WWC1
80 60 40 20 0 20 40 60 80 100
2D spectral count
3D spectral count
C
mRNA
log2FC
-2 0 2
2D ← higher in → 3D

Figure 2.4: The comparison of BirA*-PAR6B vicinal proteins in 2D and 3D screens by proteomics analysis. (A) Venn diagram showing the number of BirA*-PAR6B vicinal proteins that were identified in 2D and 3D BioID screens. (B) Graph showing the spectral count of the BirA*-PAR6B proximal proteins which were identified in 2D and 3D screens. Proteins in red are more than 5-fold enrichments of peptide spectra in 3D screens. (C) RNA-seq data showing the difference of gene expression in 2D and 3D samples. Higher expression of mRNA in 3D samples are shown in green, higher expression of mRNA in 2D samples are shown in blue.

2.2.4 PARD3B localizes to the apical membrane and is required for lumen formation

Since the association of PARD3B with the Par-complex is not well established, we were surprised to find it in proximity to PAR6B in our experiments. Moreover, we were intrigued that it was enriched in 3D samples compared to 2D samples. We first confirmed the result obtained from mass spectrometry analysis that PARD3B is enriched using streptavidin pull-downs from Caco-2 cells expressing BirA*-PAR6B in 3D versus 2D culture (Figure 2.5 A). Moreover, PARD3 was a less abundant proximity partner for PAR6B in 3D versus 2D, whereas PRKCI and PRKCZ were equivalent as detected by immunoblot, suggesting there may be a Par3 isoform switch between 2D and 3D cultures. Consistent with this idea, we observed opposite expression profiles between the major splice form of PARD3 (150 kDa) and PARD3B in 2D and 3D Caco-2 cells in whole cell lysates (Figure 2.5 A, B). Expression of *PARD3* and *PARD3B* mRNA was not substantially different between 2D and 3D cultures, nor was their expression changed in 2D cultures following treatment with the proteasome inhibitor MG132, indicating that the difference in expression of Par3 isoforms between 2D and 3D environments is not controlled by transcription or proteasomal degradation (Supplemental Figure S2.3 A). Consistent with previous results (Kohjima et al., 2002), we were unable to detect an association between endogenous PARD3B and PARD6B or PARD3 by co-immunoprecipitation (Figure 2.5 B, Supplemental Figure S2.3 B), suggesting that association of PARD3B with the Par-complex may not be stable under immunoprecipitation conditions used. Finally, we examined the localization of PARD3B in both 2D and 3D cultures, which revealed colocalization with PAR6B (Figure 2.5 C). Taken together, this data suggests a role for PARD3B which is associated with PAR6B, although more thorough studies will need to be performed to further understand a PARD3B-containing polarity complex.

To examine the function of PARD3B in lumen formation, we evaluated two independent shRNA targeting PARD3B in Caco-2 cells grown in 3D culture. Whereas control cells generated cysts with a single prominent lumen, cells expressing shRNA to PARD3B formed cysts with small multiple lumen (Figure 2.5 D, E), reminiscent of the multi-lumen phenotype observed when PARD3, PRKCI, or PARD6B are depleted in 3D culture (Durgan et al., 2011; Hao et al., 2010). In 2D cultures, expression of PARD3B shRNA did not impair cell polarization or junction formation, as determined by immunostaining for PARD6B and F-actin (Supplemental Figure S2.3 C). Collectively these results demonstrate that PARD3B is required for lumen formation and support a role for PARD3B as part of a Par complex in this process.

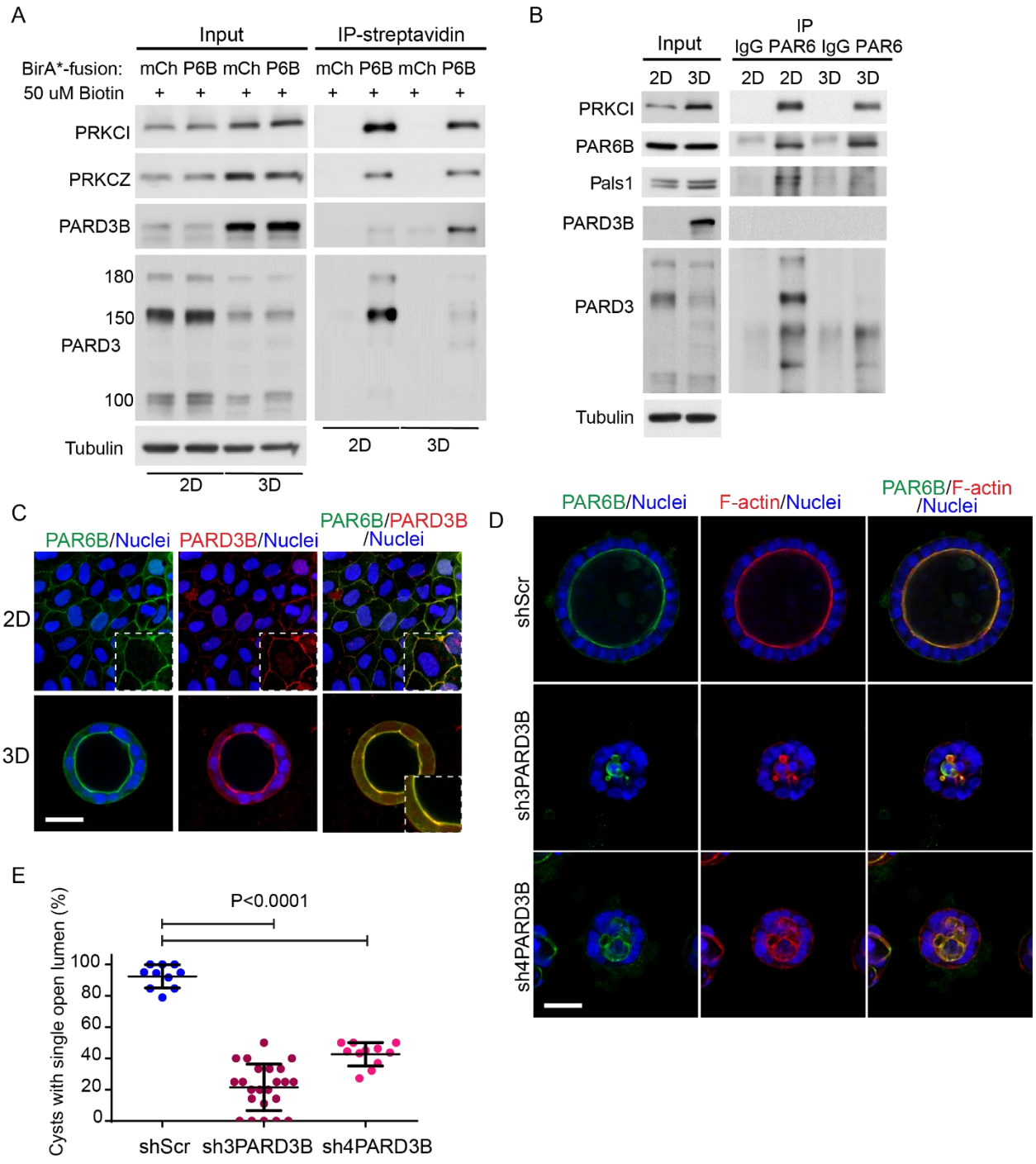
A
Input
IP-streptavidin
BirA*-fusion: mCh P6B mCh P6B mCh P6B mCh P6B
50 uM Biotin + + + + + + + +
PRKCI
PRKCZ
PARD3B
180
150
PARD3
100
Tubulin
2D 3D
2D 3D
B
Input
IP
IgG PAR6 IgG PAR6
2D 3D 2D 2D 3D 3D
PRKCI
PAR6B
Pals1
PARD3B
PARD3
Tubulin
C
PAR6B/Nuclei
PARD3B/Nuclei
PAR6B/PARD3B /Nuclei
2D
3D
D
PAR6B/Nuclei
F-actin/Nuclei
PAR6B/F-actin /Nuclei
shScr
sh3PARD3B
sh4PARD3B
E
P<0.0001
Cysts with single open lumen (%)
100
80
60
40
20
0
shScr
sh3PARD3B
sh4PARD3B

Figure 2.5: PARD3B is proximal to PAR6B and is required for lumen formation. (A) Pull-downs were performed with streptavidin in 2D and 3D BirA*-mCherry and BirA*-PAR6B-expressing Caco-2 cells. (B) Immunoprecipitation were performed with anti-PAR6B in 2D and 3D Caco-2 cells. (C) Confocal images were captured for 2D (top panel) and 3D (bottom panel) BirA*-PAR6B-expressing Caco-2 cells immunostained for PAR6B (green) and PARD3B (red). (D) Confocal images were captured for 3D shScr, sh3PARD3B, and sh4PARD3B knock-down Caco-2 cysts immunostained for PAR6B (green) and F-actin (red). (E) Quantification of the percentage of cysts with single open lumen in 3D shScr, sh3PARD3B, and sh4PARD3B knock-down Caco-2 cells. Scale Bars: C, 30µm; D, 50µm.

2.2.5 Hornerin (HRNR) and RALB are novel proteins involved in lumen formation

To determine whether additional PAR6B-proximity proteins identified in our BioID screen were also involved in lumen formation, we further examined RALB and HRNR, both of which have not previously been associated with lumen formation or apical-basal polarity. To investigate if RALB is involved in lumen formation, we examined 3D Caco-2 cells expressing control shRNA (shScr), or two-independent shRNA directed to RALB (sh1-RALB and sh5-RALB). Whereas cells form a single layer surrounding the lumen in control cysts, in cysts expressing RALB-shRNA, cells displayed collapsed and disorganized lumen and had regions of stratification (Figure 2.6 A, B). Despite RALB-shRNA-expressing cysts have a smaller size, the number of cells/cyst cross section was not different from control (Figure 2.6 C). In 2D cultures, RALB-depleted cells were similar to controls and had no obvious alterations in cell polarity or epithelial organization (Figure 2.6 D).

Similarly, we investigated a potential role for HRNR in lumen formation and epithelial organization. In 3D cysts, expression of two independent HRNR-shRNA resulted in multiple microlumen and disorganized structures with small, condensed nuclei (Figure 2.7 A-C). Moreover, HRNR-shRNA cells in 2D cultures also showed severe epithelial disorganization, with large cells with irregular nuclear size, and disrupted cortical PAR6B and F-actin (Figure 2.7 D-F). These data indicate that HRNR has a previously unappreciated role in epithelial organization and lumen formation.

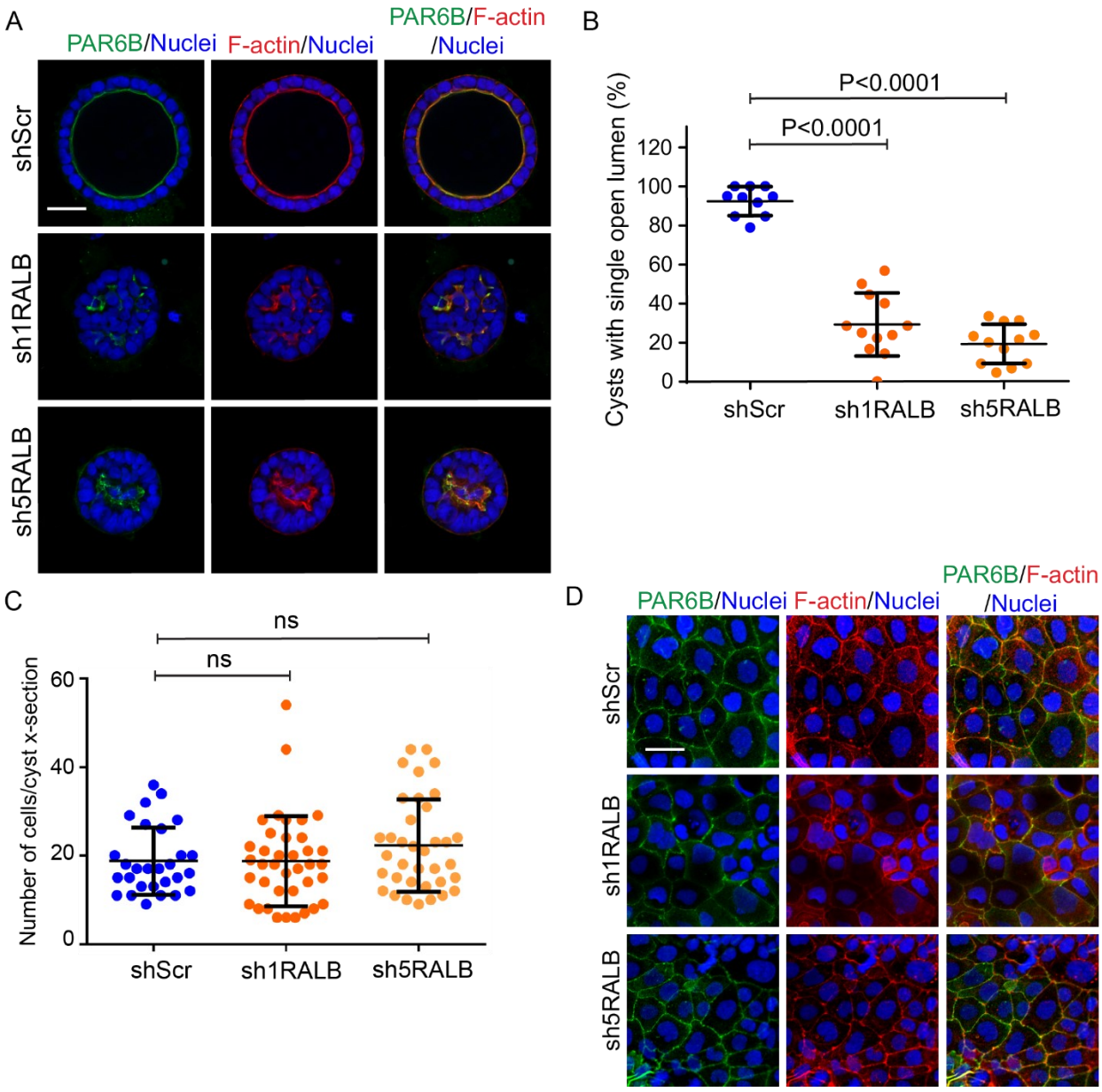
A
PAR6B/Nuclei
F-actin/Nuclei
PAR6B/F-actin
/Nuclei
shScr
sh1RALB
sh5RALB
B
P<0.0001
P<0.0001
Cysts with single open lumen (%)
120
100
80
60
40
20
0
shScr
sh1RALB
sh5RALB
C
ns
ns
Number of cells/cyst x-section
60
40
20
0
shScr
sh1RALB
sh5RALB
D
PAR6B/Nuclei
F-actin/Nuclei
PAR6B/F-actin
/Nuclei
shScr
sh1RALB
sh5RALB

Figure 2.6: RALB knockdown disrupts the morphology of 3D Caco-2 cysts. (A) Confocal images were captured for 3D shScr, sh1RALB, and sh5RALB knock-down Caco-2 cysts immunostained for PAR6B (green) and F-actin (red). (B) Quantification of the percentage of cysts with single open lumen in 3D shScr, sh1RALB, and sh5RALB knock-down Caco-2 cysts. (C) Quantification of the number of cells per cross-section cyst in 3D shScr, sh1RALB, and sh5RALB knock-down Caco-2 cysts. (D) Confocal images were captured for 2D shScr, sh1RALB, and sh5RALB knock-down Caco-2 cells immunostained for PAR6B (green) and F-actin (red). Scale Bars: A,D, 50μm.

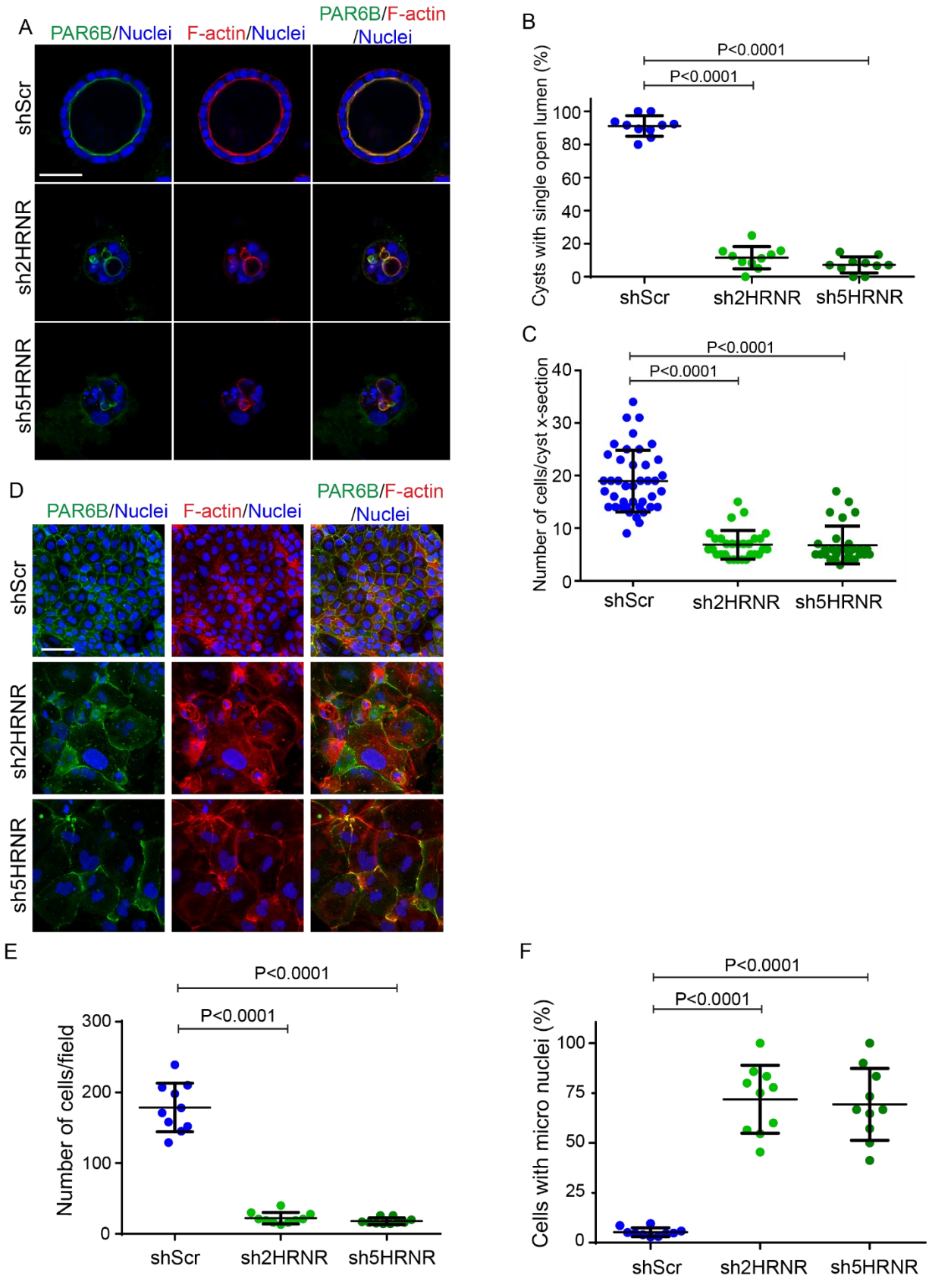
A
PAR6B/Nuclei
F-actin/Nuclei
PAR6B/F-actin /Nuclei
shScr
sh2HRNR
sh5HRNR
B
P<0.0001
P<0.0001
Cysts with single open lumen (%)
100
80
60
40
20
0
shScr
sh2HRNR
sh5HRNR
C
P<0.0001
P<0.0001
Number of cells/cyst x-section
40
30
20
10
0
shScr
sh2HRNR
sh5HRNR
D
PAR6B/Nuclei
F-actin/Nuclei
PAR6B/F-actin /Nuclei
shScr
sh2HRNR
sh5HRNR
E
P<0.0001
P<0.0001
Number of cells/field
300
200
100
0
shScr
sh2HRNR
sh5HRNR
F
P<0.0001
P<0.0001
Cells with micro nuclei (%)
100
75
50
25
0
shScr
sh2HRNR
sh5HRNR

Figure 2.7: HRNR knockdown disrupts morphology of 2D and 3D Caco-2 cells. (A) Confocal images were captured for 3D shScr, sh2HRNR, and sh5HRNR knock-down Caco-2 cysts immunostained for PAR6B (green) and F-actin (red). (B) Quantification of the percentage of cysts with single open lumen in 3D shScr, sh2HRNR, and sh5HRNR knock-down Caco-2 cysts. (C) Quantification of the number of cells per cross-section cyst in 3D shScr, sh2HRNR, and sh5HRNR knock-down Caco-2 cysts. (D) Confocal images were captured for 2D shScr, sh2HRNR, and sh5HRNR knock-down Caco-2 cells immunostained for PAR6B (green) and F-actin (red). (E) Quantification of the number of cells per field in 2D shScr, sh2HRNR, and sh5HRNR knock-down Caco-2 cells. (F) Quantification of the percentage of cells with micro nuclei in 2D shScr, sh2HRNR, and sh5HRNR knock-down Caco-2 cells. Scale Bars: A, 50μm; D, 100μm.

2.3 Discussion

We took advantage of BioID to identify novel proteins involved in cell polarity and lumen formation. Based on our mass spectrometry results, we show that BioID identifies well-characterized protein interactors of PAR6B in both 2D and 3D culture as well as novel proximity proteins. An alternative approach to identify novel genes associated with polarization or lumen formation would be to perform a high-throughput functional screen using shRNA or CRISPR libraries. Limitations to this approach are that effects observed may be indirectly related to polarity signaling (Jackson and Linsley, 2010; Lin et al., 2005). An advantage of a proximity-based screen is that it identifies proteins that are likely part of a complex with a protein of interest, which is validated by a functional assay. Moreover, we present a novel 3D suspension culture method that is amenable to generating large numbers of cells for use with mass spectrometric analysis, while minimizing the use of BME, the most expensive component for 3D culture.

To date, the function and the binding partners of PARD3B remain unclear. In one study, PARD3B was shown to have differential binding to different PAR6B isoforms (Gao et al., 2002). However, another study indicated that PARD3B is incapable of binding to PAR6B and aPKC (Kohjima et al., 2002). Although we did not detect an interaction between PAR6B and PARD3B using conventional coimmunoprecipitation experiments, we did find that they were proximal based on our BioID data. This could reflect that a PARD3B/PAR6B complex is not stable under the same conditions used to isolate PARD3/PAR6B complexes and may explain differences in the literature. Moreover, we show that PARD3B localizes to the apical domain and is necessary for lumen formation. Therefore, our data support that PARD3B is a component of, or functionally coupled to the Par polarity complex. Interestingly, we found that PARD3B was expressed at lower

levels in 2D versus 3D cultures, and that depletion of PARD3B did not impact polarization in 2D cultures. Previous studies indicated that genes involved in lumen formation are upregulated in 3D epithelial cultures (Roman-Fernandez et al., 2018). We found that PARD3B protein, but not mRNA, was up-regulated in 3D cultures, suggesting that protein translation or stability may also play a role in regulating polarity proteins involved in lumen formation.

Moreover, we performed BirA*-PKC in 3D model to investigate the proximal interactor for PKC (see Chapter 4), strikingly, BirA*-aPKC mass spectrometry results also indicated that PARD3B may be also associated with aPKC, this is a novel finding since PARD3B had been shown not interact with PAR6B and PKC, suggesting that it is crucial to set up 3D model to examine the protein-protein interactions and their functions.

Hornerin/HRNR is a S100 protein family member, which are involved in numerous biological functions including inflammatory and immune responses, calcium homeostasis, the dynamics of cytoskeleton constituents, as well as fundamental cellular processes and signaling cascades (Marenholz et al., 2004). HRNR has been studied mostly in the skin epithelium (Henry et al., 2011; Makino et al., 2001; Takaishi et al., 2005; Wu et al., 2009), but is also expressed in human breast tissue, mammary epithelial, stromal cells and extracellular matrix (Fleming et al., 2012; Fleming et al., 2010). HRNR has been shown to act as a regulator of tumor vascularity (Gutknecht et al., 2017) and HRNR fragments have distinctive intracellular localization in breast cancer cells indicating there are unknown functions of HRNR (Fleming et al., 2012). However, HRNR had not been investigated in cell polarity or lumen formation prior to this study and future studies will be necessary to understand its role in polarized epithelia and whether a defect in

lumen architecture reflect a general defect in epithelial organization, or a more specific role in lumen formation.

RALB, a member of a subfamily of Ras-related GTPases, binds to its effectors such as exocyst once it is activated and to mediate epithelial tight junction formation (Hazelett et al., 2011; Rosse et al., 2006). Moreover, the binding of RALB-exocyst (Exo84) recruits to the midbody of cytokinetic bridge to drive abscission during cytokinesis (Cascone et al., 2008). This indicates that the association of PAR6B and RALB may involve in early cell polarization or mitotic process. However, the mechanism of how RALB regulate in cell polarity or lumen formation requires further investigation.

2.4 Materials and Methods

2.4.1 Cell culture

Human intestinal epithelial cell line Caco-2 cells were purchased from American Type Culture Collection (ATCC). Caco-2 cells were cultured at 37°C in 5% CO_2 in DMEM (Wisent #319-005-CL) supplemented with 10% fetal bovine serum (Wisent #080-150), 100 U/ml penicillin, 0.1 mg/ml streptomycin (Wisent #450201EL). Human embryonic kidney cell line HEK293LT (ATCC), were cultured at 37°C in 5% CO_2 in DMEM supplemented with 10% fetal bovine serum, 100 U/ml penicillin, 0.1 mg/ml streptomycin. For semi embedded 3D cell culture, Caco-2 cells were seeded in 8 well µ-slide (Ibidi #80826) on top of a layer of 100% GelTrex (ThermoFisher Scientific #A1413202) in media supplemented 2% GelTrex at 37 °C under humidified atmosphere of 5 % CO_2. GelTrex is a growth factor basement membrane matrix extract (BME) that contains laminin, collagen IV, entactin, and heparin sulfate proteoglycans which mimic the basement membrane context. For suspension -cell culture, cells were seeded on polyHEMA-coated plate in media supplemented 2% GelTrex at 37 °C under humidified atmosphere of 5 % CO_2.

To obtain enough cells and cysts number for mass spectrometry analysis, one million of low expression cells of BirA*-mCherry and BirA*-PAR6B were seeded on four 15 cm plates in 2D or 3D cell culture, 2D or 3D cells were collected after 24 hrs incubation with 50 µM biotin. Biotinylated proteins were lysed and isolated by binding to streptavidin beads and identified by mass spectrometry.

2.4.2 DNA and shRNA constructs

PAR6B was amplified by PCR from human cDNA. myc-BioID2-MCS was a gift from Kyle Roux (Addgene plasmid # 74223). pWPI was a gift from Didier Trono (Addgene plasmid #12254). The PCR products were digested and inserted into myc-BioID2-MCS. Fused products were digested and were inserted into pWPI for virus production. Plasmids were verified by DNA sequencing.

shRNAs targeting human PARD3B, RALB, and HRNR mRNA were cloned in pLKO. Lentiviral supernatants were produced in HEK293LT cells as described previously. Caco-2 cells were infected with lentiviral supernatants and selected by the addition of 20 μg/ml puromycin for 10 days.

The shRNA used were acquired from the McGill Platform for Cellular Perturbation (MPCP) sh3PARD3B CCGGCCATGCTTTGAGAACTGTCAACTCGAGTTGACAGTTCTCAAAGCATGGTTTTTG, sh4PARD3B CCGGCCTGGTTACTGGGTGAAGATTCTCGAGAATCTTCACCCAGTAACCAGGTTTTTG, sh1RALB CCGGCGTGATGAGTTAAAGTTGTATCTCGAGATACAACTTTAACTCATCACGTTTTTG, sh5RALB CCGGGAGTTTGTAGAAGACTATGAACTCGAGTTCATAGTCTTCTACAAACTCTTTTTG, sh2HRNR CCGGGCTTTAGTCAACACAAGTCTACTCGAGTAGACTTGTGTTGACTAAAGCTTTTTTG, sh5HRNR CCGGGCAGCGGTAGTGTCTTTACTTCTCGAGAAGTAAAGACACTACCGCTGCTTTTTTG) and a non-targeting scrambled shRNA was used as a control.

2.4.3 Transient transfection

HEK293LT cells were seeded at 2×10^6 cells per well in 100mm dishes and transfected with plasmids using Polyethylenimine (PEI) as per manufacturer's instructions (Sigma # 408727). All experiments were performed 24 h post-transfection.

2.4.4 Lentivirus production

Lentivirus was produced by calcium phosphate transfection of HEK293LT cells in 15-cm dishes using 50 µg of lentiviral plasmid, 37.5 µg of packaging plasmid (psPAX2), and 15 µg of vesicular stomatitis virus G (VSVG) coat protein plasmid (pMD2.G). Viral supernatants were collected after 48 hrs. Viral supernatants were concentrated by precipitation in 40% polyethylene glycol 8000 (Bioshop # PEG800.1) followed by centrifugation and then re-suspended in the culture medium. Concentrated virus was aliquoted and frozen at -80°C then titred using HEK293LT cells.

2.4.5 Affinity capture of biotinylated proteins

Cells were incubated for 24 h in complete media supplemented with 50 µM biotin. After two PBS washes, cells were lysed in 600µl ice cold RIPA lysis buffer (50 mM Tris–HCl (pH 7.5), 150 mM NaCl, 1% NP-40, 1 mM EDTA, 1 mM EGTA, 0.1% SDS and 0.5% sodium deoxycholate. PMSF (1 mM), DTT (1 mM) and Sigma protease inhibitor cocktail (P8340, 1:500). The lysates were treated with benzonase for 1h on ice an equal volume RIPA lysis buffer was added. For each sample, 30 µl of streptavidin-sepharose bead slurry (GE Healthcare, Cat 17-5113-01) was pre-washed three times with 1 mL of lysis buffer by pelleting the beads with 400g centrifugation and aspirating off the supernatant before adding the next wash. After three sessions of sonication and centrifugation at 16,500g, supernatants with biotinylated proteins were incubated pre-washed streptavidin beads for 3 h at 4 °C with rotation. Beads were collected and washed twice with RIPA buffer and three times with 1 mL with 50 mM ammonium bicarbonate (pH 8.0). Beads were then resuspended in 100 µl of 50 mM ammonium bicarbonate, 10% of the sample was saved for immunoblotting analysis. Bound proteins were removed from the magnetic beads with

100 µl of Laemmli SDS-sample buffer saturated with biotin at 98°C for 10 mins. BioID samples and controls were analyzed by mass spectrometry in at least three biological replicates.

2.4.6 Immunoblotting and immunoprecipitation

Growth medium was removed from the dishes, and cells cultured in 3D were washed twice with ice-cold PBS. RIPA buffer (50 mM Tris-HCl, pH 8, 0.15 M NaCl, 0.1% SDS, 1% NP-40, 1% sodium deoxycholate, 50 mM NaF, 5 mM orthovanadate, 1 mM DTT) with proteinase inhibitor cocktail (Sigma # 11836170001) was used to lyse cells. Cell lysates were centrifuged at 13,000 rpm at 4°C for 20 min, and the supernatant was collected. Total proteins were denatured by SDS sample buffer and boiling in water for 5 min. The total proteins were separated by SDS-PAGE and transferred to Nitrocellulose membrane (Bio-rad # 1620115). Membranes were blocked in Tris-buffered saline containing 5% milk and 0.1% Tween 20. The primary antibodies and secondary horseradish peroxidase antibody were used. The primary antibodies were used as follows: aPKCι 1/1000 (BD Transduction #610175); PKCzeta 1/1000 (Cell signaling #9368S), α-Tubulin 1/5000 (Sigma #T9026), PAR6B 1/1000 (Santa Cruz #sc-67393), mCherry 1/1000 (Abcam #ab167453), GAPDH 1/1000 (Novus Biologicals #NB300-322), myc 1/1000 (Origene # TA150121), PARD3A (Sigma #07-330) and PARD3B 1/1000 (Santa Cruz #sc-398761). The proteins were detected by enhanced chemiluminescence method. Bands were visualized using SuperSignal West Pico Chemiluminescent Substrate (Bio-rad #1705061) and exposure to UltraCruz radiographic film (Santa Cruz # sc-201696). For immunoprecipitation, cells were washed twice with ice-cold PBS and then lysed in NP40 buffer (150 mM NaCl, 1% NP-40, 50 mM Tris-HCl, pH 8.0) containing a protease inhibitor cocktail. Lysates were precleared with MagnaBeads (Thermo Fisher Scientific

#12321D) and then incubated with 2 µg of antibody or isotype control overnight at 4°C. Antibodies were captured with MagnaBeads and washed three times with NP40 buffer.

2.4.7 Immunostaining and imaging

3D cysts were fixed with 2% paraformaldehyde/PBS for 10 min and permeabilized in 0.5% Triton X-100/10%Goat serum/10% fish gelatin/PBS for 1 hour and incubated overnight in primary antibodies. The primary antibodies were used as follows: PAR6B 1/200 (Santa Cruz #sc-67393), aPKCι 1/100 (BD Transduction #610175), PARD3B 1/100 (Santa Cruz #sc-398761), myc 1/100 (Origene # TA150121), GFP 1/500 (Abcam #ab13970), and Phalloidin 1/100 (Invitrogen #A34055). The secondary antibodies conjugated to Alexa488, Alexa546 and Alexa647 (Jackson ImmunoResearch Laboratories) were used at 1:750. DNA was detected with Hoechst dye 33258. Confocal imaging was performed using LSM700 from Zeiss with 20X/0.8NA or 40X/1.4NA objective lenses and processed using FIJI/ImageJ software.

2.4.8 Statistical Analysis

Comparison of two unpaired independent means was performed using a student's t-test. Statistics were determined using Excel, and GraphPad Prism 6. All images are representative from at least three replicates.

2.5 Acknowledgements

We acknowledge Sara Banerjee from Université Laval for her technical expertise for SAINT analysis.

2.6 References

Aranda, V., Haire, T., Nolan, M.E., Calarco, J.P., Rosenberg, A.Z., Fawcett, J.P., Pawson, T., and Muthuswamy, S.K. (2006). Par6-aPKC uncouples ErbB2 induced disruption of polarized epithelial organization from proliferation control. Nat Cell Biol 8, 1235-1245.

Assemat, E., Bazellieres, E., Pallesi-Pocachard, E., Le Bivic, A., and Massey-Harroche, D. (2008). Polarity complex proteins. Biochim Biophys Acta 1778, 614-630.

Baker, B.M., and Chen, C.S. (2012). Deconstructing the third dimension: how 3D culture microenvironments alter cellular cues. J Cell Sci 125, 3015-3024.

Cascone, I., Selimoglu, R., Ozdemir, C., Del Nery, E., Yeaman, C., White, M., and Camonis, J. (2008). Distinct roles of RalA and RalB in the progression of cytokinesis are supported by distinct RalGEFs. EMBO J 27, 2375-2387.

Choi-Rhee, E., Schulman, H., and Cronan, J.E. (2004). Promiscuous protein biotinylation by Escherichia coli biotin protein ligase. Protein Sci 13, 3043-3050.

Cronan, J.E. (2005). Targeted and proximity-dependent promiscuous protein biotinylation by a mutant Escherichia coli biotin protein ligase. J Nutr Biochem 16, 416-418.

Durgan, J., Kaji, N., Jin, D., and Hall, A. (2011). Par6B and atypical PKC regulate mitotic spindle orientation during epithelial morphogenesis. J Biol Chem 286, 12461-12474.

Edmondson, R., Broglie, J.J., Adcock, A.F., and Yang, L. (2014). Three-dimensional cell culture systems and their applications in drug discovery and cell-based biosensors. Assay Drug Dev Technol 12, 207-218.

Fleming, J.M., Ginsburg, E., Oliver, S.D., Goldsmith, P., and Vonderhaar, B.K. (2012). Hornerin, an S100 family protein, is functional in breast cells and aberrantly expressed in breast cancer. BMC Cancer 12, 266.

Fleming, J.M., Miller, T.C., Quinones, M., Xiao, Z., Xu, X., Meyer, M.J., Ginsburg, E., Veenstra, T.D., and Vonderhaar, B.K. (2010). The normal breast microenvironment of premenopausal women differentially influences the behavior of breast cancer cells in vitro and in vivo. BMC Med 8, 27.

Gao, L., and Macara, I.G. (2004). Isoforms of the polarity protein par6 have distinct functions. J Biol Chem 279, 41557-41562.

Gao, L., Macara, I.G., and Joberty, G. (2002). Multiple splice variants of Par3 and of a novel related gene, Par3L, produce proteins with different binding properties. Gene 294, 99-107.

Gutknecht, M.F., Seaman, M.E., Ning, B., Cornejo, D.A., Mugler, E., Antkowiak, P.F., Moskaluk, C.A., Hu, S., Epstein, F.H., and Kelly, K.A. (2017). Identification of the S100 fused-type protein hornerin as a regulator of tumor vascularity. Nat Commun 8, 552.

Hao, Y., Du, Q., Chen, X., Zheng, Z., Balsbaugh, J.L., Maitra, S., Shabanowitz, J., Hunt, D.F., and Macara, I.G. (2010). Par3 controls epithelial spindle orientation by aPKC-mediated phosphorylation of apical Pins. Curr Biol 20, 1809-1818.

Hazelett, C.C., Sheff, D., and Yeaman, C. (2011). RalA and RalB differentially regulate development of epithelial tight junctions. Mol Biol Cell 22, 4787-4800.

Henry, J., Hsu, C.Y., Haftek, M., Nachat, R., de Koning, H.D., Gardinal-Galera, I., Hitomi, K., Balica, S., Jean-Decoster, C., Schmitt, A.M., et al. (2011). Hornerin is a component of the epidermal cornified cell envelopes. FASEB J 25, 1567-1576.

Huo, Y., and Macara, I.G. (2014). The Par3-like polarity protein Par3L is essential for mammary stem cell maintenance. Nat Cell Biol 16, 529-537.

Jackson, A.L., and Linsley, P.S. (2010). Recognizing and avoiding siRNA off-target effects for target identification and therapeutic application. Nat Rev Drug Discov 9, 57-67.

Jaffe, A.B., Kaji, N., Durgan, J., and Hall, A. (2008). Cdc42 controls spindle orientation to position the apical surface during epithelial morphogenesis. J Cell Biol 183, 625-633.

Joberty, G., Petersen, C., Gao, L., and Macara, I.G. (2000). The cell-polarity protein Par6 links Par3 and atypical protein kinase C to Cdc42. Nat Cell Biol 2, 531-539.

Johansson, A., Driessens, M., and Aspenstrom, P. (2000). The mammalian homologue of the Caenorhabditis elegans polarity protein PAR-6 is a binding partner for the Rho GTPases Cdc42 and Rac1. J Cell Sci 113 (Pt 18), 3267-3275.

Kapalczynska, M., Kolenda, T., Przybyla, W., Zajaczkowska, M., Teresiak, A., Filas, V., Ibbs, M., Blizniak, R., Luczewski, L., and Lamperska, K. (2018). 2D and 3D cell cultures - a comparison of different types of cancer cell cultures. Arch Med Sci 14, 910-919.

Kim, D.I., Jensen, S.C., Noble, K.A., Kc, B., Roux, K.H., Motamedchaboki, K., and Roux, K.J. (2016). An improved smaller biotin ligase for BioID proximity labeling. Mol Biol Cell 27, 1188-1196.

Kim, D.I., and Roux, K.J. (2016). Filling the Void: Proximity-Based Labeling of Proteins in Living Cells. Trends Cell Biol 26, 804-817.

Kohjima, M., Noda, Y., Takeya, R., Saito, N., Takeuchi, K., and Sumimoto, H. (2002). PAR3beta, a novel homologue of the cell polarity protein PAR3, localizes to tight junctions. Biochem Biophys Res Commun 299, 641-646.

Kwon, K., and Beckett, D. (2000). Function of a conserved sequence motif in biotin holoenzyme synthetases. Protein Sci 9, 1530-1539.

Kwon, K., Streaker, E.D., Ruparelia, S., and Beckett, D. (2000). Multiple disordered loops function in corepressor-induced dimerization of the biotin repressor. J Mol Biol 304, 821-833.

Lambert, J.P., Tucholska, M., Go, C., Knight, J.D., and Gingras, A.C. (2015). Proximity biotinylation and affinity purification are complementary approaches for the interactome mapping of chromatin-associated protein complexes. J Proteomics 118, 81-94.

Lemmers, C., Michel, D., Lane-Guermonprez, L., Delgrossi, M.H., Medina, E., Arsanto, J.P., and Le Bivic, A. (2004). CRB3 binds directly to Par6 and regulates the morphogenesis of the tight junctions in mammalian epithelial cells. Mol Biol Cell 15, 1324-1333.

Li, P., Li, J., Wang, L., and Di, L.J. (2017). Proximity Labeling of Interacting Proteins: Application of BioID as a Discovery Tool. Proteomics 17.

Lin, D., Edwards, A.S., Fawcett, J.P., Mbamalu, G., Scott, J.D., and Pawson, T. (2000). A mammalian PAR-3-PAR-6 complex implicated in Cdc42/Rac1 and aPKC signalling and cell polarity. Nat Cell Biol 2, 540-547.

Lin, X.Y., Ruan, X., Anderson, M.G., McDowell, J.A., Kroeger, P.E., Fesik, S.W., and Shen, Y. (2005). siRNA-mediated off-target gene silencing triggered by a 7 nt complementation. Nucleic Acids Research 33, 4527-4535.

Makino, T., Takaishi, M., Morohashi, M., and Huh, N.H. (2001). Hornerin, a novel profilaggrin-like protein and differentiation-specific marker isolated from mouse skin. J Biol Chem 276, 47445-47452.

Marenholz, I., Heizmann, C.W., and Fritz, G. (2004). S100 proteins in mouse and man: from evolution to function and pathology (including an update of the nomenclature). Biochem Biophys Res Commun 322, 1111-1122.

Noda, Y., Takeya, R., Ohno, S., Naito, S., Ito, T., and Sumimoto, H. (2001). Human homologues of the Caenorhabditis elegans cell polarity protein PAR6 as an adaptor that links the small GTPases Rac and Cdc42 to atypical protein kinase C. Genes Cells 6, 107-119.

Nolan, M.E., Aranda, V., Lee, S., Lakshmi, B., Basu, S., Allred, D.C., and Muthuswamy, S.K. (2008). The polarity protein Par6 induces cell proliferation and is overexpressed in breast cancer. Cancer Res 68, 8201-8209.

Ozdamar, B., Bose, R., Barrios-Rodiles, M., Wang, H.R., Zhang, Y., and Wrana, J.L. (2005). Regulation of the polarity protein Par6 by TGFbeta receptors controls epithelial cell plasticity. Science 307, 1603-1609.

Rodriguez-Boulan, E., and Macara, I.G. (2014). Organization and execution of the epithelial polarity programme. Nat Rev Mol Cell Biol 15, 225-242.

Roman-Fernandez, A., Roignot, J., Sandilands, E., Nacke, M., Mansour, M.A., McGarry, L., Shanks, E., Mostov, K.E., and Bryant, D.M. (2018). The phospholipid PI(3,4)P2 is an apical identity determinant. Nat Commun 9, 5041.

Rosse, C., Hatzoglou, A., Parrini, M.C., White, M.A., Chavrier, P., and Camonis, J. (2006). RalB mobilizes the exocyst to drive cell migration. Mol Cell Biol 26, 727-734.

Roux, K.J., Kim, D.I., Raida, M., and Burke, B. (2012). A promiscuous biotin ligase fusion protein identifies proximal and interacting proteins in mammalian cells. J Cell Biol 196, 801-810.

Takaishi, M., Makino, T., Morohashi, M., and Huh, N.H. (2005). Identification of human hornerin and its expression in regenerating and psoriatic skin. J Biol Chem 280, 4696-4703.

Varnaite, R., and MacNeill, S.A. (2016). Meet the neighbors: Mapping local protein interactomes by proximity-dependent labeling with BioID. Proteomics 16, 2503-2518.

Wu, Z., Meyer-Hoffert, U., Reithmayer, K., Paus, R., Hansmann, B., He, Y., Bartels, J., Glaser, R., Harder, J., and Schroder, J.M. (2009). Highly complex peptide aggregates of the S100 fused-type protein hornerin are present in human skin. J Invest Dermatol 129, 1446-1458.

Yamanaka, T., Horikoshi, Y., Sugiyama, Y., Ishiyama, C., Suzuki, A., Hirose, T., Iwamatsu, A., Shinohara, A., and Ohno, S. (2003). Mammalian Lgl forms a protein complex with PAR-6 and aPKC independently of PAR-3 to regulate epithelial cell polarity. Curr Biol 13, 734-743.

2.7 Supplemental Figures

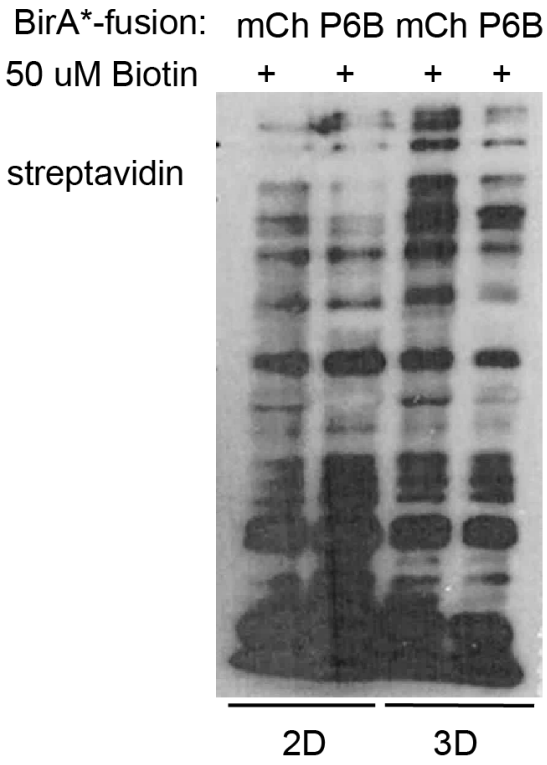

Supplemental Figure S2.1: Validation of BioID approach in 2D and 3D samples. Associated with Figure 2.2. (A) Western blotting showing BirA*-PAR6B and BirA*-mCherry promiscuously biotinylate endogenous proximal proteins in 2D and 3D cell culture samples. The expression levels of identified proteins were determined with streptavidin-HRP.

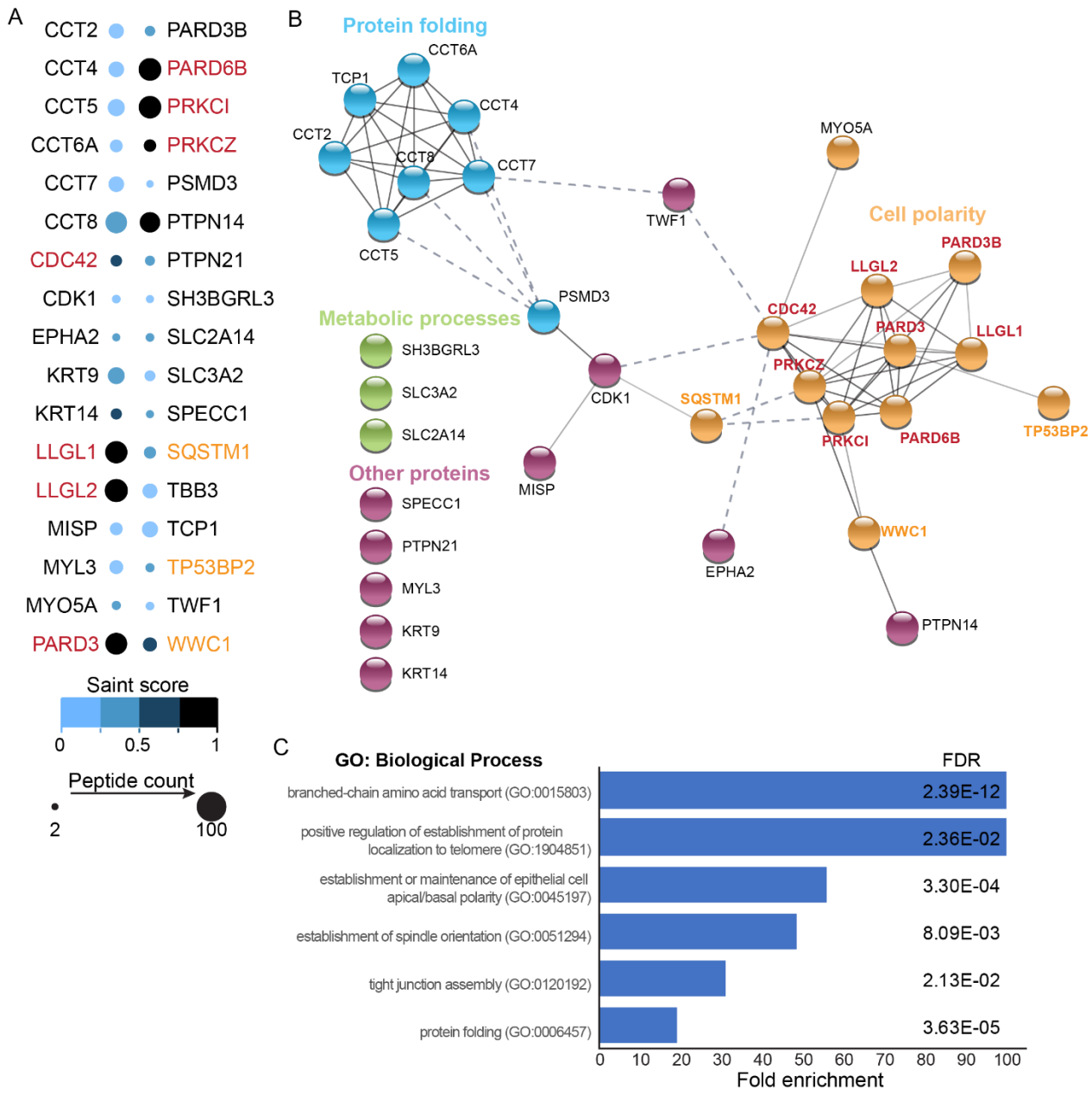
A
CCT2
CCT4
CCT5
CCT6A
CCT7
CCT8
CDC42
CDK1
EPHA2
KRT9
KRT14
LLGL1
LLGL2
MISP
MYL3
MYO5A
PARD3
PARD3B
PARD6B
PRKCI
PRKCZ
PSMD3
PTPN14
PTPN21
SH3BGRL3
SLC2A14
SLC3A2
SPECC1
SQSTM1
TBB3
TCP1
TP53BP2
TWF1
WWC1
Saint score
0
0.5
1
Peptide count
2
100
B
Protein folding
CCT6A
TCP1
CCT4
CCT2
CCT8
CCT7
CCT5
MYO5A
TWF1
Cell polarity
PARD3B
LLGL2
PSMD3
CDC42
PARD3
LLGL1
Metabolic processes
PRKCZ
SH3BGRL3
SLC3A2
SLC2A14
CDK1
SQSTM1
TP53BP2
PRKCI
PARD6B
Other proteins
MISP
SPECC1
PTPN21
MYL3
KRT9
KRT14
EPHA2
WWC1
PTPN14
C
GO: Biological Process
FDR
branched-chain amino acid transport (GO:0015803)
2.39E-12
positive regulation of establishment of protein localization to telomere (GO:1904851)
2.36E-02
establishment or maintenance of epithelial cell apical/basal polarity (GO:0045197)
3.30E-04
establishment of spindle orientation (GO:0051294)
8.09E-03
tight junction assembly (GO:0120192)
2.13E-02
protein folding (GO:0006457)
3.63E-05
0
10
20
30
40
50
60
70
80
90
100
Fold enrichment

Supplemental Figure S2.2: Identification of BirA*-PAR6B vicinal proteins in 2D cell culture samples by proteomics analysis. Associated with Figure 2.3. (A) Saint scores and peptide counts for PAR6B targets identified in 2D BirA*-PAR6B-expressing Caco-2 cells are shown with different color and size, which were analysed by SAINT analysis. BioID was successful at identifying known interaction partners such as CDC42, LGL1/2, PARD3, WWC1, and aPKC, novel vicinal proteins were also identified. (B) The interaction between proteins which were identified in 2D BirA*-PAR6B-expressing Caco-2 cells by BioID based on the STRING database. Line darkness indicates the strength of the predicted relationship between the proteins. (C) Graph showing fold enrichment of different biological processes of BirA*-PAR6B vicinal proteins in 2D samples based on Gene Ontology.

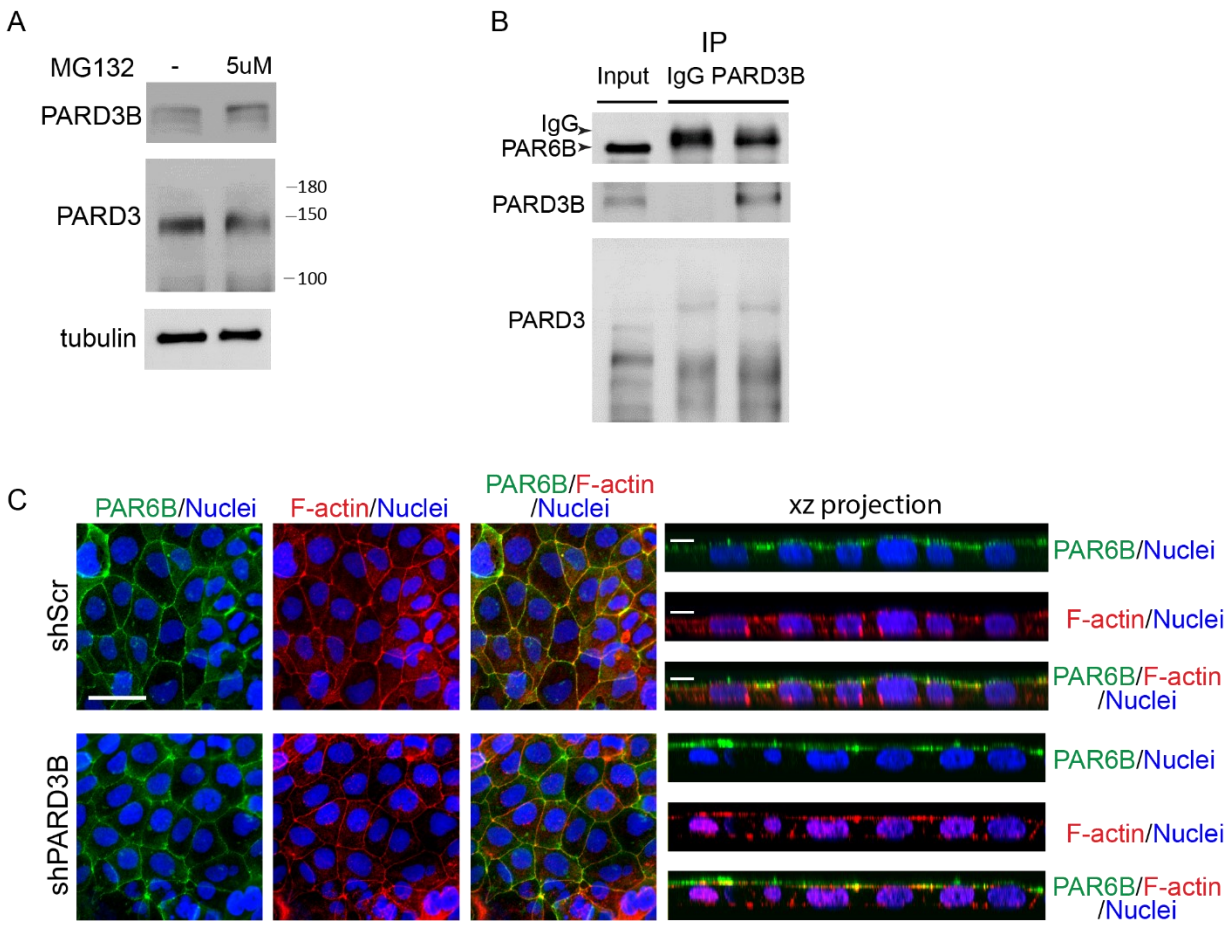

Supplemental Figure S2.3: PARD3B knockdown did not disrupt the morphology of 2D Caco-2 cells. Associated with Figure 2.5. (A) Caco-2 cells were treated with solvent or 5uM proteasome inhibitor MG132 for 24 hrs. The presence of PARD3B, PARD3, tubulin was determined by western blot analysis. (B) Immunoprecipitation were performed with anti-PARD3B in 2D Caco-2 cells. (C) Confocal images were captured for 2D PARD3B knockdown Caco-2 cells immunostained for PAR6B (green) and F-actin (red). Orthogonal slices through a field of cells stained for PAR6B (green) and F-actin (red) in 2D PARD3B knockdown Caco-2 cells. Scale Bars: C, 50μm (left panel); 10μm (right panel).

Conceptual link for Chapter 3

In Chapter 2 I found that the most abundant PAR6B-proximity proteins are known interactors, which is not surprising. However, I detected several proteins with lower peptide spectral counts from mass spectrometry and demonstrated that they have pivotal functions in polarity and lumen formation. Inspired by this, I observed that some proteins did not pass our selection criteria, with a small number of peptides in few replicates, but with a relatively high number of total spectral counts compared to the controls. This drove me to find additional candidates that might have functions in polarity and lumen formation. Manual inspection of these proteins identified CD13 (aminopeptidase N), an apically localized transmembrane protein, with unknown roles in polarity or lumen formation. Interestingly, CD13 has a very short intracellular domain (8 amino acids) with a single lysine residue capable of biotinylation by BioID methods. Given this, it seems unlikely that CD13 would pass typical statistical methods to identify high-probability hits using methods such as Saint analysis. Therefore, based on manual selection of this candidate, I depleted CD13 in epithelial cells to determine if it had a role in epithelial organization or lumen formation. This initial experiment was successful and demonstrated that CD13 was required for polarity orientation. The characterization of CD13 with apical polarity complexes and a role in lumen formation is presented in Chapter 3.

Chapter 3: CD13 orients the apical-basal polarity axis necessary for lumen formation

Authors: Li-Ting Wang[1,2], Abira Rajah[3], Claire M Brown[3,4], Luke McCaffrey[1,2,5,6,7]

[1]Rosalind and Morris Goodman Cancer Research Centre, McGill University, Montreal, Canada
[2]Division of Experimental Medicine, McGill University, Montreal, Canada
[3]Department of Physiology, McGill University, Montreal, Canada
[4]Advanced BioImaging Facility (ABIF) McGill University, Montreal, Canada
[5]Gerald Bronfman Department of Oncology, McGill University, Montreal, Canada
[6]Department of Biochemistry, McGill University, Montreal, Canada
[7]Correspondence: luke.mccaffrey@mcgill.ca

Keywords: cell polarity, apical, Rab11, epithelial cyst, trafficking

Abstract

Polarized epithelial cells can organize into complex structures such as tubes and acini with a characteristic central lumen. Lumen formation requires that cells coordinately orient their polarity axis so that the basolateral domain is on the outside and apical domain inside epithelial structures. We have identified the transmembrane Aminopeptidase N (CD13/APN/ANPEP) as a key determinant of epithelial polarity orientation. CD13 localizes to the apical membrane and associates with an apical complex with Par6 and Pals1, but not Par3. CD13 also associates with Rab11 at the plasma membrane and is decorated by Rab11-endosomes during apical membrane initiation. CD13-deficient cells display inverted polarity in which apical proteins are retained on the outer cell periphery instead of basolateral proteins, have altered Rab11 trafficking patterns, and fail to form a central lumen. We present a model by which CD13 acts as a membrane receptor for Rab11-mediated endocytosis of apical cargo that is necessary to reorient apical proteins from the periphery to internal sites necessary for lumen formation.

3.1 Introduction

Epithelial cells are a major building block of numerous tissues and organs that provide a barrier between tissue compartments and the external environment (Macara et al., 2014). An important property of many epithelial cells is establishing polarity along an apical-basal axis such that the apical membrane faces a lumen that is contiguous with the external environment. This creates a barrier that allows selective vectoral transport of macromolecules for absorption or secretion. In addition, polarized epithelial cells spatially regulate signaling pathways that control diverse cellular properties including stem cell renewal, differentiation, survival, proliferation, metabolism, motility, and adhesion that control tissue growth and organization (Nelson et al., 2013; Rodriguez-Boulan and Macara, 2014; Roignot et al., 2013). Disrupted apical-basal cell polarity and associated signaling pathways is frequent in epithelial malignancies, which account for greater than 80% of human cancers (Halaoui and McCaffrey, 2015a).

Epithelial cells are characterized by the presence of multiple dynamic complexes that associate with unique apical and basolateral membrane domains that are separated by tight junctions (Macara et al., 2014). Many established regulators of apical-basal polarity are multi-domain scaffold and adaptor proteins, that associate with transmembrane proteins that anchor them to the plasma membrane (McCaffrey and Macara, 2012). For example, Crb3 is a transmembrane apical protein that interacts with Pals1, Patj, and Par6 to form an apical Crumbs complex (Roh et al., 2003). Podocalyxin is another apical transmembrane protein that associates with Ezrin, which binds filamentous actin and links the apical membrane to the cytoskeleton (Orlando et al., 2001). Meanwhile, transmembrane junctional proteins bind to Par3 as part of an apical-lateral Par-complex associated with Par6 and aPKC (Horikoshi et al., 2009). Therefore, Par6

is a multi-functional polarity adaptor that can associate with multiple polarity complexes through protein-protein interaction sites including a PDZ domain that binds Pals1 or Par3, a semi-CRIB domain that binds Cdc42, and a PB1 domain forms a heterodimeric PB1-PB1 interaction with aPKC.

Epithelial cells cultured in 3D basement membrane extract rich in laminin are a well-established model of apical-basal polarity (Caplan et al., 1987; Yu et al., 2005). In this model, apical and basolateral proteins are initially co-distributed on the plasma membrane of single cells. Following the first cell division, an apical membrane initiation site (AMIS) is established at the location of the cytokinetic midbody (Fremont and Echard, 2018). Rab-positive recycling endosomes have been identified as important players of apical trafficking (Nokes et al., 2008; Sato et al., 2007; van Ijzendoorn, 2006). Rab-dependent endocytosis internalizes apical membrane proteins and delivers them to the nascent apical domain at the middle cell clusters, thus establishing an apical-basal polarity axis with an internal apical membrane that expands to establish a central lumen. Rab11 is an apically located small GTP-binding protein that plays a central role in transcytosis and recycling of apical proteins for lumen formation in diverse epithelial systems (Bhartur et al., 2000; Bryant et al., 2010b; Casanova et al., 1999; Desclozeaux et al., 2008; Golachowska et al., 2010; Goldenring et al., 1996; Li et al., 2007; Prekeris et al., 2000; Roman-Fernandez and Bryant, 2016; Shaye et al., 2008; Shivas et al., 2010; Winter et al., 2012). For example, Rab11 and the exocyst complex are required for lumen formation by delivering Crb to the apical surface via the Golgi and then apical recycling endosomes (ARE) (Roeth et al., 2009; Schluter et al., 2009a).

Strikingly, depletion of mammalian polarity proteins often results in multi-lumen phenotypes resulting from misoriented cell divisions (Durgan et al., 2011; Hao et al., 2010; Jaffe et al., 2008b). However, the apical-basal polarity axis remains intact with the apical domain oriented towards the interior and the basolateral domain oriented to the periphery of multicellular structures. Notably, inverted (inside-out) polarity is observed in some developmental contexts (e.g., preimplantation embryo) and is associated with metastasis of colorectal cancer cells (Zajac et al., 2018). However, the mechanisms that control the orientation of apical-basal polarity remain to be fully elucidated.

CD13 (Aminopeptidase N, APN) is a type II membrane-bound zinc dependent metalloprotease that is widely expressed on cell surface of epithelial, immune, and fibroblasts. It can also exist as a soluble form in plasma, serum, and urine (Favaloro et al., 1993). CD13 has a short amino-terminal intracellular domain, a helical transmembrane anchor, an extracellular stalk that connects the C-terminal catalytic ectodomain. The peptidolytic ectodomain cleaves terminal amino acids from of peptides in diverse physiological processes including angiotensin activation, amino acid metabolism, ECM degradation, neuropeptide processing, and trimming peptides bound to MHC-II complexes (Bauvois, 2004; Mina-Osorio, 2008; Wong et al., 2012). In contrast, several studies have indicated that CD13 also functions independent of enzymatic activity, including cell-cell adhesion between inflammatory cells, intracellular trafficking in monocytes, and migration of fibroblasts and immune cells (Bauvois, 2004; Chang et al., 2005; Curnis et al., 2000; Pasqualini et al., 2000). Many non-catalytic functions instead require a tyrosine (Y6) in the highly conserved intracellular domain. Y6 can be phosphorylated in a Src-dependent manner, and mutation to phenylalanine abrogates cell adhesion (Mina-Osorio et al.,

2006; Subramani et al., 2013) and β1-integrin recycling during cell migration (Ghosh et al., 2019b). Other non-catalytic functions for CD13 include acting as a receptor for coronaviruses, and it has been used as a receptor for tumor-homing peptides that guide experimental anti-cancer drugs to tumours expressing high levels of CD13 (Bogenrieder et al., 1997; Di Matteo et al., 2011; Guzman-Rojas et al., 2012; Ito et al., 2009; Kehlen et al., 2003; Rocken et al., 2005; Terauchi et al., 2007). In epithelial cells, CD13 localizes to the apical membrane, however its function in this cell type has largely remained elusive.

Here, we characterize CD13 as a novel polarity protein which involved in early polarization, where it is required to promote the association and recruitment of polarity proteins to the emerging apical domain. Our data demonstrate that depletion of CD13 expression impairs the localization of apical traffic protein-Rab11 and impairs transcytosis of apical components, resulting in an inverted apical-basal polarity axis. Collectively, these observations reveal CD13 as a crucial element of the endocytic machinery that controls the site of apical membrane specification and lumen formation.

3.2 Results

3.2.1 CD13 associates with Par6 at the apical membrane.

We identified CD13 in a BioID screen for proteins potentially associating with aPKC and Par6 in Caco-2 cells, an established cellular model to study apical-basal polarity (Durgan et al., 2011; Jaffe et al., 2008b). CD13 was previously reported to localize at the apical membrane in epithelia and its expression increases during apical-basal polarization in Caco-2 cells (Vogel et al., 1992; Wessels et al., 1990). We therefore hypothesized that CD13 may have a role in apical-basal

polarity. We first established that endogenous CD13 and exogenous CD13-V5 were enriched at the luminal membrane of 3D Caco-2 cysts and they colocalized with Par6 and other apical markers (aPKC, Ezrin, Pals1, F-actin) (Figure 3.1 A,B; Supplemental Figure S3.1 A-D). Staining against endogenous CD13 also revealed substantial cytoplasmic staining that persisted following CD13 knock-down, indicating that this is non-specific staining by the antibody (Supplemental Figure S3.1 E). CD13 did not overlap with E-cadherin or ZO-1, indicating that it does not localize to adherens or tight junctions (Supplemental Figure S3.1 F,G).

To determine if CD13 formed a complex with Par6 and/or aPKC, we performed co-immunoprecipitation experiments from 3D Caco-2 cell lysates. These results confirm that CD13 associates with Par6 and aPKC (Figure 3.1 C). Par6 can associate with either Par3 or Pals1 as part of the Par or Crumbs complexes respectively (Joberty et al., 2000; Wang et al., 2004). We detected Pals1 co-precipitating with CD13, whereas we did not detect Par3 in CD13 co-immunoprecipitates. This indicating that CD13 interacts with Par6 as part of the Crumbs complex and is independent of the Par complex (Figure 3.1 D, E). This was confirmed by co-precipitation of CD13 with Crumbs3 (Supplemental Figure S3.1 H). We next wondered if CD13 was required for the association of Par6 with the Crumbs complex. We therefore knocked down CD13 using two independent shRNA and immunoprecipitated Par6. These data revealed that the association of Par6 with Pals1 was reduced by CD13 knockdown, whereas the association between Par6 and aPKC or Par6 and Par3 were not affected (Figure 3.1 F). These data provide further support that CD13 associates with Par6 and the Crumbs complex but not Par3. This is consistent with our localization data showing CD13 enriched in the apical membrane, but not tight junctions, which contain Par3.

As an adaptor, Par6 associates with known partners through conserved protein-protein interaction domains, including PB1, semi-CRIB, and PDZ (Rodriguez-Boulan and Macara, 2014). To determine if the association of CD13 with Par6 was dependent on these regions, we generated Par6 variants with internal deletions of each domain (Figure 3.1 G) and tested their ability to associate with CD13. As expected, $Par6^{\Delta PB1}$ and $Par6^{\Delta PDZ}$ disrupted interactions with aPKC and Pals1, respectively (Figure 3.1 H). Whereas CD13 retained the capacity to associate with $Par6^{\Delta sCRIB}$ and $Par6^{\Delta PDZ}$, it did not associate with $Par6^{\Delta PB1}$ (Figure 3.1 H).

PB1 domains form heterodimeric (PB1-PB1) connections between proteins and mutation of lysine 19 ($Par6^{K19A}$) in the PB1 domain of Par6 disrupts its association with aPKC (Nolan et al., 2008). Since CD13 does not have a PB1 domain, it cannot form a canonical PB1-PB1 interaction with Par6. We therefore wondered if CD13 associated with Par6 through aPKC or by a different mechanism. To test this, we expressed and immunoprecipitated wild-type Par6 or $Par6^{K19A}$. As expected $Par6^{K19A}$ did not associate with aPKC, however, it retained an association with CD13 (Figure 3.1 I). Consistent with our domain-deletion experiments, inactivating point mutations in the semi-CRIB ($Par6^{\Delta P136}$) and PDZ domain ($Par6^{M235W}$) did not impact the association of CD13 with Par6 (Figure 3.1 I). Therefore, CD13 associates with Par6 through the PB1 domain-dependent mechanism that does not require aPKC binding to Par6. Together, these data demonstrate that CD13 localizes to the apical membrane and is part of an apical complex with Par6.

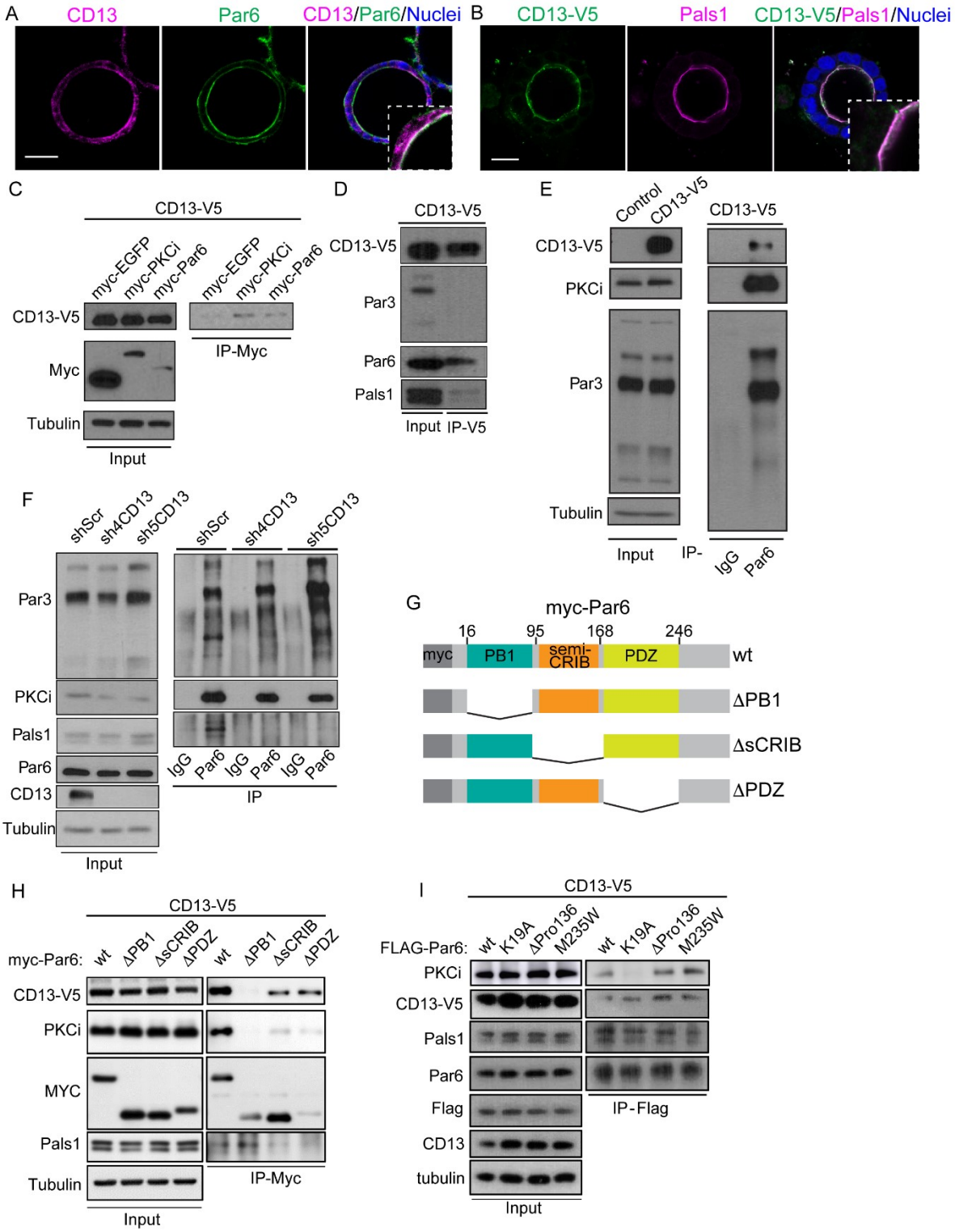
A
CD13
Par6
CD13/Par6/Nuclei
B
CD13-V5
Pals1
CD13-V5/Pals1/Nuclei
C
CD13-V5
myc-EGFP
myc-PKCi
myc-Par6
CD13-V5
Myc
Tubulin
Input
IP-Myc
D
CD13-V5
CD13-V5
Par3
Par6
Pals1
Input
IP-V5
E
Control
CD13-V5
CD13-V5
CD13-V5
PKCi
Par3
Tubulin
Input
IP-
IgG
Par6
F
shScr
sh4CD13
sh5CD13
Par3
PKCi
Pals1
Par6
CD13
Tubulin
Input
IP
G
myc-Par6
16
95
168
246
myc
PB1
semi-CRIB
PDZ
wt
ΔPB1
ΔsCRIB
ΔPDZ
H
CD13-V5
myc-Par6:
wt
ΔPB1
ΔsCRIB
ΔPDZ
CD13-V5
PKCi
MYC
Pals1
Tubulin
IP-Myc
Input
I
CD13-V5
FLAG-Par6:
wt
K19A
ΔPro136
M235W
PKCi
CD13-V5
Pals1
Par6
Flag
CD13
tubulin
IP-Flag
Input

Figure 3.1: CD13 localizes at the apical domain of 3D Caco-2 cysts and associates with PB1 domain of Par6. (A) Confocal images of polarized 3D cysts of cultured Caco-2 cells immunostained for CD13 (magenta) and Par6 (green). (B) Confocal images of polarized 3D cysts of cultured Caco-2 cells immunostained for CD13-V5 (green) and Pals1 (magenta). (C) Co-immunoprecipitation of CD13 and EGFP, PKCι or Par6 was performed with anti-myc in HEK293 cells. The presence of CD13 in immunoprecipitates was determined by western blot analysis. (D) Immunoprecipitation was performed with anti-V5 in stably expressed CD13-V5 Caco-2 cells. (E) Immunoprecipitation was performed with anti-IgG or anti-PAR6 in stably expressed CD13-V5 Caco-2 cells. (F) Immunoprecipitation was performed with anti-PAR6 in shScr, sh4-CD13 and sh5-CD13 knock-down Caco-2 cells. (G) Schematic diagram showing different deletion domains of PAR6. (H) Co-immunoprecipitation of CD13 and wild type or Par6 deletion mutants was performed with anti-myc in HEK293 cells. (I) Co-immunoprecipitation of CD13 and wild type, mutant flag-Par6 (K19A, M235W), or deletion proline 136 was performed with anti-flag in HEK293 cells. Bars: A and B, 50μm.

3.2.2 CD13 is required to orient apical-basal polarity in Caco-2 cells.

A role for CD13 in cell polarity is not known. To investigate if CD13 is involved in lumenogenesis, we examined cyst formation of Caco-2 cells expressing control shRNA (shScr) or two-independent shRNA (sh4-CD13 and sh5-CD13), which efficiently reduced CD13 protein expression by >85% (Figure 3.1 F). After 9 days in culture, control cysts formed with a single prominent lumen, whereas CD13-depleted cysts were significantly smaller and fewer were able to form a single prominent lumen (94% for shScr; 38-43% for shCD13; Figure 3.2 A-C). We attempted to delete CD13 from Caco-2 cells using CRISPR/Cas9, however we were unable to recover viable clones (not shown). To investigate the effect on apical-basal polarity, we immunostained cysts for Par6. Whereas control cysts predominantly localized Par6 internal at the central lumen, CD13-depleted cysts showed diverse localization patterns for Par6 (Figure 3.2 D). Internal (luminal) apical staining was observed in some CD13-depleted structures, which had a single prominent lumen, similar to control cysts (Figure 3.2 E-F). A second phenotype exhibited Par6 localization to the outer edge of CD13-depleted structures (peripheral). Finally, some CD13-depleted structures displayed an intermediate of these two phenotypes (mixed) (Figure 3.2 D-F). In mixed cases, we observed multiple microlumen or misshapen collapsed lumen with weak staining of apical markers (Figure 3.2 E). We confirmed apical reorientation to the periphery of CD13-depleted Caco-2 cysts with an independent apical marker, Ezrin (Figure 3.2 G,H).

In normal polarized epithelial cells, apical and basal markers are mutually exclusive. Since we frequently observed apical markers mis-localized to the outer edge of CD13-depleted cell structures, we wondered if there was mixing of apical and basal proteins or whether apical and basal membranes remained mutually exclusive. β1-integrin-containing complexes localizes to the

basal surface and associate with ECM proteins like laminin (Yu et al., 2005), which was observed in control Caco-2 cysts. In contrast, we observed that β1-integrin was often mis-localized to intercellular patches and laminin was not sequestered around the periphery of CD13-depleted cysts (Figure 3.2 G,I,J). E-cadherin was localized to cell-cell contacts in both control and CD13-depleted cells and therefore not affected by CD13-depletion. Interestingly, in some cases we observed both internal and peripheral apical localization in different cells within the same 3D structure, indicating that polarity orientation is not coordinated between adjacent cells (Supplemental Figure S3.2 A). Collectively, these results indicate that CD13 is required to establish the correct orientation of apical-basal polarity and subsequent lumen formation in Caco-2 cysts.

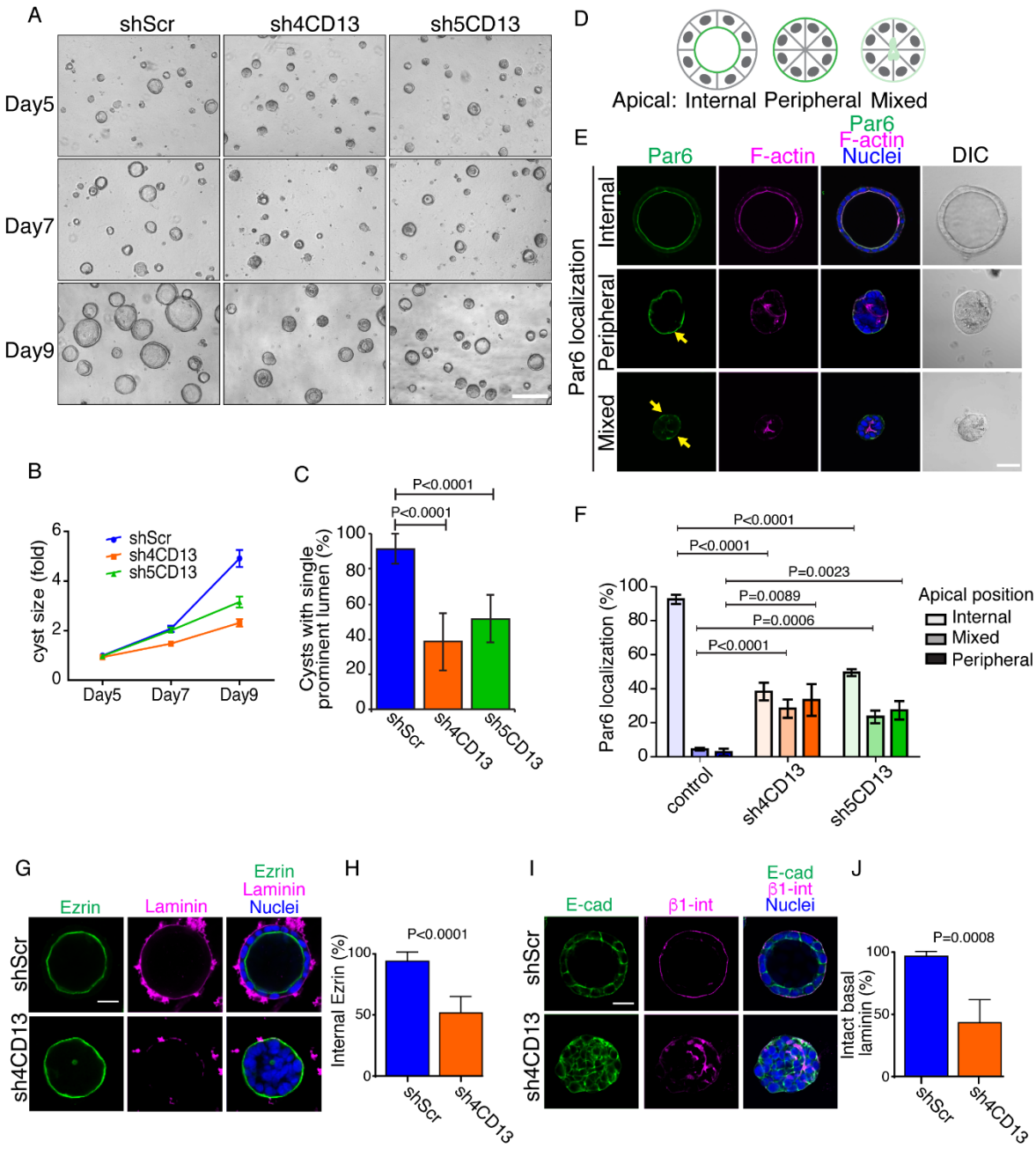
A
shScr
sh4CD13
sh5CD13
Day5
Day7
Day9
B
cyst size (fold)
shScr
sh4CD13
sh5CD13
Day5
Day7
Day9
C
P<0.0001
P<0.0001
Cysts with single prominent lumen (%)
shScr
sh4CD13
sh5CD13
D
Apical: Internal Peripheral Mixed
E
Par6
F-actin
Par6
F-actin
Nuclei
DIC
Par6 localization
Internal
Peripheral
Mixed
F
P<0.0001
P<0.0001
P=0.0023
P=0.0089
P=0.0006
P<0.0001
Par6 localization (%)
Apical position
Internal
Mixed
Peripheral
control
sh4CD13
sh5CD13
G
Ezrin
Laminin
Ezrin
Laminin
Nuclei
shScr
sh4CD13
H
P<0.0001
Internal Ezrin (%)
shScr
sh4CD13
I
E-cad
β1-int
E-cad
β1-int
Nuclei
shScr
sh4CD13
J
P=0.0008
Intact basal laminin (%)
shScr
sh4CD13

Figure 3.2: Knockdown CD13 decreases the size of cysts and mislocalizes apical proteins to the periphery of 3D Caco-2 cysts. (A) Phase contrast images showing the phenotype of shScr, sh4- and sh5-CD13 knock-down in 3D Caco-2 cysts after 5, 7, and 9 days in culture. (B) Quantification of the size of 3D Caco-2 structures for shScr (n=806), sh4-CD13 (n=961) and sh5-CD13 (n=1312) knock-down after 5, 7, and 9 days in culture. (C) Quantification of cysts with single prominent lumen of shScr (n=806), sh4-CD13 (n=961) and sh5-CD13 (n=1312) knock-down in 3D Caco-2 cysts on day 10. (D) The schematic diagram showing different phenotypes (internal, peripheral, mixed) of apical Par6. (E) Images for Par6 (green) and F-actin (magenta) showing different Par6 localization (internal, peripheral, mixed) in 3D Caco-2 cysts. Yellow arrow heads indicate peripheral Par6 localization. (F) Quantification of Par6 localization (internal, peripheral, mixed) of shScr (n=358), sh4-CD13 (=336) and sh5-CD13 (n=187) knock-down in 3D Caco-2 cysts after 10 days in culture. (G) Images for Ezrin (green) and laminin (magenta) showing cells have lost general apical-basal identity in CD13 knock-down 3D Caco-2 cysts. (H) Quantification of internal Ezrin in shScr (n=168) and sh4-CD13 (n=150) 3D Caco-2 cysts after 10 days in culture. (I) Images for E-cad (green) and β1-integrin (magenta) showing cell polarity are disrupted in CD13 knock-down 3D Caco-2 cysts. (J) Quantification of intact basal laminin in shScr (n=71) and sh4CD13 (n=35) 3D Caco-2 cysts after 10 days in culture. Bars: A, 200μm; E, 50μm; G and I, 30μm.

3.2.3 CD13 is required to position apical membrane-initiation site between cells

Lumen formation occurs through initial specification of an apical membrane site that matures into a pre-luminal apical patch (PAP), and then expands to open a luminal cavity (Bryant et al., 2010a). To determine if CD13 was involved in early stages of apical membrane establishment, we first examined CD13 localization in pre-luminal stages when apical-membrane specification occurs. Prior to apical membrane initiation, we observed CD13 at the cell-cell adhesion that was decorated with E-cadherin (Supplemental Figure S3.3 A). The apical membrane initiation site (AMIS) is established by recruitment of apical membrane determinants with coincident displacement of E-cadherin. At this stage, we observed recruitment of CD13 at focal sites of E-cadherin displacement (Supplemental Figure S3.3 Aii, white arrow). The apical foci of CD13 expanded to form a pre-luminal apical patch (PAP), which was strongly anti-correlated with E-cad localization (Supplemental Figure S3.3 A,B).

Since CD13 can associate with Par6, we also investigated their co-localization during apical membrane initiation. Par6 did not colocalize with CD13 at the cell-cell adhesion stage, prior to apical membrane initiation, but was colocalized with CD13 at the AMIS and PAP stages (Figure 3.3 A). Similar results were obtained with Pals1 (Supplemental Figure S3.3 C). The unique localization of CD13 at the cell adhesion followed by its accumulation at the AMIS prompted us to investigate the dynamics of this event in more detail using time-lapse imaging. For this, we expressed mCherry-tagged CD13 (CD13-mCh) and GFP-tagged Par6 (GFP-Par6) in Caco-2 cells, and imaged from single cell stage (before apical membrane initiation) through lumen formation. After the first cell division, CD13-mCh transiently localized to the cell-cell contact surface, confirming our data from fixed images (Figure 3.3 A,B). Cell contact-associated CD13-mCh was

then redistributed diffusely in the cytoplasm and coalesced into puncta that eventually aggregated into a compacted blob that subsequently expanded to form a nascent lumen (Figure 3.3 B). The early CD13-mCh puncta were mostly GFP-Par6-negative, and aggregation of these puncta into a larger single patch was co-incident with GFP-Par6 accumulation (Figure 3.3 C; Supplemental Video S3.1). This result suggests that Par6 may help stabilize CD13 during apical membrane specification and lumen formation. Therefore, these data demonstrate that CD13 accumulates at a site for apical membrane initiation and subsequent lumen formation.

To explore a role for CD13 in apical membrane initiation we examined the consequences of CD13-depletion on cells 24 hrs after seeding. At this time, cells have divided (i.e., 2-cell stage) and 80% of control cells (shScr) have initiated apical membrane specification, as marked by Par6 accumulation at the interior (Figure 3.4 A, B). At this time, some control cells had minor residual Par6 on the periphery, which represent 3D structures that had not yet fully polarized (Figs. 4A, C, and 3A). In contrast, 40-60% of CD13-depleted cells failed to accumulate any Par6 at an internal site and >90% instead retained Par6 on the periphery (Figure 3.4 A-C). This does not result from delayed apical specification at internal sites in 2-cell structures, because we also observed Par6 on the periphery in 4-cell structures when a lumen has initiated in controls, and after 10-days in culture, when control structures have a well-established lumen (Figs. 2E,F, 4A). Similar effects were observed with independent apical markers, Pals1 and Ezrin, and tight junction maker ZO-1 (Supplemental Figure S3.4 A-F).

In the subset of CD13-depleted 2-cell structures with internal Par6 accumulation, we also observed robust Par6 staining on the periphery (Figure 3.4 D). Moreover, we observed that the position of internal Par6 accumulation at internal sites was offset to the side of the 2-cell

structure and not between the nuclei (Figure 3.4 D). To quantify this, we calculated the Par6 Offset Index, in which a value of 1 represents the middle of the structure, and values approaching 0 are displaced towards the periphery (Figure 3.4 E). This reveals that whereas control cells typically accumulate Par6 at the center of 2-cell structures (Offset $Index_{shScr}$ = 0.91 +/- 0.1), internal Par6 accumulation is offset towards the periphery of CD13-depleted 3D structures (Offset $Index_{shCD13\text{-}4}$ = 0.19 +/- 0.16); Figure 3.4 E,F).

Previous studies reported that the cytokinetic midbody positions the apical membrane initiation site (Li et al., 2014; Schluter et al., 2009a; Wang et al., 2014). Therefore, we examined whether the midbody position was affected by CD13 knockdown. We did not observe apoptosis or multi-nucleated cells in control or CD13-knockdown, indicating that cell-division per se was not blocked under these conditions (not shown). In control cells, the midbody formed between nuclei at the middle of 2-cell structures (Offset $Index_{shScr}$ = 0.82 +/- 0.19) with Par6 accumulating at the center of the midbody. In contrast the midbody in CD13-depleted cells was displaced towards the cell edge (Offset $Index_{shCD13\text{-}4}$ = 0.35-0.45 +/- 0.32-0.35) and Par6 did not accumulate at the midbody (Figure 3.4 G-I) indicating that trafficking of proteins to initiate apical membrane at the midbody was impaired. Collectively, these data indicate that CD13 is required to direct apical membrane components to the midbody to initiate internal apical membrane formation.

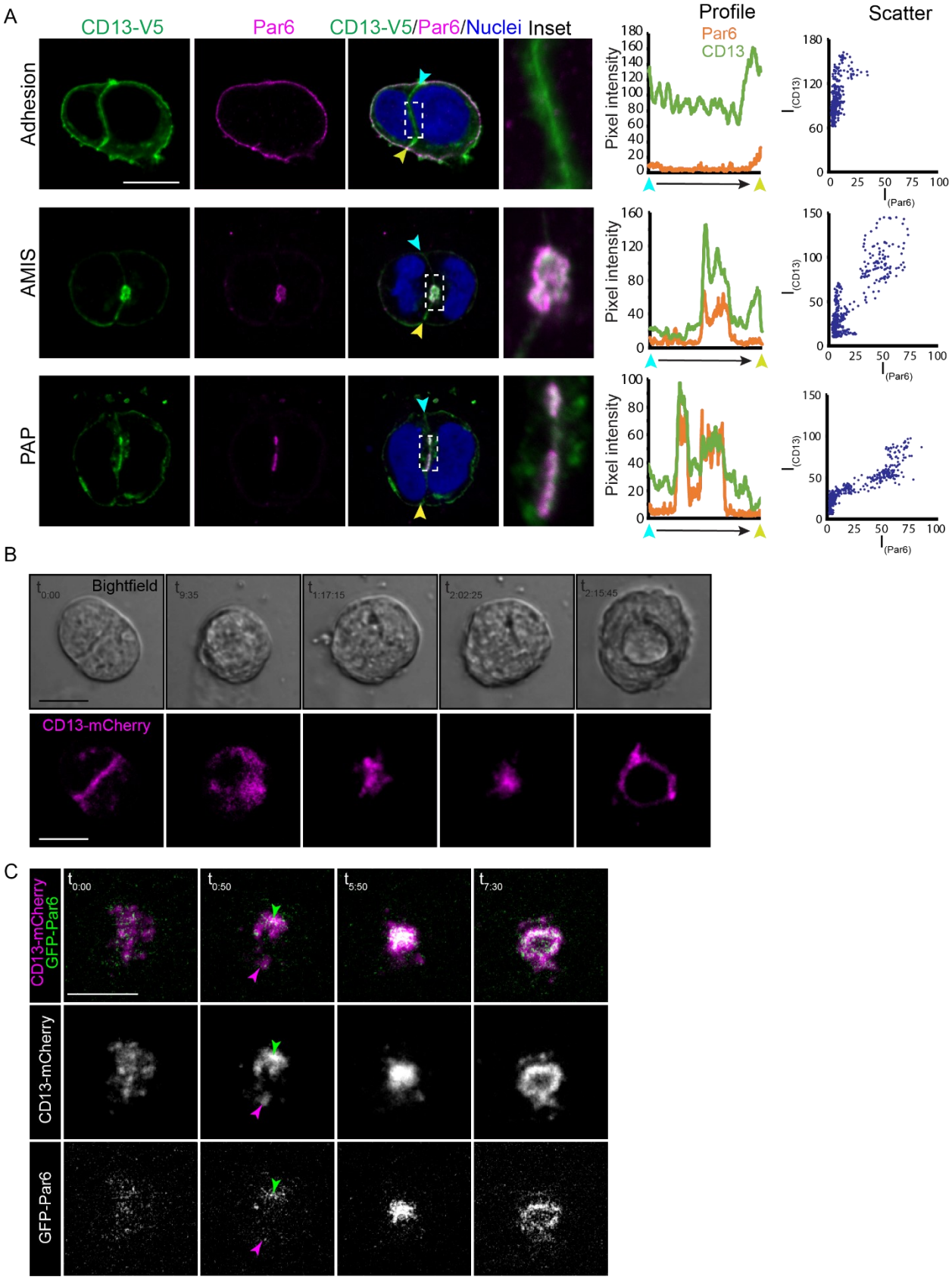
A
CD13-V5
Par6
CD13-V5/Par6/Nuclei
Inset
Profile
Scatter
Adhesion
AMIS
PAP
Par6
CD13
Pixel intensity
I(CD13)
I(Par6)
B
Bightfield
CD13-mCherry
C
CD13-mCherry
GFP-Par6

Figure 3.3: CD13 is recruited to the apical membrane-initiation site before Par6 in 3D Caco-2 cysts. (A) Left-confocal images for CD13-V5 (green) and Par6 (magenta) showing the localization of CD13 and Par6 at adhesion, AMIS, and PAP stage in 2-cell 3D Caco-2 structures. Middle-Profiles depicting fluorescent intensity (8-bit) of Par6 and CD13 along the cell-cell edge from blue to yellow arrows. Right-Scatter plots showing the relationships between Par6 and CD13 pixel intensities. (B) DIC/fluorescence images showing selected frames from time-lapse series during cell polarization of 3D cultured Caco-2 cells. Images were captured every 25 min for 62 hrs. (C) Fluorescence images showing selected frames from a time-lapse series of CD13-mCh and GFP-Par6 in Caco-2 3D structures. Cells were virus-infected with CD13-mCherry and EGFP-Par6 in 2D culture and transferred to 3D culture to perform live imaging. Images were captured every 25 min for 8 h Green and magenta arrows show the colocalization of Par6 and CD13. Bars: A, B, 10µm.

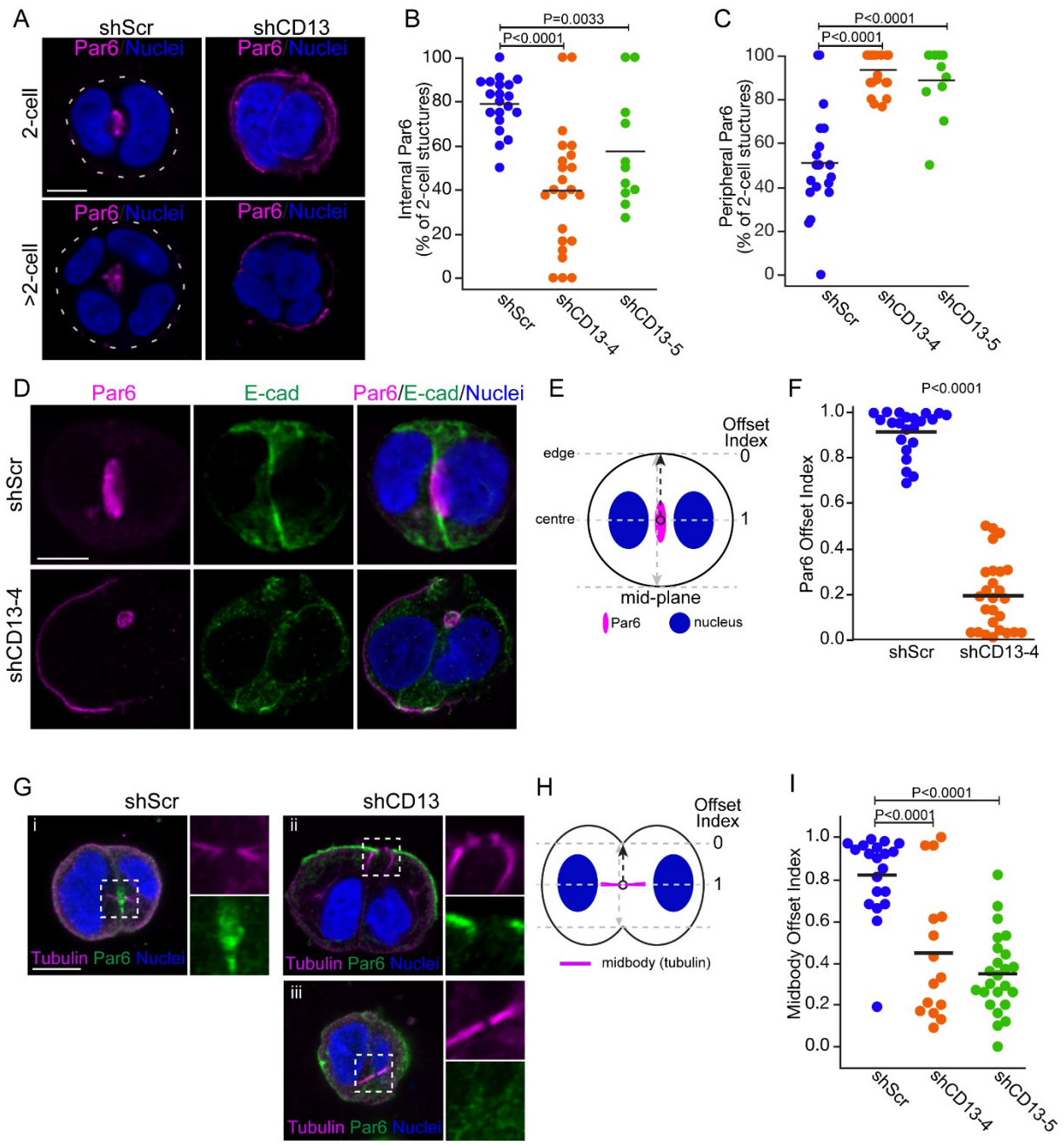
A
shScr
shCD13
Par6/Nuclei
2-cell
>2-cell
B
P=0.0033
P<0.0001
Internal Par6 (% of 2-cell stuctures)
shScr
shCD13-4
shCD13-5
C
P<0.0001
P<0.0001
Peripheral Par6 (% of 2-cell stuctures)
D
Par6
E-cad
Par6/E-cad/Nuclei
shCD13-4
E
Offset Index
edge
centre
mid-plane
Par6
nucleus
F
P<0.0001
Par6 Offset Index
G
Tubulin Par6 Nuclei
H
midbody (tubulin)
I
Midbody Offset Index

Figure 3.4: Depletion of CD13 disrupts early polarization of 3D Caco-2 cysts by mislocalizing Par6 and the midbody. (A) Confocal images of Par6 (magenta) in control (shScr) and CD13 knock-down 3D Caco-2 structures. (B and C) Quantification of the percentage of 3D structures with internal (B) and peripheral (C) Par6 localization in control shScr (n=173), sh4-CD13 knock-down (n=151) and sh5-CD13 knock-down (n=89) 3D Caco-2 structures. (D) Confocal images of Par6 (magenta) and E-cad (green) in control and CD13 knockdown 3D Caco-2 structures. (E) Diagram showing the offset index of Par6 in 2-cell 3D Caco-2 structures. A value of one indicates a midbody at the centre of the 3D structure, and values approaching 0 represent midbody positioned closer to the edge. (F) Quantification of Par6 offset index from shScr (n=22) and sh4-CD13 knock-down (n=26) 2-cell 3D Caco-2 structures. (G) Confocal images of tubulin (magenta) and Par6 (green) in 2-cell 3D Caco-2 structures. (H) Diagram showing the offset index of the midbody. for the edge and the centre (where midbody locates) on 2-cell structure. (I) Quantification of midbody offset index from shScr (n=20), sh4-CD13 knock-down (n=15) and sh5-CD13 knock-down (n=24) on 2-cell 3D Caco-2 structures. Bars: A, D, G, 10µm.

3.2.4 CD13 associates with Rab11 and directs protein trafficking

The Rab family of GTPases have important roles in vesicle trafficking, and the Rab11 family plays a vital role in transcytosis and lumenogenesis (Bryant et al., 2010b; Casanova et al., 1999; Desclozeaux et al., 2008; Li et al., 2007; Roman-Fernandez and Bryant, 2016; Shaye et al., 2008). In migrating cells, CD13 was also shown to regulate integrin endocytosis by Rab11 (Ghosh et al., 2019a). To determine if CD13 may influence Rab11-dependent endocytosis during epithelial polarization, we first investigated the localization of CD13 and Rab11 during apical membrane initiation in Caco-2 cells. In single cells prior to polarization, we observed partial colocalization of CD13 and Rab11 at the plasma membrane and some vesicles (Figure 3.5 A). During apical membrane initiation (AMIS), Rab11 was observed diffusely surrounding CD13, which became more concentrated to a ring of Rab11 that decorated the edge of CD13 in the pre-luminal apical patch (PAP) (Figure 3.5 A). This localization pattern demonstrates that CD13 accumulation at the future apical membrane site precedes Rab11. Therefore, we examined whether Rab11 trafficking was influenced by CD13 during apical membrane initiation and lumen formation. In control cells, Rab11 was distributed to the plasma membrane in single cells, which was redistributed to areas between the nuclei and accumulated adjacent to Par6-positive apical membrane in 2-cell structures and at later stages (>2 cells) when the lumen begins to form (Figure 3.5 B, C). In CD13-depleted cells, Rab11 was also distributed at the plasma membrane in single cells, but failed to accumulate between nuclei of 2-cell and >2-cell structures, instead it accumulated with no obvious pattern, and often at multiple sites that were not necessarily adjacent to Par6-positive apical membrane (Figure 3.5 B, C). Using live imaging, we observed that accumulation of Rab11 occurred within a similar timescale between control and CD13-depleted samples (Figure 3.5 D;

Supplemental Video S3.2; Supplemental Video S3.3), suggesting that CD13 does not control the kinetics of Rab11 accumulation, but is necessary for correct positioning of Rab11 to the center of structures.

To determine if CD13 could associate with Rab11, we first co-expressed GFP-Rab11 and CD13-V5 in HEK293 or Caco-2 and performed co-immunoprecipitation experiments. From this data, we observed Rab11 in CD13 precipitates supporting a potential association between the two proteins (Figure 3.5 E, 6E). To determine if CD13 and Rab11 were associated at the plasma membrane of Caco-2 cells, we performed temporal image correlation microscopy (tICM) to investigate the correlated dynamics of GFP-tagged Rab11 and mCherry-tagged CD13 in time and space using total internal reflectance fluorescence (TIRF) microscopy. ICM relies on the coupled fluctuations of two different-colored fluorescent molecules moving in and out of the illumination beam and can determine if two different molecules associate in a physical complex, but cannot reveal direct binding. Whereas the cross-correlation amplitude between GFP control and CD13-mCherry was negligible, we observed a high cross correlation amplitude between GFP-Rab11 and CD13-mCherry (Figure 3.5 F-H). These results indicate that CD13 associates with Rab11 and is required for Rab11 accumulation at internal apical membrane sites.

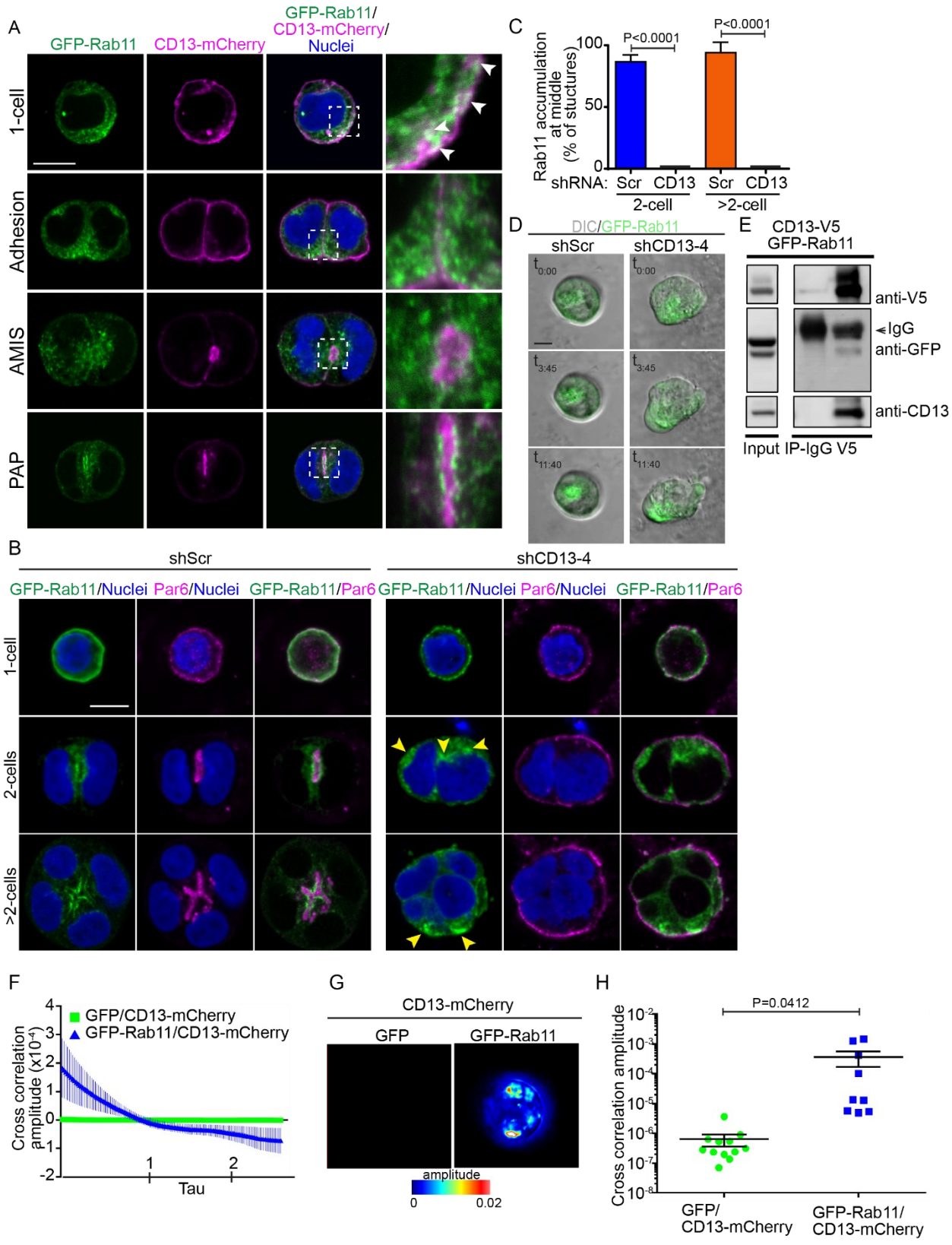
A
GFP-Rab11
CD13-mCherry
GFP-Rab11/
CD13-mCherry/
Nuclei
1-cell
Adhesion
AMIS
PAP
C
Rab11 accumulation at middle (% of stuctures)
100
50
0
P<0.0001
P<0.0001
shRNA: Scr CD13 Scr CD13
2-cell
>2-cell
D
DIC/GFP-Rab11
shScr
shCD13-4
t0:00
t3:45
t11:40
E
CD13-V5
GFP-Rab11
anti-V5
IgG
anti-GFP
anti-CD13
Input IP-IgG V5
B
shScr
shCD13-4
GFP-Rab11/Nuclei Par6/Nuclei GFP-Rab11/Par6
1-cell
2-cells
>2-cells
F
GFP/CD13-mCherry
GFP-Rab11/CD13-mCherry
Cross correlation amplitude (x10-4)
Tau
G
CD13-mCherry
GFP
GFP-Rab11
amplitude
0
0.02
H
P=0.0412
Cross correlation amplitude
GFP/
CD13-mCherry
GFP-Rab11/
CD13-mCherry

Figure 3.5: Knockdown CD13 disrupts early polarization by mislocalizing Rab11 to the periphery of 3D cultured Caco-2 cells. (A) Confocal images for GFP-Rab11 (green) and CD13-mCherry (magenta) showing the relative localization of CD13 and Rab11 at 1-cell, and adhesion, AMIS, and PAP stage in 2-cell 3D Caco-2 structures. White arrow shows the colocalization of Rab11 and CD13. (B) Confocal images of GFP-Rab11 (green) and Par6 (magenta) showing Rab11 mislocalizing to the periphery in CD13 knock-down 3D Caco-2 cysts. Yellow arrow shows the mislocalized Rab11. (C) Quantification of the percentage of Rab11 accumulation at the middle of shScr (n=92) and shCD13 (n=24) at 2 cell and >2 cell 3D Caco-2 structures. (D) DIC/confocal images showing selected frames from time-lapse series of shScr and shCD13-4 3D Caco-2 structures. Images were captured every 25 min for 12 h. (E) Co-immunoprecipitation of CD13-V5 and GFP-Rab11 was performed with anti-V5 in HEK293 cells. The presence of Rab11 in immunoprecipitates was determined by western blot analysis using anti-GFP. (F) Relative cross correlation amplitude profile of cells co-expressing GFP or Rab11-GFP and CD13-mCherry fusions over time. Tau represents the time separation between two acquired images. (G) Co-binding intensity profile of Caco-2 cells co-expressing GFP (n=12) or Rab11-GFP (n=9) with CD13-mCherry. (H) Relative cross correlation amplitude profile of cells co-expressing GFP (n=18) or Rab11-GFP (n=17) with CD13-mCherry fusions at the first time-point. Bars: A, 50µm; C, 10µm; F, 5µm.

3.2.5 The CD13 intracellular domain is required to orient apical-basal polarity

Next, we examined regions of CD13 that were required for polarization in Caco-2 cells. CD13 has an extracellular M1 peptidase domain and a short N-terminal intracellular domain. To evaluate whether peptidase activity was necessary for CD13 polarity functions, we conducted rescue experiments in CD13 depleted cells using vectors that expressed wild-type CD13 or a series of catalytically inactive mutants (H388A, H392A, or E411A) and examined polarity orientation (Figure 3.6 A). In all cases polarity orientation was restored, indicating that CD13 catalytic activity is not essential for orienting apical-basal polarity (Figure 3.6 B,C, Supplemental Figure S3.5 A,B). Tyrosine (Y6) within the intracellular domain was previously reported to be necessary for some non-catalytic functions of CD13 (Subramani et al., 2013). We therefore investigated if this residue was also necessary to establish the orientation of apical-basal polarity in Caco-2 cysts by re-expressing wild-type or Y6 mutant (Y6F) in control and CD13-depleted cells. Whereas wild-type CD13 was able to restore the correct apical polarity orientation, Y6F failed to restore polarity orientation (Figure 3.6 B,C). CD13 containing other mutations within the intracellular domain were also able to restore polarity orientation, demonstrating specificity of the tyrosine residue (Figure 3.6 A-C, Supplemental Figure S3.5 A,B).

We extended these studies to evaluate CD13-Y6F at early stages when apical membrane is initiated at internal sites (2-cell). Consistent with our above data, the CD13-Y6F mutant was deficient in restoring internal apical sites in CD13-depleted cells (Figure 3.6 D). Interestingly, we did not observe mis-oriented polarity in control cysts with endogenous CD13 that express CD13-YF6, indicating that it does not behave as a dominant negative protein (Figure 3.6 B-D). Moreover, we observe in both early (2-cell) and mature (>10 cells) 3D structures, that CD13-Y6F was

localized to intracellular vesicles instead of the outer plasma membrane and did not overlap with or associated with endogenous Par6 (Figure 3.6 D, E). Therefore, these results indicate that the Tyr-6 is required for CD13 localization to the plasma membrane and association with Par6.

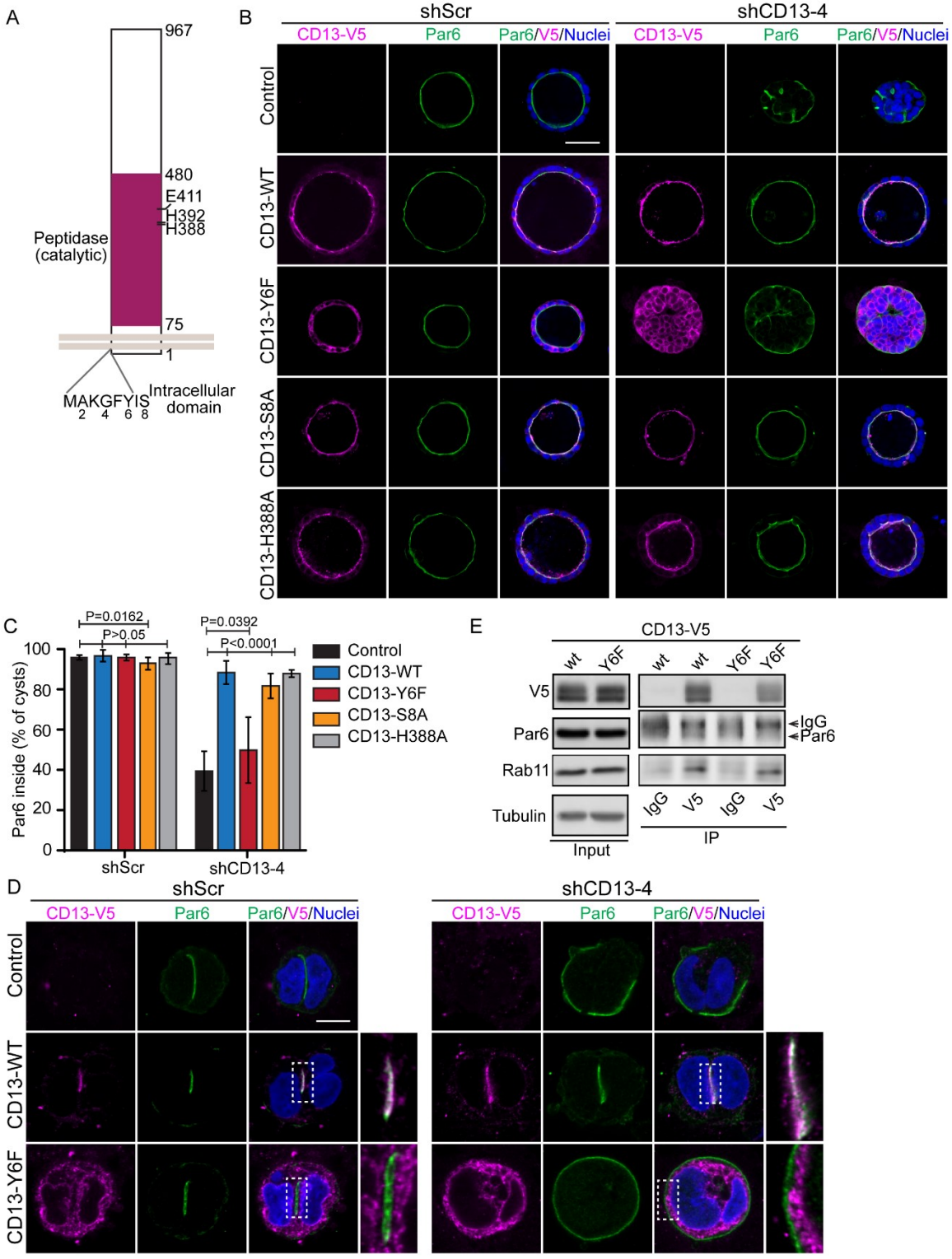
A
967
480
E411
H392
H388
Peptidase
(catalytic)
75
1
MAKGFYIS
2 4 6 8
Intracellular
domain
B
shScr
shCD13-4
CD13-V5
Par6
Par6/V5/Nuclei
Control
CD13-WT
CD13-Y6F
CD13-S8A
CD13-H388A
C
P=0.0162
P>0.05
P=0.0392
P<0.0001
Par6 inside (% of cysts)
100
80
60
40
20
0
shScr
shCD13-4
Control
CD13-WT
CD13-Y6F
CD13-S8A
CD13-H388A
D
shScr
shCD13-4
CD13-V5
Par6
Par6/V5/Nuclei
Control
CD13-WT
CD13-Y6F
E
CD13-V5
wt
Y6F
V5
Par6
Rab11
Tubulin
IgG
Par6
Input
IP
IgG
V5

Figure 3.6: The intracellular domain of CD13 is required to maintain apical-basal polarity. (A) Schematic diagram showing mutation sites at intracellular and peptidase domain of CD13. (B) Images for CD13-V5 (magenta) and Par6 (green) showing the rescue phenotype in wild type and different CD13 mutants of shScr and shCD13 3D Caco-2 cysts. (C) Quantification of the percentage of Par6 internally in wildtype (shScr, n =515; shCD13, n=292), CD13-Y6F (shScr, n=462; shCD13, n=433), CD13-S8A (shScr, n=541; shCD13, n=333), and CD13-H388A (shScr, n=452; shCD13, n=336) of shScr (n=428) and shCD13 (n=492) 3D Caco-2 cysts. (D) Images for CD13-V5 (magenta) and Par6 (green) showing the rescue phenotype in wild type and CD13-Y6F mutant of shScr and shCD13 3D Caco-2 cysts on 2-cell structures. (E) Immunoprecipitation was performed with anti-IgG or anti-V5 in stably expressed CD13-wild type or CD13-Y6F Caco-2 cells. Bars: B, 50µm, D, 10µm.

3.3 Discussion

Together, our results demonstrate that CD13 (also known as APN and ANPEP) is a novel factor that controls epithelial lumen formation by directing the orientation of apical-basal polarity. Silencing of CD13 induced an inverted polarity phenotype in Caco-2 cysts, which was characterized by apical complexes and tight junctions positioned at the periphery of cell aggregates, while basolateral proteins were excluded from the outer edge and interactions with the matrix were impaired (Figure 3.7 A). The formation of a central lumen requires precise coordination of multiple intra- and intercellular events that establish a polarity axis, position apical determinants between cells, and separate cell-cell contacts to expand a central luminal cavity (Blasky et al., 2015; Bryant et al., 2010b; Datta et al., 2011; Fremont and Echard, 2018). This architecture is essential for normal tissue function and epithelial homeostasis and is frequently disrupted or lost in diseases including cancer (Halaoui and McCaffrey, 2015b; Saito et al., 2018).

Par6 can associate with two apically directed polarity complexes: The Par complex by binding Par3 at tight-junctions, or the Crumbs complex through Pals1 and Crumbs3 at the apical membrane (Joberty et al., 2000; Wang et al., 2004). Our results show that CD13 is an apical protein, which is supported by previous studies showing that CD13 localizes to the apical brush border (Fairweather et al., 2012; Riemann et al., 1999). We extend this to demonstrate that CD13 associates with an apical complex containing Par6, aPKC, Pals1, and Crb3, but not Par3 (Figure 3.7 B). This interaction requires the PB1-domain of Par6 and the intracellular domain of CD13. Although Par6 interacts with aPKC through its PB1 domain (Wilson et al., 2003), a point-mutation in the PB1-domain of Par6 that disrupted its interaction with aPKC retained the capacity to

associate with CD13. Moreover, deletion or mutation of other protein-protein interaction domains within Par6 that mediate its known interactions (Rodriguez-Boulan and Macara, 2014) also retained the ability to associate with CD13. Therefore, we conclude that Par6 either binds CD13 directly through its PB1 domain, or indirectly through an unidentified intermediate. Efforts to detect a direct interaction between purified Par6 and a peptide of the CD13 intracellular domain were unsuccessful (data not shown), and we cannot distinguish these possibilities at present. Therefore, CD13 associates with an apical Crumbs complex containing Par6.

Our imaging data reveal that CD13 is dynamically localized during apical membrane initiation and lumen formation in a pattern that is distinct from other apical proteins. In non-polarized cells, apical proteins are distributed to the cell periphery and re-distributed to the midbody thorough Rab11-mediated endocytosis to form an apical membrane initiation site that marks the position of the future lumen (Jaffe et al., 2008a; Roman-Fernandez and Bryant, 2016; Schluter et al., 2009b; Wang et al., 2000). While CD13 also localized to the periphery in non-polar cells, unlike other apical proteins, it temporarily localized to the cell-cell adhesion that is also positive for E-cadherin. CD13 then redistributed through vesicles that accumulated internally, co-incident with delivery of other apical proteins that converged to establish an internal apical membrane site that excludes E-cadherin (Figure 3.7 C).

Cell division represents the earliest known symmetry breaking event to position a central lumen in 3D cysts and *in vivo* (Cerruti et al., 2013; Mangan et al., 2016; Rathbun et al., 2020). However, the cues that initiate internalization of apical proteins from the periphery to establish an internal apical site are currently unknown. We propose that CD13 represents this long sought-after factor, which regulates Rab11-dependent endocytosis of apical proteins necessary to

establish an internal lumen. In support of this model, our results show that CD13 colocalizes and associates with Rab11 in the peripheral plasma membrane and a subset of vesicles in non-polarized cells. Second, Rab11-postive endosomes are recruited to and decorate CD13 patches at internal sites. Third, in the absence of CD13, cells fail to internalize apical proteins and redistribute them to the midbody. Forth, Rab11 is mislocalized and does not accumulate at a single internal site in CD13-deficient cells. Therefore, based on our results, it is likely that CD13 acts at multiple steps in orienting apical-basal polarity with a major role as a membrane cue for Rab11-dependent apical protein endocytosis.

Rab11 is required for mitotic spindle orientation through affecting dynein-dependent endosome localization at poles (Hehnly and Doxsey, 2014). Rab11 also plays an important role in regulating the trafficking of proteins for cell abscission and loss of Rab11 causes cytokinetic failure and multinucleated cells (Mangan et al., 2016). We did not observe cytokinetic deficiencies or multinucleated cells in our experiments, indicating that CD13 regulates a subset of Rab11-dependent endocytic events, likely restricted to apical membrane trafficking in epithelial cells. However, we cannot exclude other trafficking roles for CD13 that are context specific. For example, in mouse embryonic fibroblasts, CD13 is required for endocytosis of β1-integrin to Rab11-positive endosomes during cell migration (Ghosh et al., 2019b).

Although cell division appeared able to proceed in CD13-deficient cells, we did observe asymmetric placement of the midbody away from the center of cell aggregates. Interestingly, the relationship between the apical domain and midbody is bi-directional. In addition to the midbody serving to direct endocytic trafficking of apical proteins, apical proteins also direct the position of the midbody, and depletion of some apical proteins can cause displacement of the midbody

that leads to ectopic lumen formation (Jaffe et al., 2008b; Lujan et al., 2016). In the context of CD13, we speculate that apical membrane retained at the periphery of cell aggregates may cause the midbody to be pulled away from the center, although alternatives where CD13 more directly controls midbody position are also possible.

Our data indicate that catalytic activity of CD13 is dispensable for its role in organizing apical-basal polarity. However, the tyrosine residue within the short intracellular domain (Tyr6) is specifically required to establish an internal apical domain and lumen. Consistent with this, other studies have found the same tyrosine residue is required for non-catalytic functions, including cell adhesion and migration (Ghosh et al., 2019b; Subramani et al., 2013), indicating that this residue may have diverse roles in regulating diverse functions through the intracellular domain. Our results reveal that Y6 was necessary for the association with Par6 whereas this residue was dispensable for CD13 to associate with Rab11. This supports a role for CD13 in linking the apical polarity complex to Rab11 at the plasma membrane to allow apical protein endocytosis. As a model, we propose that CD13 associates with the apical Crumbs complex through Par6, which acts as a surface receptor to recruit Rab11 (Figure 3.7 C step 1). Rab11 then mediates the internalization of apical proteins into endosomes (Figure 3.7 C step 2). Rab11 then delivers apical proteins to midbody, which coalesce with CD13 to establish an internal apical site necessary for lumen formation (Figure 3.7 C step 3). Since Rab11-positive endosomes accumulate on the edge of CD13 patches, we hypothesize that CD13 may also capture or retain apical endosomes at this site with newly delivered apical proteins. This model is supported by our detailed microscopic and live imaging analysis.

In summary, our study identifies CD13 as an essential protein required for symmetry breaking by enabling endocytosis of apical proteins for redistribution to an internal position necessary for lumen formation.

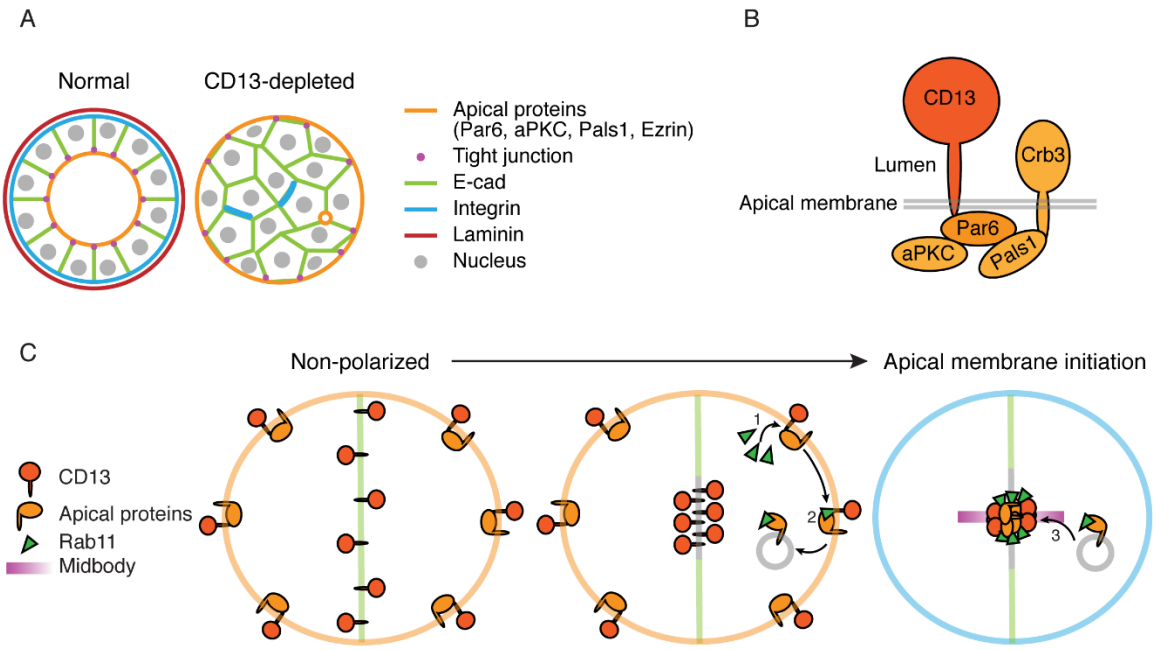

Figure 3.7: Proposed model for CD13 functions in apical specification in Caco-2 cells (A) Organization of control Caco-2 3D structures displaying apical-basal polarity and epithelial organization, and CD-13-depleted cells showing inverted apical-basal polarity and impaired lumen formation. (B) CD13 associates with apical complex containing Par6, aPKC, Pals1, and Crb3. (C) Proposed events by which CD13 functions to establish the orientation of apical-basal polarity. See discussion for a further explanation.

3.4 Materials and Methods

3.4.1 Cell culture

The Caco-2 human intestinal epithelial cell line was purchased from American Type Culture Collection (HTB-37). Caco-2 cells were cultured at 37°C in 5% CO_2 in DMEM (Wisent #319-005-CL) supplemented with 10% fetal bovine serum (Wisent #080-150), 100 U/ml penicillin, 0.1 mg/ml streptomycin (Wisent #450201EL). For 3D culture, Caco-2 cells were seeded in 8-well µ-slides (Ibidi #80826) at a density of 1.25 $x10^4$ cells per well on top of a thin layer of 100% GelTrex (ThermoFisher Scientific #A1413202) in media supplemented 2% GelTrex. After one or ten days in adherent culture, cells were collected for immunofluorescence. Human embryonic kidney cell line HEK293LT (ATCC), were cultured at 37°C in 5% CO_2 in DMEM supplemented with 10% fetal bovine serum, 100 U/ml penicillin, 0.1 mg/ml streptomycin.

3.4.2 DNA and shRNA constructs

The pLX317-CD13-V5 plasmids were purchased from Sigma (TRCN, CD13 TRCN0000476147). pK-myc-Par6C was a gift from Ian Macara (Addgene plasmid # 15474). pWPI was a gift from Didier Trono (Addgene plasmid #12254). GFP-Rab11 were provided by Robert Lodge. pSecTag_Myc-CRB3A were provided by Patrick Laprise. pWPI-myc-EGFP, pWPI-myc-aPKCι, pWPI-myc-Par6, pWPI-CD13-mCh, pWPI-EGFP-Par6, pWPI-flag-Par6wt were obtained by subcloning cDNA products to pWPI. pLX317-CD13^{Y6F}-V5, pLX317-CD13^{Y6E}-V5, pLX317-CD13^{S8A}-V5, pLX317-CD13^{S8D}-V5, pLX317-CD13^{H388A}-V5, pLX317-CD13^{H392A}-V5, pLX317-CD13^{E411A}-V5, pK-myc-Par6C$^{\Delta 16-95}$, pK-myc-Par6C$^{\Delta 95-168}$, pK-myc-Par6C$^{\Delta 168-246}$, pWPI-flag-Par6^{K19A}, pWPI-flag-Par6$^{\Delta Pro136}$, and pWPI-flag-Par6^{M235W}were generated using the QuikChange II site directed mutagenesis kit according to manufacturer's instructions (Agilent #200523).

shRNAs targeting human *CD13* mRNA were cloned in pLKO. Lentiviral supernatants were produced in HEK293LT cells as described previously. Caco-2 cells were infected with lentiviral supernatants and selected by the addition of 20 μg/ml puromycin for 10 days.

The shRNA used were acquired from the McGill Platform for Cellular Perturbation (MPCP) sh1CD13 CCGGCCCTCTTCATTCACTTCAGAACTCGAGTTCTGAAGTGAATGAAGAGGGTTTTTG, sh2CD13 CCGGCCTCAATGTGACGGGCTATTACTCGAGTAATAGCCCGTCACATTGAGGTTTTTG, sh3CD13 CCGGCCTGAGCTACTTCAAGCTCATCTCGAGATGAGCTTGAAGTAGCTCAGGTTTTTG, sh4CD13 CCGGCCACAGCAAGAAGCTCAACTACTCGAGTAGTTGAGCTTCTTGCTGTGGTTTTTG, sh5CD13 CCGGGTGACCATAGAGTGGTGGAATCTCGAGATTCCACCACTCTATGGTCACTTTTTG) and a non-targeting scrambled shRNA was used as a control.

3.4.3 Transient transfection

HEK293LT cells were seeded at 2×10^6 cells per well in 100mm dishes and transfected with plasmids using Polyethylenimine (PEI) as per manufacturer's instructions (Sigma # 408727). Caco-2 cells were seeded at 4×10^4 cells per well in 24 well and transfected with plasmids using Lipofectamine LTX as per manufacturer's instructions (Invitrogen #15338030). All experiments were performed 24 h post-transfection.

3.4.4 Lentivirus production

Lentivirus was produced using calcium phosphate transfection of HEK293LT cells in 15-cm dishes with 50 μg of lentiviral plasmid, 37.5 μg of packaging plasmid (psPAX2), and 15 μg of VSVG coat protein plasmid (pMD2.G). Viral supernatants were collected after 48 hrs and were concentrated by precipitation in 40% polyethylene glycol 8000 (Bioshop # PEG800.1) followed by

centrifugation and then re-suspended in the culture medium. Concentrated virus was aliquoted and frozen at -80°C, then an aliquot was titred in HEK293LT cells.

3.4.5 Immunoblotting and immunoprecipitation

Cells were lysed in RIPA lysis buffer (50 mM Tris-HCl, pH 8, 0.15 M NaCl, 0.1% SDS, 1% NP-40, 1% sodium deoxycholate, 50 mM NaF, 5 mM orthovanadate, 1 mM DTT) supplemented with proteinase inhibitor cocktail (Sigma # 11836170001). Total proteins were separated by SDS-PAGE and transferred to Nitrocellulose membrane (Bio-rad # 1620115). The primary antibodies used were: aPKCι 1/1000 (BD Transduction #610175), α-Tubulin 1/5000 (Sigma #T9026), Par3 1/1000 (Millipore #07-330); Par6B 1/1000 (Santa Cruz #sc-67393), V5 1/5000 (Thermo Fisher Scientific # R960-25); flag 1/1000 (Delta Biolabs # DB125), CD13 1/1000 (Abcam # ab108382), Pals1 1/1000 (proteintech group #17710-1-AP), myc 1/1000 (Origene # TA150121), and GFP 1/1000 (Abcam #ab13970). For immunoprecipitation, cells were washed twice with ice-cold PBS and then lysed in NP40 lysis buffer (150 mM NaCl, 1% NP-40, 50 mM Tris-HCl, 10 mM NaF, 1 mM $NaVO_4$, pH 8.0) containing a protease inhibitor cocktail and calyculin A. Lysates were precleared with MagnaBeads (Thermo Fisher Scientific #12321D) and then incubated with 2 µg of antibody or isotype control overnight at 4°C. Antibodies were captured with MagnaBeads and washed three times with NP40 buffer.

3.4.6 Immunostaining and imaging

Cells from three-dimensional cultures were fixed with 2% paraformaldehyde/PBS for 10 min, permeabilized in 0.5% Triton X-100/10% Goat serum/10% fish gelatin/PBS for 1 hr and incubated overnight in primary antibodies. The primary antibodies were used at the following dilutions: Par6B 1/200 (Santa Cruz #sc-67393), aPKCι 1/100 (BD Transduction #610175), Par3

1/200 (Millipore #07-330), CD13 1/100 (Abcam #ab108382), E-cadherin 1/200 (Cell Signaling #3195S), ZO-1 1/100 (Cell Signaling #8193), Ezrin 1/200 (Cell Signaling #3145), Pals1 1/100 (proteintech group #17710-1-AP), β1-integrin 1/200 (Abcam #ab30394), V5 1/200 (Thermo Fisher Scientific # R960-25), laminin 1/200 (Abcam #ab11575), α-Tubulin 1/200 (Sigma #T9026) and Phalloidin 1/100 (Invitrogen #A34055). The secondary antibodies conjugated to Alexa488, Alexa546 and Alexa647 (Jackson ImmunoResearch Laboratories) were used at 1:750. DNA was detected with Hoechst dye 33258. Confocal imaging was performed using LSM700 from Zeiss with 20X/0.8NA or 40X/1.4NA objective lenses and processed using FIJI/ImageJ software.

3.4.7 Live-imaging

Live-imaging of Caco-2 3D structures was performed using a LSM700 confocal microscope with a LD plan-Neofluar 20X/0.4NA Korr M27 objective lens with 1% laser power and ZEN software (Zeiss). Caco-2 cells were virus-infected with CD13-mCherry, EGFP-Par6, or GFP-Rab11 in 2D culture for stable gene expression. Cells were seeded in 3D culture prior to performing live imaging. 8-bit images were captured every 25 min with 5 slices (28 µm), two channels in an environmental chamber (37 °C, 5% CO_2).

3.4.8 Temporal image correlation microscopy (tICM)

To measure the proteins dynamics, the tICM were implemented using a TIRF (total internal reflectance fluorescence) microscope. Caco-2 cells were transient transfected with CD13-mCherry and GFP-Rab11 in 2D culture. After 24 hours, cells were seeded on 8 well ibidi plate supplemented with 5% GelTrex-media at 37°C in 5% CO_2 in DMEM supplemented with 10% fetal bovine serum, 100 U/ml penicillin, 0.1 mg/ml streptomycin for 24 hours prior to performing live imaging. TIRF was obtained using a Spectral Diskovery unit (Spectral Applied Research,

Richmond Hill, ON) attached to an inverted Leica DMI6000B microscope (Leica Microsystems, Wetzler, Germany) with a Leica Plan ApoChromat 63x/1. 47 NA TIRF oil immersion objective lens. The platform incorporates a 488 nm diode laser, 561 nm diode-pumped solid-state laser, 642 nm didode laser (Spectral Applied Research) with two ImagEMX2 Digital EM-CCD Cameras (Hamamatsu, Hamamatsu City, Japan). A 100-Watt X-Cite 120 LED (370-700 nm) source was applied to allow visualization of fluorescence proteins by eye. The platform was integrated with MetaMorph 7.1 image acquisition software (Molecular Devices Inc.) Each image was set to collect 1000 frames with a 30 ms interval.

3.4.9 Statistical Analysis

Comparison of two unpaired independent means was performed using a student's t-test. Statistics were determined using Excel, and GraphPad Prism 6. All images are representative from at least three replicates.

3.5 Acknowledgements

This work was supported by a Canadian Institutes of Health Research grant (PJT-156271) to LM. LM is a Fonds Recherche du Québec – Santé Research Scholar.

3.6 References

Bauvois, B. (2004). Transmembrane proteases in cell growth and invasion: new contributors to angiogenesis? Oncogene 23, 317-329.

Bhartur, S.G., Calhoun, B.C., Woodrum, J., Kurkjian, J., Iyer, S., Lai, F., and Goldenring, J.R. (2000). Genomic structure of murine Rab11 family members. Biochem Biophys Res Commun 269, 611-617.

Blasky, A.J., Mangan, A., and Prekeris, R. (2015). Polarized protein transport and lumen formation during epithelial tissue morphogenesis. Annu Rev Cell Dev Biol 31, 575-591.

Bogenrieder, T., Finstad, C.L., Freeman, R.H., Papandreou, C.N., Scher, H.I., Albino, A.P., Reuter, V.E., and Nanus, D.M. (1997). Expression and localization of aminopeptidase A, aminopeptidase N, and dipeptidyl peptidase IV in benign and malignant human prostate tissue. Prostate 33, 225-232.

Bryant, D.M., Datta, A., Rodriguez-Fraticelli, A.E., Peranen, J., Martin-Belmonte, F., and Mostov, K.E. (2010a). A molecular network for de novo generation of the apical surface and lumen. Nature cell biology 12, 1035-1045.

Bryant, D.M., Datta, A., Rodriguez-Fraticelli, A.E., Peranen, J., Martin-Belmonte, F., and Mostov, K.E. (2010b). A molecular network for de novo generation of the apical surface and lumen. Nat Cell Biol 12, 1035-1045.

Caplan, M.J., Stow, J.L., Newman, A.P., Madri, J., Anderson, H.C., Farquhar, M.G., Palade, G.E., and Jamieson, J.D. (1987). Dependence on pH of polarized sorting of secreted proteins. Nature 329, 632-635.

Casanova, J.E., Wang, X., Kumar, R., Bhartur, S.G., Navarre, J., Woodrum, J.E., Altschuler, Y., Ray, G.S., and Goldenring, J.R. (1999). Association of Rab25 and Rab11a with the apical recycling system of polarized Madin-Darby canine kidney cells. Mol Biol Cell 10, 47-61.

Cerruti, B., Puliafito, A., Shewan, A.M., Yu, W., Combes, A.N., Little, M.H., Chianale, F., Primo, L., Serini, G., Mostov, K.E., et al. (2013). Polarity, cell division, and out-of-equilibrium dynamics control the growth of epithelial structures. J Cell Biol 203, 359-372.

Chang, Y.W., Chen, S.C., Cheng, E.C., Ko, Y.P., Lin, Y.C., Kao, Y.R., Tsay, Y.G., Yang, P.C., Wu, C.W., and Roffler, S.R. (2005). CD13 (aminopeptidase N) can associate with tumor-associated antigen L6 and enhance the motility of human lung cancer cells. Int J Cancer 116, 243-252.

Curnis, F., Sacchi, A., Borgna, L., Magni, F., Gasparri, A., and Corti, A. (2000). Enhancement of tumor necrosis factor alpha antitumor immunotherapeutic properties by targeted delivery to aminopeptidase N (CD13). Nat Biotechnol 18, 1185-1190.

Datta, A., Bryant, D.M., and Mostov, K.E. (2011). Molecular regulation of lumen morphogenesis. Curr Biol 21, R126-136.

Desclozeaux, M., Venturato, J., Wylie, F.G., Kay, J.G., Joseph, S.R., Le, H.T., and Stow, J.L. (2008). Active Rab11 and functional recycling endosome are required for E-cadherin trafficking and lumen formation during epithelial morphogenesis. Am J Physiol Cell Physiol 295, C545-556.

Di Matteo, P., Arrigoni, G.L., Alberici, L., Corti, A., Gallo-Stampino, C., Traversari, C., Doglioni, C., and Rizzardi, G.P. (2011). Enhanced expression of CD13 in vessels of inflammatory and neoplastic tissues. J Histochem Cytochem 59, 47-59.

Durgan, J., Kaji, N., Jin, D., and Hall, A. (2011). Par6B and atypical PKC regulate mitotic spindle orientation during epithelial morphogenesis. J Biol Chem 286, 12461-12474.

Fairweather, S.J., Broer, A., O'Mara, M.L., and Broer, S. (2012). Intestinal peptidases form functional complexes with the neutral amino acid transporter B(0)AT1. Biochem J 446, 135-148.

Favaloro, E.J., Browning, T., and Facey, D. (1993). CD13 (GP150; aminopeptidase-N): predominant functional activity in blood is localized to plasma and is not cell-surface associated. Exp Hematol 21, 1695-1701.

Fremont, S., and Echard, A. (2018). Membrane Traffic in the Late Steps of Cytokinesis. Curr Biol 28, R458-R470.

Ghosh, M., Lo, R., Ivic, I., Aguilera, B., Qendro, V., Devarakonda, C., and Shapiro, L.H. (2019b). CD13 tethers the IQGAP1-ARF6-EFA6 complex to the plasma membrane to promote ARF6 activation, beta1 integrin recycling, and cell migration. Sci Signal 12.

Golachowska, M.R., Hoekstra, D., and van, I.S.C. (2010). Recycling endosomes in apical plasma membrane domain formation and epithelial cell polarity. Trends Cell Biol 20, 618-626.

Goldenring, J.R., Smith, J., Vaughan, H.D., Cameron, P., Hawkins, W., and Navarre, J. (1996). Rab11 is an apically located small GTP-binding protein in epithelial tissues. Am J Physiol 270, G515-525.

Guzman-Rojas, L., Rangel, R., Salameh, A., Edwards, J.K., Dondossola, E., Kim, Y.G., Saghatelian, A., Giordano, R.J., Kolonin, M.G., Staquicini, F.I., et al. (2012). Cooperative effects of aminopeptidase N (CD13) expressed by nonmalignant and cancer cells within the tumor microenvironment. Proc Natl Acad Sci U S A 109, 1637-1642.

Halaoui, R., and McCaffrey, L. (2015a). Rewiring cell polarity signaling in cancer. Oncogene 34, 939-950.

Halaoui, R., and McCaffrey, L. (2015b). Rewiring cell polarity signaling in cancer. Oncogene 34, 939-950.

Hao, Y., Du, Q., Chen, X., Zheng, Z., Balsbaugh, J.L., Maitra, S., Shabanowitz, J., Hunt, D.F., and Macara, I.G. (2010). Par3 controls epithelial spindle orientation by aPKC-mediated phosphorylation of apical Pins. Curr Biol 20, 1809-1818.

Hehnly, H., and Doxsey, S. (2014). Rab11 endosomes contribute to mitotic spindle organization and orientation. Dev Cell 28, 497-507.

Horikoshi, Y., Suzuki, A., Yamanaka, T., Sasaki, K., Mizuno, K., Sawada, H., Yonemura, S., and Ohno, S. (2009). Interaction between PAR-3 and the aPKC-PAR-6 complex is indispensable for apical domain development of epithelial cells. J Cell Sci 122, 1595-1606.

Ito, S., Miyahara, R., Takahashi, R., Nagai, S., Takenaka, K., Wada, H., and Tanaka, F. (2009). Stromal aminopeptidase N expression: correlation with angiogenesis in non-small-cell lung cancer. Gen Thorac Cardiovasc Surg 57, 591-598.

Jaffe, A.B., Kaji, N., Durgan, J., and Hall, A. (2008a). Cdc42 controls spindle orientation to position the apical surface during epithelial morphogenesis. The Journal of cell biology 183, 625-633.

Jaffe, A.B., Kaji, N., Durgan, J., and Hall, A. (2008b). Cdc42 controls spindle orientation to position the apical surface during epithelial morphogenesis. J Cell Biol 183, 625-633.

Joberty, G., Petersen, C., Gao, L., and Macara, I.G. (2000). The cell-polarity protein Par6 links Par3 and atypical protein kinase C to Cdc42. Nat Cell Biol 2, 531-539.

Kehlen, A., Lendeckel, U., Dralle, H., Langner, J., and Hoang-Vu, C. (2003). Biological significance of aminopeptidase N/CD13 in thyroid carcinomas. Cancer Res 63, 8500-8506.

Li, B.X., Satoh, A.K., and Ready, D.F. (2007). Myosin V, Rab11, and dRip11 direct apical secretion and cellular morphogenesis in developing Drosophila photoreceptors. J Cell Biol 177, 659-669.

Li, D., Mangan, A., Cicchini, L., Margolis, B., and Prekeris, R. (2014). FIP5 phosphorylation during mitosis regulates apical trafficking and lumenogenesis. EMBO Rep 15, 428-437.

Lujan, P., Varsano, G., Rubio, T., Hennrich, M.L., Sachsenheimer, T., Galvez-Santisteban, M., Martin-Belmonte, F., Gavin, A.C., Brugger, B., and Kohn, M. (2016). PRL-3 disrupts epithelial architecture by altering the post-mitotic midbody position. J Cell Sci 129, 4130-4142.

Macara, I.G., Guyer, R., Richardson, G., Huo, Y., and Ahmed, S.M. (2014). Epithelial homeostasis. Curr Biol 24, R815-825.

Mangan, A.J., Sietsema, D.V., Li, D., Moore, J.K., Citi, S., and Prekeris, R. (2016). Cingulin and actin mediate midbody-dependent apical lumen formation during polarization of epithelial cells. Nat Commun 7, 12426.

McCaffrey, L.M., and Macara, I.G. (2012). Signaling pathways in cell polarity. Cold Spring Harb Perspect Biol 4.

Mina-Osorio, P. (2008). The moonlighting enzyme CD13: old and new functions to target. Trends in molecular medicine 14, 361-371.

Mina-Osorio, P., Shapiro, L.H., and Ortega, E. (2006). CD13 in cell adhesion: aminopeptidase N (CD13) mediates homotypic aggregation of monocytic cells. J Leukoc Biol 79, 719-730.

Nelson, W.J., Dickinson, D.J., and Weis, W.I. (2013). Roles of cadherins and catenins in cell-cell adhesion and epithelial cell polarity. Prog Mol Biol Transl Sci 116, 3-23.

Nokes, R.L., Fields, I.C., Collins, R.N., and Folsch, H. (2008). Rab13 regulates membrane trafficking between TGN and recycling endosomes in polarized epithelial cells. J Cell Biol 182, 845-853.

Nolan, M.E., Aranda, V., Lee, S., Lakshmi, B., Basu, S., Allred, D.C., and Muthuswamy, S.K. (2008). The polarity protein Par6 induces cell proliferation and is overexpressed in breast cancer. Cancer Res 68, 8201-8209.

Orlando, R.A., Takeda, T., Zak, B., Schmieder, S., Benoit, V.M., McQuistan, T., Furthmayr, H., and Farquhar, M.G. (2001). The glomerular epithelial cell anti-adhesin podocalyxin associates with the actin cytoskeleton through interactions with ezrin. J Am Soc Nephrol 12, 1589-1598.

Pasqualini, R., Koivunen, E., Kain, R., Lahdenranta, J., Sakamoto, M., Stryhn, A., Ashmun, R.A., Shapiro, L.H., Arap, W., and Ruoslahti, E. (2000). Aminopeptidase N is a receptor for tumor-homing peptides and a target for inhibiting angiogenesis. Cancer Res 60, 722-727.

Prekeris, R., Klumperman, J., and Scheller, R.H. (2000). A Rab11/Rip11 protein complex regulates apical membrane trafficking via recycling endosomes. Mol Cell 6, 1437-1448.

Rathbun, L.I., Colicino, E.G., Manikas, J., O'Connell, J., Krishnan, N., Reilly, N.S., Coyne, S., Erdemci-Tandogan, G., Garrastegui, A., Freshour, J., et al. (2020). Cytokinetic bridge triggers de novo lumen formation in vivo. Nat Commun 11, 1269.

Riemann, D., Kehlen, A., and Langner, J. (1999). CD13--not just a marker in leukemia typing. Immunol Today 20, 83-88.

Rocken, C., Licht, J., Roessner, A., and Carl-McGrath, S. (2005). Canalicular immunostaining of aminopeptidase N (CD13) as a diagnostic marker for hepatocellular carcinoma. J Clin Pathol 58, 1069-1075.

Rodriguez-Boulan, E., and Macara, I.G. (2014). Organization and execution of the epithelial polarity programme. Nat Rev Mol Cell Biol 15, 225-242.

Roeth, J.F., Sawyer, J.K., Wilner, D.A., and Peifer, M. (2009). Rab11 helps maintain apical crumbs and adherens junctions in the Drosophila embryonic ectoderm. PLoS One 4, e7634.

Roh, M.H., Fan, S., Liu, C.J., and Margolis, B. (2003). The Crumbs3-Pals1 complex participates in the establishment of polarity in mammalian epithelial cells. J Cell Sci 116, 2895-2906.

Roignot, J., Peng, X., and Mostov, K. (2013). Polarity in mammalian epithelial morphogenesis. Cold Spring Harb Perspect Biol 5.

Roman-Fernandez, A., and Bryant, D.M. (2016). Complex Polarity: Building Multicellular Tissues Through Apical Membrane Traffic. Traffic 17, 1244-1261.

Saito, Y., Desai, R.R., and Muthuswamy, S.K. (2018). Reinterpreting polarity and cancer: The changing landscape from tumor suppression to tumor promotion. Biochim Biophys Acta Rev Cancer 1869, 103-116.

Sato, T., Mushiake, S., Kato, Y., Sato, K., Sato, M., Takeda, N., Ozono, K., Miki, K., Kubo, Y., Tsuji, A., et al. (2007). The Rab8 GTPase regulates apical protein localization in intestinal cells. Nature 448, 366-369.

Schluter, M.A., Pfarr, C.S., Pieczynski, J., Whiteman, E.L., Hurd, T.W., Fan, S., Liu, C.J., and Margolis, B. (2009a). Trafficking of Crumbs3 during cytokinesis is crucial for lumen formation. Mol Biol Cell 20, 4652-4663.

Schluter, M.A., Pfarr, C.S., Pieczynski, J., Whiteman, E.L., Hurd, T.W., Fan, S., Liu, C.J., and Margolis, B. (2009b). Trafficking of Crumbs3 during cytokinesis is crucial for lumen formation. Molecular biology of the cell 20, 4652-4663.

Shaye, D.D., Casanova, J., and Llimargas, M. (2008). Modulation of intracellular trafficking regulates cell intercalation in the Drosophila trachea. Nat Cell Biol 10, 964-970.

Shivas, J.M., Morrison, H.A., Bilder, D., and Skop, A.R. (2010). Polarity and endocytosis: reciprocal regulation. Trends Cell Biol 20, 445-452.

Subramani, J., Ghosh, M., Rahman, M.M., Caromile, L.A., Gerber, C., Rezaul, K., Han, D.K., and Shapiro, L.H. (2013). Tyrosine phosphorylation of CD13 regulates inflammatory cell-cell adhesion and monocyte trafficking. J Immunol 191, 3905-3912.

Terauchi, M., Kajiyama, H., Shibata, K., Ino, K., Nawa, A., Mizutani, S., and Kikkawa, F. (2007). Inhibition of APN/CD13 leads to suppressed progressive potential in ovarian carcinoma cells. BMC Cancer 7, 140.

van Ijzendoorn, S.C. (2006). Recycling endosomes. J Cell Sci 119, 1679-1681.

Vogel, L.K., Spiess, M., Sjostrom, H., and Noren, O. (1992). Evidence for an apical sorting signal on the ectodomain of human aminopeptidase N. J Biol Chem 267, 2794-2797.

Wang, Q., Hurd, T.W., and Margolis, B. (2004). Tight junction protein Par6 interacts with an evolutionarily conserved region in the amino terminus of PALS1/stardust. J Biol Chem 279, 30715-30721.

Wang, T., Yanger, K., Stanger, B.Z., Cassio, D., and Bi, E. (2014). Cytokinesis defines a spatial landmark for hepatocyte polarization and apical lumen formation. J Cell Sci 127, 2483-2492.

Wang, X., Kumar, R., Navarre, J., Casanova, J.E., and Goldenring, J.R. (2000). Regulation of vesicle trafficking in madin-darby canine kidney cells by Rab11a and Rab25. J Biol Chem 275, 29138-29146.

Wessels, H.P., Hansen, G.H., Fuhrer, C., Look, A.T., Sjostrom, H., Noren, O., and Spiess, M. (1990). Aminopeptidase N is directly sorted to the apical domain in MDCK cells. J Cell Biol 111, 2923-2930.

Wilson, M.I., Gill, D.J., Perisic, O., Quinn, M.T., and Williams, R.L. (2003). PB1 domain-mediated heterodimerization in NADPH oxidase and signaling complexes of atypical protein kinase C with Par6 and p62. Mol Cell 12, 39-50.

Winter, J.F., Hopfner, S., Korn, K., Farnung, B.O., Bradshaw, C.R., Marsico, G., Volkmer, M., Habermann, B., and Zerial, M. (2012). Caenorhabditis elegans screen reveals role of PAR-5 in RAB-11-recycling endosome positioning and apicobasal cell polarity. Nat Cell Biol 14, 666-676.

Wong, A.H., Zhou, D., and Rini, J.M. (2012). The X-ray crystal structure of human aminopeptidase N reveals a novel dimer and the basis for peptide processing. J Biol Chem 287, 36804-36813.

Yu, W., Datta, A., Leroy, P., O'Brien, L.E., Mak, G., Jou, T.S., Matlin, K.S., Mostov, K.E., and Zegers, M.M. (2005). Beta1-integrin orients epithelial polarity via Rac1 and laminin. Mol Biol Cell 16, 433-445.

Zajac, O., Raingeaud, J., Libanje, F., Lefebvre, C., Sabino, D., Martins, I., Roy, P., Benatar, C., Canet-Jourdan, C., Azorin, P., et al. (2018). Tumour spheres with inverted polarity drive the formation of peritoneal metastases in patients with hypermethylated colorectal carcinomas. Nat Cell Biol 20, 296-306.

3.7 Supplemental Figures

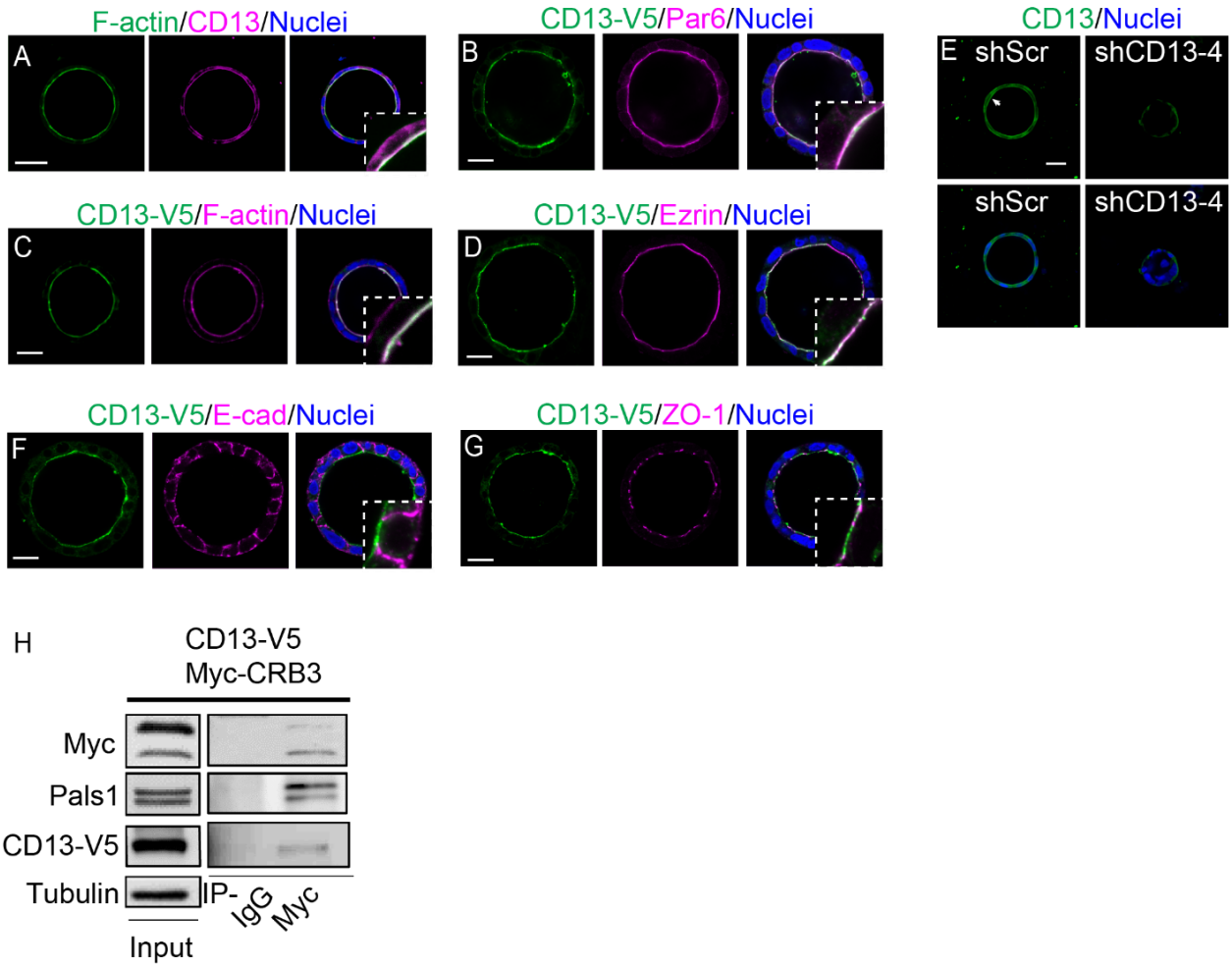

Supplemental Figure S3.1: CD13 associates with apical proteins and localizes at the apical domain of 3D Caco-2 cysts at day 10. Associated with Figure 3.1. (A) Images of polarized 3D cysts of cultured Caco-2 cells for F-actin (green) and CD13 (magenta). (B) Images of polarized 3D cysts of cultured Caco-2 cells for CD13-V5 (green) and Par6 (magenta). (C) Images of polarized 3D cysts of cultured Caco-2 cells for CD13-V5 (green) and F-actin (magenta). (D) Images of polarized 3D cysts of cultured Caco-2 cells for CD13-V5 (green) and Ezrin (magenta). (E) Images of control and knockdown CD13 3D cysts of cultured Caco-2 cells for CD13 (green). (F) Images of polarized 3D cysts of cultured Caco-2 cells for CD13-V5 (green) and E-cad (magenta). (G) Images of polarized 3D cysts of cultured Caco-2 cells for CD13-V5 (green) and ZO-1 (magenta). (H) Co-immunoprecipitation of CD13 and CRB3 was performed with anti-IgG or anti-myc in HEK293 cells. The presence of CD13 in immunoprecipitates was determined by western blot analysis using anti-V5. Bars: A-G, 20µm.

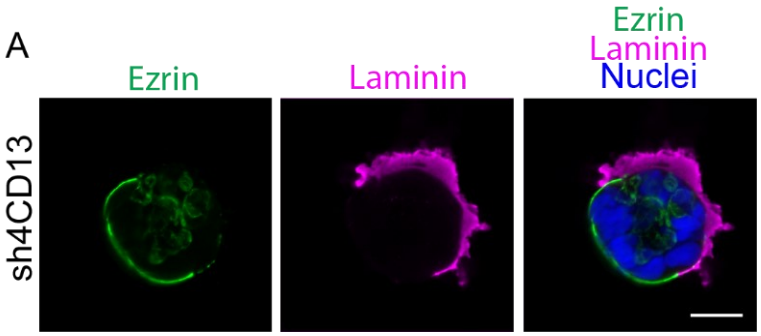

Supplemental Figure S3.2: CD13 depletion disrupts the basement membrane of 3D Caco-2 cysts. Associated with Figure 3.2. (A) Images for Ezrin (green) and laminin (magenta) showing cyst has lost apical-basal identity in CD13 knock-down 3D Caco-2 cysts. Bars: A, 30 µm.

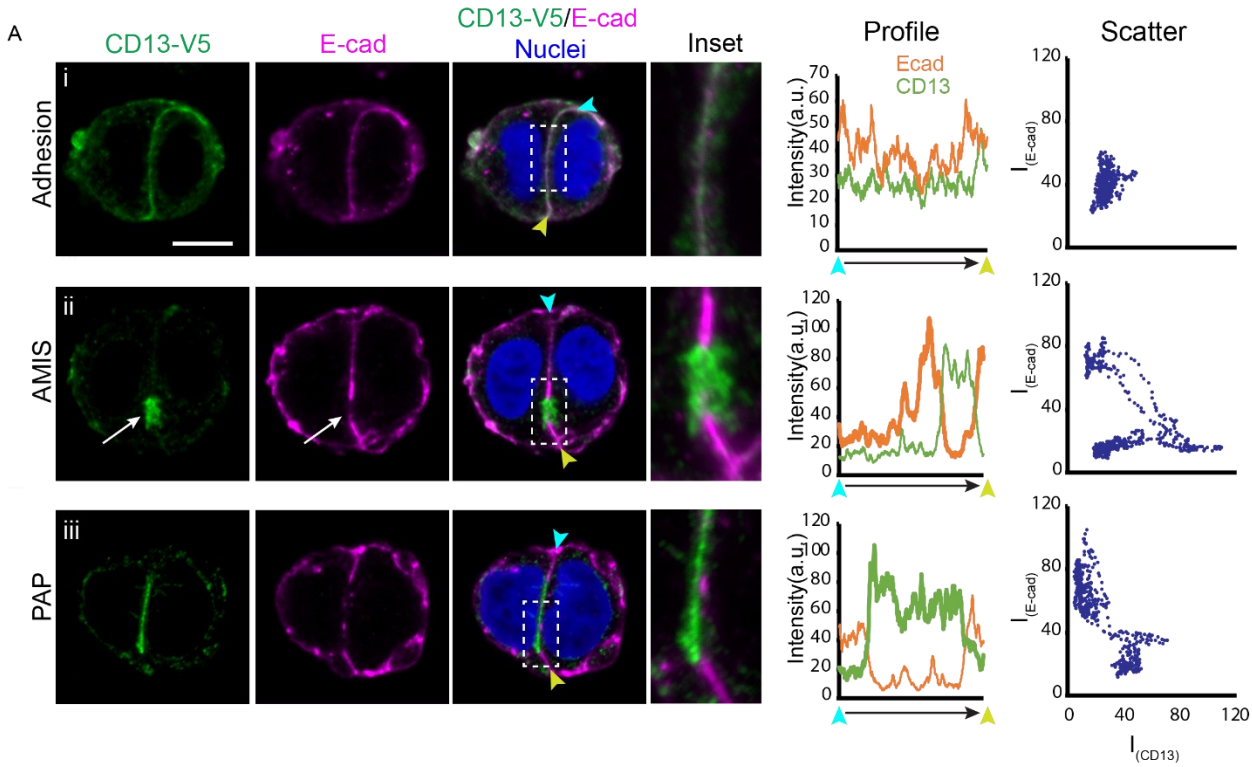
A
CD13-V5
E-cad
CD13-V5/E-cad
Nuclei
Inset
Profile
Scatter
Ecad
CD13
Adhesion
AMIS
PAP
i
ii
iii
Intensity(a.u.)
I(E-cad)
I(CD13)

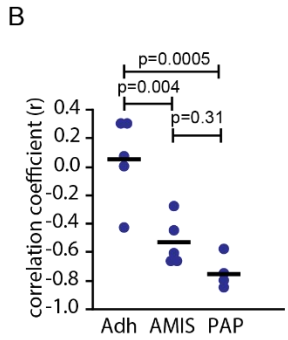
B
p=0.0005
p=0.004
p=0.31
correlation coefficient (r)
Adh
AMIS
PAP

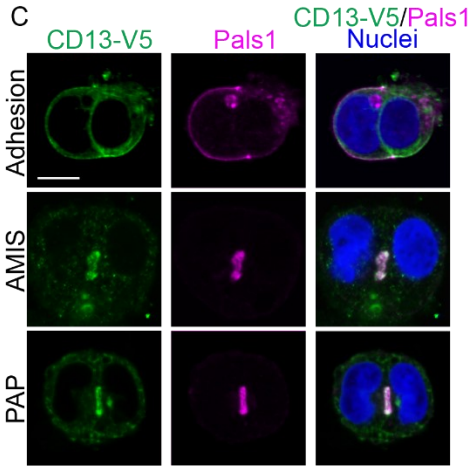
C
CD13-V5
Pals1
CD13-V5/Pals1
Nuclei
Adhesion
AMIS
PAP

Supplemental Figure S3.3: Recruitment of CD13 to focal sites with E-cadherin displacement in early 3D Caco-2 cysts. Associated with Figure 3.3. (A) Images for CD13-V5 (green) and E-cad (magenta) showing the relative localization of CD13 and E-cad at adhesion, AMIS, and PAP stage in two cell structures of 3D Caco-2 cysts. Graphic profile depicting changes in fluorescent intensity (A.U.) from blue to yellow arrows. Adjacent scatter plots showing the relationships between CD13 and E-cad. (B) Quantification of the correlation coefficient of CD13 and E-cad at adhesion, AMIS, and PAP stage in two cell structures of 3D Caco-2 cysts. (C) Images for CD13-V5 (green) and Pals1 (magenta) showing CD13 is recruited to the pre-luminal apical patch before Pals1 in two cell structures of 3D Caco-2 cysts. Bars: A, C, 10 µm.

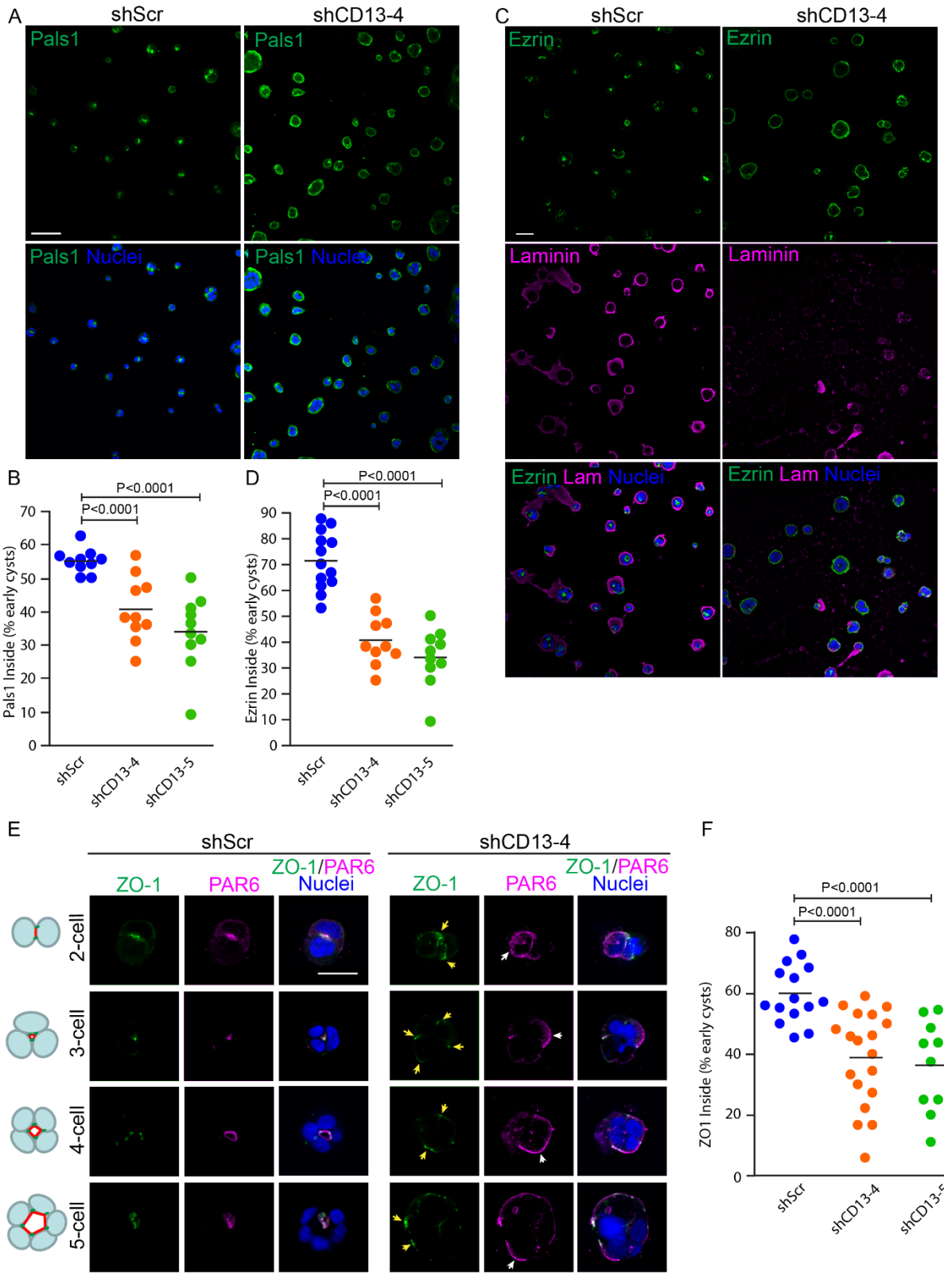
A
shScr
shCD13-4
Pals1
Pals1 Nuclei
B
P<0.0001
P<0.0001
Pals1 Inside (% early cysts)
shScr
shCD13-4
shCD13-5
C
Ezrin
Laminin
Ezrin Lam Nuclei
D
P<0.0001
P<0.0001
Ezrin Inside (% early cysts)
E
ZO-1
PAR6
ZO-1/PAR6 Nuclei
2-cell
3-cell
4-cell
5-cell
F
P<0.0001
P<0.0001
ZO1 Inside (% early cysts)

Supplemental Figure S3.4: CD13 depletion disrupts early polarization in 3D Caco-2 cysts. Associated with Figure 3.4. (A) Low-power confocal images for Pals1 (green) showing mislocalized Pals1 in CD13 knock-down 3D Caco-2 cysts at early stages. (B) Quantification of the percentage of Pals1 localization of shScr (n=235), sh4-CD13 knock-down (n=326) and sh5-CD13 knock-down (n=154) in 3D Caco-2 cysts at early stages. (C) Images for Ezrin (green) and laminin (magenta) showing cysts have lost general apical identity in CD13 knock-down 3D Caco-2 cysts at early stages. (D) Quantification of the percentage of Ezrin localization of shScr (n=153), sh4-CD13 knock-down (n=162) and sh5-CD13 knock-down (n=147) in 3D Caco-2 cysts at early stages. (E) Images for ZO-1 (green) and Par6 (magenta) showing ZO-1 and Par6 mislocalizing to the periphery in CD13 knock-down 3D Caco-2 cysts at early stages. (F) Quantification of the percentage of ZO-1 localization of shScr (n=302), sh4-CD13 knock-down (n=278) and sh5-CD13 knock-down (n=146) in 3D Caco-2 cysts at early stages. Bars: A, C, 100µm; E, 30µm.

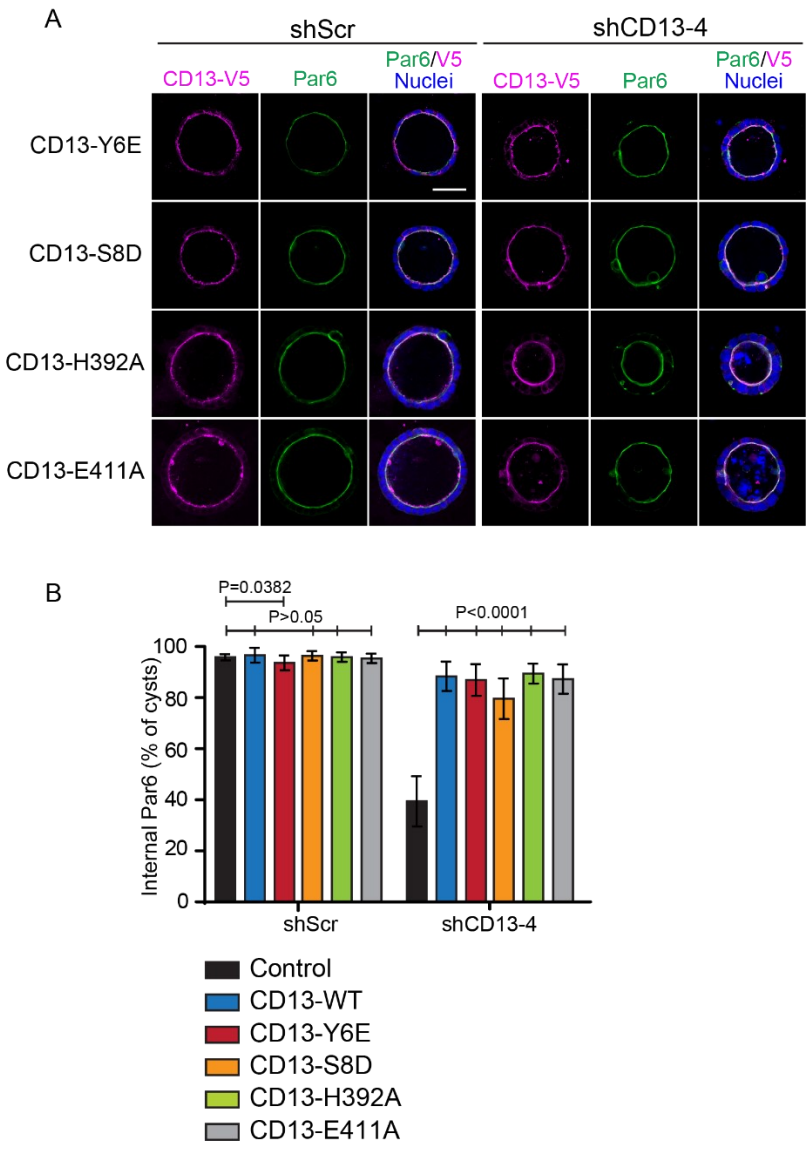

Supplemental Figure S3.5: The intracellular domain of CD13 is required to maintain apical-basal polarity. Associated with Figure 3.6. (A) Images for CD13-V5 (magenta) and Par6 (green) showing the rescue phenotype in different CD13 mutants of shScr and shCD13 3D Caco-2 cysts. (B) Quantification of the percentage of Par6 internally in wildtype (n of shScr=515, shCD13=292), CD13-Y6E (n of shScr=555, shCD13=285), CD13-S8D (n of shScr=400, shCD13=337), CD13-H392A (n of shScr=475, shCD13=298), and CD13-E411A (n of shScr=513, shCD13=283) of shScr (n=428) and shCD13 (n=492) 3D Caco-2 cysts. Bars: A, 50µm.

Conceptual link for Chapter 4

Approximately 85% of cancers arise from epithelial cells. Cancer progression is associated with extensive epithelial remodelling, in which luminal cavities fill with malignant cancer cells. In Chapters 2 and 3, I reported on mechanisms that promote lumen formation. In this chapter I explore changes in cell polarity associated with cancer progression. Since aPKCι/PRKCI is frequently over-expressed in tumours and is required for KRAS-mediated tumourigenesis, I evaluated differences in PRKCI-proximity proteins in the absence or presence of $KRAS^{G12V}$ using BioID. This identified PTPN14 as a proximity protein to PRKCI, which was reduced in $KRAS^{G12V}$-expressing cells. In Chapter 2, I reported that PTPN14 was also a high-confidence interactor with PAR6B, suggesting that PTPN14 is associated with an apical complex with PAR6B and PRKCI. In Chapter 4, I explore a potential role for PTPN14 as a tumour-suppressor by regulating apical-basal polarity.

Chapter 4: Protein tyrosine phosphatase N14 associates with the Par complex and regulates KRAS-dependent transformation

Authors: Li-Ting Wang[1,2] and Luke McCaffrey[1,2,3,4]

[1]Rosalind and Morris Goodman Cancer Research Centre, McGill University, Montreal, QC, Canada H3A 1A3
[2]Division of Experimental Medicine, McGill University, Montreal, QC, Canada H4A 3J1
[3]Gerald Bronfman Department of Oncology, McGill University, QC, Canada H4A 3T2
[4]Correspondence: luke.mccaffrey@mcgill.ca

Keywords: cell polarity, apical, epithelial cyst, BioID, PTPN14, KRAS

Abstract

Changes in epithelial polarity are coupled with cancer progression. Here, we implemented a BioID screen in 3D culture to identify PRKCI-proximity proteins in control and $KRAS^{G12V}$-transformed Caco-2 cells. From this screen we identified PTPN14 and found that it localizes at apical domain and associates with PRKCI. Both PTPN14 and PRKCI protein levels are reduced by $KRAS^{G12V}$ expression, with PTPN14 downstream of PRKCI. We report that PTPN14 is dispensable for growth and polarization of control Caco-2 cysts, whereas re-introduction of PTPN14 suppressed $KRAS^{G12V}$-induced transformation by restricting $KRAS^{G12V}$-induced cell growth and restoring apical-basal polarity and a central lumen. This demonstrates that PTPN14 is an important tumour suppressor that maintains cell polarization to restrict cancer development.

4.1 Introduction

Altered epithelial cell polarity is associated with development of carcinoma (Halaoui et al., 2017). Cell polarity proteins play a fundamental role in regulating many aspects of epithelial growth control and maintaining apical-basal polarity by controlling the localization of key mediators involved in regulating stem cell renewal, proliferation, apoptosis, survival, differentiation, cell motility, cell adhesion, and tissue organization (Rodriguez-Boulan and Macara, 2014), processes involved in both development and cancer progression. The Par, Crumbs, and Scribble complexes are three major polarization complexes that localize to the apical (Par and Crumbs) or basal (Scribble) membranes and regulate epithelial organization (Rodriguez-Boulan and Macara, 2014).

Most proteins in the apical polarity complexes are adaptors or scaffolding proteins, except for atypical protein kinase C (aPKC, which has two isoforms, PRKCI and PRKCZ) which regulates polarization and signaling by phosphorylating diverse target proteins to regulate their function or localization (Gunaratne et al., 2013; Rodriguez-Boulan and Macara, 2014; Smith et al., 2007; Suzuki et al., 2004). aPKCι/PRKCI is required for cell polarity, proliferation and migration and is commonly up-regulated in multiple cancer types including breast (Kojima et al., 2008), prostate (Yu et al., 2004), pancreas (Evans et al., 2003) and colon cancer (Murray et al., 2004).

Recent studies indicate that PRKCI is required for Ras-induced transformation and tumorigenesis in many cancer types (Murray et al., 2004; Murray et al., 2009; Regala et al., 2009; Regala et al., 2005a). For example, studies demonstrate that PKCι is required for KRAS-driven transformed growth *in vitro* and tumorigenicity *in vivo* through a KRAS-PKC-Rac1-Pak-Mek-Erk

signaling axis in pancreatic ductal adenocarcinoma (PDAC) and non-small cell lung cancer (NSCLC) cells (Regala et al., 2005; Scotti et al., 2010).

The proto-oncogenic Ras proteins are GTPases that are regulated through GEFs and GAPs. GEFs act as Ras activators by promoting the exchange of a bound GDP molecule with a GTP molecule (Zhang et al., 2005a). In the GTP-bound state, Ras can expose two regions named switch I and switch II to form a conformation that allows Ras to recruit effector proteins and activate various signalling pathways (Pacold et al., 2000). On the other hand, GAPs amplify 100,000-fold the endogenous GTPase activity of Ras and return it to the GDP-bound state. (Gideon et al., 1992). Ras proteins, including harvey rat sarcoma viral oncogene (HRAS), kirsten rat sarcoma viral oncogene (KRAS), and neuroblastoma RAS viral oncogene (NRAS), share over 90% sequence identity at the amino acid level (Baines et al., 2011).

KRAS is the most prevalent and most oncogenic among Ras isoforms and is one of the most frequently mutated genes (21%) across all cancers, with the highest prevalence in pancreatic, colorectal, endometrial, biliary tract, lung, and cervical cancers (Nakhaeizadeh et al., 2016; Prior et al., 2012; Schubbert et al., 2007). Recurrent point mutations typically occur at codons 12, 13, or 61 and promote GTP binding to produce a constitutive activate protein (Quinlan and Settleman, 2009). Mutations at codon 12 of KRAS are the most frequent, with G to T transitions at the second base of codon 12 produces G12V mutations, which are among the second common mutations of KRAS (Prior et al., 2012).

Several studies have demonstrated a relationship between KRAS and polarity. For example, mutations in the *KRAS* gene disrupt apical-basal polarity through inhibiting normal glycosylation of the β1-integrin chain of the collagen receptor in colon epithelial cells (Yan et al., 1997a).

Moreover, oncogenic KRAS expression is associated with up-regulated carcinoembryonic antigen (CEA) expression and disruption of epithelial cell polarization (Yan et al., 1997b). A recent study indicated that recurrent KRAS mutations lead to papillary renal neoplasm with reverse polarity (PRNRP) (Al-Obaidy et al., 2019). Activated KRAS also involves loss of apical-basal polarity, luminal cavity formation with apoptosis in human CRC HCT116 3D cell culture (Tsunoda et al., 2010). Furthermore, mutation or inhibition of the kinase activity of RAF (rapidly accelerated fibrosarcoma), a KRAS effector, results in tumour growth and apical-basal polarity disruption in human colorectal cancer (Borovski et al., 2017; Magudia et al., 2012; Patankar et al., 2019).

PTPN14, also known as PEZ, PTP36 and PTPD2, is a 130 kDa cytosolic non-receptor protein tyrosine phosphatase (PTP) that is highly expressed in multiple tissues including kidney, skeletal muscle, lungs, and placenta (Smith et al., 1995; Uhlen et al., 2015). PTPN14 has a FERM protein-binding domain at N-terminal, a linker central region contains an acidic region and two PPxY motifs, and a PTP catalytic domain at its C-terminus (Barr et al., 2006; Chishti et al., 1998; Smith et al., 1995). The PPxY motifs of PTPN14 directly bind to the WW domains of YAP and KIBRA (kidney and brain protein) which are components of the Hippo signalling pathway and negatively regulate YAP in a cell density-dependent manner, indicating the important role of PTPN14 in Hippo signaling pathway (Liu et al., 2013; Michaloglou et al., 2013; Poernbacher et al., 2012; Wang et al., 2012a; Wilson et al., 2014). KIBRA is a scaffold protein with WW, C2-like and aPKC-binding domains and it can be phosphorylated by aPKC (Buther et al., 2004). PTPN14 forms a complex with KIBRA and LATS (large tumor suppressor) and regulates the Hippo signaling pathway by dephosphorylating Yap to exclude it from the nucleus and negatively regulates its transcriptional co-activator activity (Liu et al., 2013; Wang et al., 2012; Wilson et al., 2014).

PTPN14 has an important developmental role and regulates of organogenesis, TGFβ expression, lymphangiogenesis, cell-cell adhesion, cell-matrix adhesion, cell migration, and cell growth. Knockdown of PTPN14 results in developmental defects in the brain, heart, pharyngeal arches, and somites in zebrafish embryos (Wyatt et al., 2007) and gives rise to developmental defects in *Drosophila* (Poernbacher et al., 2012). Overexpression of PTPN14 induces EMT by provoking TGFβ signaling through Smad4 in epithelial MDCK cells (Wyatt et al., 2007). In addition, PTPN14 dephosphorylates β-catenin at adherens junctions and blocking this led to decreased cell-cell adhesion and enhanced cell motility (Wadham et al., 2003).

PTPN14 has been shown to act both a tumor promoter or tumor suppressor depending on the context, indicating the level of PTPN14 activity may be critical to maintain the cellular homeostasis or that different substrates in different contexts dictates its contribution to cancer. *PTPN14* is altered in a variety of human cancers including breast, skin, and liver cancers, mostly by gene amplification (Bonilla et al., 2016; Cerami et al., 2012; Gao et al., 2013; Li et al., 2011; Sjoblom et al., 2006). Inhibition of PTPN14 expression attenuated ERBB2-mediated morphological changes such as multiacinar phenotype in 3D mammary organoid, showing PTPN14 acts as a positive regulator of ERBB2 signalling in human breast cancer (Ramesh et al., 2015). On the other hand, PTPN14 deficiency leads to lymphatic hyperplasia with lymphedema, suggesting the tumor suppressive role of PTPN14 in lymphangiogenesis (Au et al., 2010). Moreover, PTPN14 suppressed the invasiveness and metastasis of triple-negative breast cancer cells in breast cancer xenografts model through restricting the intracellular trafficking of soluble and membrane bound proteins, protein kinase C delta (PRKCD) and Ras and Rab interactor 1 (RIN1), which are correlated with decreased overall survival in breast cancer (Belle et al., 2015).

Another study has shown that PTPN14 might be involved in regulating the migratory and proliferative properties in colorectal cancer since PTPN14 directly dephosphorylates breast cancer anti-estrogen resistance protein 1 (BCAR1/p130cas) at tyrosine residue 128 (Y128) which regulates cell growth, migration, and invasion (Cabodi et al., 2006; Zhang et al., 2013).

Here, we applied BioID to identify PRKCI-proximity proteins in control and $KRAS^{G12V}$-transformed epithelial cells. We show that PTPN14 associates with PRKCI and is localized at the apical domain in polarized epithelial cells. In $KRAS^{G12V}$-transformed cells, PTPN14 is down-regulated, which is permissive for overgrowth and disruption of epithelial architecture, since re-expression of PTPN14 promotes polarity, lumen formation, and suppressed growth, which is independent of Yap. We therefore reveal that PTPN14 can act as a tumour suppressor by regulating cell polarity and epithelial organization.

4.2 Results

4.2.1 BirA*-PRKCI expression in 3D Caco-2 cells

To understand changes in polarity signaling during cell transformation, we implemented a BioID screen of PRKCI-proximity proteins using Caco-2 cells, a human intestinal adenocarcinoma cell line. This ideal model readily forms polarized epithelial structures in 3D culture, which can be transformed by expressing $KRAS^{G12V}$ to generate enlarged irregularly shaped structures without a lumen that resemble cancerous tissue (Figure 4.4 B). To determine if oncogenic KRAS altered proteins associated with the apical polarity complex, we performed BioID with BirA*-PRKCI in Caco-2 cells expressing $KRAS^{G12V}$, or the control parental cell line. BirA*-EGFP was expressed in both parental and $KRAS^{G12V}$-expressing Caco-2 cells as a BirA* control. To generate cells that

stably express a transcriptionally functional myc-epitope conjugated BirA*-PRKCI-fusion protein construct, the promiscuous biotin ligase, BirA mutant (R118G, hereafter called BirA*), was fused to EGFP as control or PRKCI and expressed in Caco-2 cells. We chose to study the aPKC-iota isoform (PRKCI) since it is a major effector of the apical polarity complexes and has been implicated in numerous cancers (Fields and Regala, 2007; Murray et al., 2011).

The expression of BirA*-PRKCI in pWPI vector is driven by an EF1α promoter and an internal ribosomal entry site (IRES) directs expression of GFP. To obtain the endogenous expression level where exogenous BirA*-PRKCI levels are similar to endogenous levels of PRKCI, Caco-2 cells were virus infected with low dose of lentivirus virus (multiplicity of infection (MOI) = 0.2) of BirA*-PRKCI and were sorted with low (25%), medium (50%), high (75%) expression according to the expression of GFP (Figure 4.1 A). BirA*-PRKCI expression at low expression (25%) reaches the level as endogenous PRKCI in Caco-2 cells, which were confirmed by western blotting and immunostaining (Figure 4.1 B-D). We confirmed that BirA*-PRKCI was expressed at a physiological level and localized to the apical membrane and did not interfere with polarization or lumen formation (Figure 4.1 C).

To validate the construct for BioID approach, HEK293 cells were transient transfected with pWPI-BirA*-PRKCI or pWPI-BirA*-EGFP and the expression of the fusion protein was detected by anti-Myc (Supplemental Figure S4.1 A) and the biotinylation of the proximity interactors of the BirA*-PRKCI or BirA*-EGFP were detected by HRP (horseradish peroxidase) streptavidin (Supplemental Figure S4.1 B). To obtain enough cysts for mass spectrometry analysis, one million Caco-2 cells expressing BirA*-EGFP or BirA*-PRKCI were seeded into four 15 cm plates for 9 days in 3D culture, cysts were collected after 24 hrs of incubation with 50 µM biotin.

Furthermore, we confirmed that BirA*-PRKCI biotinylated two direct binding partners, PAR6B and PARD3, further confirming that BirA*-PRKCI is functional within Caco-2 cells. Interestingly, we observed similar amounts of PAR6B and PARD3 in the streptavidin pull-down from parental and $KRAS^{G12V}$-expressing Caco-2 cells, indicating that this oncogene does not disrupt the core components of the Par complex (Supplemental Figure S4.1 C). Novel interactions were validated by co-immunoprecipitation experiments and analysed using Scaffold, Cytoscape, and compared to Biogrid, and Crapome databases.

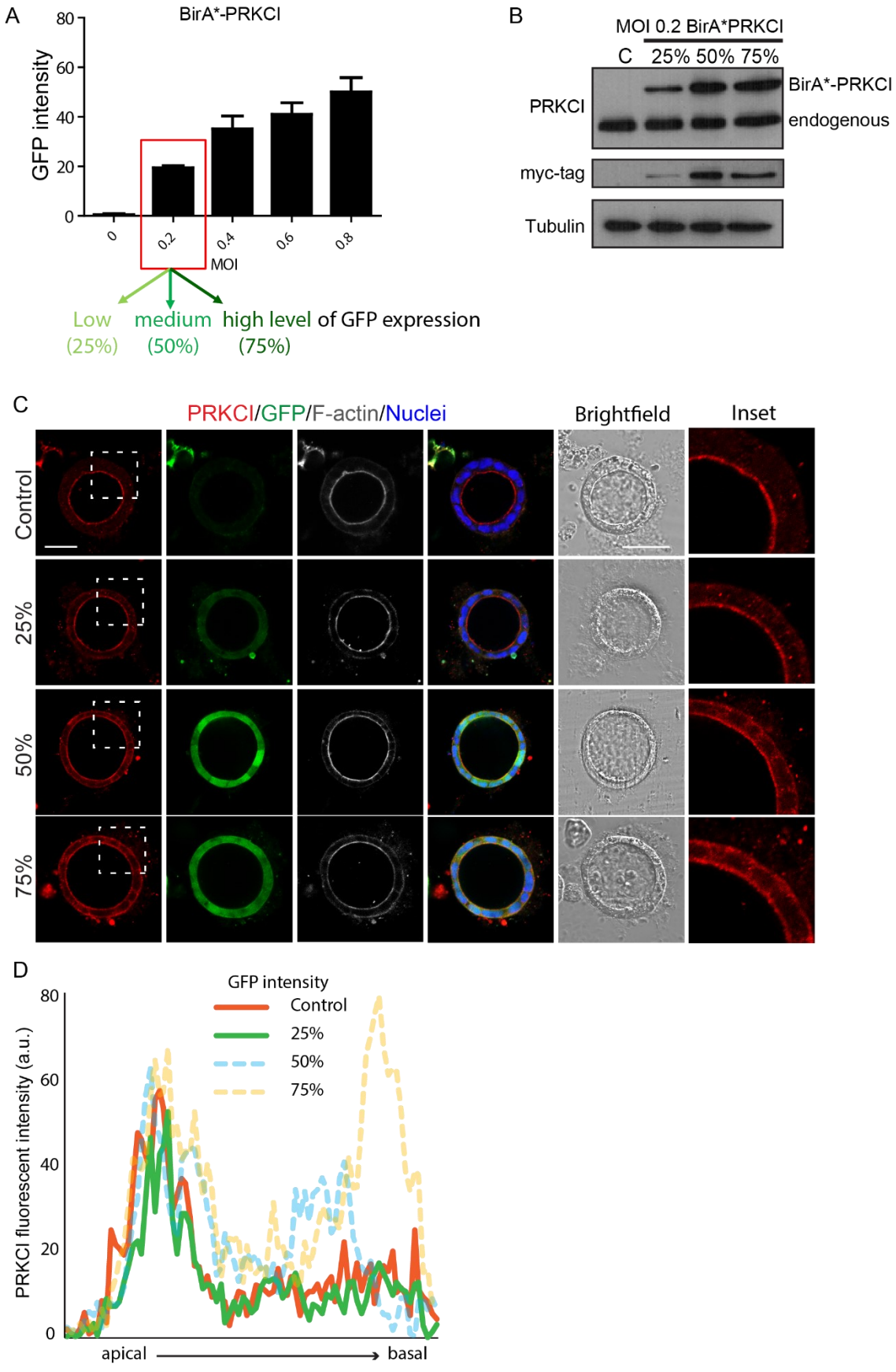
A
BirA*-PRKCI
GFP intensity
80
60
40
20
0
0
0.2
0.4
0.6
0.8
MOI
Low (25%)
medium (50%)
high level (75%)
of GFP expression
B
MOI 0.2 BirA*PRKCI
C
25% 50% 75%
PRKCI
BirA*-PRKCI
endogenous
myc-tag
Tubulin
C
PRKCI/GFP/F-actin/Nuclei
Brightfield
Inset
Control
25%
50%
75%
D
GFP intensity
Control
25%
50%
75%
PRKCI fluorescent intensity (a.u.)
80
60
40
20
0
apical
basal

Figure 4.1: Optimization of the BirA*-PRKCI expression in Caco-2 cells. (A) Graph showing the percentage of GFP expression in Caco-2 cells with different dose of lentivirus virus (0-0.8 MOI) of BirA*-PRKCI. Different expression (25%-low, 50%-medium, 75%-high level) of BirA*-PRKCI with 0.2 MOI in Caco-2 cells were generated by fluorescent activated cell sorting (FACS). (B) Caco-2 cells expressed with different level of exogenous myc epitope-tagged BirA*-PRKCI were validated by western blotting with anti-PRKCI, and anti-myc. (C) Confocal images were captured for Caco-2 cysts expressed with different level of BirA*-PRKCI immunostained for PRKCI (red), GFP (GFP) and F-actin (grey) showing the localization of PRKCI. (D) Line plot showing the PRKCI fluorescent intensities from apical to basal membrane of Caco-2 cysts expressed with different level (control-red, 25%-green, 50%-blue, 75%-yellow) of BirA*-PRKCI. Each line is from a single representative cell. Scale Bars: C, 50µm.

4.2.2 Identification of PRKCI-proximity proteins in parental and KRAS^{G12V}-transformed Caco-2 cells

To identify apical proteins proximal to PRKCI in parental and KRAS^{G12V}-transformed samples, we grew cells for 9 days in suspension culture, a time when the lumen is fully established. At this time, we added biotin for 24 hrs, then lysed cells and pulled-down biotinylated proteins using streptavidin beads. From triplicate experiments, we filtered the list of PRKCI-proximity proteins using SAINT scores and peptide counts as cut-offs. Prey from BirA*-PRKCI in control and KRAS^{G12V}-transformed Caco-2 samples were plotted according to the spectral counts and SAINT score, indicating the abundance of proximal proteins of PRKCI in control and KRAS^{G12V}-transformed Caco-2 samples (Figure 4.2 A). Of the PRKCI-proximal proteins identified in parental and KRAS^{G12V}-transformed samples, 6 were common, 5 specific to control samples and 6 specific to KRAS^{G12V}-transformed samples (Figure 4.2 B). High confidence interactions included polarity proteins known to directly associated with PRKCI (LGL1/2, PARD6B, SQSTM1) (Sanchez et al., 1998; Yamanaka et al., 2003), as well proteins that have not been reported in the literature such as PTPN14 (Figure 4.2 A). PTPN14 was identified as a significant novel proximal protein for BirA*-PRKCI in both control and KRAS^{G12V}-transformed Caco-2 samples (Figure 4.2 A). Moreover, SAINT analysis indicates that PTPN14 shows higher abundance in control samples compared to KRAS^{G12V}-transformed samples according to the total spectral counts which is consistent with other studies showing that PTPN14 acts as a tumor suppressor (Laczmanska and Sasiadek, 2011; Wang et al., 2004) (Figure 4.2 A,C). To further explore relationships between PRKCI proximity proteins in control and KRAS^{G12V}-transformed Caco-2 samples, we used STRING protein-protein interaction networks as well as Gene Ontology for candidates from control and KRAS^{G12V}-

transformed Caco-2 samples (Figure 4.2 D, and Supplemental Figure S4.2 A,B). This identified two clusters related to 1) Cell polarity and trafficking, 2) Cell movement/Cell adhesion (Control/ $KRAS^{G12V}$).

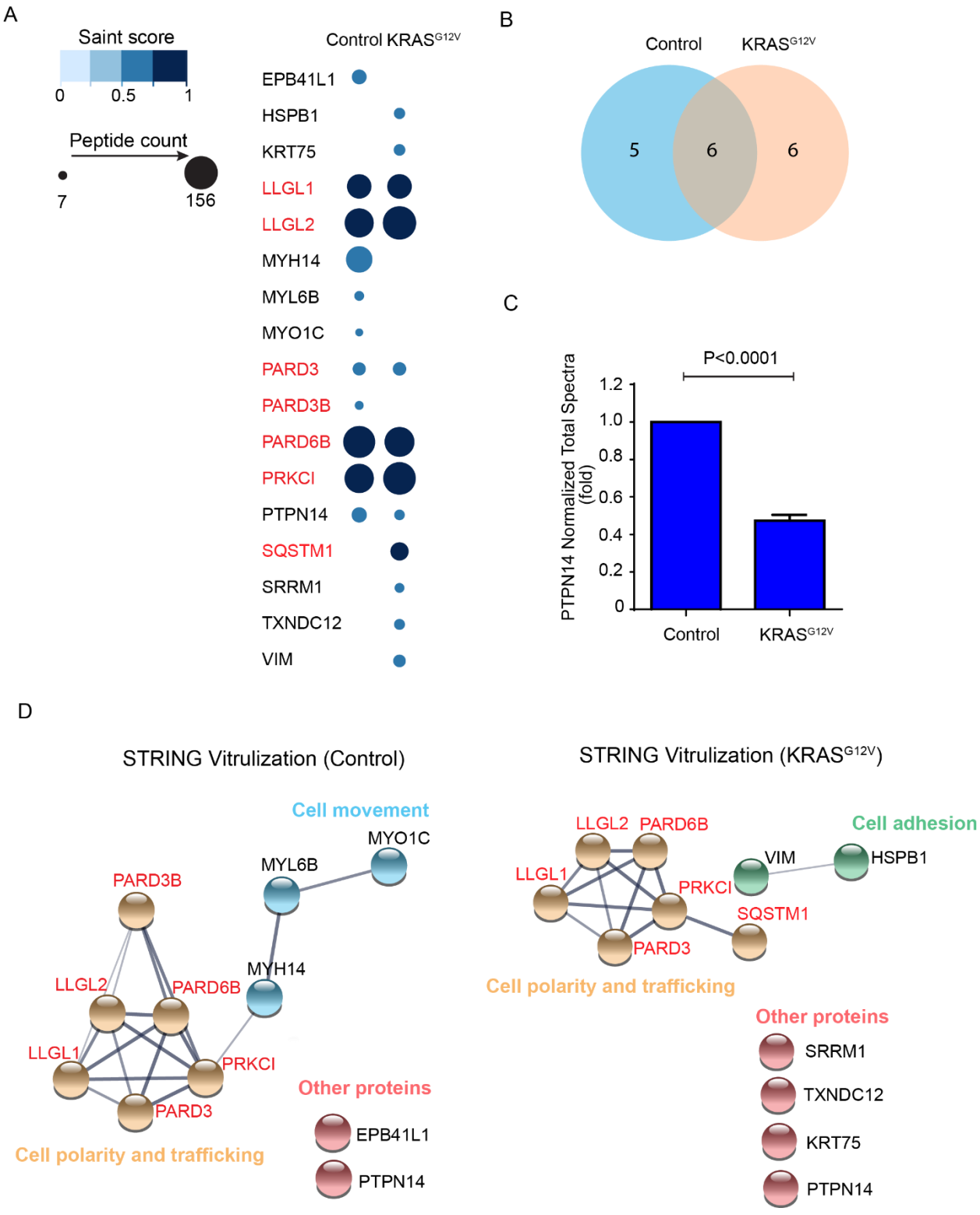
A
Saint score
0
0.5
1
Peptide count
7
156
Control KRASG12V
EPB41L1
HSPB1
KRT75
LLGL1
LLGL2
MYH14
MYL6B
MYO1C
PARD3
PARD3B
PARD6B
PRKCI
PTPN14
SQSTM1
SRRM1
TXNDC12
VIM
B
Control
KRASG12V
5
6
6
C
P<0.0001
PTPN14 Normalized Total Spectra (fold)
1.2
1.0
0.8
0.6
0.4
0.2
0
Control
KRASG12V
D
STRING Vitrulization (Control)
Cell movement
MYO1C
MYL6B
PARD3B
MYH14
LLGL2
PARD6B
LLGL1
PRKCI
PARD3
Cell polarity and trafficking
Other proteins
EPB41L1
PTPN14
STRING Vitrulization (KRASG12V)
LLGL2
PARD6B
Cell adhesion
VIM
HSPB1
LLGL1
PRKCI
SQSTM1
PARD3
Cell polarity and trafficking
Other proteins
SRRM1
TXNDC12
KRT75
PTPN14

Figure 4.2: Identification of BirA*-PRKCI vicinal proteins in control or KRAS^{G12V}-transformed Caco-2 samples by proteomics analysis. (A) Significance Analysis of INTeractome (SAINT) analysis were analyzed using 1.0% False Discovery Rate (FDR) as protein and peptide threshold with 1 as minimum number of peptides. Total spectrum count was analyzed. SAINT scored probability of identified proteins to be true interactors from 0 to 1, where 0 indicates a false interactor and 1 indicates a true interactor. The cutoff for identifying BirA*-PRKCI vicinal proteins here is 0.5. The Saint score and peptide counts for PRKCI targets identified in control or KRAS^{G12V}-transformed Caco-2 samples are shown with different color and size. BioID was successful at identifying known interaction partners for PRKCI such as LGL1/2, PARD3, PARD6B, and SQSTM1 (in red), novel vicinal proteins were also identified. (B) Venn diagram showing the number of BirA*-PRKCI vicinal proteins which were identified in control and KRAS^{G12V} screens. (C) Quantification of the fold change of PTPN14 normalized total spectra in control or KRAS^{G12V} screens. (D) STRING virtualization showing the interaction between proteins which were identified in BirA*-PRKCI-expressing control or KRAS^{G12V}-transformed Caco-2 samples by BioID based on the STRING database. Line darkness indicates the strength of the predicted relationship between the proteins. Known interactors for PRKCI are shown in red.

4.2.3 PTPN14 is associated with the Par complex and is dispensable for lumen formation in Caco-2 cells

We previously identified PTPN14 as a high-confidence hit in a BioID screen for PAR6B proximity proteins in Caco-2 cells. The presence of PTPN14 in proximity to PRKCI here provides additional evidence that PTPN14 is likely associated with the Par-complex. To confirm this, we first examined the localization of PTPN14, and detected endogenous PTPN14 and exogenous V5-tagged PTPN14 (PTPN14-V5) localized apically with apical markers-PAR6B and F-actin in polarized Caco-2 cyst (Figure 4.3 A,B, and Supplemental Figure S4.3 A). To confirm the interaction between PRKCI and PTPN14, we performed co-immunoprecipitation experiments between PTPN14-V5 and myc-tagged-PRKCI or myc-EGFP in HEK293 cells. We were able to detect myc co-precipitating with V5 (Figure 4.3 C), indicating that PTPN14 associates with PRKCI, which supports the results from BioID. To determine if endogenous PTPN14 formed part of a complex with PRKCI, we performed immunoprecipitation experiments from control and $KRAS^{G12V}$-transformed 3D Caco-2 cell lysates. We not only detect PARD3 and PAR6B but also detect endogenous PTPN14 in immunoprecipitates in control myc-PRKCI expressed 3D Caco-2 cysts (Figure 4.4 D). Taken together, these data indicate that PTPN14 is part of a complex with PRKCI, PAR6B, and PARD3.

A role for PTPN14 in cell polarity or lumen formation has not been previously reported. Given that we found it associated with the Par complex, we further investigated a role for PTPN14 in apical-basal polarity by depleting it using two-independent shRNA (sh3-CD13 and sh5-CD13) (Supplemental Figure S4.3 B). We did not observe any obvious defects in the overall cyst morphology or lumen formation (Figure 4.3 D,E). However, the apical localization of PRKCI was moderately reduced in PTPN14-deficient cells, whereas localization of basolateral marker E-

cadherin appeared unaffected (Figure 4.3 D,F,G). Collectively, these results suggest that PTPN14 is required to efficiently polarize PRKCI but is dispensable for lumen formation in Caco-2 cysts. However, we cannot exclude that residual PTPN14 may be sufficient to maintain polarity and lumen formation.

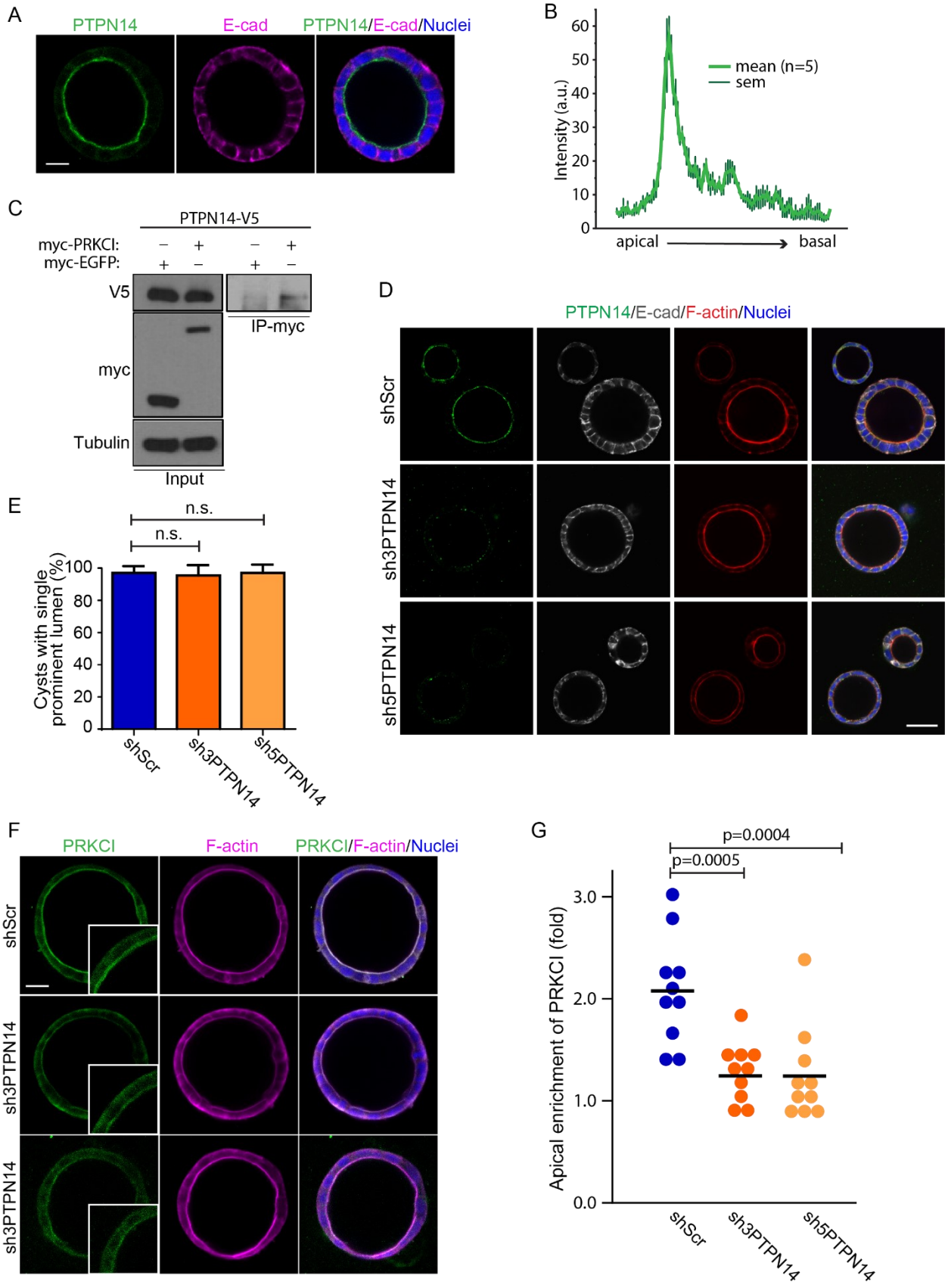
A
PTPN14
E-cad
PTPN14/E-cad/Nuclei
B
mean (n=5)
sem
Intensity (a.u.)
apical
basal
C
PTPN14-V5
myc-PRKCI:
myc-EGFP:
V5
IP-myc
myc
Tubulin
Input
D
PTPN14/E-cad/F-actin/Nuclei
shScr
sh3PTPN14
sh5PTPN14
E
n.s.
n.s.
Cysts with single prominent lumen (%)
shScr
sh3PTPN14
sh5PTPN14
F
PRKCI
F-actin
PRKCI/F-actin/Nuclei
shScr
sh3PTPN14
sh3PTPN14
G
p=0.0004
p=0.0005
Apical enrichment of PRKCI (fold)
shScr
sh3PTPN14
sh5PTPN14

Figure 4.3: PTPN14 is associated with PRKCI and is dispensable for lumen formation in Caco-2 cells. (A) Confocal images were captured for polarized Caco-2 cysts immunostained for PTPN14 (green) and E-cad (magenta) showing PTPN14 localizes to apical membrane. (B) Line plot showing PTPN14 fluorescent intensities from apical to basal membrane of polarized Caco-2 cysts. (C) Co-immunoprecipitation of PTPN14-V5 and myc-EGFP or myc-PRKCI was performed with anti-myc in transient transfected HEK293 cells. The presence of PTPN14 in immunoprecipitates was determined by western blot analysis using anti-V5. (D) Confocal images were captured for shScr, sh3- and sh5-PTPN14 knock-down Caco-2 cysts immunostained for PTPN14 (green), E-cad (grey), and F-actin (red). (E) Quantification of the percentage of cysts with single prominent lumen in shScr, sh3- and sh5-PTPN14 knock-down Caco-2 cysts. (F) Confocal images for PRKCI (green) and F-actin (magenta) showing the phenotype of shScr, sh3- and sh5-PTPN14 knock-down Caco-2 cysts. (G) Quantification of the fold change of apical enrichment of PRKCI in shScr, sh3- and sh5-PTPN14 knock-down Caco-2 cysts. Scale Bars: A, 20µm; D, 50µm; F, 30µm.

4.2.4 PTPN14 suppresses KRAS^{G12V}-induced transformation in Caco-2 cells

To explore a potential role for PTPN14 and PRKCI in KRAS transformation, Caco-2 cells were stably modified to express constitutively active KRAS^{G12V}. Immunoblot analysis of cell lysates indicated that PTPN14 and PRKCI protein were downregulated in KRAS^{G12V}-transformed Caco-2 cysts compared to controls, whereas mRNA was unaffected (Figure 4.4 A, and Supplemental Figure S4.4 A). KRAS^{G12V}-expression generated solid spheres of cells with collapsed small lumen demarcated by F-actin (Figure 4.4 B, and Supplemental Figure S4.4 B). The apical membrane of these structures had reduced enrichment of PRKCI compared to controls and PTPN14 was not detected at the apical membrane (Figure 4.4 B,C, and Supplemental Figure S4.4 B).

Since polarity was altered by KRAS^{G12V} expression, we investigated whether it affected PAR6B and PARD3 expression and ability assemble the Par complex. We observed that PAR6B was also reduced in KRAS^{G12V}-expressing samples, consistent with co-stability of PRKCI and PAR6B (Durgan et al., 2011), whereas PARD3-expression was not affected by KRAS^{G12V} (Figure 4.4 D). To determine if KRAS^{G12V}-expression affected the ability of the Par complex to form, we expressed myc-PRKCI in Caco-2 cells and immunoprecipitated with anti-myc antibodies. Under these experimental conditions, PAR6B was detected in the pull-down of both control and KRAS^{G12V}-expressing cells, consistent with their constitutive association (Figure 4.4 D). The reduced PAR6B band intensity in the KRAS^{G12V} compared to control pull-down likely reflects lower expression levels of PAR6B in these KRAS^{G12V} cells. In contrast, PARD3 was not detected in the myc-PRKCI pull-down containing KRAS^{G12V} (Figure 4.4 D). Since we were able to detect PARD3 in proximity to PRKCI at similar levels in control and KRAS^{G12V}-expressing cells using BioID with BirA*-PRKCI

(Supplemental Figure S4.1 C, and Figure 4.2 A), these results together suggests that $KRAS^{G12V}$ may affect the stability of the Par-complex rather than its formation *per se*.

Given the association between PRKCI and PTPN14 and the co-downregulation of both proteins in response to $KRAS^{G12V}$-expression, we wondered whether one may regulate the expression of the other. To understand this potential relationship, we knockdown PRKCI or PTPN14 in Caco-2 cells. Whereas knockdown of PRKCI resulted in a strong reduction in PTPN14-protein, knockdown of PTPN14 caused an up-regulation of PRKCI-expression (Figure 4.4 E,F). This indicates that PTPN14 associates with PRKCI and each reciprocally influences the protein expression of the other. Since PTPN14-expression requires PRKCI, it is possible that reduction of PTPN14 in $KRAS^{G12V}$-expressing cells is a consequence of reduced PRKCI expression. However, we cannot exclude that PTPN14 may be affected by $KRAS^{G12V}$ through an alternative mechanism.

To determine if reduced PTPN14 in $KRAS^{G12V}$-expressing cells has a functional consequence for the malignant phenotype (enlarged solid structures with reduced polarity), we enforced expression of V5-tagged PTPN14 in $KRAS^{G12V}$-expressing Caco-2 cells using lentivirus. Strikingly, overexpression of PTPN14 resulted in reformation of a prominent open lumen, enrichment of PRKCI to the apical membrane, and reduced the size of $KRAS^{G12V}$-expressing Caco-2 cells (Figure 4.4 G-I). Moreover, in 2D cultures, enforced expression of PTPN14 reduced the growth of $KRAS^{G12V}$-expressing cells (Supplemental Figure S4.4 C,D). Overall, these findings highlight that disruption of cell polarity by $KRAS^{G12V}$ acts through PTPN14 and highlight its pivotal functions in apical-basal polarity organization during cancer progression.

Previous studies have shown that PTPN14 is a tumour suppressor that regulates Yap/Hippo signaling (Liu et al., 2013; Michaloglou et al., 2013; Wilson et al., 2014) and Yap has

been shown that it acts as a major effector of mutant KRAS during tumor progression (Zhang et al., 2014). In a KRAS-induced pancreatic cancer model, PTPN14 was required for Yap-dependent tumourigenesis (Mello et al., 2017). We therefore wondered whether PTPN14 may regulate $KRAS^{G12V}$-induced malignant transformation through YAP. However, consistent with previous reports (Elbediwy et al., 2016), we did not observe YAP-translocation to the nucleus in $KRAS^{G12V}$-transformed Caco-2 cells (Supplemental Figure S4.5 A,B). As a positive control, we could detect oncogene-induced YAP nuclear translocation in Caco-2 cells expressing constitutively active SRC^{E527K} (Supplemental Figure S4.5 C). Therefore, our data indicate that PTPN14 likely acts as a tumour suppressor through an alternative signaling mechanism related to PRKCI regulation rather than Hippo signaling in this model of $KRAS^{G12V}$ malignant transformation.

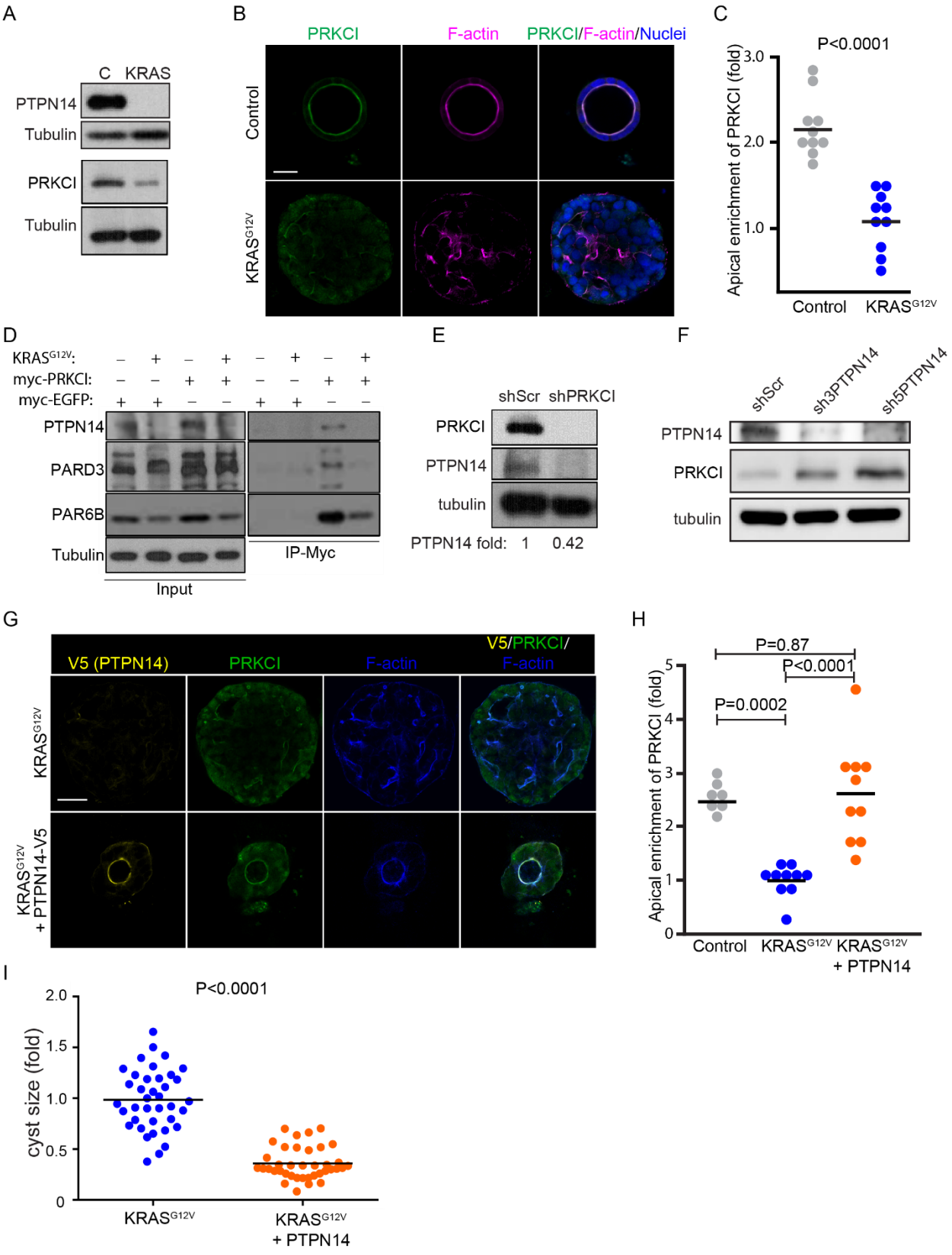
A
C KRAS
PTPN14
Tubulin
PRKCI
Tubulin
B
PRKCI
F-actin
PRKCI/F-actin/Nuclei
Control
KRASG12V
C
P<0.0001
Apical enrichment of PRKCI (fold)
3.0
2.0
1.0
Control
KRASG12V
D
KRASG12V:
myc-PRKCI:
myc-EGFP:
PTPN14
PARD3
PAR6B
Tubulin
IP-Myc
Input
E
shScr shPRKCI
PRKCI
PTPN14
tubulin
PTPN14 fold: 1 0.42
F
shScr
sh3PTPN14
sh5PTPN14
PTPN14
PRKCI
tubulin
G
V5 (PTPN14)
PRKCI
F-actin
V5/PRKCI/
F-actin
KRASG12V
KRASG12V
+ PTPN14-V5
H
P=0.87
P<0.0001
P=0.0002
Apical enrichment of PRKCI (fold)
5
4
3
2
1
0
Control
KRASG12V
KRASG12V
+ PTPN14
I
P<0.0001
cyst size (fold)
2.0
1.5
1.0
0.5
0
KRASG12V
KRASG12V
+ PTPN14

Figure 4.4: PTPN14 suppresses KRAS^{G12V}-induced transformation in Caco-2 cells. (A) Western blotting was performed with anti-PRKCI and anti-PTPN14 in control and KRAS^{G12V}-transformed Caco-2 cysts. (B) Confocal images were captured for control and KRAS^{G12V}-transformed Caco-2 cysts immunostained PRKCI (green) and F-actin (magenta) showing the expression and localization of PRKCI. (C) Quantification of the fold change of apical enrichment of PRKCI in control and KRAS^{G12V}-transformed Caco-2 cysts. (D) Immunoprecipitation of myc-EGFP or myc-PRKCI was performed with anti-myc in control and KRAS^{G12V}-transformed Caco-2 cysts. (E) Western blotting was performed with anti-PRKCI and anti-PTPN14 in PRKCI knockdown Caco-2 cells. PTPN14 is downregulated in PRKCI knockdown Caco-2 cells. (F) Western blotting was performed with anti-PRKCI and anti-PTPN14 in shScr, sh3- and sh5-PTPN14 knock-down Caco-2 cells. PRKCI is up-regulated in PTPN14 knockdown Caco-2 cells. (G) Confocal images were captured for KRAS^{G12V}-transformed Caco-2 cysts with or without PTPN14 overexpression immunostained for PTPN14-V5 (yellow), PRKCI (green), and F-actin (blue). (H) Quantification of the fold change of apical enrichment of PRKCI in control, KRAS^{G12V}-transformed Caco-2 cysts, and KRAS^{G12V}-transformed Caco-2 cysts with PTPN14 overexpression. (I) Quantification of the fold change of cyst size of cultured KRAS^{G12V}-transformed Caco-2 cysts with or without PTPN14 overexpression. Scale Bars: B, 30μm; G, 100μm.

4.3 Discussion

In this study we used BioID to investigate novel proximal proteins to PRKCI in 3D epithelial cultures and compared polarized cells with those transformed by $KRAS^{G12V}$. Malignant transformation of epithelia is associated with increased proliferation, loss of apical-basal polarity and disruption of epithelial organization by stratification or lumen filling (Halaoui et al., 2017). We successfully detected high-confidence associations (Saint score > 0.75) with PAR6B, a constitutive partner for PRKCI and both LLGL1 and LLGL2, known phosphorylation targets for PRKCI, thus validating that both interactors and substrates were detected in this screen. We observed a high-confidence association with p62 only in $KRAS^{G12V}$-expressing cells. p62 regulates proliferation, metabolism, stress signaling and autophagy and is known that it binds directly to aPKC isoforms through the PB1 domain (Moscat and Diaz-Meco, 2012). This supports that p62 is a key aPKC effector that contributes to cancer progression.

We also identified PTPN14 as a PRKCI-proximity interaction, which is consistent with our previous results (see Chapter 2) in which we also found PTPN14 as a PAR6B-proximal protein. We report that PTPN14 localizes to the apical membrane and associates with PAR6B and PRKCI, and collectively, this supports that PTPN14 is part of a PAR6B/PRKCI complex. Interestingly, PRKCI was important for PTPN14 protein levels. Previous studies have shown that PAR6B and aPKC are interdependent for protein stability to control epithelial organization: aPKC prevents PAR6B from degradation in a kinase-independent manner, on the other hand, PAR6B is required for maintaining aPKC in an inactive conformation (Durgan et al., 2011). Our data (Figure 4.4 E,F) show that PRKCI regulates PTPN14 protein levels, suggesting that PTPN14 might be similarly regulated as part of a complex.

The physical link between PAR6B/PRKCI and PTPN14 is currently unknown, however, one possibility is through KIBRA. PTPN14 interacts with KIBRA which is a cytoplasmic protein and has been shown to regulate a variety of cellular functions including cell growth, apoptosis, directional cell migration, mitotic spindle assembly and MAPK activation (Wilson et al., 2016). KIBRA has two N-terminal WW domains, a C2 domain, a glutamic acid-rich domain and a PDZ binding motif. The WW domains of KIBRA contain two conserved tryptophan residues which are required for recognizing proline-rich sequences PPxY (Kremerskothen et al., 2003). KIBRA can localize at the apical domain and influences cell polarity by inhibiting aPKC, but is also an aPKC substrate (Buther et al., 2004; Jin et al., 2015; Yoshihama et al., 2011). Furthermore, studies indicate that KIBRA can interact with Par complex or PTPN14 to activate LATS1 and negatively regulate the YAP in hippo signaling pathway (Moleirinho et al., 2013; Wilson et al., 2014; Xiao et al., 2011). This suggests that PTPN14 might be in a complex or cooperate with KIBRA to regulate cell polarity, however, this needs to be formally tested.

Although there is not extensive literature regarding cell polarity and PTPN14, a few studies describe the role of PTPN14 that can be indirectly linked to cell polarity. In mammary 3D epithelial cells, PTPN14 is required for ERBB2-mediated loss of polarity and lumen filling (Ramesh et al., 2015). Moreover, Kibra was identified to be a Patj interactor in yeast two-hybrid screen using a podocyte cDNA library and modulates the motility of podocytes (Duning et al., 2008). Our data show that depletion of PTPN14 has a modest effect on polarity and decreases the enrichment of PRKCI at the apical membrane, however this is insufficient to affect lumen formation or epithelial organization. This could result from residual PTPN14 being sufficient for lumenogenesis, or that

PTPN14 is required for optimal PRKCI polarization, but not to establish apical-basal polarity *per se*.

PTPN14 has been shown to act as a tumor suppressor since it has been demonstrated that there are PTPN14 mutations which leads to a loss of enzyme function of PTPN14 in colorectal cancers (Laczmanska and Sasiadek, 2011; Wang et al., 2004). Furthermore, PTPN14 expression was significantly lower in liver metastases compared to primary tumors, which were investigated by orthotopic implantation of the human pancreatic cancer cell line MiaPaca-2 in severe combined immunodeficiency (SCID) mice (Niedergethmann et al., 2007). In this study, we also found PTPN14 acts as tumor suppressor since PTPN14 expression is downregulated in $KRAS^{G12V}$-transformed cells and overexpression of PTPN14 repolarizes the phenotype of $KRAS^{G12V}$-transformed Caco-2 cysts. Moreover, we show the regulation of PTPN14 by $KRAS^{G12V}$ transformation is post-transcriptional since the mRNA level of PTPN14 and PRKCI have no change in $KRAS^{G12V}$-transformed Caco-2 cells, suggesting that the regulation PTPN14 and PRKCI by $KRAS^{G12V}$ transformation could be due to translational modification or protein stability. Strikingly, we report that forced expression of PTPN14 in $KRAS^{G12V}$-expressing cells was able to reverse malignant characteristics including overgrowth, loss of polarity, and lumen filling, providing strong evidence that PTPN14 is a potent tumour suppressor.

A major pathway by which PTPN14 functions as a tumour suppressor is by negatively regulating Yap signaling. Moreover, previous studies have also shown that overexpression of aPKC isoforms induced overgrowth by inducing YAP signaling (Archibald et al., 2015). Some reports indicate that RAS depended on its ability to stabilize YAP by counteracting Hippo pathway activity in some contexts (Hong et al., 2014). However, we did not observe changes in Yap

localization in our model, which is consistent with previous reports that KRAS acts independent of Yap signaling in Caco-2 cells (Elbediwy et al., 2016). The mechanism by which re-introduction of PTPN14 repolarize the $KRAS^{G12V}$-transformed cell and the regulation of the association of PRKCI and PTPN14 which is involved in $KRAS^{G12V}$ transformation are unclear at present and will need further investigation. Collectively, our study indicates that PTPN14 acts as a tumour suppressor through Yap-independent functions by regulating apical cell polarity.

4.4 Materials and Methods

4.4.1 Cell culture

The Caco-2 human intestinal epithelial cell line was purchased from American Type Culture Collection (HTB-37). Caco-2 cells were cultured at 37°C in 5% CO_2 in DMEM (Wisent #319-005-CL) supplemented with 10% fetal bovine serum (Wisent #080-150), 100 U/ml penicillin, 0.1 mg/ml streptomycin (Wisent #450201EL). For 3D culture, Caco-2 cells were seeded in 8 well µ-slide (Ibidi #80826) at a density of 1.25 x10^4 cells per well on top of a thin layer of 100% GelTrex (ThermoFisher Scientific #A1413202) in media supplemented 2% GelTrex. After one or ten days in adherent culture, cells were collected for immunofluorescence. Human embryonic kidney cell line HEK293LT (ATCC), were cultured at 37°C in 5% CO_2 in DMEM supplemented with 10% fetal bovine serum, 100 U/ml penicillin, 0.1 mg/ml streptomycin.

4.4.2 DNA and shRNA constructs

PRKCI was amplified by PCR from human cDNA. pcDNA3.1 mycBioID was a gift from Kyle Roux (Addgene plasmid # 35700). The PCR products were digested (by NotI and BamHI for PRKCI; by NotI and HindIII for EGFP) and inserted into pcDNA3.1 mycBioID. pWPI was a gift from Didier Trono (Addgene plasmid #12254). Products were digested by NheI and HindIII and were inserted into pWPI for virus production. The pLX317-PTPN14-V5 plasmids were purchased from Sigma (TRCN, PTPN14 TRCN0000479328).

shRNAs targeting human CD13 mRNA were cloned in pLKO Lentiviral supernatants were produced in HEK293LT cells as described previously. Caco-2 cells were infected with lentiviral supernatants and selected by the addition of 20 µg/ml puromycin for 10 days.

The shRNA used were acquired from the McGill Platform for Cellular Perturbation (MPCP)

sh1PTPN14 CCGGAGAGTCACCTCCAGACAACATCTCGAGATGTTGTCTGGAGGTGACTCTTTTTT, sh2PTPN14 CCGGGCGGTAATATACAGGTGGAATCTCGAGATTCCACCTGTATATTACCGCTTTTT, sh3PTPN14 CCGGCGGGAAGAGAATCGAGTTGATCTCGAGATCAACTCGATTCTCTTCCCGTTTTT, sh4PTPN14 CCGGCGCTCAGTACAAGTTTGTCTACTCGAGTAGACAAACTTGTACTGAGCGTTTTT, sh5PTPN14 CCGGCCTCAGAGAGTATGTGCTATTCTCGAGAATAGCACATACTCTCTGAGGTTTTT and a non-targeting scrambled shRNA was used as a control.

4.4.3 Transient transfection

HEK293LT cells were seeded at 2×10^6 cells per well in 100mm dishes and transfected with plasmids using Polyethylenimine (PEI) as per manufacturer's instructions (Sigma # 408727). Caco-2 cells were seeded at 4×10^4 cells per well in 24-well plates and transfected with plasmids using Lipofectamine LTX as per manufacturer's instructions (Invitrogen #15338030). All experiments were performed 24 h post-transfection.

4.4.4 Lentivirus production

Lentivirus was produced using calcium phosphate transfection of HEK293LT cells in 15-cm dishes with 50 µg of lentiviral plasmid, 37.5 µg of packaging plasmid (psPAX2), and 15 µg of VSVG coat protein plasmid (pMD2.G). Viral supernatants were collected after 48 hrs and were concentrated by precipitation in 40% polyethylene glycol 8000 (Bioshop # PEG800.1) followed by centrifugation and then re-suspended in the culture medium. Concentrated virus was aliquoted and frozen at -80°C, then an aliquot was titred in HEK293LT cells.

4.4.5 Affinity capture of biotinylated proteins

Biotinylation was induced by adding 50 µM biotin for 24 h to biotinylate proximal proteins (10-20 nm) to identify the interacting partners and substrates. After two PBS washes, cells were

lysed in 600µl ice cold RIPA lysis buffer (50 mM Tris-HCl (pH 7.5), 150 mM NaCl, 1% NP-40, 1 mM EDTA, 1 mM EGTA, 0.1% SDS and 0.5% sodium deoxycholate. PMSF (1 mM), DTT (1 mM) and Sigma protease inhibitor cocktail (P8340, 1:500). The lysates were treated with Benzonase for 1h on ice an equal volume RIPA lysis buffer was added. For each sample, 30 µL of streptavidin-sepharose bead slurry (GE Healthcare, Cat 17-5113-01) was pre-washed three times with 1 mL of lysis buffer by pelleting the beads with 400g centrifugation and aspirating off the supernatant before adding the next wash. After three sessions of sonication and centrifugation at 16,500g, supernatants with biotinylated proteins were incubated pre-washed streptavidin beads for 3 h at 4 °C with rotation. Beads were collected and washed twice with RIPA buffer and three times with 1 mL with 50 mM ammonium bicarbonate (pH 8.0). Beads were then resuspended in 100 µL of 50 mM ammonium bicarbonate, 10% of the sample was saved for immunoblotting analysis. Bound proteins were removed from the magnetic beads with 100 µl of Laemmli SDS-sample buffer saturated with biotin at 98°C for 10 mins. BioID samples and controls were analyzed by mass spectrometry in at least three biological replicates.

4.4.6 Immunoblotting and immunoprecipitation

Cells were lysed in RIPA lysis buffer (50 mM Tris-HCl, pH 8, 0.15 M NaCl, 0.1% SDS, 1% NP-40, 1% sodium deoxycholate, 50 mM NaF, 5 mM orthovanadate, 1 mM DTT) supplemented with proteinase inhibitor cocktail (Sigma # 11836170001). Total proteins were separated by SDS-PAGE and transferred to Nitrocellulose membrane (Bio-rad # 1620115). The primary antibodies were used as follows: aPKCι 1/1000 (BD Transduction #610175), Streptavidin 1/10000 (Jackson IR through #Cedarlane), α-Tubulin 1/5000 (Sigma #T9026), Par3 1/1000 (Millipore #07-330), Par6B 1/1000 (Santa Cruz #sc-67393), PTPN14 1/1000 (R&D Systems #MAB4458), V5 1/5000 (Thermo

Fisher Scientific # R960-25), and myc 1/1000 (Origene # TA15012). For immunoprecipitation, cells were washed twice with ice-cold PBS and then lysed in NP40 lysis buffer (150 mM NaCl, 1% NP-40, 50 mM Tris-HCl, 10 mM NaF, 1 mM $NaVO_4$, pH 8.0) containing a protease inhibitor cocktail and calyculin A. Lysates were precleared with MagnaBeads (Thermo Fisher Scientific #12321D) and then incubated with 2 µg of antibody or isotype control overnight at 4°C. Antibodies were captured with MagnaBeads and washed three times with NP40 buffer.

4.4.7 Immunostaining and imaging

Cells from three-dimensional cultures were fixed with 2% paraformaldehyde/PBS for 10 min, permeabilized in 0.5% Triton X-100/10% Goat serum/10% fish gelatin/PBS for 1 hr and incubated overnight in primary antibodies. The primary antibodies were used at the following dilutions: aPKCι 1/100 (BD Transduction #610175), PTPN14 1/1000 (R&D Systems #MAB4458), E-cadherin 1/200 (Cell Signaling #3195S), V5 1/200 (Thermo Fisher Scientific # R960-25), myc 1/100 (Origene # TA150121), GFP 1/500 (Abcam #ab13970), and Phalloidin 1/100 (Invitrogen #A34055). The secondary antibodies conjugated to Alexa488, Alexa546 and Alexa647 (Jackson ImmunoResearch Laboratories) were used at 1:750. DNA was detected with Hoechst dye 33258. Confocal imaging was performed using LSM700 from Zeiss with 20X/0.8NA or 40X/1.4NA objective lenses and processed using FIJI/ImageJ software.

4.4.8 Statistical Analysis

Comparison of two unpaired independent means was performed using a student's t-test. Statistics were determined using Excel, and GraphPad Prism 6. All images are representative from at least three replicates.

4.5 Acknowledgements

We acknowledge Sara Banerjee from Université Laval for her technical expertise for SAINT analysis.

4.6 References

Al-Obaidy, K.I., Eble, J.N., Nassiri, M., Cheng, L., Eldomery, M.K., Williamson, S.R., Sakr, W.A., Gupta, N., Hassan, O., Idrees, M.T., et al. (2019). Recurrent KRAS mutations in papillary renal neoplasm with reverse polarity. Mod Pathol.

Archibald, A., Al-Masri, M., Liew-Spilger, A., and McCaffrey, L. (2015). Atypical protein kinase C induces cell transformation by disrupting Hippo/Yap signaling. Mol Biol Cell 26, 3578-3595.

Au, A.C., Hernandez, P.A., Lieber, E., Nadroo, A.M., Shen, Y.M., Kelley, K.A., Gelb, B.D., and Diaz, G.A. (2010). Protein tyrosine phosphatase PTPN14 is a regulator of lymphatic function and choanal development in humans. Am J Hum Genet 87, 436-444.

Baines, A.T., Xu, D., and Der, C.J. (2011). Inhibition of Ras for cancer treatment: the search continues. Future Med Chem 3, 1787-1808.

Barr, A.J., Debreczeni, J.E., Eswaran, J., and Knapp, S. (2006). Crystal structure of human protein tyrosine phosphatase 14 (PTPN14) at 1.65-A resolution. Proteins 63, 1132-1136.

Belle, L., Ali, N., Lonic, A., Li, X., Paltridge, J.L., Roslan, S., Herrmann, D., Conway, J.R., Gehling, F.K., Bert, A.G., et al. (2015). The tyrosine phosphatase PTPN14 (Pez) inhibits metastasis by altering protein trafficking. Sci Signal 8, ra18.

Bonilla, X., Parmentier, L., King, B., Bezrukov, F., Kaya, G., Zoete, V., Seplyarskiy, V.B., Sharpe, H.J., McKee, T., Letourneau, A., et al. (2016). Genomic analysis identifies new drivers and progression pathways in skin basal cell carcinoma. Nat Genet 48, 398-406.

Borovski, T., Vellinga, T.T., Laoukili, J., Santo, E.E., Fatrai, S., van Schelven, S., Verheem, A., Marvin, D.L., Ubink, I., Borel Rinkes, I.H.M., et al. (2017). Inhibition of RAF1 kinase activity restores apicobasal polarity and impairs tumour growth in human colorectal cancer. Gut 66, 1106-1115.

Buther, K., Plaas, C., Barnekow, A., and Kremerskothen, J. (2004). KIBRA is a novel substrate for protein kinase Czeta. Biochem Biophys Res Commun 317, 703-707.

Cabodi, S., Tinnirello, A., Di Stefano, P., Bisaro, B., Ambrosino, E., Castellano, I., Sapino, A., Arisio, R., Cavallo, F., Forni, G., et al. (2006). p130Cas as a new regulator of mammary epithelial cell proliferation, survival, and HER2-neu oncogene-dependent breast tumorigenesis. Cancer Res 66, 4672-4680.

Cerami, E., Gao, J., Dogrusoz, U., Gross, B.E., Sumer, S.O., Aksoy, B.A., Jacobsen, A., Byrne, C.J., Heuer, M.L., Larsson, E., et al. (2012). The cBio cancer genomics portal: an open platform for exploring multidimensional cancer genomics data. Cancer Discov 2, 401-404.

Chishti, A.H., Kim, A.C., Marfatia, S.M., Lutchman, M., Hanspal, M., Jindal, H., Liu, S.C., Low, P.S., Rouleau, G.A., Mohandas, N., et al. (1998). The FERM domain: a unique module involved in the linkage of cytoplasmic proteins to the membrane. Trends Biochem Sci 23, 281-282.

Duning, K., Schurek, E.M., Schluter, M., Bayer, M., Reinhardt, H.C., Schwab, A., Schaefer, L., Benzing, T., Schermer, B., Saleem, M.A., et al. (2008). KIBRA modulates directional migration of podocytes. J Am Soc Nephrol 19, 1891-1903.

Durgan, J., Kaji, N., Jin, D., and Hall, A. (2011). Par6B and atypical PKC regulate mitotic spindle orientation during epithelial morphogenesis. J Biol Chem 286, 12461-12474.

Elbediwy, A., Vincent-Mistiaen, Z.I., Spencer-Dene, B., Stone, R.K., Boeing, S., Wculek, S.K., Cordero, J., Tan, E.H., Ridgway, R., Brunton, V.G., et al. (2016). Integrin signalling regulates YAP and TAZ to control skin homeostasis. Development 143, 1674-1687.

Evans, J.D., Cornford, P.A., Dodson, A., Neoptolemos, J.P., and Foster, C.S. (2003). Expression patterns of protein kinase C isoenzymes are characteristically modulated in chronic pancreatitis and pancreatic cancer. Am J Clin Pathol 119, 392-402.

Fields, A.P., and Regala, R.P. (2007). Protein kinase C iota: human oncogene, prognostic marker and therapeutic target. Pharmacol Res 55, 487-497.

Gao, J., Aksoy, B.A., Dogrusoz, U., Dresdner, G., Gross, B., Sumer, S.O., Sun, Y., Jacobsen, A., Sinha, R., Larsson, E., et al. (2013). Integrative analysis of complex cancer genomics and clinical profiles using the cBioPortal. Sci Signal 6, pl1.

Gideon, P., John, J., Frech, M., Lautwein, A., Clark, R., Scheffler, J.E., and Wittinghofer, A. (1992). Mutational and kinetic analyses of the GTPase-activating protein (GAP)-p21 interaction: the C-terminal domain of GAP is not sufficient for full activity. Mol Cell Biol 12, 2050-2056.

Gunaratne, A., Thai, B.L., and Di Guglielmo, G.M. (2013). Atypical protein kinase C phosphorylates Par6 and facilitates transforming growth factor beta-induced epithelial-to-mesenchymal transition. Mol Cell Biol 33, 874-886.

Halaoui, R., Rejon, C., Chatterjee, S.J., Szymborski, J., Meterissian, S., Muller, W.J., Omeroglu, A., and McCaffrey, L. (2017). Progressive polarity loss and luminal collapse disrupt tissue organization in carcinoma. Genes Dev 31, 1573-1587.

Hong, X., Nguyen, H.T., Chen, Q., Zhang, R., Hagman, Z., Voorhoeve, P.M., and Cohen, S.M. (2014). Opposing activities of the Ras and Hippo pathways converge on regulation of YAP protein turnover. EMBO J 33, 2447-2457.

Jin, A., Neufeld, T.P., and Choe, J. (2015). Kibra and aPKC regulate starvation-induced autophagy in Drosophila. Biochem Biophys Res Commun 468, 1-7.

Kojima, Y., Akimoto, K., Nagashima, Y., Ishiguro, H., Shirai, S., Chishima, T., Ichikawa, Y., Ishikawa, T., Sasaki, T., Kubota, Y., et al. (2008). The overexpression and altered localization of the atypical protein kinase C lambda/iota in breast cancer correlates with the pathologic type of these tumors. Hum Pathol 39, 824-831.

Kremerskothen, J., Plaas, C., Buther, K., Finger, I., Veltel, S., Matanis, T., Liedtke, T., and Barnekow, A. (2003). Characterization of KIBRA, a novel WW domain-containing protein. Biochem Biophys Res Commun 300, 862-867.

Laczmanska, I., and Sasiadek, M.M. (2011). Tyrosine phosphatases as a superfamily of tumor suppressors in colorectal cancer. Acta Biochim Pol 58, 467-470.

Li, M., Zhao, H., Zhang, X., Wood, L.D., Anders, R.A., Choti, M.A., Pawlik, T.M., Daniel, H.D., Kannangai, R., Offerhaus, G.J., et al. (2011). Inactivating mutations of the chromatin remodeling gene ARID2 in hepatocellular carcinoma. Nat Genet 43, 828-829.

Liu, X., Yang, N., Figel, S.A., Wilson, K.E., Morrison, C.D., Gelman, I.H., and Zhang, J. (2013). PTPN14 interacts with and negatively regulates the oncogenic function of YAP. Oncogene 32, 1266-1273.

Magudia, K., Lahoz, A., and Hall, A. (2012). K-Ras and B-Raf oncogenes inhibit colon epithelial polarity establishment through up-regulation of c-myc. J Cell Biol 198, 185-194.

Mello, S.S., Valente, L.J., Raj, N., Seoane, J.A., Flowers, B.M., McClendon, J., Bieging-Rolett, K.T., Lee, J., Ivanochko, D., Kozak, M.M., et al. (2017). A p53 Super-tumor Suppressor Reveals a Tumor Suppressive p53-Ptpn14-Yap Axis in Pancreatic Cancer. Cancer Cell 32, 460-473 e466.

Michaloglou, C., Lehmann, W., Martin, T., Delaunay, C., Hueber, A., Barys, L., Niu, H., Billy, E., Wartmann, M., Ito, M., et al. (2013). The tyrosine phosphatase PTPN14 is a negative regulator of YAP activity. PLoS One 8, e61916.

Moleirinho, S., Chang, N., Sims, A.H., Tilston-Lunel, A.M., Angus, L., Steele, A., Boswell, V., Barnett, S.C., Ormandy, C., Faratian, D., et al. (2013). KIBRA exhibits MST-independent functional regulation of the Hippo signaling pathway in mammals. Oncogene 32, 1821-1830.

Moscat, J., and Diaz-Meco, M.T. (2012). p62: a versatile multitasker takes on cancer. Trends Biochem Sci 37, 230-236.

Murray, N.R., Jamieson, L., Yu, W., Zhang, J., Gokmen-Polar, Y., Sier, D., Anastasiadis, P., Gatalica, Z., Thompson, E.A., and Fields, A.P. (2004). Protein kinase Ciota is required for Ras transformation and colon carcinogenesis in vivo. J Cell Biol 164, 797-802.

Murray, N.R., Kalari, K.R., and Fields, A.P. (2011). Protein kinase Ciota expression and oncogenic signaling mechanisms in cancer. J Cell Physiol 226, 879-887.

Murray, N.R., Weems, J., Braun, U., Leitges, M., and Fields, A.P. (2009). Protein kinase C betaII and PKCiota/lambda: collaborating partners in colon cancer promotion and progression. Cancer Res 69, 656-662.

Nakhaeizadeh, H., Amin, E., Nakhaei-Rad, S., Dvorsky, R., and Ahmadian, M.R. (2016). The RAS-Effector Interface: Isoform-Specific Differences in the Effector Binding Regions. PLoS One 11, e0167145.

Niedergethmann, M., Alves, F., Neff, J.K., Heidrich, B., Aramin, N., Li, L., Pilarsky, C., Grutzmann, R., Allgayer, H., Post, S., et al. (2007). Gene expression profiling of liver metastases and tumour invasion in pancreatic cancer using an orthotopic SCID mouse model. Br J Cancer 97, 1432-1440.

Pacold, M.E., Suire, S., Perisic, O., Lara-Gonzalez, S., Davis, C.T., Walker, E.H., Hawkins, P.T., Stephens, L., Eccleston, J.F., and Williams, R.L. (2000). Crystal structure and functional analysis of Ras binding to its effector phosphoinositide 3-kinase gamma. Cell 103, 931-943.

Patankar, M., Eskelinen, S., Tuomisto, A., Makinen, M.J., and Karttunen, T.J. (2019). KRAS and BRAF mutations induce anoikis resistance and characteristic 3D phenotypes in Caco2 cells. Mol Med Rep 20, 4634-4644.

Poernbacher, I., Baumgartner, R., Marada, S.K., Edwards, K., and Stocker, H. (2012). Drosophila Pez acts in Hippo signaling to restrict intestinal stem cell proliferation. Curr Biol 22, 389-396.

Prior, I.A., Lewis, P.D., and Mattos, C. (2012). A comprehensive survey of Ras mutations in cancer. Cancer Res 72, 2457-2467.

Quinlan, M.P., and Settleman, J. (2009). Isoform-specific ras functions in development and cancer. Future Oncol 5, 105-116.

Ramesh, M., Krishnan, N., Muthuswamy, S.K., and Tonks, N.K. (2015). A novel phosphatidic acid-protein-tyrosine phosphatase D2 axis is essential for ERBB2 signaling in mammary epithelial cells. J Biol Chem 290, 9646-9659.

Regala, R.P., Davis, R.K., Kunz, A., Khoor, A., Leitges, M., and Fields, A.P. (2009). Atypical protein kinase C ι is required for bronchioalveolar stem cell expansion and lung tumorigenesis. Cancer Res 69, 7603-7611.

Regala, R.P., Weems, C., Jamieson, L., Copland, J.A., Thompson, E.A., and Fields, A.P. (2005). Atypical protein kinase Ciota plays a critical role in human lung cancer cell growth and tumorigenicity. J Biol Chem 280, 31109-31115.

Rodriguez-Boulan, E., and Macara, I.G. (2014). Organization and execution of the epithelial polarity programme. Nat Rev Mol Cell Biol 15, 225-242.

Sanchez, P., De Carcer, G., Sandoval, I.V., Moscat, J., and Diaz-Meco, M.T. (1998). Localization of atypical protein kinase C isoforms into lysosome-targeted endosomes through interaction with p62. Mol Cell Biol 18, 3069-3080.

Schubbert, S., Shannon, K., and Bollag, G. (2007). Hyperactive Ras in developmental disorders and cancer. Nat Rev Cancer 7, 295-308.

Scotti, M.L., Bamlet, W.R., Smyrk, T.C., Fields, A.P., and Murray, N.R. (2010). Protein kinase Ciota is required for pancreatic cancer cell transformed growth and tumorigenesis. Cancer Res 70, 2064-2074.

Sjoblom, T., Jones, S., Wood, L.D., Parsons, D.W., Lin, J., Barber, T.D., Mandelker, D., Leary, R.J., Ptak, J., Silliman, N., et al. (2006). The consensus coding sequences of human breast and colorectal cancers. Science 314, 268-274.

Smith, A.L., Mitchell, P.J., Shipley, J., Gusterson, B.A., Rogers, M.V., and Crompton, M.R. (1995). Pez: a novel human cDNA encoding protein tyrosine phosphatase- and ezrin-like domains. Biochem Biophys Res Commun 209, 959-965.

Smith, C.A., Lau, K.M., Rahmani, Z., Dho, S.E., Brothers, G., She, Y.M., Berry, D.M., Bonneil, E., Thibault, P., Schweisguth, F., et al. (2007). aPKC-mediated phosphorylation regulates asymmetric membrane localization of the cell fate determinant Numb. EMBO J 26, 468-480.

Suzuki, A., Hirata, M., Kamimura, K., Maniwa, R., Yamanaka, T., Mizuno, K., Kishikawa, M., Hirose, H., Amano, Y., Izumi, N., et al. (2004). aPKC acts upstream of PAR-1b in both the establishment and maintenance of mammalian epithelial polarity. Curr Biol 14, 1425-1435.

Tsunoda, T., Takashima, Y., Fujimoto, T., Koyanagi, M., Yoshida, Y., Doi, K., Tanaka, Y., Kuroki, M., Sasazuki, T., and Shirasawa, S. (2010). Three-dimensionally specific inhibition of DNA repair-related genes by activated KRAS in colon crypt model. Neoplasia 12, 397-404.

Uhlen, M., Fagerberg, L., Hallstrom, B.M., Lindskog, C., Oksvold, P., Mardinoglu, A., Sivertsson, A., Kampf, C., Sjostedt, E., Asplund, A., et al. (2015). Proteomics. Tissue-based map of the human proteome. Science 347, 1260419.

Wadham, C., Gamble, J.R., Vadas, M.A., and Khew-Goodall, Y. (2003). The protein tyrosine phosphatase Pez is a major phosphatase of adherens junctions and dephosphorylates beta-catenin. Mol Biol Cell 14, 2520-2529.

Wang, W., Huang, J., Wang, X., Yuan, J., Li, X., Feng, L., Park, J.I., and Chen, J. (2012). PTPN14 is required for the density-dependent control of YAP1. Genes Dev 26, 1959-1971.

Wang, Z., Shen, D., Parsons, D.W., Bardelli, A., Sager, J., Szabo, S., Ptak, J., Silliman, N., Peters, B.A., van der Heijden, M.S., et al. (2004). Mutational analysis of the tyrosine phosphatome in colorectal cancers. Science 304, 1164-1166.

Wilson, K.E., Li, Y.W., Yang, N., Shen, H., Orillion, A.R., and Zhang, J. (2014). PTPN14 Forms a Complex with Kibra and LATS1 Proteins and Negatively Regulates the YAP Oncogenic Function. J Biol Chem 289, 23693-23700.

Wilson, K.E., Yang, N., Mussell, A.L., and Zhang, J. (2016). The Regulatory Role of KIBRA and PTPN14 in Hippo Signaling and Beyond. Genes (Basel) 7.

Wyatt, L., Wadham, C., Crocker, L.A., Lardelli, M., and Khew-Goodall, Y. (2007). The protein tyrosine phosphatase Pez regulates TGFbeta, epithelial-mesenchymal transition, and organ development. J Cell Biol 178, 1223-1235.

Xiao, L., Chen, Y., Ji, M., and Dong, J. (2011). KIBRA regulates Hippo signaling activity via interactions with large tumor suppressor kinases. J Biol Chem 286, 7788-7796.

Yamanaka, T., Horikoshi, Y., Sugiyama, Y., Ishiyama, C., Suzuki, A., Hirose, T., Iwamatsu, A., Shinohara, A., and Ohno, S. (2003). Mammalian Lgl forms a protein complex with PAR-6 and aPKC independently of PAR-3 to regulate epithelial cell polarity. Curr Biol 13, 734-743.

Yan, Z., Chen, M., Perucho, M., and Friedman, E. (1997a). Oncogenic Ki-ras but not oncogenic Ha-ras blocks integrin beta1-chain maturation in colon epithelial cells. J Biol Chem 272, 30928-30936.

Yan, Z., Deng, X., Chen, M., Xu, Y., Ahram, M., Sloane, B.F., and Friedman, E. (1997b). Oncogenic c-Ki-ras but not oncogenic c-Ha-ras up-regulates CEA expression and disrupts basolateral polarity in colon epithelial cells. J Biol Chem 272, 27902-27907.

Yoshihama, Y., Sasaki, K., Horikoshi, Y., Suzuki, A., Ohtsuka, T., Hakuno, F., Takahashi, S., Ohno, S., and Chida, K. (2011). KIBRA suppresses apical exocytosis through inhibition of aPKC kinase activity in epithelial cells. Curr Biol 21, 705-711.

Yu, Y.P., Landsittel, D., Jing, L., Nelson, J., Ren, B., Liu, L., McDonald, C., Thomas, R., Dhir, R., Finkelstein, S., et al. (2004). Gene expression alterations in prostate cancer predicting tumor aggression and preceding development of malignancy. J Clin Oncol 22, 2790-2799.

Zhang, B., Zhang, Y., Shacter, E., and Zheng, Y. (2005). Mechanism of the guanine nucleotide exchange reaction of Ras GTPase--evidence for a GTP/GDP displacement model. Biochemistry 44, 2566-2576.

Zhang, P., Guo, A., Possemato, A., Wang, C., Beard, L., Carlin, C., Markowitz, S.D., Polakiewicz, R.D., and Wang, Z. (2013). Identification and functional characterization of p130Cas as a substrate of protein tyrosine phosphatase nonreceptor 14. Oncogene 32, 2087-2095.

Zhang, W., Nandakumar, N., Shi, Y., Manzano, M., Smith, A., Graham, G., Gupta, S., Vietsch, E.E., Laughlin, S.Z., Wadhwa, M., et al. (2014). Downstream of mutant KRAS, the transcription regulator YAP is essential for neoplastic progression to pancreatic ductal adenocarcinoma. Sci Signal 7, ra42.

4.7 Supplemental Figures

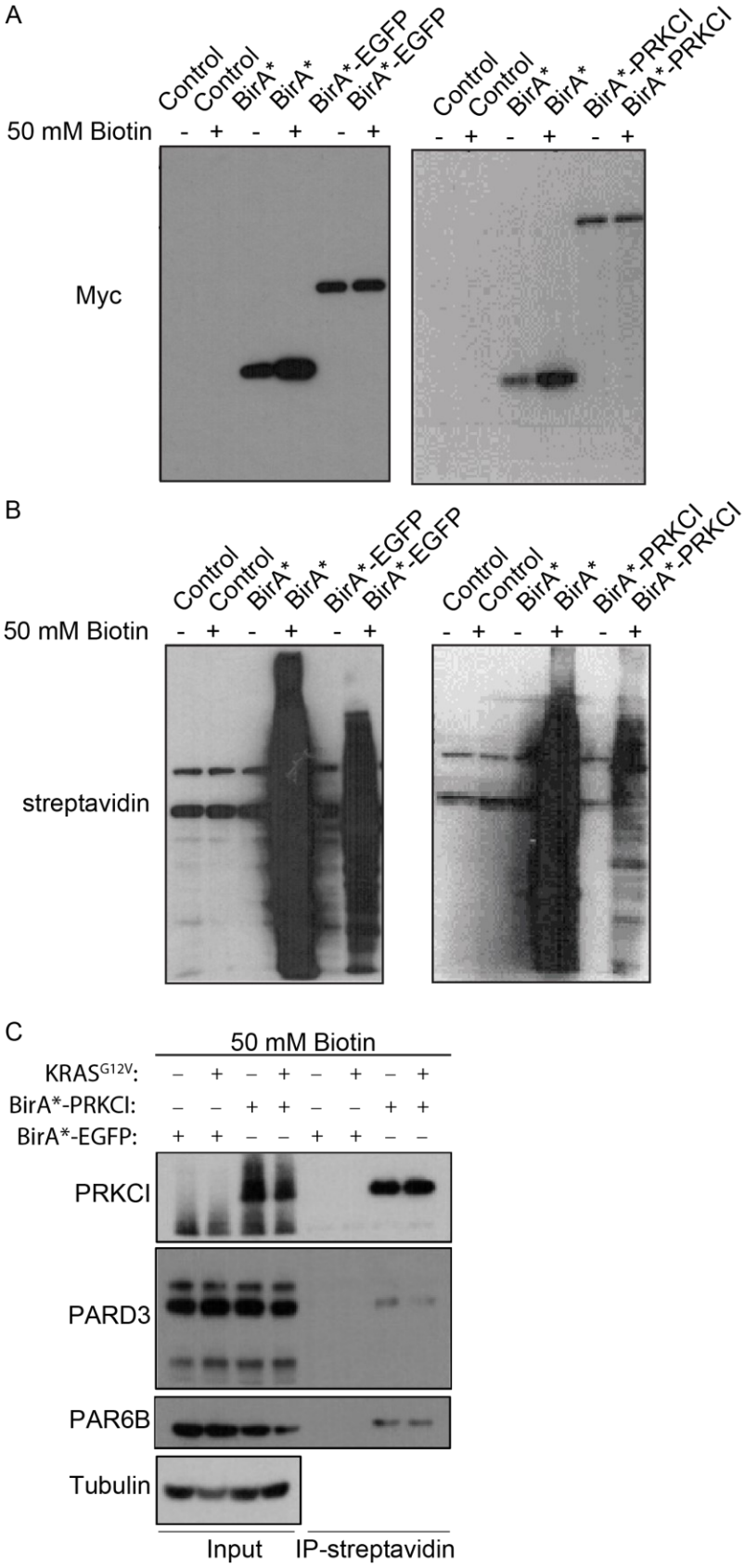

Supplemental Figure S4.1: Validation of BioID approach. Associated with Figure 4.1. (A) Myc epitope-tagged BirA*-EGFP (as wildtype) and BirA*-PRKCI in pWPI vector were generated for transient expression in HEK293 cells and cells were cultured with 50 mM biotin for 24 hours. Western blotting analysis using myc indicates the expression of BirA*, BirA*-EGFP (left panel) and BirA*-PRKCI (right panel). (B) Western blotting showing BirA*, BirA*-EGFP (left panel) and BirA*-PRKCI (right panel) promiscuously biotinylate endogenous proximal proteins which were detected with streptavidin-HRP. (C) Control and $KRAS^{G12V}$-transformed Caco-2 cells were expressed with BirA*-EGFP or BirA*-PRKCI and cultured with 50 mM biotin for 24 hours. Immunoprecipitation was performed with streptavidin beads, followed by western blotting analysis for PRKCI, PARD3, PARD6B.

A

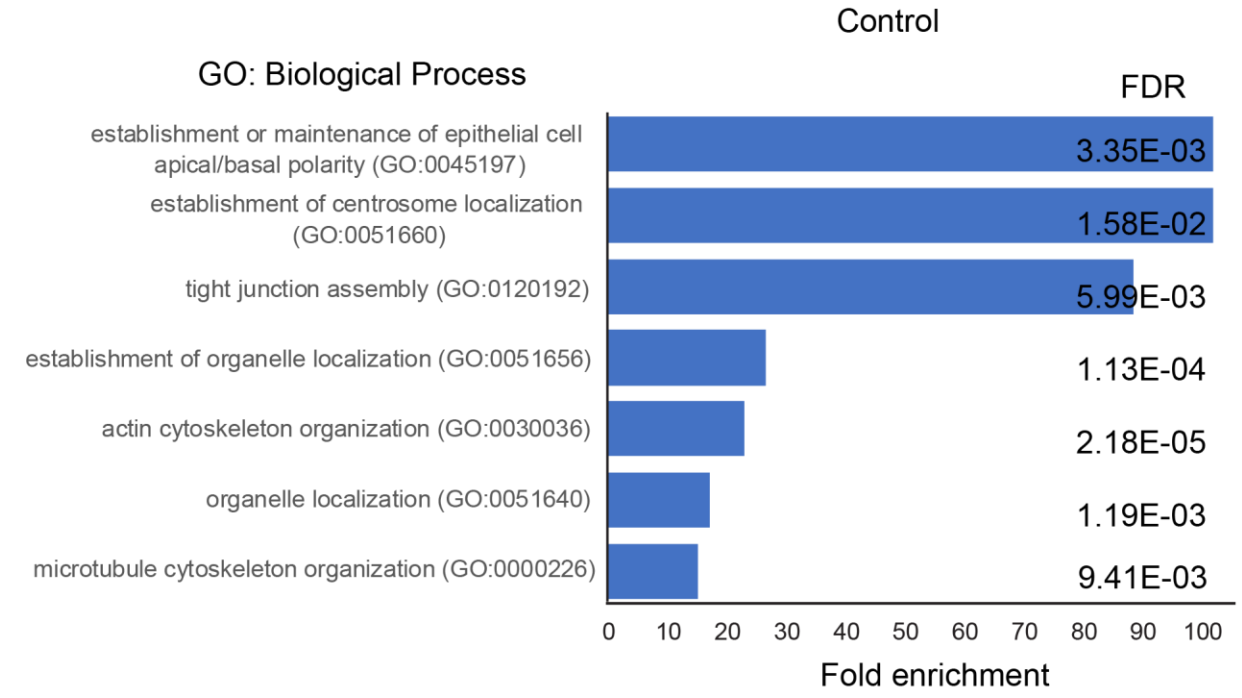
Control
GO: Biological Process
FDR
establishment or maintenance of epithelial cell apical/basal polarity (GO:0045197)
establishment of centrosome localization (GO:0051660)
tight junction assembly (GO:0120192)
establishment of organelle localization (GO:0051656)
actin cytoskeleton organization (GO:0030036)
organelle localization (GO:0051640)
microtubule cytoskeleton organization (GO:0000226)
3.35E-03
1.58E-02
5.99E-03
1.13E-04
2.18E-05
1.19E-03
9.41E-03
0 10 20 30 40 50 60 70 80 90 100
Fold enrichment

B

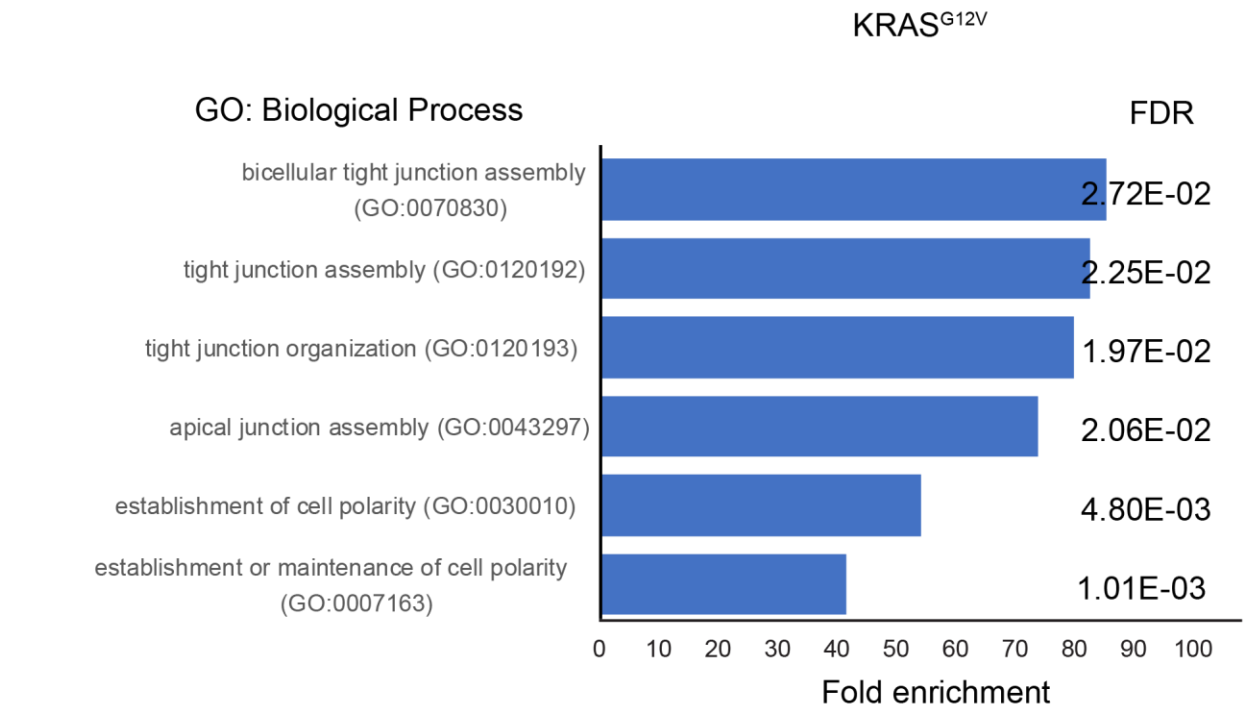
KRASG12V
GO: Biological Process
FDR
bicellular tight junction assembly (GO:0070830)
tight junction assembly (GO:0120192)
tight junction organization (GO:0120193)
apical junction assembly (GO:0043297)
establishment of cell polarity (GO:0030010)
establishment or maintenance of cell polarity (GO:0007163)
2.72E-02
2.25E-02
1.97E-02
2.06E-02
4.80E-03
1.01E-03
0 10 20 30 40 50 60 70 80 90 100
Fold enrichment

Supplemental Figure S4.2: Identification of BirA*-PRKCI vicinal proteins in control and KRAS^{G12V} screens by Gene Ontology. Associated with Figure 4.2. (A) Graph showing fold enrichment of different biological processes of BirA*-PRKCI vicinal proteins in control screens based on Gene Ontology. The BirA*-PRKCI vicinal proteins in control samples are involved in cell polarity and cytoskeleton organization. FDR: False Discovery Rates. (B) Graph showing fold enrichment of different biological processes of BirA*- PRKCI vicinal proteins in KRAS^{G12V} screens based on Gene Ontology. The BirA*-PRKCI vicinal proteins in KRAS^{G12V} screens are involved in cell polarity and junctional organization.

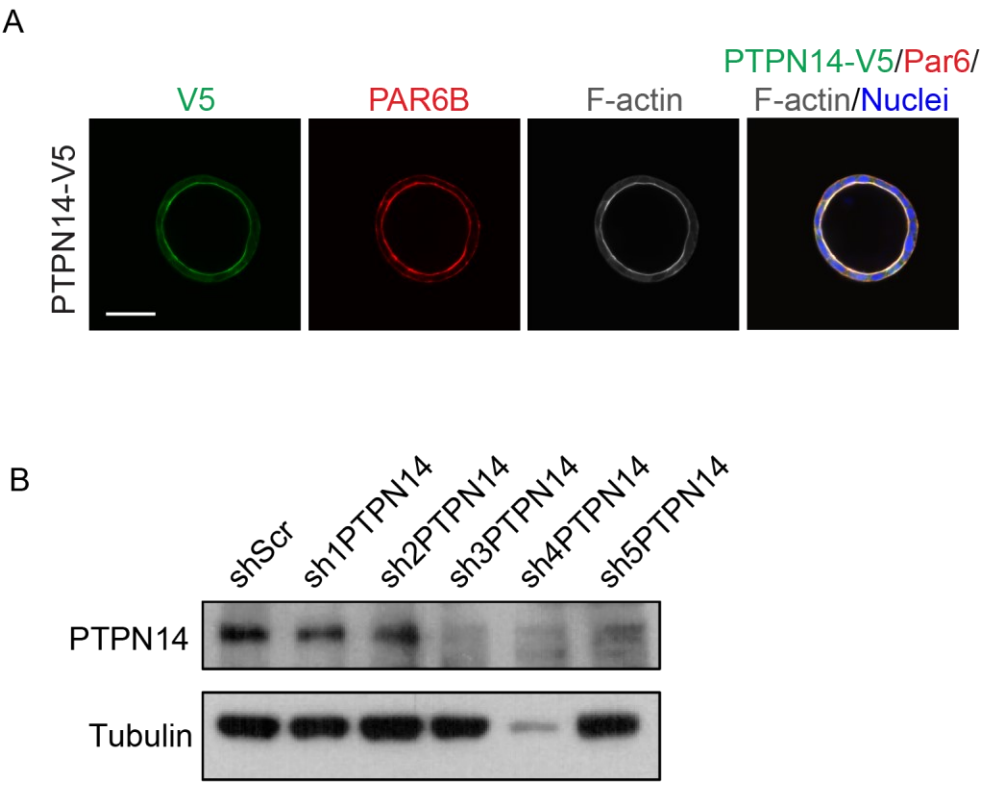

Supplemental Figure S4.3: PTPN14 is associated with PARD6B and localizes to apical membrane of polarized Caco-2 cysts. Associated with Figure 4.3. (A) Confocal images were captured for PTPN14-V5-expressed 3D Caco-2 cysts immunostained for PTPN14-V5 (green), Par6 (red), and F-actin (grey) showing the co-localization of PTPN14 and PARD6B. (B) Western blotting shows the knockdown efficiency of different shRNAs for PTPN14 in Caco-2 cells. Scale Bars: A, 50µm.

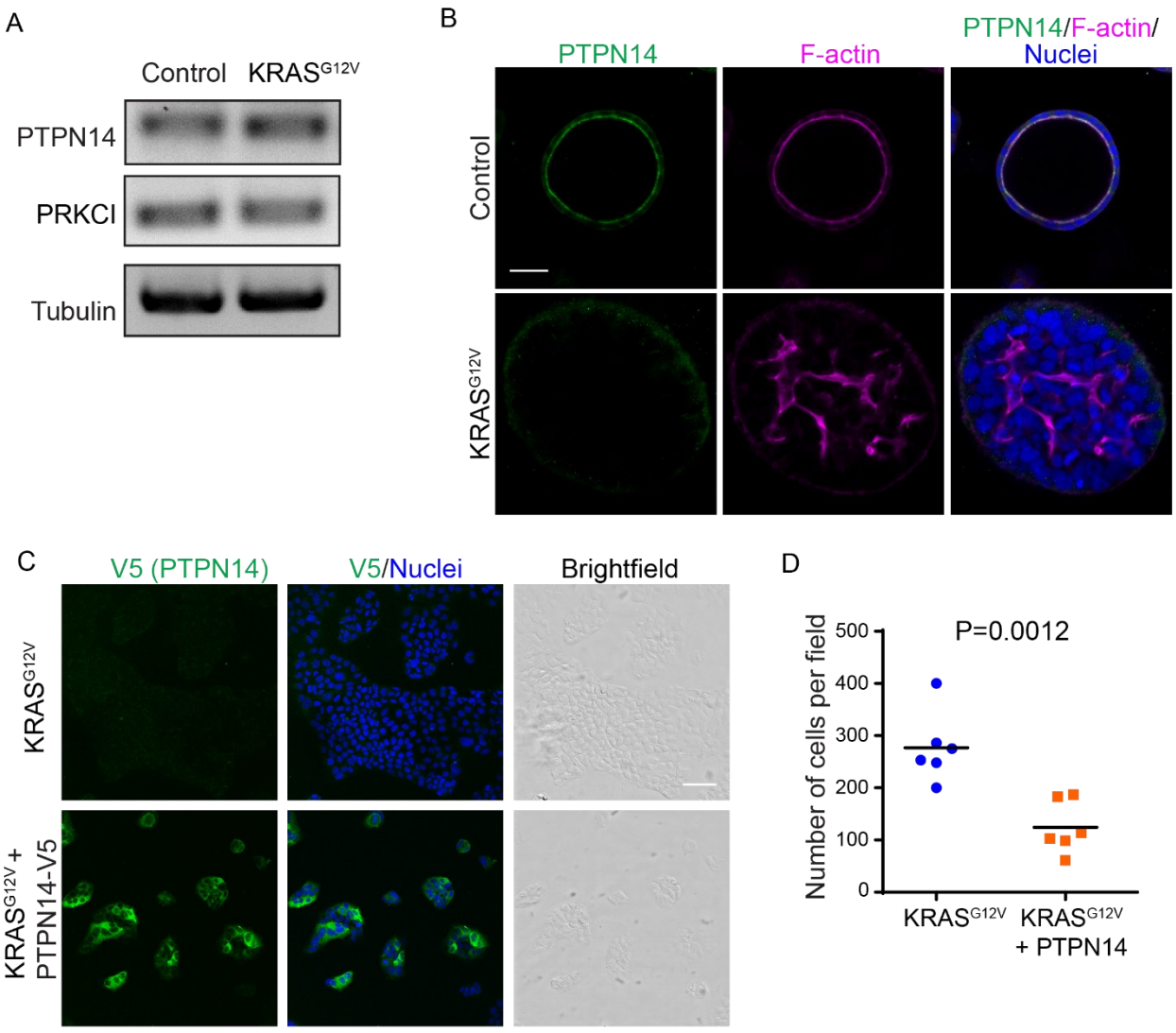

Supplemental Figure S4.4: PTPN14 suppresses KRAS^{G12V}-induced transformation in Caco-2 cells. Associated with Figure 4.4. (A) mRNA abundance of PTPN14 and PRKCI was compared between control and KRAS^{G12V}-transformed Caco-2 cells. (B) Confocal images were captured for control and KRAS^{G12V}-transformed Caco-2 cysts immunostained for PTPN14 (green) and F-actin (magenta) showing the expression and localization of PTPN14. (C) Images for PTPN14-V5 (green) showing overexpression of PTPN14 suppresses KRAS^{G12V}-induced transformation in Caco-2 cells. (D) Quantification of number of cells per field in KRAS^{G12V}-transformed Caco-2 cells with or without PTPN14 overexpression. Scale Bars: B, 30µm; C,100µm.

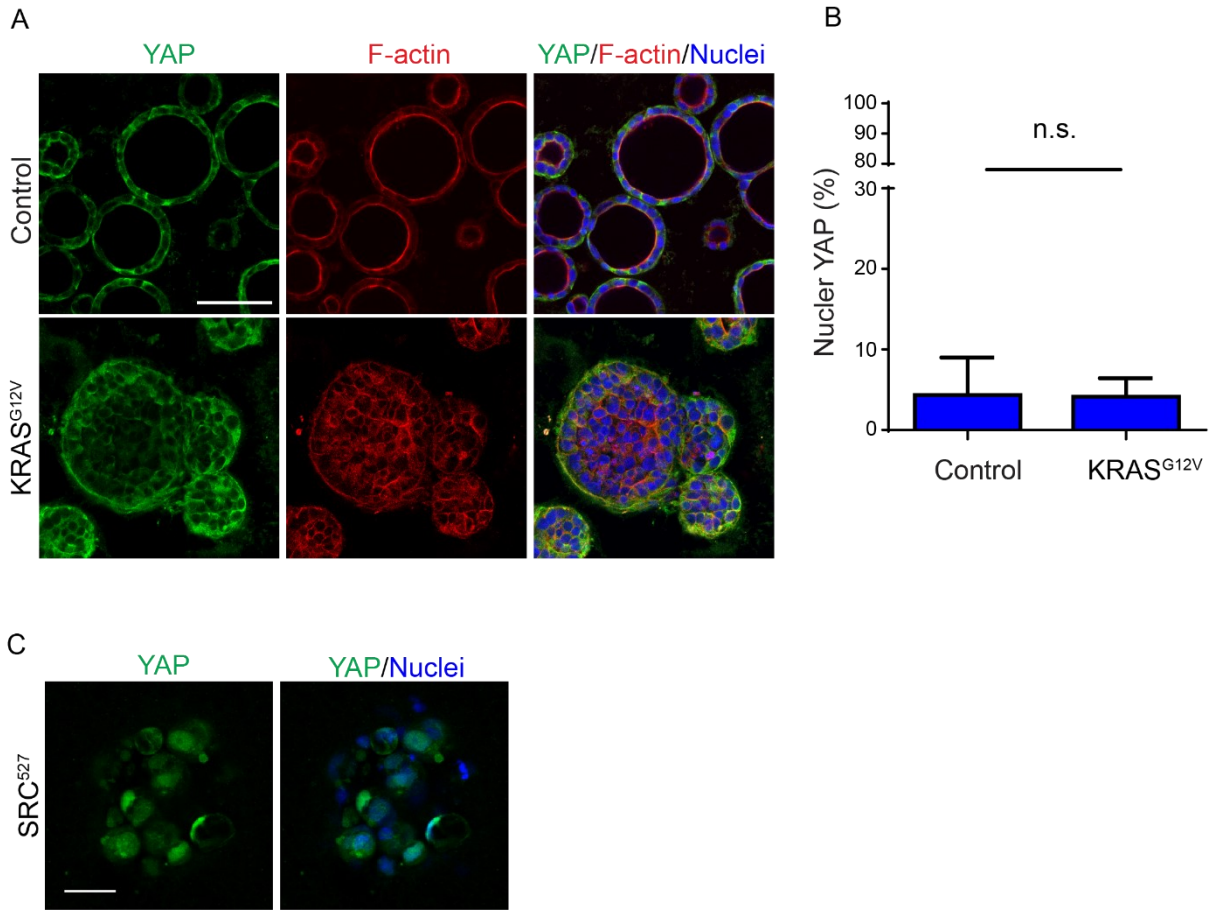

Supplemental Figure S4.5: KRAS^{G12V} expression in Caco-2 cysts does not induce Hippo signalling. Associated with Figure 4.4. (A) Confocal images for YAP (green) and F-actin (red) showing the localization of YAP in control and KRAS^{G12V}-transformed Caco-2 cysts. (B) Quantification the percentage of nuclear YAP in control and KRAS^{G12V}-transformed Caco-2 cysts. (C) Confocal images for YAP (green) showing YAP translocates to the nucleus in SRC^{527}-expressed Caco-2 cysts. Scale Bars: A, 100µm; C, 50µm.

Chapter 5: Discussion, Future Directions, and Conclusions

In this body of work, I identified and characterized the functions of novel polarity-associated proteins in lumen formation using a three-dimensional cell culture model. First, I provided an approach for proteomic studies using a 3D suspension model that efficiently generates highly polarized epithelial structures. This enables generating large batches of cells while minimizing the amount of basement membrane matrix necessary and cost. I implemented BioID to investigate the novel proteins associated with PAR6B and PRKCI/aPKCι in 3D Caco-2 cells.

Many concepts were discussed in the individual Chapters 2, 3 and 4. Here, I will expand and integrate these concepts and will present some preliminary data that extends our understanding of polarity in cancer that is related to Chapters 3 and 4. Finally, I will discuss additional questions raised by this thesis work and propose future studies to address them.

5.1 Novel proteins are involved in lumen formation were identified by 3D BioID approach

Lumen formation is a vital process for development of tissues and organs such as gut, kidney, blood vessels, and lung. Cell polarity is necessary for lumen formation, and the machinery for cell polarization is becoming better understood with recent studies using proteomics to identify the components of the cell polarity machinery. However, our understanding of lumen formation and epithelial morphogenesis lags. The results presented in this thesis integrate discovery screens (BioID) with functional studies, which is essential for identifying novel cell polarity effectors that are crucial for lumenogenesis and epithelial tissue organization. An advantage of a proximity-based screen is that it identifies proteins that are likely part of a complex with a protein of interest, which gives clues to a general mechanism, and is validated by functional assays. BioID provides a complementary approach to established methods used to

characterize potential protein-protein interactions in complexes (Choi-Rhee et al., 2004; Cronan, 2005). BioID can detect proteins that directly interact either transiently or stably, indirect interactions, or vicinal proteins that do not interact directly or indirectly (Varnaite and MacNeill, 2016). My results provide a means of identifying neighboring and potentially interacting proteins in novel 3D suspension culture method that is amenable to generating large numbers of cells necessary for mass spectrometric analysis, while minimizing the use of BME, the most expensive component for 3D culture. I implemented this 3D cell culture model for BioID to identify protein-protein interactions in cell polarity and to demonstrate that 3D cell culture presents different protein-protein interactions than 2D. This indicates that the cellular environment of different models is crucial for investigating polarity protein interactions in epithelial cell.

While unbiased approaches for statistically scoring proteomics hits using criteria such as the SAINT score are useful for identifying high-probability interactions, they are not without their limitations. For example, low abundance proteins or proteins not amenable to biotin ligation may not be readily detected and not pass through quality control criteria. In this regard, manual inspection of data can identify potential interactions that would be otherwise overlooked. Based on my mass spectrometry data, the core polarity proteins for PRKCI and PAR6B were readily identified as high-confidence hits, as well as other novel proteins including PTPN14 and HRNR. We also identified lower-confidence hits (RALB) that demonstrated involvement in cell polarity and lumen formation in functional studies. However, CD13 was only identified in a preliminary BioID screen for Par-complex proximal proteins. BioID utilizes a biotin ligase, BirA* that allows promiscuous biotinylation to exposed lysines on proximal proteins irrespective of whether they are direct or indirectly interaction or located in the same neighborhood within an approximately

10 nm radius by generating high reactive and short-lived bioAMP (Roux et al., 2012). For CD13, there is only one lysine in its intracellular domain (MA**K**GFYIS) that can be biotinylated by BirA*. Moreover, endogenous CD13 is expressed at low level in Caco-2 cells, providing potential explanations to why CD13 only showed up rarely and with low peptide counts. Therefore, this information indicates that some novel interactors may be neglected from mass spectrometer analysis by using highly stringent criteria.

5.2 The role of novel proteins in lumen formation

The formation of a central lumen requires precise coordination of multiple intra- and intercellular events that establish a polarity axis, position apical determinants between cells, and separate cell-cell contacts to expand a central luminal cavity (Blasky et al., 2015; Bryant et al., 2010; Datta et al., 2011; Fremont and Echard, 2018). This architecture is essential for normal tissue function and epithelial homeostasis, but is frequently disrupted or lost in diseases including cancer (Halaoui and McCaffrey, 2015a; Saito et al., 2018). It has been shown that lumen formation requires trafficking of apical polarity proteins such as Ezrin, Podocalyxin, and Crumbs3 from the peripheral membrane to an internal site to assist first cell division (Bryant et al., 2014; Schluter et al., 2009b). However, the cues that initiate internalization of apical proteins from the periphery to establish an internal apical site are currently unknown. For example, Crumbs3 knockout mice do not show obvious polarity and cell-cell junction defects, suggesting that compensatory mechanisms may support cell polarity. Crumbs3 has been shown to function as regulator for actomyosin dynamics or growth control, however, its intracellular domains are redundant for polarity mechanism (Charrier et al., 2015; Margolis, 2018; Whiteman et al., 2014). My results demonstrate that CD13 is a novel factor that controls epithelial lumen formation by

directing the orientation of apical-basal polarity. My imaging data reveal that CD13 is dynamically localized during apical membrane initiation and lumen formation in a pattern that is distinct from other apical proteins. In non-polarized cells, apical proteins are distributed to the cell periphery and re-distributed to the midbody through Rab11-mediated endocytosis to form an apical membrane initiation site that marks the position of the future lumen (Jaffe et al., 2008b; Roman-Fernandez and Bryant, 2016; Schluter et al., 2009a; Wang et al., 2000). While CD13 also localized to the periphery in non-polar cells, unlike other apical proteins, it temporarily localized to the cell-cell adhesion that is also positive for E-cadherin. CD13 then redistributed through vesicles that accumulated internally, co-incident with delivery of other apical proteins that converged to establish an internal apical membrane site that excludes E-cadherin. Although studies reveal diverse tissues that undergo lumen initiating *in vivo*, such as in mouse aorta (Strilic et al., 2009), zebrafish neuroepithelial (Tawk et al., 2007), Drosophila pupal photoreceptor and tracheal tube and Drosophila terminal tracheal cells (Baer et al., 2009; Gervais and Casanova, 2010), most mechanistic studies for lumen formation have been implemented using 3D *in vitro* culture models. Studies indicate that fundamental mechanisms of lumen formation observed in 3D models recapitulate events *in vivo* (Cerruti et al., 2013; Mangan et al., 2016; Rathbun et al., 2020), however, it will be important to understand additional layers of complexity during tissue morphogenesis in more complex and diverse environments found *in vivo*, and this would be important for CD13, which is expressed in multiple cell types and may regulate cell organization differently between tissue or cell types.

5.3 The role cell trafficking in lumen formation

Cell division represents the earliest known symmetry breaking event to position a central lumen in 3D cysts and *in vivo* (Cerruti et al., 2013; Mangan et al., 2016; Rathbun et al., 2020). I propose that CD13 regulates Rab11-dependent endocytosis of apical proteins necessary to establish an internal lumen. In support of this model, my results show that CD13 colocalizes and associates with Rab11 in the peripheral plasma membrane and a subset of vesicles in non-polarized cells. Second, Rab11-postive endosomes are recruited to and decorate CD13 patches at internal sites. Third, in the absence of CD13, cells fail to internalize apical proteins and redistribute them to the midbody. Forth, Rab11 is mislocalized and does not accumulate at a single internal site in CD13-deficient cells. Therefore, based on my results, it is likely that CD13 acts at multiple steps in orienting apical-basal polarity with a major role as a membrane cue for Rab11-dependent apical protein endocytosis. Rab11 is required for mitotic spindle orientation through affecting dynein-dependent endosome localization at poles (Hehnly and Doxsey, 2014). Rab11 also plays an important role in regulating the trafficking of proteins for cell abscission and loss of Rab11 causes cytokinetic failure and multinucleated cells (Mangan et al., 2016). I did not observe cytokinetic deficiencies or multinucleated cells in our experiments, indicating that CD13 may regulate a subset of Rab11-dependent endocytic events, likely restricted to apical membrane trafficking in epithelial cells. However, I cannot exclude other trafficking roles for CD13 that are context specific. For example, in mouse embryonic fibroblasts, CD13 is required for endocytosis of β1-integrin to Rab11-positive endosomes during cell migration (Ghosh et al., 2019). Since other Rab proteins-Rab4, Rab5, Rab6, Rab7, Rab8, Rab10, Rab11, Rab13, Rab14, Rab17, Rab22, Rab25, Rab27, and Rab35 have been implicated in polarized epithelial trafficking

machinery (Blum et al., 2020; Klinkert and Echard, 2016; Klinkert et al., 2016; Lu and Wilson, 2016; Rodriguez-Boulan and Macara, 2014), whether CD13 regulates other Rab proteins is unknown. Moreover, since Rab proteins are also involved in other mechanisms, there could be other alternative Rab-dependent processes that CD13 is involved in that we are not yet aware of. These questions could be answered through investigating CD13 knockdown in other Rab-dependent processes such as phagocytosis, pinocytosis, and exocytosis.

The midbody is created within the intercellular bridge during cytokinesis and directs trafficking of apical membrane to a position between cells (D'Avino and Capalbo, 2016; Overeem et al., 2015) (Jaffe et al., 2008a). Interestingly, the relationship between the apical domain and midbody is bi-directional. In addition to the midbody serving to direct endocytic trafficking of apical proteins, apical proteins also direct the position of the midbody, and depletion of some apical proteins can cause displacement of the midbody that leads to ectopic lumen formation (Jaffe et al., 2008a; Lujan et al., 2016). Although my findings show that cell division appeared able to proceed in CD13-deficient cells, I did observe asymmetric placement of the midbody away from the center of cell aggregates. In the context of CD13 depletion, I speculate that apical membrane retained at the periphery of cell aggregates may cause the midbody to be pulled away from the center, although alternatives where CD13 more directly controls midbody position are also possible (Mangan et al., 2016). Therefore, this information demonstrates that lumen formation is a complex and dynamic process that requires spatial and temporal coordination for epithelial lumen morphogenesis.

5.4 Loss of apical-basal polarity is reversed upon polarity protein induction.

The progression of carcinoma (epithelial cancers) is associated with loss of apical-basal polarity, and collapse and filling of the lumen to generate solid ducts (Halaoui et al., 2017). Since CD13 is essential for lumen formation, we hypothesized that CD13 may be important to regulate lumen integrity in malignant cells. To explore this possibility, we immunostained PAR6B and CD13 in human breast tissue samples and observed that CD13 colocalizes with PAR6B to the apical membrane in normal ducts, but CD13 and PAR6B are lost from the apical membrane in pre-invasive and invasive regions (Figure 5.1 A; arrow), indicating that disrupted CD13 is associated with loss of cell polarity and disease progression.

Since CD13 is a potent promoter of apical-basal polarity in Caco-2 cells, and $KRAS^{G12V}$ expression disrupts polarity and generates solid structures in 3D culture, I have begun to explore a role for CD13 in regulating polarity during malignant-transformation. To understand a role for CD13 in malignant cells we evaluated Caco2 cells expressing oncogenic KRAS ($KRAS^{G12V}$), an important driver of colon cancer (Hardiman, 2018). I modified Caco-2 cells to stably express constitutively active $KRAS^{G12V}$ and observed that the protein level of induced CD13 increased 8-9-fold in 3D Caco-2 cysts (Figure 5.1 B). To further examine a role of CD13 and apical-basal polarity in $KRAS^{G12V}$ transformation, cDNA for EGFP or CD13 under doxycycline-inducible promoter for inducible CD13 expression was introduced to cells using lentivirus. CD13 or EGFP expression were induced by adding of doxycycline to the culture every two days (Figure 5.1 C). Non-transformed Caco-2 cells formed polarized cysts in 3D culture with a regular, hollow central lumen, however, $KRAS^{G12V}$-transformed cysts produce solid, irregular structures with disrupted cell polarity, as expected (Figure 5.1 D). However, when CD13 was induced in $KRAS^{G12V}$-transformed Caco-2 cysts

(cultured 4 days prior to CD13 induction and 6 days after) I observed that $KRAS^{G12V}$-transformed Caco-2 cysts reverted to structures with apical-basal polarity and a hollow lumen (Figure 5.1 E, F; Figure 5.2). To investigate the dynamics of lumen formation, I labeled cells with GFP-tagged PAR6B and tracked cell cysts for several hours after induction. Strikingly, CD13 induction reversed the transformation phenotype to polarized normal like cyst (Figure 5.3 A). This demonstrates that disruption of cell polarity was reversible upon CD13 induction. Interestingly, in cysts with heterogeneous CD13 expression in individual cells, I observed that the lumen collapse around cells with undetectable or low expression of CD13 in the apical domain in CD13-induced $KRAS^{G12V}$-transformed Caco-2 cysts (Figure 5.3 B). This suggests that the requirement for CD13 in cell polarity not only in normal condition cysts but also oncogene-transformed epithelial cells. Overall, these findings highlight that disruption of cell polarity by $KRAS^{G12V}$ constitutively expression is reversible upon CD13 induction. Thus, CD13 is an apical determinant regulator of epithelial cell polarity during lumen formation that is required for polarization and suppressing carcinogenesis. Future studies investigating the mechanism of repolarization of CD13 in cancer progression will help to understand how CD13 suppress the progression of epithelial cancers.

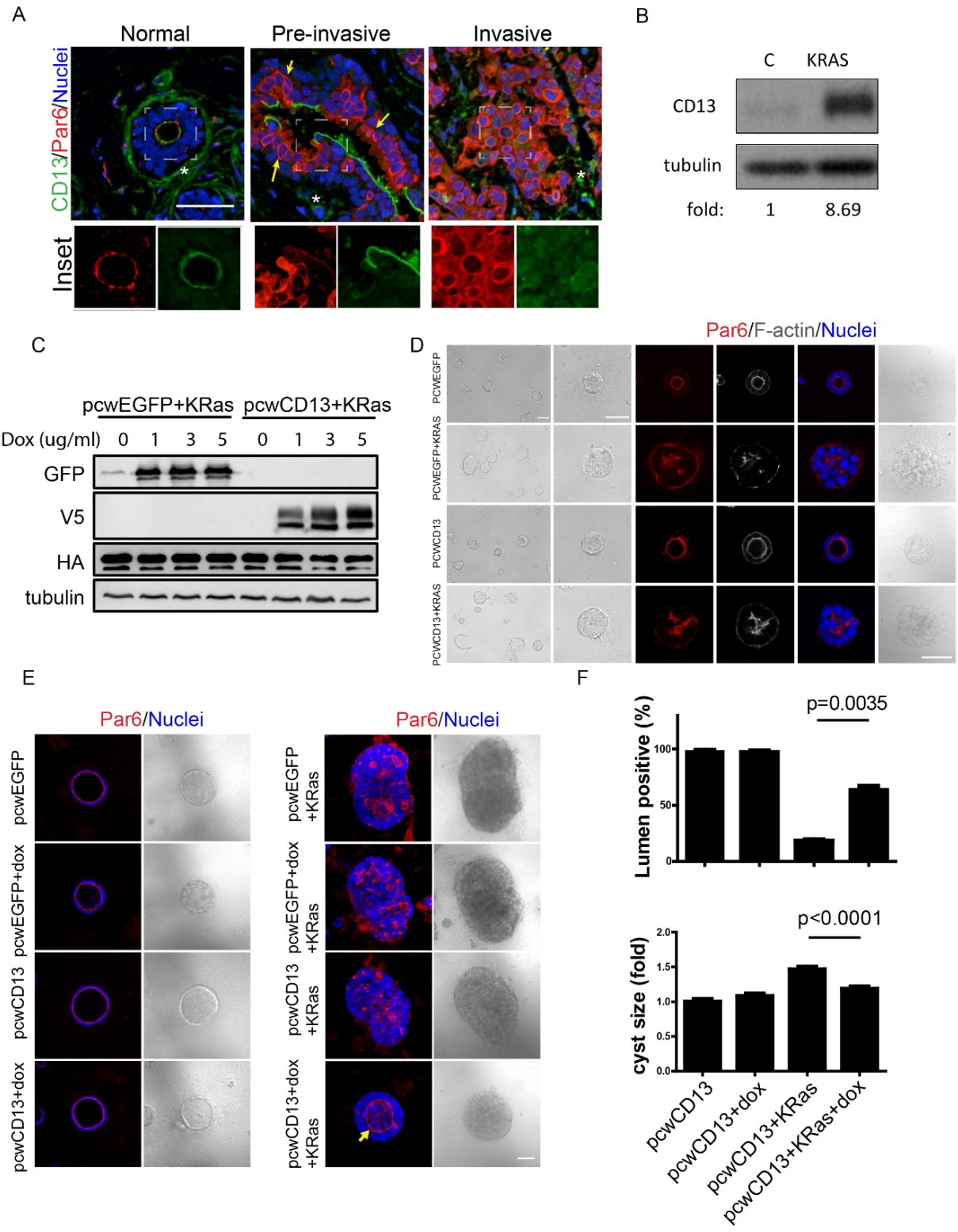
A
Normal
Pre-invasive
Invasive
CD13/Par6/Nuclei
Inset
B
C
KRAS
CD13
tubulin
fold:
1
8.69
C
pcwEGFP+KRas
pcwCD13+KRas
Dox (ug/ml)
0
1
3
5
0
1
3
5
GFP
V5
HA
tubulin
D
Par6/F-actin/Nuclei
PCWEGFP
PCWEGFP+KRAS
PCWCD13
PCWCD13+KRAS
E
Par6/Nuclei
Par6/Nuclei
pcwEGFP
pcwEGFP+dox
pcwCD13
pcwCD13+dox
pcwEGFP +KRas
pcwEGFP+dox +KRas
pcwCD13 +KRas
pcwCD13+dox +KRas
F
p=0.0035
Lumen positive (%)
100
50
0
p<0.0001
cyst size (fold)
2.0
1.5
1.0
0.5
0.0
pcwCD13
pcwCD13+dox
pcwCD13+KRas
pcwCD13+KRas+dox

Figure 5.1 Loss of apical-basal polarity is reversed upon CD13 induction. (A) Image of human breast tissue immunostained for PAR6B (red) and CD13 (green) showing CD13 colocalizing with PAR6B to the apical membrane in normal ducts. CD13 is lost from the apical membrane in pre-invasive regions with Par6 in the cytoplasm. Asterisk (*) shows stromal CD13 staining. Yellow arrows show cytoplasmic Par6. (B) Western blotting was performed with anti-CD13 in $KRAS^{G12V}$-transformed 3D cysts of cultured Caco-2 cells. (C) Western blotting was performed with anti-GFP, V5, and HA in $KRAS^{G12V}$-transformed Caco-2 cells with or without doxycycline-induced EGFP or CD13 expression. (D) Image of day4 3D cysts of cultured $KRAS^{G12V}$-transformed Caco-2 cells without doxycycline-induced EGFP or CD13 expression immunostained for Par6 (red) and F-actin (grey). (E) Image of 3D cysts of cultured $KRAS^{G12V}$-transformed (right panel) Caco-2 cells with or without doxycycline-induced EGFP or CD13 expression immunostained for Par6 (red). Yellow arrow heads indicate polarized Par6. (F) Quantification of lumen positive (top) and cyst size (bottom) of 3D cysts of cultured $KRAS^{G12V}$-transformed Caco-2 cells with or without doxycycline-induced CD13 expression. Bars: A, D, E, 50µm

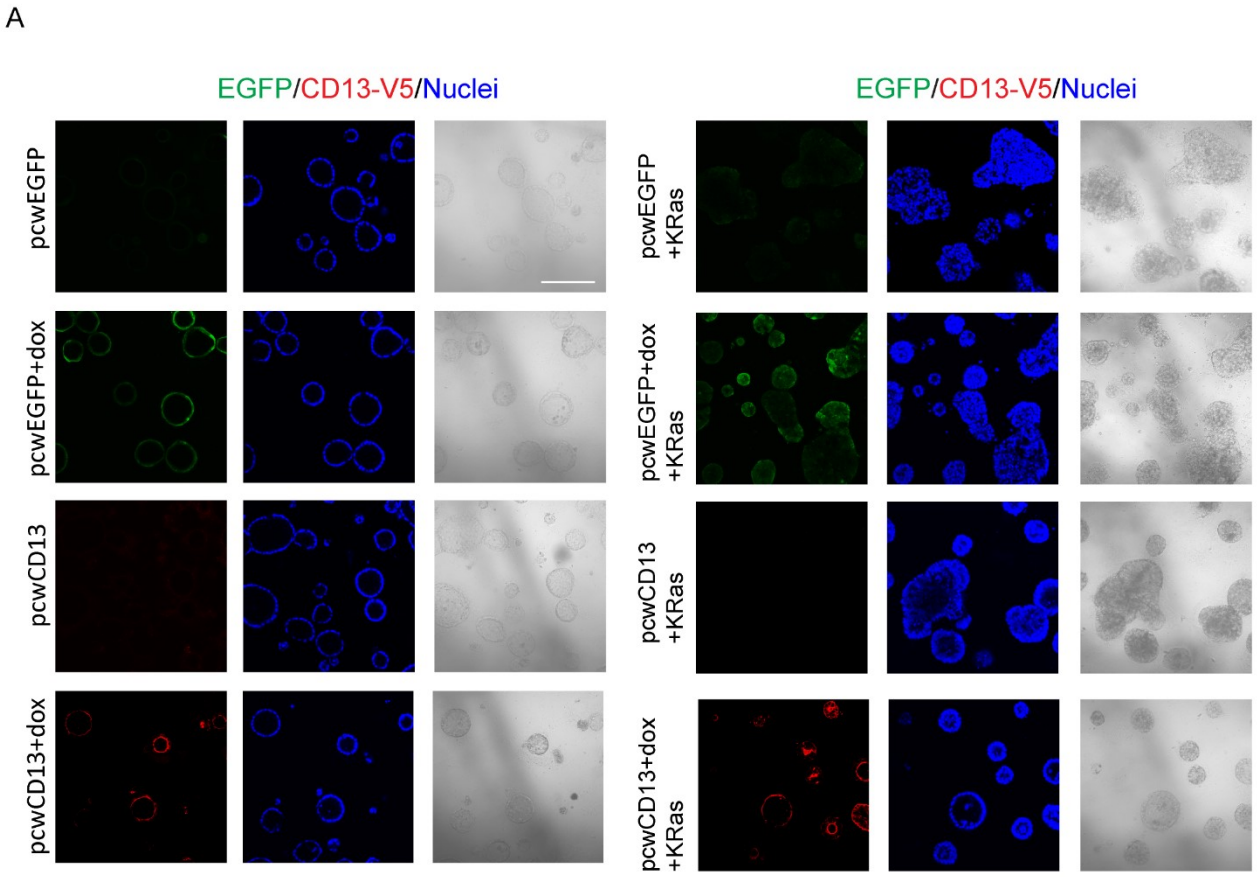

Figure 5.2 Loss of apical-basal polarity is reversed upon CD13 induction. (A) Widefield images of wild type (left panel) or $KRAS^{G12V}$-transformed (right panel) 3D Caco-2 cysts with or without doxycycline-induced EGFP or CD13 expression immunostained for EGFP (green) and CD13-V5 (red). Bars: A, 200µm

A

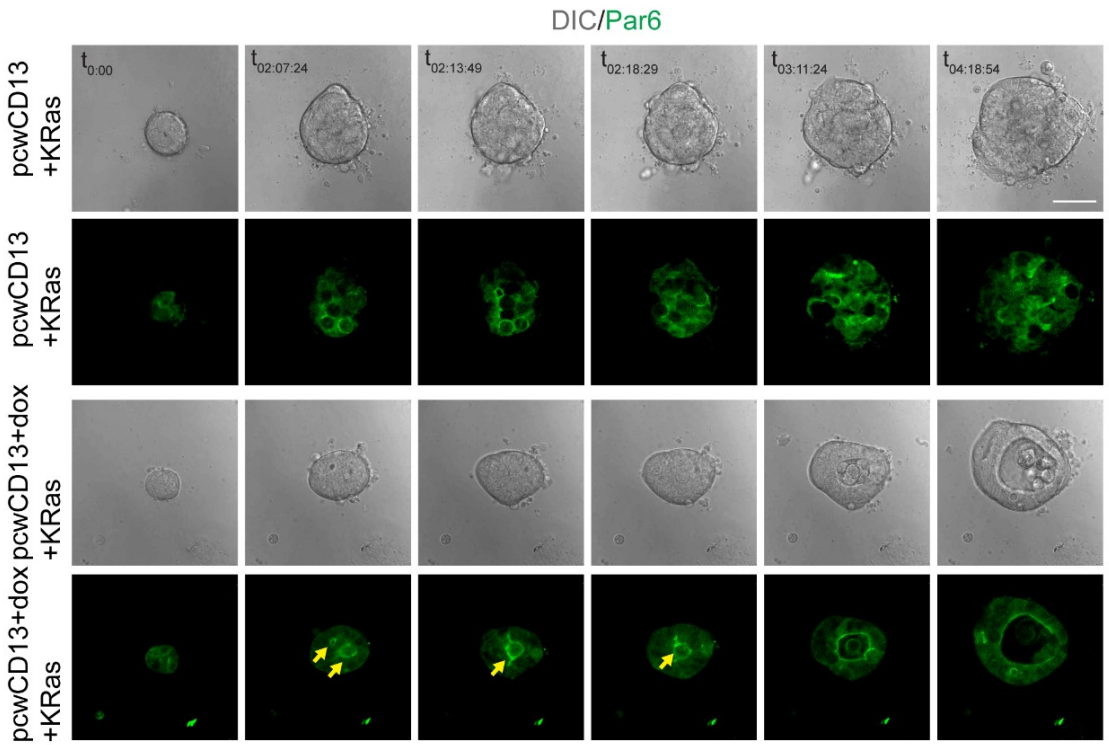
DIC/Par6
pcwCD13 +KRas
pcwCD13 +KRas
pcwCD13+dox +KRas
pcwCD13+dox +KRas
t0:00
t02:07:24
t02:13:49
t02:18:29
t03:11:24
t04:18:54

B

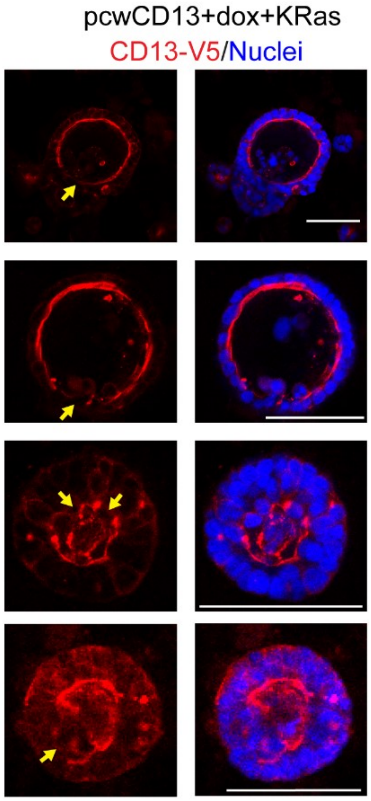
pcwCD13+dox+KRas
CD13-V5/Nuclei

Figure 5.3 CD13 is involved in cell repolarization in KRAS^{G12V}-transformed cysts. (A) DIC/fluorescence images showing selected frames from time-lapse series of GFP-Par6 during cell polarization in inducible-CD13 of KRAS^{G12V}-transformed Caco-2 cysts. Images were captured every 35 min for 115 hrs. Yellow arrows show the coalescence lumen formation. (B) Confocal images of KRAS^{G12V}-transformed Caco-2 cysts with CD13 induction immunostained for CD13-V5 (red). Yellow arrows indicate the area where CD13 is absent in heterogeneous cysts. Images are examples from different samples. Bars: A, 30µm; B, 100µm.

5.5 The role of novel proteins in epithelial polarity programme

CD13 is a widely expressed protein that has been shown to localize to the apical brush border (Fairweather et al., 2012; Riemann et al., 1999). The results presented in this thesis show that CD13 associates with an apical polarity complex containing PAR6B, aPKC, PALS1, and CRB3, but not PARD3. Moreover, I show that PAR6B-CD13 interaction requires the PB1-domain of Par6 and the intracellular domain of CD13. However, although PAR6B interacts with aPKC through its PB1 domain (Wilson et al., 2003), a point-mutation in the PB1-domain of PAR6B that disrupted its interaction with aPKC retained the capacity to associate with CD13, deletion or mutation of other protein-protein interaction domains within PAR6B that mediate its known interactions (Rodriguez-Boulan and Macara, 2014) also retained the ability to associate with CD13. This indicates that PAR6B either binds CD13 directly through its PB1 domain, or indirectly through an unidentified intermediate. My data indicate that catalytic activity of CD13 is dispensable for its role in organizing apical-basal polarity. However, the tyrosine residue within the short intracellular domain (Tyr6) is specifically required to establish an internal apical domain and lumen. Consistent with this, other studies have found the same tyrosine residue is required for non-catalytic functions, including cell adhesion and migration (Ghosh et al., 2019; Subramani et al., 2013), indicating that this residue may have diverse roles in regulating diverse functions through the intracellular domain. My results reveal that Tyr6 was necessary for the association with Par6 whereas this residue was dispensable for CD13 to associate with Rab11. This supports a role for CD13 in linking the apical polarity complex to Rab11 at the plasma membrane to allow apical protein endocytosis.

Based on my observations, silencing of CD13 induced an inverted polarity phenotype in Caco-2 cysts, which was characterized by apical complexes and tight junctions positioned at the periphery of cell aggregates, while basolateral proteins were excluded from the outer edge and interactions with the matrix were impaired. Polarity inversion phenotypes have been examined and several mechanisms involved in polarity inversion, including defects of trafficking mechanism so that polarity proteins could not internalize into internal domain, or polarity proteins could not be trafficked properly directly to the apical initiation site (Klinkert et al., 2016). Alternatively, signaling pathways from extracellular matrix components also have obvious effect on apical-basal identity, for example, cysts performed inverted polarity due to dominant-negative Rac1 (O'Brien et al., 2001), depleting small GTPase Arf6 (Monteleon et al., 2012), or blocking of β1-integrin function (Bryant et al., 2014). In our model, since CD13 is involved not only in cell trafficking but also the integrity of basement membrane. what remains unknown is whether CD13 orients apical-basal polarity only by maintaining the trafficking of apical proteins or whether it also induces changes in basement membrane during lumen formation. In addition, there could be alternative mechanisms by which CD13 regulates polarity that we are not yet aware of. For example, recent studies demonstrate that apical junction proteins undergo phase separation to establish of apical-basal polarity (Rouaud et al., 2020). In *Drosophila* neuroblasts asymmetric divisions, N-terminal domain of PARD3 autonomously promotes phase separation and the binding of PAR6B also helps to promote PARD3 phase separation (Liu et al., 2020). Since CD13 also promotes apical-basal cell polarization establishment, it might also be involved in a phase separation mechanism. Related to this, we observed coalescence of CD13 at the site of apical membrane initiation. These questions could be answered through a more extensive

investigation of CD13 and polarity protein dynamics and further understanding these interactions. This could be supplemented with studies in corresponding mouse models to validate the cellular and molecular mechanisms of tissue physiology.

Whether the involvement of CD13 in cell polarity is a common mechanism in other cell types and tissues is not fully understood, since CD13-null mice show few developmental, fertility, behavioral or physiological abnormalities (Rangel et al., 2007; Winnicka et al., 2010). Moreover, during tissue morphogenesis, the loss of deleted molecules often results in gain of function in similar molecules to compensate for the deficit (Maddison and Clarke, 2005), so it is possible another protein ca substitutes the function of CD13 to integrate the apical-basal polarity programme. It is possible that since the formation of epithelial tissue such as ducts and sheets are the major of tissue function, some polarity machineries may provide redundant mechanisms to ensure proper tissue morphogenesis.

My thesis work focused on understanding a mechanism for lumen formation through CD13. However, I identify additional novel regulators of epithelial morphogenesis and lumen formation that were functionally validated, including HRNR and RALB. The depletion phenotypes of these are distinct from each other and from CD13, suggesting that diverse cellular events may be crucial for lumen formation. Future studies should focus on clarifying the interaction of HRNR and RALB with apical polarity complexes and understanding mechanistically how they contribute to polarity and lumen formation.

Finally, loss of apical-basal polarity is associated with tumour progression. The data I presented for both PTPN14 and CD13 supports that loss of polarity is an essential step for initiating tumours, at least in the context of $KRAS^{G12V}$. Remarkably, inducing apical-basal polarity

after cells develop a malignant phenotype (i.e., overgrowth, loss of polarity, lumen filling) can reverse this phenotype and returns cells to a normal architecture, while oncogene expression persists. Although KRAS mutations are prevalent in human cancers, no treatment is currently available that targets KRAS. My studies indicate that restoring polarity may be an option to block malignant growth in cells expressing oncogenic KRAS, and possibly other oncogenes.

5.6 Conclusions

The objective of my thesis studies were to further investigate the functions of polarity signaling and lumen formation. The first objective was to identify novel regulators of lumen formation in three-dimensional organotypic cultures by using a proximity proteomics screen. I identified proximal protiens for PAR6B, including PARD3B, HRNR, and RALB that are required for proper lumen formation. This adds previously unidentified components that regulate lumen formation, and indicates that an intricate signaling network is required for epithelial morphogenesis. The suspension culture model provides an applicable approach to explore three-dimensional protein-protein interaction networks and represents a robust model for functional validation.

The second objective was to examine the cell polarity functions in lumenogenesis and epithelial polarity. I found that CD13 localizes to the apical membrane and associates with an apical complex with Crumbs complex. CD13-deficient cells display inverted polarity in which apical proteins are retained on the outer cell periphery instead of basolateral proteins, have altered Rab11 trafficking patterns, and fail to form a central lumen. This novel finding demonstrates that CD13 acts as a membrane receptor for Rab11-mediated endocytosis of apical

cargo that is necessary to reorient apical proteins from the periphery to internal sites necessary for lumen formation.

The final objective was to investigate polarity effectors important for malignant transformation. I implemented BioID in 3D cultures expressing oncogenic $KRAS^{G12V}$, a frequent mutation in human cancers. I identified PTPN14 which localizes at apical domain and is associated with Par complex. I found that PTPN14 is a potent tumour suppressor of $KRAS^{G12V}$ that appears to act independent of Yap. This reveals that PTPN14 is a novel PAR6B/PRKCI-associated protein that is required for maintaining cell polarization to restrict cancer development. The collection of findings in this thesis further highlight that importance of three-dimensional culture model for investigating polarity interactions and contributes substantially to our understanding of the mechanisms for polarization and lumen formation.

Bibliography

Adey, N.B., Huang, L., Ormonde, P.A., Baumgard, M.L., Pero, R., Byreddy, D.V., Tavtigian, S.V., and Bartel, P.L. (2000). Threonine phosphorylation of the MMAC1/PTEN PDZ binding domain both inhibits and stimulates PDZ binding. Cancer Res *60*, 35-37.

Aguilar-Aragon, M., Fletcher, G., and Thompson, B.J. (2020). The cytoskeletal motor proteins Dynein and MyoV direct apical transport of Crumbs. Dev Biol *459*, 126-137.

Ajduk, A., and Zernicka-Goetz, M. (2016). Polarity and cell division orientation in the cleavage embryo: from worm to human. Mol Hum Reprod *22*, 691-703.

Albertson, R., and Doe, C.Q. (2003). Dlg, Scrib and Lgl regulate neuroblast cell size and mitotic spindle asymmetry. Nat Cell Biol *5*, 166-170.

Altschuler, Y., Liu, S., Katz, L., Tang, K., Hardy, S., Brodsky, F., Apodaca, G., and Mostov, K. (1999). ADP-ribosylation factor 6 and endocytosis at the apical surface of Madin-Darby canine kidney cells. J Cell Biol *147*, 7-12.

Anastas, J.N., Biechele, T.L., Robitaille, M., Muster, J., Allison, K.H., Angers, S., and Moon, R.T. (2012). A protein complex of SCRIB, NOS1AP and VANGL1 regulates cell polarity and migration, and is associated with breast cancer progression. Oncogene *31*, 3696-3708.

Andrade-Vieira, R., Xu, Z., Colp, P., and Marignani, P.A. (2013). Loss of LKB1 expression reduces the latency of ErbB2-mediated mammary gland tumorigenesis, promoting changes in metabolic pathways. PLoS One *8*, e56567.

Aranda, V., Haire, T., Nolan, M.E., Calarco, J.P., Rosenberg, A.Z., Fawcett, J.P., Pawson, T., and Muthuswamy, S.K. (2006). Par6-aPKC uncouples ErbB2 induced disruption of polarized epithelial organization from proliferation control. Nat Cell Biol *8*, 1235-1245.

Aranda, V., Nolan, M.E., and Muthuswamy, S.K. (2008). Par complex in cancer: a regulator of normal cell polarity joins the dark side. Oncogene *27*, 6878-6887.

Archibald, A., Al-Masri, M., Liew-Spilger, A., and McCaffrey, L. (2015a). Atypical protein kinase C induces cell transformation by disrupting Hippo/Yap signaling. Mol Biol Cell *26*, 3578-3595.

Archibald, A., Mihai, C., Macara, I.G., and McCaffrey, L. (2015b). Oncogenic suppression of apoptosis uncovers a Rac1/JNK proliferation pathway activated by loss of Par3. Oncogene *34*, 3199-3206.

Assemat, E., Bazellieres, E., Pallesi-Pocachard, E., Le Bivic, A., and Massey-Harroche, D. (2008). Polarity complex proteins. Biochim Biophys Acta *1778*, 614-630.

Baer, M.M., Chanut-Delalande, H., and Affolter, M. (2009). Cellular and molecular mechanisms underlying the formation of biological tubes. Curr Top Dev Biol *89*, 137-162.

Baker, B.M., and Chen, C.S. (2012). Deconstructing the third dimension: how 3D culture microenvironments alter cellular cues. J Cell Sci *125*, 3015-3024.

Balklava, Z., Pant, S., Fares, H., and Grant, B.D. (2007). Genome-wide analysis identifies a general requirement for polarity proteins in endocytic traffic. Nat Cell Biol *9*, 1066-1073.

Bardeesy, N., Sinha, M., Hezel, A.F., Signoretti, S., Hathaway, N.A., Sharpless, N.E., Loda, M., Carrasco, D.R., and DePinho, R.A. (2002). Loss of the Lkb1 tumour suppressor provokes intestinal polyposis but resistance to transformation. Nature *419*, 162-167.

Beauchamp, P., Moritz, W., Kelm, J.M., Ullrich, N.D., Agarkova, I., Anson, B.D., Suter, T.M., and Zuppinger, C. (2015). Development and Characterization of a Scaffold-Free 3D Spheroid Model of Induced Pluripotent Stem Cell-Derived Human Cardiomyocytes. Tissue Eng Part C Methods *21*, 852-861.

Bedzhov, I., and Zernicka-Goetz, M. (2014). Self-organizing properties of mouse pluripotent cells initiate morphogenesis upon implantation. Cell *156*, 1032-1044.

Bell, G.P., Fletcher, G.C., Brain, R., and Thompson, B.J. (2015). Aurora kinases phosphorylate Lgl to induce mitotic spindle orientation in Drosophila epithelia. Curr Biol *25*, 61-68.

Benton, R., and St Johnston, D. (2003). Drosophila PAR-1 and 14-3-3 inhibit Bazooka/PAR-3 to establish complementary cortical domains in polarized cells. Cell *115*, 691-704.

Bergstralh, D.T., and St Johnston, D. (2012). Epithelial cell polarity: what flies can teach us about cancer. Essays Biochem *53*, 129-140.

Bernascone, I., Hachimi, M., and Martin-Belmonte, F. (2017). Signaling Networks in Epithelial Tube Formation. Cold Spring Harb Perspect Biol *9*.

Bhartur, S.G., Calhoun, B.C., Woodrum, J., Kurkjian, J., Iyer, S., Lai, F., and Goldenring, J.R. (2000). Genomic structure of murine Rab11 family members. Biochem Biophys Res Commun *269*, 611-617.

Bilder, D. (2004). Epithelial polarity and proliferation control: links from the Drosophila neoplastic tumor suppressors. Genes Dev *18*, 1909-1925.

Bilder, D., Li, M., and Perrimon, N. (2000). Cooperative regulation of cell polarity and growth by Drosophila tumor suppressors. Science *289*, 113-116.

Bilder, D., and Perrimon, N. (2000). Localization of apical epithelial determinants by the basolateral PDZ protein Scribble. Nature *403*, 676-680.

Bilder, D., Schober, M., and Perrimon, N. (2003). Integrated activity of PDZ protein complexes regulates epithelial polarity. Nat Cell Biol *5*, 53-58.

Bisi, S., Marchesi, S., Rizvi, A., Carra, D., Beznoussenko, G.V., Ferrara, I., Deflorian, G., Mironov, A., Bertalot, G., Pisati, F*., et al.* (2020). IRSp53 controls plasma membrane shape and polarized transport at the nascent lumen in epithelial tubules. Nat Commun *11*, 3516.

Blasky, A.J., Mangan, A., and Prekeris, R. (2015). Polarized protein transport and lumen formation during epithelial tissue morphogenesis. Annu Rev Cell Dev Biol *31*, 575-591.

Blum, I.R., Behling-Hess, C., Padilla-Rodriguez, M., Momtaz, S., Cox, C., and Wilson, J.M. (2020). Rab22a regulates the establishment of epithelial polarity. Small GTPases.

Breslin, S., and O'Driscoll, L. (2013). Three-dimensional cell culture: the missing link in drug discovery. Drug Discov Today *18*, 240-249.

Bryant, D.M., Datta, A., Rodriguez-Fraticelli, A.E., Peranen, J., Martin-Belmonte, F., and Mostov, K.E. (2010). A molecular network for de novo generation of the apical surface and lumen. Nat Cell Biol *12*, 1035-1045.

Bryant, D.M., Roignot, J., Datta, A., Overeem, A.W., Kim, M., Yu, W., Peng, X., Eastburn, D.J., Ewald, A.J., Werb, Z.*, et al.* (2014). A molecular switch for the orientation of epithelial cell polarization. Dev Cell *31*, 171-187.

Buther, K., Plaas, C., Barnekow, A., and Kremerskothen, J. (2004). KIBRA is a novel substrate for protein kinase Czeta. Biochem Biophys Res Commun *317*, 703-707.

Cao, F., Miao, Y., Xu, K., and Liu, P. (2015). Lethal (2) giant larvae: an indispensable regulator of cell polarity and cancer development. Int J Biol Sci *11*, 380-389.

Carthew, R.W. (2005). Adhesion proteins and the control of cell shape. Curr Opin Genet Dev *15*, 358-363.

Casanova, J.E., Wang, X., Kumar, R., Bhartur, S.G., Navarre, J., Woodrum, J.E., Altschuler, Y., Ray, G.S., and Goldenring, J.R. (1999). Association of Rab25 and Rab11a with the apical recycling system of polarized Madin-Darby canine kidney cells. Mol Biol Cell *10*, 47-61.

Catterall, R., Lelarge, V., and McCaffrey, L. (2020). Genetic alterations of epithelial polarity genes are associated with loss of polarity in invasive breast cancer. Int J Cancer *146*, 1578-1591.

Cerruti, B., Puliafito, A., Shewan, A.M., Yu, W., Combes, A.N., Little, M.H., Chianale, F., Primo, L., Serini, G., Mostov, K.E.*, et al.* (2013). Polarity, cell division, and out-of-equilibrium dynamics control the growth of epithelial structures. J Cell Biol *203*, 359-372.

Chaicharoenaudomrung, N., Kunhorm, P., and Noisa, P. (2019). Three-dimensional cell culture systems as an in vitro platform for cancer and stem cell modeling. World J Stem Cells *11*, 1065-1083.

Charrier, L.E., Loie, E., and Laprise, P. (2015). Mouse Crumbs3 sustains epithelial tissue morphogenesis in vivo. Sci Rep *5*, 17699.

Chen, X., and Macara, I.G. (2005). Par-3 controls tight junction assembly through the Rac exchange factor Tiam1. Nat Cell Biol *7*, 262-269.

Choi-Rhee, E., Schulman, H., and Cronan, J.E. (2004). Promiscuous protein biotinylation by Escherichia coli biotin protein ligase. Protein Sci *13*, 3043-3050.

Cronan, J.E. (2005). Targeted and proximity-dependent promiscuous protein biotinylation by a mutant Escherichia coli biotin protein ligase. J Nutr Biochem *16*, 416-418.

Cukierman, E., Pankov, R., and Yamada, K.M. (2002). Cell interactions with three-dimensional matrices. Curr Opin Cell Biol *14*, 633-639.

D'Avino, P.P., and Capalbo, L. (2016). Regulation of midbody formation and function by mitotic kinases. Semin Cell Dev Biol *53*, 57-63.

Dahan, I., Petrov, D., Cohen-Kfir, E., and Ravid, S. (2014). The tumor suppressor Lgl1 forms discrete complexes with NMII-A and Par6alpha-aPKCzeta that are affected by Lgl1 phosphorylation. J Cell Sci *127*, 295-304.

Dahan, I., Yearim, A., Touboul, Y., and Ravid, S. (2012). The tumor suppressor Lgl1 regulates NMII-A cellular distribution and focal adhesion morphology to optimize cell migration. Mol Biol Cell *23*, 591-601.

Datta, A., Bryant, D.M., and Mostov, K.E. (2011). Molecular regulation of lumen morphogenesis. Curr Biol *21*, R126-136.

Davalos, V., Moutinho, C., Villanueva, A., Boque, R., Silva, P., Carneiro, F., and Esteller, M. (2012). Dynamic epigenetic regulation of the microRNA-200 family mediates epithelial and mesenchymal transitions in human tumorigenesis. Oncogene *31*, 2062-2074.

Deen, P.M., Croes, H., van Aubel, R.A., Ginsel, L.A., and van Os, C.H. (1995). Water channels encoded by mutant aquaporin-2 genes in nephrogenic diabetes insipidus are impaired in their cellular routing. J Clin Invest *95*, 2291-2296.

Desai, R.A., Gao, L., Raghavan, S., Liu, W.F., and Chen, C.S. (2009). Cell polarity triggered by cell-cell adhesion via E-cadherin. J Cell Sci *122*, 905-911.

Desclozeaux, M., Venturato, J., Wylie, F.G., Kay, J.G., Joseph, S.R., Le, H.T., and Stow, J.L. (2008). Active Rab11 and functional recycling endosome are required for E-cadherin trafficking and lumen formation during epithelial morphogenesis. Am J Physiol Cell Physiol *295*, C545-556.

Di Paolo, G., and De Camilli, P. (2006). Phosphoinositides in cell regulation and membrane dynamics. Nature *443*, 651-657.

Dias Gomes, M., Letzian, S., Saynisch, M., and Iden, S. (2019). Polarity signaling ensures epidermal homeostasis by coupling cellular mechanics and genomic integrity. Nat Commun *10*, 3362.

Durgan, J., Kaji, N., Jin, D., and Hall, A. (2011). Par6B and atypical PKC regulate mitotic spindle orientation during epithelial morphogenesis. J Biol Chem *286*, 12461-12474.

Ebnet, K., Suzuki, A., Horikoshi, Y., Hirose, T., Meyer Zu Brickwedde, M.K., Ohno, S., and Vestweber, D. (2001). The cell polarity protein ASIP/PAR-3 directly associates with junctional adhesion molecule (JAM). EMBO J *20*, 3738-3748.

Edmondson, R., Broglie, J.J., Adcock, A.F., and Yang, L. (2014). Three-dimensional cell culture systems and their applications in drug discovery and cell-based biosensors. Assay Drug Dev Technol *12*, 207-218.

Elias, S., McGuire, J.R., Yu, H., and Humbert, S. (2015). Huntingtin Is Required for Epithelial Polarity through RAB11A-Mediated Apical Trafficking of PAR3-aPKC. PLoS Biol *13*, e1002142.

Ellenbroek, S.I., Iden, S., and Collard, J.G. (2012). Cell polarity proteins and cancer. Semin Cancer Biol *22*, 208-215.

Etienne-Manneville, S. (2008). Polarity proteins in migration and invasion. Oncogene *27*, 6970-6980.

Etienne-Manneville, S., Manneville, J.B., Nicholls, S., Ferenczi, M.A., and Hall, A. (2005). Cdc42 and Par6-PKCzeta regulate the spatially localized association of Dlg1 and APC to control cell polarization. J Cell Biol *170*, 895-901.

Eva, R., Koseki, H., Kanamarlapudi, V., and Fawcett, J.W. (2017). EFA6 regulates selective polarised transport and axon regeneration from the axon initial segment. J Cell Sci *130*, 3663-3675.

Fairn, G.D., Hermansson, M., Somerharju, P., and Grinstein, S. (2011). Phosphatidylserine is polarized and required for proper Cdc42 localization and for development of cell polarity. Nat Cell Biol *13*, 1424-1430.

Fairweather, S.J., Broer, A., O'Mara, M.L., and Broer, S. (2012). Intestinal peptidases form functional complexes with the neutral amino acid transporter B(0)AT1. Biochem J *446*, 135-148.

Ferrari, A., Veligodskiy, A., Berge, U., Lucas, M.S., and Kroschewski, R. (2008). ROCK-mediated contractility, tight junctions and channels contribute to the conversion of a preapical patch into apical surface during isochoric lumen initiation. J Cell Sci *121*, 3649-3663.

Fields, A.P., and Regala, R.P. (2007). Protein kinase C iota: human oncogene, prognostic marker and therapeutic target. Pharmacol Res *55*, 487-497.

Fogg, V.C., Liu, C.J., and Margolis, B. (2005). Multiple regions of Crumbs3 are required for tight junction formation in MCF10A cells. J Cell Sci *118*, 2859-2869.

Franz, A., and Riechmann, V. (2010). Stepwise polarisation of the Drosophila follicular epithelium. Dev Biol *338*, 136-147.

Fremont, S., and Echard, A. (2018). Membrane Traffic in the Late Steps of Cytokinesis. Curr Biol *28*, R458-R470.

Galvez-Santisteban, M., Rodriguez-Fraticelli, A.E., Bryant, D.M., Vergarajauregui, S., Yasuda, T., Banon-Rodriguez, I., Bernascone, I., Datta, A., Spivak, N., Young, K.*, et al.* (2012). Synaptotagmin-like proteins control the formation of a single apical membrane domain in epithelial cells. Nat Cell Biol *14*, 838-849.

Gao, L., and Macara, I.G. (2004). Isoforms of the polarity protein par6 have distinct functions. J Biol Chem *279*, 41557-41562.

Gao, L., Macara, I.G., and Joberty, G. (2002). Multiple splice variants of Par3 and of a novel related gene, Par3L, produce proteins with different binding properties. Gene *294*, 99-107.

Gardiol, D., Kuhne, C., Glaunsinger, B., Lee, S.S., Javier, R., and Banks, L. (1999). Oncogenic human papillomavirus E6 proteins target the discs large tumour suppressor for proteasome-mediated degradation. Oncogene *18*, 5487-5496.

Gassama-Diagne, A., Yu, W., ter Beest, M., Martin-Belmonte, F., Kierbel, A., Engel, J., and Mostov, K. (2006). Phosphatidylinositol-3,4,5-trisphosphate regulates the formation of the basolateral plasma membrane in epithelial cells. Nat Cell Biol *8*, 963-970.

Gaudet, S., Langlois, M.J., Lue, R.A., Rivard, N., and Viel, A. (2011). The MEK2-binding tumor suppressor hDlg is recruited by E-cadherin to the midbody ring. BMC Cell Biol *12*, 55.

Gervais, L., and Casanova, J. (2010). In vivo coupling of cell elongation and lumen formation in a single cell. Curr Biol *20*, 359-366.

Ghosh, M., Lo, R., Ivic, I., Aguilera, B., Qendro, V., Devarakonda, C., and Shapiro, L.H. (2019). CD13 tethers the IQGAP1-ARF6-EFA6 complex to the plasma membrane to promote ARF6 activation, beta1 integrin recycling, and cell migration. Sci Signal *12*.

Godde, N.J., Sheridan, J.M., Smith, L.K., Pearson, H.B., Britt, K.L., Galea, R.C., Yates, L.L., Visvader, J.E., and Humbert, P.O. (2014). Scribble modulates the MAPK/Fra1 pathway to disrupt luminal and ductal integrity and suppress tumour formation in the mammary gland. PLoS Genet *10*, e1004323.

Golachowska, M.R., Hoekstra, D., and van, I.S.C. (2010). Recycling endosomes in apical plasma membrane domain formation and epithelial cell polarity. Trends Cell Biol *20*, 618-626.

Goldenring, J.R., Smith, J., Vaughan, H.D., Cameron, P., Hawkins, W., and Navarre, J. (1996). Rab11 is an apically located small GTP-binding protein in epithelial tissues. Am J Physiol *270*, G515-525.

Grindstaff, K.K., Yeaman, C., Anandasabapathy, N., Hsu, S.C., Rodriguez-Boulan, E., Scheller, R.H., and Nelson, W.J. (1998). Sec6/8 complex is recruited to cell-cell contacts and specifies transport vesicle delivery to the basal-lateral membrane in epithelial cells. Cell *93*, 731-740.

Gunaratne, A., Thai, B.L., and Di Guglielmo, G.M. (2013). Atypical protein kinase C phosphorylates Par6 and facilitates transforming growth factor beta-induced epithelial-to-mesenchymal transition. Mol Cell Biol *33*, 874-886.

Halaoui, R., and McCaffrey, L. (2015a). Rewiring cell polarity signaling in cancer. Oncogene *34*, 939-950.

Halaoui, R., and McCaffrey, L. (2015b). Rewiring cell polarity signaling in cancer. Oncogene *34*, 939-950.

Halaoui, R., Rejon, C., Chatterjee, S.J., Szymborski, J., Meterissian, S., Muller, W.J., Omeroglu, A., and McCaffrey, L. (2017). Progressive polarity loss and luminal collapse disrupt tissue organization in carcinoma. Genes Dev *31*, 1573-1587.

Hardiman, K.M. (2018). Update on Sporadic Colorectal Cancer Genetics. Clin Colon Rectal Surg *31*, 147-152.

Hayase, J., Kamakura, S., Iwakiri, Y., Yamaguchi, Y., Izaki, T., Ito, T., and Sumimoto, H. (2013). The WD40 protein Morg1 facilitates Par6-aPKC binding to Crb3 for apical identity in epithelial cells. J Cell Biol *200*, 635-650.

Hehnly, H., and Doxsey, S. (2014). Rab11 endosomes contribute to mitotic spindle organization and orientation. Dev Cell *28*, 497-507.

Hidalgo-Carcedo, C., Hooper, S., Chaudhry, S.I., Williamson, P., Harrington, K., Leitinger, B., and Sahai, E. (2011). Collective cell migration requires suppression of actomyosin at cell-cell contacts mediated by DDR1 and the cell polarity regulators Par3 and Par6. Nat Cell Biol *13*, 49-58.

Hirose, T., Izumi, Y., Nagashima, Y., Tamai-Nagai, Y., Kurihara, H., Sakai, T., Suzuki, Y., Yamanaka, T., Suzuki, A., Mizuno, K*., et al.* (2002). Involvement of ASIP/PAR-3 in the promotion of epithelial tight junction formation. J Cell Sci *115*, 2485-2495.

Hoege, C., Constantinescu, A.T., Schwager, A., Goehring, N.W., Kumar, P., and Hyman, A.A. (2010). LGL can partition the cortex of one-cell Caenorhabditis elegans embryos into two domains. Curr Biol *20*, 1296-1303.

Huang, L., and Muthuswamy, S.K. (2010). Polarity protein alterations in carcinoma: a focus on emerging roles for polarity regulators. Curr Opin Genet Dev *20*, 41-50.

Huebner, R.J., Lechler, T., and Ewald, A.J. (2014). Developmental stratification of the mammary epithelium occurs through symmetry-breaking vertical divisions of apically positioned luminal cells. Development *141*, 1085-1094.

Humbert, P.O., Dow, L.E., and Russell, S.M. (2006). The Scribble and Par complexes in polarity and migration: friends or foes? Trends Cell Biol *16*, 622-630.

Huo, Y., and Macara, I.G. (2014). The Par3-like polarity protein Par3L is essential for mammary stem cell maintenance. Nat Cell Biol *16*, 529-537.

Hurd, T.W., Gao, L., Roh, M.H., Macara, I.G., and Margolis, B. (2003). Direct interaction of two polarity complexes implicated in epithelial tight junction assembly. Nat Cell Biol *5*, 137-142.

Hutagalung, A.H., and Novick, P.J. (2011). Role of Rab GTPases in membrane traffic and cell physiology. Physiol Rev *91*, 119-149.

Iden, S., and Collard, J.G. (2008). Crosstalk between small GTPases and polarity proteins in cell polarization. Nat Rev Mol Cell Biol *9*, 846-859.

Iden, S., van Riel, W.E., Schafer, R., Song, J.Y., Hirose, T., Ohno, S., and Collard, J.G. (2012). Tumor type-dependent function of the par3 polarity protein in skin tumorigenesis. Cancer cell *22*, 389-403.

Iizuka-Kogo, A., Ishidao, T., Akiyama, T., and Senda, T. (2007). Abnormal development of urogenital organs in Dlgh1-deficient mice. Development *134*, 1799-1807.

Irazoqui, J.E., Gladfelter, A.S., and Lew, D.J. (2003). Scaffold-mediated symmetry breaking by Cdc42p. Nat Cell Biol *5*, 1062-1070.

Iruela-Arispe, M.L., and Beitel, G.J. (2013). Tubulogenesis. Development *140*, 2851-2855.

Itoh, M., Sasaki, H., Furuse, M., Ozaki, H., Kita, T., and Tsukita, S. (2001). Junctional adhesion molecule (JAM) binds to PAR-3: a possible mechanism for the recruitment of PAR-3 to tight junctions. J Cell Biol *154*, 491-497.

Izumi, Y., Hirose, T., Tamai, Y., Hirai, S., Nagashima, Y., Fujimoto, T., Tabuse, Y., Kemphues, K.J., and Ohno, S. (1998). An atypical PKC directly associates and colocalizes at the epithelial tight junction with ASIP, a mammalian homologue of Caenorhabditis elegans polarity protein PAR-3. J Cell Biol *143*, 95-106.

Jaffe, A.B., Kaji, N., Durgan, J., and Hall, A. (2008a). Cdc42 controls spindle orientation to position the apical surface during epithelial morphogenesis. J Cell Biol *183*, 625-633.

Jaffe, A.B., Kaji, N., Durgan, J., and Hall, A. (2008b). Cdc42 controls spindle orientation to position the apical surface during epithelial morphogenesis. The Journal of cell biology *183*, 625-633.

Jarolim, P., Shayakul, C., Prabakaran, D., Jiang, L., Stuart-Tilley, A., Rubin, H.L., Simova, S., Zavadil, J., Herrin, J.T., Brouillette, J.*, et al.* (1998). Autosomal dominant distal renal tubular acidosis is associated in three families with heterozygosity for the R589H mutation in the AE1 (band 3) Cl-/HCO3- exchanger. J Biol Chem *273*, 6380-6388.

Jewett, C.E., and Prekeris, R. (2018). Insane in the apical membrane: Trafficking events mediating apicobasal epithelial polarity during tube morphogenesis. Traffic.

Joberty, G., Petersen, C., Gao, L., and Macara, I.G. (2000). The cell-polarity protein Par6 links Par3 and atypical protein kinase C to Cdc42. Nat Cell Biol *2*, 531-539.

Johansson, A., Driessens, M., and Aspenstrom, P. (2000). The mammalian homologue of the Caenorhabditis elegans polarity protein PAR-6 is a binding partner for the Rho GTPases Cdc42 and Rac1. J Cell Sci *113 (Pt 18)*, 3267-3275.

Jossin, Y., Lee, M., Klezovitch, O., Kon, E., Cossard, A., Lien, W.H., Fernandez, T.E., Cooper, J.A., and Vasioukhin, V. (2017). Llgl1 Connects Cell Polarity with Cell-Cell Adhesion in Embryonic Neural Stem Cells. Dev Cell *41*, 481-495 e485.

Kadoshima, T., Sakaguchi, H., Nakano, T., Soen, M., Ando, S., Eiraku, M., and Sasai, Y. (2013). Self-organization of axial polarity, inside-out layer pattern, and species-specific progenitor dynamics in human ES cell-derived neocortex. Proc Natl Acad Sci U S A *110*, 20284-20289.

Kallay, L.M., McNickle, A., Brennwald, P.J., Hubbard, A.L., and Braiterman, L.T. (2006). Scribble associates with two polarity proteins, Lgl2 and Vangl2, via distinct molecular domains. J Cell Biochem *99*, 647-664.

Kamberov, E., Makarova, O., Roh, M., Liu, A., Karnak, D., Straight, S., and Margolis, B. (2000). Molecular cloning and characterization of Pals, proteins associated with mLin-7. J Biol Chem *275*, 11425-11431.

Kapalczynska, M., Kolenda, T., Przybyla, W., Zajaczkowska, M., Teresiak, A., Filas, V., Ibbs, M., Blizniak, R., Luczewski, L., and Lamperska, K. (2018). 2D and 3D cell cultures - a comparison of different types of cancer cell cultures. Arch Med Sci *14*, 910-919.

Karp, C.M., Tan, T.T., Mathew, R., Nelson, D., Mukherjee, C., Degenhardt, K., Karantza-Wadsworth, V., and White, E. (2008). Role of the polarity determinant crumbs in suppressing mammalian epithelial tumor progression. Cancer Res *68*, 4105-4115.

Kashyap, A., Zimmerman, T., Ergul, N., Bosserhoff, A., Hartman, U., Alla, V., Bataille, F., Galle, P.R., Strand, S., and Strand, D. (2013). The human Lgl polarity gene, Hugl-2, induces MET and suppresses Snail tumorigenesis. Oncogene *32*, 1396-1407.

Kemphues, K.J., Priess, J.R., Morton, D.G., and Cheng, N.S. (1988). Identification of genes required for cytoplasmic localization in early C. elegans embryos. Cell *52*, 311-320.

Khursheed, M., and Bashyam, M.D. (2014). Apico-basal polarity complex and cancer. J Biosci *39*, 145-155.

Kim, J.Y., Valencia, T., Abu-Baker, S., Linares, J., Lee, S.J., Yajima, T., Chen, J., Eroshkin, A., Castilla, E.A., Brill, L.M*., et al.* (2013). c-Myc phosphorylation by PKCzeta represses prostate tumorigenesis. Proc Natl Acad Sci U S A *110*, 6418-6423.

Klinkert, K., and Echard, A. (2016). Rab35 GTPase: A Central Regulator of Phosphoinositides and F-actin in Endocytic Recycling and Beyond. Traffic *17*, 1063-1077.

Klinkert, K., Rocancourt, M., Houdusse, A., and Echard, A. (2016). Rab35 GTPase couples cell division with initiation of epithelial apico-basal polarity and lumen opening. Nat Commun *7*, 11166.

Kohjima, M., Noda, Y., Takeya, R., Saito, N., Takeuchi, K., and Sumimoto, H. (2002). PAR3beta, a novel homologue of the cell polarity protein PAR3, localizes to tight junctions. Biochem Biophys Res Commun *299*, 641-646.

Krahn, M.P., Klopfenstein, D.R., Fischer, N., and Wodarz, A. (2010). Membrane targeting of Bazooka/PAR-3 is mediated by direct binding to phosphoinositide lipids. Curr Biol *20*, 636-642.

Krahn, M.P., and Wodarz, A. (2012). Phosphoinositide lipids and cell polarity: linking the plasma membrane to the cytocortex. Essays Biochem *53*, 15-27.

Lancaster, M.A., and Knoblich, J.A. (2014). Organogenesis in a dish: modeling development and disease using organoid technologies. Science *345*, 1247125.

Langhans, S.A. (2018). Three-Dimensional in Vitro Cell Culture Models in Drug Discovery and Drug Repositioning. Front Pharmacol *9*, 6.

Lapierre, L.A., Avant, K.M., Caldwell, C.M., Oztan, A., Apodaca, G., Knowles, B.C., Roland, J.T., Ducharme, N.A., and Goldenring, J.R. (2012). Phosphorylation of Rab11-FIP2 regulates polarity in MDCK cells. Mol Biol Cell *23*, 2302-2318.

Lapierre, L.A., Manning, E.H., Mitchell, K.M., Caldwell, C.M., and Goldenring, J.R. (2017). Interaction of phosphorylated Rab11-FIP2 with Eps15 regulates apical junction composition. Mol Biol Cell *28*, 1088-1100.

Laprise, P., Lau, K.M., Harris, K.P., Silva-Gagliardi, N.F., Paul, S.M., Beronja, S., Beitel, G.J., McGlade, C.J., and Tepass, U. (2009). Yurt, Coracle, Neurexin IV and the Na(+),K(+)-ATPase form a novel group of epithelial polarity proteins. Nature *459*, 1141-1145.

Laprise, P., Viel, A., and Rivard, N. (2004). Human homolog of disc-large is required for adherens junction assembly and differentiation of human intestinal epithelial cells. J Biol Chem *279*, 10157-10166.

Lazaro-Dieguez, F., Cohen, D., Fernandez, D., Hodgson, L., van Ijzendoorn, S.C., and Musch, A. (2013). Par1b links lumen polarity with LGN-NuMA positioning for distinct epithelial cell division phenotypes. J Cell Biol *203*, 251-264.

Lee, C.Y., Robinson, K.J., and Doe, C.Q. (2006). Lgl, Pins and aPKC regulate neuroblast self-renewal versus differentiation. Nature *439*, 594-598.

Lee, J.L., and Streuli, C.H. (2014). Integrins and epithelial cell polarity. J Cell Sci *127*, 3217-3225.

Lee, S., Fan, S., Makarova, O., Straight, S., and Margolis, B. (2002). A novel and conserved protein-protein interaction domain of mammalian Lin-2/CASK binds and recruits SAP97 to the lateral surface of epithelia. Mol Cell Biol *22*, 1778-1791.

Legouis, R., Jaulin-Bastard, F., Schott, S., Navarro, C., Borg, J.P., and Labouesse, M. (2003). Basolateral targeting by leucine-rich repeat domains in epithelial cells. EMBO Rep *4*, 1096-1102.

Lemmers, C., Medina, E., Delgrossi, M.H., Michel, D., Arsanto, J.P., and Le Bivic, A. (2002). hINADl/PATJ, a homolog of discs lost, interacts with crumbs and localizes to tight junctions in human epithelial cells. J Biol Chem *277*, 25408-25415.

Lemmers, C., Michel, D., Lane-Guermonprez, L., Delgrossi, M.H., Medina, E., Arsanto, J.P., and Le Bivic, A. (2004). CRB3 binds directly to Par6 and regulates the morphogenesis of the tight junctions in mammalian epithelial cells. Mol Biol Cell *15*, 1324-1333.

Li, B.X., Satoh, A.K., and Ready, D.F. (2007). Myosin V, Rab11, and dRip11 direct apical secretion and cellular morphogenesis in developing Drosophila photoreceptors. J Cell Biol *177*, 659-669.

Li, D., Mangan, A., Cicchini, L., Margolis, B., and Prekeris, R. (2014). FIP5 phosphorylation during mitosis regulates apical trafficking and lumenogenesis. EMBO Rep *15*, 428-437.

Lin, D., Edwards, A.S., Fawcett, J.P., Mbamalu, G., Scott, J.D., and Pawson, T. (2000). A mammalian PAR-3-PAR-6 complex implicated in Cdc42/Rac1 and aPKC signalling and cell polarity. Nat Cell Biol *2*, 540-547.

Linch, M., Sanz-Garcia, M., Soriano, E., Zhang, Y., Riou, P., Rosse, C., Cameron, A., Knowles, P., Purkiss, A., Kjaer, S.*, et al.* (2013). A cancer-associated mutation in atypical protein kinase Ciota occurs in a substrate-specific recruitment motif. Sci Signal *6*, ra82.

Ling, C., Zheng, Y., Yin, F., Yu, J., Huang, J., Hong, Y., Wu, S., and Pan, D. (2010). The apical transmembrane protein Crumbs functions as a tumor suppressor that regulates Hippo signaling by binding to Expanded. Proc Natl Acad Sci U S A *107*, 10532-10537.

Liu, Z., Yang, Y., Gu, A., Xu, J., Mao, Y., Lu, H., Hu, W., Lei, Q.Y., Li, Z., Zhang, M.*, et al.* (2020). Par complex cluster formation mediated by phase separation. Nat Commun *11*, 2266.

Lizcano, J.M., Goransson, O., Toth, R., Deak, M., Morrice, N.A., Boudeau, J., Hawley, S.A., Udd, L., Makela, T.P., Hardie, D.G.*, et al.* (2004). LKB1 is a master kinase that activates 13 kinases of the AMPK subfamily, including MARK/PAR-1. EMBO J *23*, 833-843.

Lu, R., and Wilson, J.M. (2016). Rab14 specifies the apical membrane through Arf6-mediated regulation of lipid domains and Cdc42. Sci Rep *6*, 38249.

Lubarsky, B., and Krasnow, M.A. (2003). Tube morphogenesis: making and shaping biological tubes. Cell *112*, 19-28.

Lujan, P., Varsano, G., Rubio, T., Hennrich, M.L., Sachsenheimer, T., Galvez-Santisteban, M., Martin-Belmonte, F., Gavin, A.C., Brugger, B., and Kohn, M. (2016). PRL-3 disrupts epithelial architecture by altering the post-mitotic midbody position. J Cell Sci *129*, 4130-4142.

Maddison, K., and Clarke, A.R. (2005). New approaches for modelling cancer mechanisms in the mouse. J Pathol *205*, 181-193.

Maehama, T., and Dixon, J.E. (1998). The tumor suppressor, PTEN/MMAC1, dephosphorylates the lipid second messenger, phosphatidylinositol 3,4,5-trisphosphate. J Biol Chem *273*, 13375-13378.

Makarova, O., Roh, M.H., Liu, C.J., Laurinec, S., and Margolis, B. (2003). Mammalian Crumbs3 is a small transmembrane protein linked to protein associated with Lin-7 (Pals1). Gene *302*, 21-29.

Mangan, A.J., Sietsema, D.V., Li, D., Moore, J.K., Citi, S., and Prekeris, R. (2016). Cingulin and actin mediate midbody-dependent apical lumen formation during polarization of epithelial cells. Nat Commun *7*, 12426.

Margolis, B. (2018). The Crumbs3 Polarity Protein. Cold Spring Harb Perspect Biol *10*.

Martin-Belmonte, F., Gassama, A., Datta, A., Yu, W., Rescher, U., Gerke, V., and Mostov, K. (2007). PTEN-mediated apical segregation of phosphoinositides controls epithelial morphogenesis through Cdc42. Cell *128*, 383-397.

Mathew, D., Gramates, L.S., Packard, M., Thomas, U., Bilder, D., Perrimon, N., Gorczyca, M., and Budnik, V. (2002). Recruitment of scribble to the synaptic scaffolding complex requires GUK-holder, a novel DLG binding protein. Curr Biol *12*, 531-539.

McCaffrey, L.M., and Macara, I.G. (2011). Epithelial organization, cell polarity and tumorigenesis. Trends Cell Biol *21*, 727-735.

McCaffrey, L.M., Montalbano, J., Mihai, C., and Macara, I.G. (2012). Loss of the Par3 polarity protein promotes breast tumorigenesis and metastasis. Cancer Cell *22*, 601-614.

Mechler, B.M., McGinnis, W., and Gehring, W.J. (1985). Molecular cloning of lethal(2)giant larvae, a recessive oncogene of Drosophila melanogaster. EMBO J *4*, 1551-1557.

Meder, D., Shevchenko, A., Simons, K., and Fullekrug, J. (2005). Gp135/podocalyxin and NHERF-2 participate in the formation of a preapical domain during polarization of MDCK cells. J Cell Biol *168*, 303-313.

Medina, E., Lemmers, C., Lane-Guermonprez, L., and Le Bivic, A. (2002). Role of the Crumbs complex in the regulation of junction formation in Drosophila and mammalian epithelial cells. Biol Cell *94*, 305-313.

Metais, J.Y., Navarro, C., Santoni, M.J., Audebert, S., and Borg, J.P. (2005). hScrib interacts with ZO-2 at the cell-cell junctions of epithelial cells. FEBS Lett *579*, 3725-3730.

Michel, D., Arsanto, J.P., Massey-Harroche, D., Beclin, C., Wijnholds, J., and Le Bivic, A. (2005). PATJ connects and stabilizes apical and lateral components of tight junctions in human intestinal cells. J Cell Sci *118*, 4049-4057.

Mizuno, K., Suzuki, A., Hirose, T., Kitamura, K., Kutsuzawa, K., Futaki, M., Amano, Y., and Ohno, S. (2003). Self-association of PAR-3-mediated by the conserved N-terminal domain contributes to the development of epithelial tight junctions. J Biol Chem *278*, 31240-31250.

Montanez-Sauri, S.I., Beebe, D.J., and Sung, K.E. (2015). Microscale screening systems for 3D cellular microenvironments: platforms, advances, and challenges. Cell Mol Life Sci *72*, 237-249.

Monteleon, C.L., Sedgwick, A., Hartsell, A., Dai, M., Whittington, C., Voytik-Harbin, S., and D'Souza-Schorey, C. (2012). Establishing epithelial glandular polarity: interlinked roles for ARF6, Rac1, and the matrix microenvironment. Mol Biol Cell *23*, 4495-4505.

Morais-de-Sa, E., Mirouse, V., and St Johnston, D. (2010). aPKC phosphorylation of Bazooka defines the apical/lateral border in Drosophila epithelial cells. Cell *141*, 509-523.

Moscat, J., Diaz-Meco, M.T., Albert, A., and Campuzano, S. (2006). Cell signaling and function organized by PB1 domain interactions. Mol Cell *23*, 631-640.

Mrozowska, P.S., and Fukuda, M. (2016). Regulation of podocalyxin trafficking by Rab small GTPases in 2D and 3D epithelial cell cultures. J Cell Biol *213*, 355-369.

Mulders, S.M., Knoers, N.V., Van Lieburg, A.F., Monnens, L.A., Leumann, E., Wuhl, E., Schober, E., Rijss, J.P., Van Os, C.H., and Deen, P.M. (1997). New mutations in the AQP2 gene in nephrogenic diabetes insipidus resulting in functional but misrouted water channels. J Am Soc Nephrol *8*, 242-248.

Murray, N.R., Jamieson, L., Yu, W., Zhang, J., Gokmen-Polar, Y., Sier, D., Anastasiadis, P., Gatalica, Z., Thompson, E.A., and Fields, A.P. (2004). Protein kinase Ciota is required for Ras transformation and colon carcinogenesis in vivo. J Cell Biol *164*, 797-802.

Murray, N.R., Kalari, K.R., and Fields, A.P. (2011). Protein kinase Ciota expression and oncogenic signaling mechanisms in cancer. J Cell Physiol *226*, 879-887.

Musch, A., Cohen, D., Yeaman, C., Nelson, W.J., Rodriguez-Boulan, E., and Brennwald, P.J. (2002). Mammalian homolog of Drosophila tumor suppressor lethal (2) giant larvae interacts with basolateral exocytic machinery in Madin-Darby canine kidney cells. Mol Biol Cell *13*, 158-168.

Muthuswamy, S.K., and Xue, B. (2012). Cell polarity as a regulator of cancer cell behavior plasticity. Annu Rev Cell Dev Biol *28*, 599-625.

Nakayama, M., Goto, T.M., Sugimoto, M., Nishimura, T., Shinagawa, T., Ohno, S., Amano, M., and Kaibuchi, K. (2008). Rho-kinase phosphorylates PAR-3 and disrupts PAR complex formation. Dev Cell *14*, 205-215.

Nam, J.M., Onodera, Y., Bissell, M.J., and Park, C.C. (2010). Breast cancer cells in three-dimensional culture display an enhanced radioresponse after coordinate targeting of integrin alpha5beta1 and fibronectin. Cancer Res *70*, 5238-5248.

Navarro, C., Nola, S., Audebert, S., Santoni, M.J., Arsanto, J.P., Ginestier, C., Marchetto, S., Jacquemier, J., Isnardon, D., Le Bivic, A.*, et al.* (2005). Junctional recruitment of mammalian Scribble relies on E-cadherin engagement. Oncogene *24*, 4330-4339.

Noda, Y., Takeya, R., Ohno, S., Naito, S., Ito, T., and Sumimoto, H. (2001). Human homologues of the Caenorhabditis elegans cell polarity protein PAR6 as an adaptor that links the small GTPases Rac and Cdc42 to atypical protein kinase C. Genes Cells *6*, 107-119.

Nolan, M.E., Aranda, V., Lee, S., Lakshmi, B., Basu, S., Allred, D.C., and Muthuswamy, S.K. (2008). The polarity protein Par6 induces cell proliferation and is overexpressed in breast cancer. Cancer Res *68*, 8201-8209.

Novick, P. (2016). Regulation of membrane traffic by Rab GEF and GAP cascades. Small GTPases *7*, 252-256.

O'Brien, L.E., Jou, T.S., Pollack, A.L., Zhang, Q., Hansen, S.H., Yurchenco, P., and Mostov, K.E. (2001). Rac1 orientates epithelial apical polarity through effects on basolateral laminin assembly. Nat Cell Biol *3*, 831-838.

Overeem, A.W., Bryant, D.M., and van, I.S.C. (2015). Mechanisms of apical-basal axis orientation and epithelial lumen positioning. Trends Cell Biol *25*, 476-485.

Ozdamar, B., Bose, R., Barrios-Rodiles, M., Wang, H.R., Zhang, Y., and Wrana, J.L. (2005). Regulation of the polarity protein Par6 by TGFbeta receptors controls epithelial cell plasticity. Science *307*, 1603-1609.

Oztan, A., Silvis, M., Weisz, O.A., Bradbury, N.A., Hsu, S.C., Goldenring, J.R., Yeaman, C., and Apodaca, G. (2007). Exocyst requirement for endocytic traffic directed toward the apical and basolateral poles of polarized MDCK cells. Mol Biol Cell *18*, 3978-3992.

Park, C.C., Zhang, H., Pallavicini, M., Gray, J.W., Baehner, F., Park, C.J., and Bissell, M.J. (2006). Beta1 integrin inhibitory antibody induces apoptosis of breast cancer cells, inhibits growth, and distinguishes malignant from normal phenotype in three dimensional cultures and in vivo. Cancer Res *66*, 1526-1535.

Peterman, E., and Prekeris, R. (2019). The postmitotic midbody: Regulating polarity, stemness, and proliferation. J Cell Biol *218*, 3903-3911.

Porter, A.P., White, G.R.M., Mack, N.A., and Malliri, A. (2019). The interaction between CASK and the tumour suppressor Dlg1 regulates mitotic spindle orientation in mammalian epithelia. J Cell Sci *132*.

Prekeris, R., Klumperman, J., and Scheller, R.H. (2000). A Rab11/Rip11 protein complex regulates apical membrane trafficking via recycling endosomes. Mol Cell *6*, 1437-1448.

Qin, Y., Capaldo, C., Gumbiner, B.M., and Macara, I.G. (2005). The mammalian Scribble polarity protein regulates epithelial cell adhesion and migration through E-cadherin. J Cell Biol *171*, 1061-1071.

Rangel, R., Sun, Y., Guzman-Rojas, L., Ozawa, M.G., Sun, J., Giordano, R.J., Van Pelt, C.S., Tinkey, P.T., Behringer, R.R., Sidman, R.L.*, et al.* (2007). Impaired angiogenesis in aminopeptidase N-null mice. Proc Natl Acad Sci U S A *104*, 4588-4593.

Rathbun, L.I., Colicino, E.G., Manikas, J., O'Connell, J., Krishnan, N., Reilly, N.S., Coyne, S., Erdemci-Tandogan, G., Garrastegui, A., Freshour, J.*, et al.* (2020). Cytokinetic bridge triggers de novo lumen formation in vivo. Nat Commun *11*, 1269.

Regala, R.P., Weems, C., Jamieson, L., Copland, J.A., Thompson, E.A., and Fields, A.P. (2005). Atypical protein kinase Ciota plays a critical role in human lung cancer cell growth and tumorigenicity. J Biol Chem *280*, 31109-31115.

Riemann, D., Kehlen, A., and Langner, J. (1999). CD13--not just a marker in leukemia typing. Immunol Today *20*, 83-88.

Rink, J., Ghigo, E., Kalaidzidis, Y., and Zerial, M. (2005). Rab conversion as a mechanism of progression from early to late endosomes. Cell *122*, 735-749.

Rodriguez-Boulan, E., Kreitzer, G., and Musch, A. (2005). Organization of vesicular trafficking in epithelia. Nat Rev Mol Cell Biol *6*, 233-247.

Rodriguez-Boulan, E., and Macara, I.G. (2014). Organization and execution of the epithelial polarity programme. Nat Rev Mol Cell Biol *15*, 225-242.

Roh, M.H., Liu, C.J., Laurinec, S., and Margolis, B. (2002a). The carboxyl terminus of zona occludens-3 binds and recruits a mammalian homologue of discs lost to tight junctions. J Biol Chem *277*, 27501-27509.

Roh, M.H., Makarova, O., Liu, C.J., Shin, K., Lee, S., Laurinec, S., Goyal, M., Wiggins, R., and Margolis, B. (2002b). The Maguk protein, Pals1, functions as an adapter, linking mammalian homologues of Crumbs and Discs Lost. J Cell Biol *157*, 161-172.

Roland, J.T., Bryant, D.M., Datta, A., Itzen, A., Mostov, K.E., and Goldenring, J.R. (2011). Rab GTPase-Myo5B complexes control membrane recycling and epithelial polarization. Proc Natl Acad Sci U S A *108*, 2789-2794.

Roman-Fernandez, A., and Bryant, D.M. (2016). Complex Polarity: Building Multicellular Tissues Through Apical Membrane Traffic. Traffic *17*, 1244-1261.

Rosse, C., Linch, M., Kermorgant, S., Cameron, A.J., Boeckeler, K., and Parker, P.J. (2010). PKC and the control of localized signal dynamics. Nat Rev Mol Cell Biol *11*, 103-112.

Rouaud, F., Sluysmans, S., Flinois, A., Shah, J., Vasileva, E., and Citi, S. (2020). Scaffolding proteins of vertebrate apical junctions: structure, functions and biophysics. Biochim Biophys Acta Biomembr *1862*, 183399.

Roux, K.J., Kim, D.I., Raida, M., and Burke, B. (2012). A promiscuous biotin ligase fusion protein identifies proximal and interacting proteins in mammalian cells. J Cell Biol *196*, 801-810.

Russ, A., Louderbough, J.M., Zarnescu, D., and Schroeder, J.A. (2012). Hugl1 and Hugl2 in mammary epithelial cells: polarity, proliferation, and differentiation. PLoS One *7*, e47734.

Saadaoui, M., Machicoane, M., di Pietro, F., Etoc, F., Echard, A., and Morin, X. (2014). Dlg1 controls planar spindle orientation in the neuroepithelium through direct interaction with LGN. J Cell Biol *206*, 707-717.

Saito, Y., Desai, R.R., and Muthuswamy, S.K. (2018). Reinterpreting polarity and cancer: The changing landscape from tumor suppression to tumor promotion. Biochim Biophys Acta Rev Cancer *1869*, 103-116.

Schluter, M.A., Pfarr, C.S., Pieczynski, J., Whiteman, E.L., Hurd, T.W., Fan, S., Liu, C.J., and Margolis, B. (2009a). Trafficking of Crumbs3 during cytokinesis is crucial for lumen formation. Molecular biology of the cell *20*, 4652-4663.

Schluter, M.A., Pfarr, C.S., Pieczynski, J., Whiteman, E.L., Hurd, T.W., Fan, S., Liu, C.J., and Margolis, B. (2009b). Trafficking of Crumbs3 during cytokinesis is crucial for lumen formation. Mol Biol Cell *20*, 4652-4663.

Schneeberger, K., Roth, S., Nieuwenhuis, E.E.S., and Middendorp, S. (2018). Intestinal epithelial cell polarity defects in disease: lessons from microvillus inclusion disease. Dis Model Mech *11*.

Schober, M., Schaefer, M., and Knoblich, J.A. (1999). Bazooka recruits Inscuteable to orient asymmetric cell divisions in Drosophila neuroblasts. Nature *402*, 548-551.

Shaye, D.D., Casanova, J., and Llimargas, M. (2008). Modulation of intracellular trafficking regulates cell intercalation in the Drosophila trachea. Nat Cell Biol *10*, 964-970.

Shin, K., Straight, S., and Margolis, B. (2005). PATJ regulates tight junction formation and polarity in mammalian epithelial cells. J Cell Biol *168*, 705-711.

Shin, K., Wang, Q., and Margolis, B. (2007). PATJ regulates directional migration of mammalian epithelial cells. EMBO Rep *8*, 158-164.

Shivas, J.M., Morrison, H.A., Bilder, D., and Skop, A.R. (2010). Polarity and endocytosis: reciprocal regulation. Trends Cell Biol *20*, 445-452.

Slaughter, B.D., Smith, S.E., and Li, R. (2009). Symmetry breaking in the life cycle of the budding yeast. Cold Spring Harb Perspect Biol *1*, a003384.

Smith, C.A., Lau, K.M., Rahmani, Z., Dho, S.E., Brothers, G., She, Y.M., Berry, D.M., Bonneil, E., Thibault, P., Schweisguth, F*., et al.* (2007). aPKC-mediated phosphorylation regulates asymmetric membrane localization of the cell fate determinant Numb. EMBO J *26*, 468-480.

St Johnston, D., and Ahringer, J. (2010). Cell polarity in eggs and epithelia: parallels and diversity. Cell *141*, 757-774.

Steinberg, S.F. (2008). Structural basis of protein kinase C isoform function. Physiol Rev *88*, 1341-1378.

Stephens, R., Lim, K., Portela, M., Kvansakul, M., Humbert, P.O., and Richardson, H.E. (2018). The Scribble Cell Polarity Module in the Regulation of Cell Signaling in Tissue Development and Tumorigenesis. J Mol Biol *430*, 3585-3612.

Sternlicht, M.D. (2006). Key stages in mammary gland development: the cues that regulate ductal branching morphogenesis. Breast Cancer Res *8*, 201.

Straight, S.W., Pieczynski, J.N., Whiteman, E.L., Liu, C.J., and Margolis, B. (2006). Mammalian lin-7 stabilizes polarity protein complexes. J Biol Chem *281*, 37738-37747.

Straight, S.W., Shin, K., Fogg, V.C., Fan, S., Liu, C.J., Roh, M., and Margolis, B. (2004). Loss of PALS1 expression leads to tight junction and polarity defects. Mol Biol Cell *15*, 1981-1990.

Strilic, B., Kucera, T., Eglinger, J., Hughes, M.R., McNagny, K.M., Tsukita, S., Dejana, E., Ferrara, N., and Lammert, E. (2009). The molecular basis of vascular lumen formation in the developing mouse aorta. Dev Cell *17*, 505-515.

Subramani, J., Ghosh, M., Rahman, M.M., Caromile, L.A., Gerber, C., Rezaul, K., Han, D.K., and Shapiro, L.H. (2013). Tyrosine phosphorylation of CD13 regulates inflammatory cell-cell adhesion and monocyte trafficking. J Immunol *191*, 3905-3912.

Sun, Y., Aiga, M., Yoshida, E., Humbert, P.O., and Bamji, S.X. (2009). Scribble interacts with beta-catenin to localize synaptic vesicles to synapses. Mol Biol Cell *20*, 3390-3400.

Suzuki, A., Hirata, M., Kamimura, K., Maniwa, R., Yamanaka, T., Mizuno, K., Kishikawa, M., Hirose, H., Amano, Y., Izumi, N*., et al.* (2004). aPKC acts upstream of PAR-1b in both the establishment and maintenance of mammalian epithelial polarity. Curr Biol *14*, 1425-1435.

Suzuki, A., and Ohno, S. (2006). The PAR-aPKC system: lessons in polarity. J Cell Sci *119*, 979-987.

Suzuki, A., Yamanaka, T., Hirose, T., Manabe, N., Mizuno, K., Shimizu, M., Akimoto, K., Izumi, Y., Ohnishi, T., and Ohno, S. (2001). Atypical protein kinase C is involved in the evolutionarily conserved par protein complex and plays a critical role in establishing epithelia-specific junctional structures. J Cell Biol *152*, 1183-1196.

Szymaniak, A.D., Mahoney, J.E., Cardoso, W.V., and Varelas, X. (2015). Crumbs3-Mediated Polarity Directs Airway Epithelial Cell Fate through the Hippo Pathway Effector Yap. Dev Cell *34*, 283-296.

Tabuse, Y., Izumi, Y., Piano, F., Kemphues, K.J., Miwa, J., and Ohno, S. (1998). Atypical protein kinase C cooperates with PAR-3 to establish embryonic polarity in Caenorhabditis elegans. Development *125*, 3607-3614.

Taniguchi, K., Shao, Y., Townshend, R.F., Tsai, Y.H., DeLong, C.J., Lopez, S.A., Gayen, S., Freddo, A.M., Chue, D.J., Thomas, D.J*., et al.* (2015). Lumen Formation Is an Intrinsic Property of Isolated Human Pluripotent Stem Cells. Stem Cell Reports *5*, 954-962.

Tawk, M., Araya, C., Lyons, D.A., Reugels, A.M., Girdler, G.C., Bayley, P.R., Hyde, D.R., Tada, M., and Clarke, J.D. (2007). A mirror-symmetric cell division that orchestrates neuroepithelial morphogenesis. Nature *446*, 797-800.

ten Klooster, J.P., Jaffer, Z.M., Chernoff, J., and Hordijk, P.L. (2006). Targeting and activation of Rac1 are mediated by the exchange factor beta-Pix. J Cell Biol *172*, 759-769.

Tepass, U. (2012). The apical polarity protein network in Drosophila epithelial cells: regulation of polarity, junctions, morphogenesis, cell growth, and survival. Annu Rev Cell Dev Biol *28*, 655-685.

Thiery, J.P., Acloque, H., Huang, R.Y., and Nieto, M.A. (2009). Epithelial-mesenchymal transitions in development and disease. Cell *139*, 871-890.

Thuenauer, R., Hsu, Y.C., Carvajal-Gonzalez, J.M., Deborde, S., Chuang, J.Z., Romer, W., Sonnleitner, A., Rodriguez-Boulan, E., and Sung, C.H. (2014). Four-dimensional live imaging of apical biosynthetic trafficking reveals a post-Golgi sorting role of apical endosomal intermediates. Proc Natl Acad Sci U S A *111*, 4127-4132.

Tushir, J.S., Clancy, J., Warren, A., Wrobel, C., Brugge, J.S., and D'Souza-Schorey, C. (2010). Unregulated ARF6 activation in epithelial cysts generates hyperactive signaling endosomes and disrupts morphogenesis. Mol Biol Cell *21*, 2355-2366.

Varnaite, R., and MacNeill, S.A. (2016). Meet the neighbors: Mapping local protein interactomes by proximity-dependent labeling with BioID. Proteomics *16*, 2503-2518.

Ventura, G., Moreira, S., Barros-Carvalho, A., Osswald, M., and Morais-de-Sa, E. (2020). Lgl cortical dynamics are independent of binding to the Scrib-Dlg complex but require Dlg-dependent restriction of aPKC. Development *147*.

Vogel, G.F., Klee, K.M., Janecke, A.R., Muller, T., Hess, M.W., and Huber, L.A. (2015). Cargo-selective apical exocytosis in epithelial cells is conducted by Myo5B, Slp4a, Vamp7, and Syntaxin 3. J Cell Biol *211*, 587-604.

von Stein, W., Ramrath, A., Grimm, A., Muller-Borg, M., and Wodarz, A. (2005). Direct association of Bazooka/PAR-3 with the lipid phosphatase PTEN reveals a link between the PAR/aPKC complex and phosphoinositide signaling. Development *132*, 1675-1686.

Wang, Q., Chen, X.W., and Margolis, B. (2007). PALS1 regulates E-cadherin trafficking in mammalian epithelial cells. Mol Biol Cell *18*, 874-885.

Wang, T., Yanger, K., Stanger, B.Z., Cassio, D., and Bi, E. (2014). Cytokinesis defines a spatial landmark for hepatocyte polarization and apical lumen formation. J Cell Sci *127*, 2483-2492.

Wang, X., Kumar, R., Navarre, J., Casanova, J.E., and Goldenring, J.R. (2000). Regulation of vesicle trafficking in madin-darby canine kidney cells by Rab11a and Rab25. J Biol Chem *275*, 29138-29146.

Wang, Y.C., Khan, Z., Kaschube, M., and Wieschaus, E.F. (2012). Differential positioning of adherens junctions is associated with initiation of epithelial folding. Nature *484*, 390-393.

Watts, J.L., Etemad-Moghadam, B., Guo, S., Boyd, L., Draper, B.W., Mello, C.C., Priess, J.R., and Kemphues, K.J. (1996). par-6, a gene involved in the establishment of asymmetry in early C. elegans embryos, mediates the asymmetric localization of PAR-3. Development *122*, 3133-3140.

Whiteman, E.L., Fan, S., Harder, J.L., Walton, K.D., Liu, C.J., Soofi, A., Fogg, V.C., Hershenson, M.B., Dressler, G.R., Deutsch, G.H.*, et al.* (2014). Crumbs3 is essential for proper epithelial development and viability. Mol Cell Biol *34*, 43-56.

Wildenberg, G.A., Dohn, M.R., Carnahan, R.H., Davis, M.A., Lobdell, N.A., Settleman, J., and Reynolds, A.B. (2006). p120-catenin and p190RhoGAP regulate cell-cell adhesion by coordinating antagonism between Rac and Rho. Cell *127*, 1027-1039.

Willenborg, C., Jing, J., Wu, C., Matern, H., Schaack, J., Burden, J., and Prekeris, R. (2011). Interaction between FIP5 and SNX18 regulates epithelial lumen formation. J Cell Biol *195*, 71-86.

Wilson, M.I., Gill, D.J., Perisic, O., Quinn, M.T., and Williams, R.L. (2003). PB1 domain-mediated heterodimerization in NADPH oxidase and signaling complexes of atypical protein kinase C with Par6 and p62. Mol Cell *12*, 39-50.

Wilson, P.D. (2011). Apico-basal polarity in polycystic kidney disease epithelia. Biochim Biophys Acta *1812*, 1239-1248.

Winnicka, B., O'Conor, C., Schacke, W., Vernier, K., Grant, C.L., Fenteany, F.H., Pereira, F.E., Liang, B., Kaur, A., Zhao, R.*, et al.* (2010). CD13 is dispensable for normal hematopoiesis and myeloid cell functions in the mouse. J Leukoc Biol *88*, 347-359.

Winter, J.F., Hopfner, S., Korn, K., Farnung, B.O., Bradshaw, C.R., Marsico, G., Volkmer, M., Habermann, B., and Zerial, M. (2012). Caenorhabditis elegans screen reveals role of PAR-5 in RAB-11-recycling endosome positioning and apicobasal cell polarity. Nat Cell Biol *14*, 666-676.

Yamanaka, T., Horikoshi, Y., Sugiyama, Y., Ishiyama, C., Suzuki, A., Hirose, T., Iwamatsu, A., Shinohara, A., and Ohno, S. (2003). Mammalian Lgl forms a protein complex with PAR-6 and aPKC independently of PAR-3 to regulate epithelial cell polarity. Curr Biol *13*, 734-743.

Yamanaka, T., Horikoshi, Y., Suzuki, A., Sugiyama, Y., Kitamura, K., Maniwa, R., Nagai, Y., Yamashita, A., Hirose, T., Ishikawa, H.*, et al.* (2001). PAR-6 regulates aPKC activity in a novel way and mediates cell-cell contact-induced formation of the epithelial junctional complex. Genes Cells *6*, 721-731.

Yamashita, Y.M., Yuan, H., Cheng, J., and Hunt, A.J. (2010). Polarity in stem cell division: asymmetric stem cell division in tissue homeostasis. Cold Spring Harb Perspect Biol *2*, a001313.

Yeaman, C., Ayala, M.I., Wright, J.R., Bard, F., Bossard, C., Ang, A., Maeda, Y., Seufferlein, T., Mellman, I., Nelson, W.J.*, et al.* (2004). Protein kinase D regulates basolateral membrane protein exit from trans-Golgi network. Nat Cell Biol *6*, 106-112.

Yonemura, S. (2014). Differential sensitivity of epithelial cells to extracellular matrix in polarity establishment. PLoS One *9*, e112922.

Yu, J., Zheng, Y., Dong, J., Klusza, S., Deng, W.M., and Pan, D. (2010). Kibra functions as a tumor suppressor protein that regulates Hippo signaling in conjunction with Merlin and Expanded. Dev Cell *18*, 288-299.

Zeitler, J., Hsu, C.P., Dionne, H., and Bilder, D. (2004). Domains controlling cell polarity and proliferation in the Drosophila tumor suppressor Scribble. J Cell Biol *167*, 1137-1146.

Zerial, M., and McBride, H. (2001). Rab proteins as membrane organizers. Nat Rev Mol Cell Biol *2*, 107-117.

Zhan, L., Rosenberg, A., Bergami, K.C., Yu, M., Xuan, Z., Jaffe, A.B., Allred, C., and Muthuswamy, S.K. (2008). Deregulation of scribble promotes mammary tumorigenesis and reveals a role for cell polarity in carcinoma. Cell *135*, 865-878.

Zhang, K., Zhao, H., Ji, Z., Zhang, C., Zhou, P., Wang, L., Chen, Q., Wang, J., Zhang, P., Chen, Z.*, et al.* (2016). Shp2 promotes metastasis of prostate cancer by attenuating the PAR3/PAR6/aPKC polarity protein complex and enhancing epithelial-to-mesenchymal transition. Oncogene *35*, 1271-1282.

Zhang, X., Wang, P., Gangar, A., Zhang, J., Brennwald, P., TerBush, D., and Guo, W. (2005). Lethal giant larvae proteins interact with the exocyst complex and are involved in polarized exocytosis. J Cell Biol *170*, 273-283.

Zhou, W., and Hong, Y. (2012). Drosophila Patj plays a supporting role in apical-basal polarity but is essential for viability. Development *139*, 2891-2896.